

4. SITE 897¹

Shipboard Scientific Party²

HOLE 897A

Date occupied: 31 March 1993
Date departed: 1 April 1993
Time on hole: 1 day, 5 hr, 45 min
Position: 40°50.32'N, 12°28.44'W
Bottom felt (drill-pipe measurement from rig floor, m): 5331.0
Distance between rig floor and sea level (m): 11.05
Water depth (drill-pipe measurement from sea level, m): 5320.0
Total depth (from rig floor, m): 5386.20
Penetration (m): 55.20
Number of cores (including cores having no recovery): 6
Total length of cored section (m): 55.20
Total core recovered (m): 17.37
Core recovery (%): 31.5
Oldest sediment cored:
Depth (mbsf): 55.20
Nature: nannofossil ooze/interbedded silty turbidites
Age: Pleistocene
Measured velocity (km/s): 1.51

HOLE 897B

Date occupied: 1 April 1993
Date departed: 2 April 1993
Time on hole: 19 hr, 0 min
Position: 40°50.32'N, 12°28.44'W
Bottom felt (drill-pipe measurement from rig floor, m): 5331.0
Distance between rig floor and sea level (m): 11.08
Water depth (drill-pipe measurement from sea level, m): 5319.9
Total depth (from rig floor, m): 5393.00
Penetration (m): 62.00
Number of cores (including cores having no recovery): 1
Total length of cored section (m): 10.00
Total core recovered (m): 0.00
Core recovery (%): 0

HOLE 897C

Date occupied: 2 April 1993
Date departed: 9 April 1993
Time on hole: 7 days, 8 hr, 30 min

Position: 40°50.33'N, 12°28.44'W
Bottom felt (drill-pipe measurement from rig floor, m): 5326.3
Distance between rig floor and sea level (m): 11.14
Water depth (drill-pipe measurement from sea level, m): 5315.2
Total depth (from rig floor, m): 6071.20
Penetration (m): 744.90
Number of cores (including cores with no recovery): 73
Total length of cored section (m): 695.00
Total core recovered (m): 352.81
Core recovery (%): 50.8
Oldest sediment cored:
Depth (mbsf): 677.5
Nature: claystone, sandstone, conglomerate
Age: Early Cretaceous
Measured velocity (km/s): 1.70
Basement:
Depth (mbsf): 744.90
Nature: serpentinized peridotites
Measured velocity (km/s): 3.37

HOLE 897D

Date occupied: 9 April 1993
Date departed: 17 April 1993
Time on hole: 7 days, 23 hr, 15 min
Position: 40°50.31'N, 12°28.51'W
Bottom felt (drill-pipe measurement from rig floor, m): 5327.0
Distance between rig floor and sea level (m): 11.23
Water depth (drill-pipe measurement from sea level, m): 5315.8
Total depth (from rig floor, m): 6164.20
Penetration (m): 837.20
Number of cores (including cores having with no recovery): 25
Total length of cored section (m): 241.20
Total core recovered (m): 117.94
Core recovery (%): 48.75
Oldest sediment cored:
Depth (mbsf): 693.80
Nature: nannofossil-foraminifer chalk, claystone
Age: Early Cretaceous
Measured velocity (km/s): 2.07
Basement:
Depth (mbsf): 837.20
Nature: serpentinized peridotite
Measured velocity (km/s): 3.0-5.4

Principal results: Site 897 is situated in the Iberia Abyssal Plain over a north-south basement ridge within the ocean/continent transition (OCT) zone. Geophysical modeling had predicted that the ridge lay at, or close to, the

¹ Sawyer, D.S., Whitmarsh, R.B., Klaus, A., et al., 1994. *Proc. ODP, Init. Repts.*, 149: College Station, TX (Ocean Drilling Program).

² Shipboard Scientific Party is as given in list of participants preceding the contents.

ocean/continent boundary and might consist of serpentinized peridotite. The site is one of a transect across the OCT designed to study the petrological changes in the basement rocks within the OCT as a means of identifying the processes that accompanied continental break-up and the onset of steady-state seafloor spreading. Cores were obtained from three holes that penetrated up to 694 m of Pleistocene to Early Cretaceous age sediments and from two holes that penetrated up to 143 m of basement.

1. The basement is composed of serpentinized, relatively undepleted peridotite that originated in the upper mantle and was exposed at the seafloor during, and for several tens of m.y. after, the time of continental break-up.

2. A unit containing late Hauterivian(?), early Barremian to late Aptian sediments immediately overlies basement and contains fragments of peridotite and continental basement rocks. The unit was deposited during the Early Cretaceous by a series of mass flows. The composition of the sediments suggest that continental basement rocks were located upslope, or a few tens of meters downslope, of the site.

3. A significant depositional hiatus starting in the middle Miocene, correlatable with a regional angular unconformity on seismic reflection profiles, may be related to northwest-southeast compression on this margin during a Compressional phase in the Betic Mountains in southern Spain and structural inversion in the Lusitanian Basin of Portugal.

Four lithologic units have been identified at Site 897:

1. Unit I (0-292.0 mbsf) is a Pleistocene to early Pliocene silty clay to clayey silt with nannofossil clay with graded silt and fine sand beds. The unit mainly consists of terrigenous turbidites.

2. Subunit IIA (292.0-301.2 mbsf) is an early Pliocene to late Miocene nannofossil claystone with claystone and nannofossil silty claystone of turbiditic and hemipelagic/pelagic origin.

Subunit IIB (301.2-359.8 mbsf) is a late to early Miocene calcareous claystone and claystone with silty claystone and clayey siltstone. The Subunit mainly consists of calcareous turbidites with significant reworking by contour currents.

Subunit IIC (359.8-619.7 mbsf in Hole 897C; base at 622.9 mbsf in Hole 897D) is an early Miocene to middle Eocene silty claystone to clayey siltstone with calcareous claystone. The subunit consists mainly of calcareous turbidites with significant reworking by contour currents.

3. Subunit IIIA (619.7-639.4 mbsf in Hole 897C; 622.9-645.2 mbsf in Hole 897D) is an unfossiliferous claystone. The subunit consists of a pelagic/hemipelagic facies deposited below the carbonate compensation depth (CCD).

Subunit IIIB (639.4-648.7 mbsf in Hole 897C; 645.2-655.2 mbsf in Hole 897D) is an unfossiliferous clayey conglomerate and sandy silty claystone with clayey sandstone.

4. Unit IV (648.7-677.5 mbsf in Hole 897C; 655.2-693.8 mbsf in Hole 897D) consists of late Aptian to Hauterivian sandstone, dolomite, limestone, calcareous claystone with peridotite clasts and megaclasts. The unit is a mass-flow deposit.

The sedimentary section provided a discontinuous fossil record from the Pleistocene through Early Cretaceous. Calcareous nannofossils are generally present, except in Unit III. Planktonic and benthic foraminifers are abundant to common in the Pleistocene and upper Pliocene deposits, but rare to absent throughout most of the remaining cored interval. One hiatus was observed in the upper Pliocene. Two unconformities in the Miocene together represent a 10.5-Ma hiatus from middle Miocene to late Miocene. Although the age of Unit III is uncertain, it is likely that an earlier hiatus in deposition occurred from the Early Cretaceous to the middle to late Eocene.

The mass-flow deposit immediately above the basement, containing basement blocks, was emplaced during late Hauterivian(?), early Barremian and late Aptian times. Therefore, the peridotite was exposed at the seafloor and contributed clasts to the mass flows during the Early Cretaceous.

Holes 897C and 897D penetrated 67 m and 143 m, respectively, of basement rock. The entire basement section consists of peridotite that has

been almost completely serpentinized and partially brecciated during and after serpentinization. About 90% of the peridotite is undifferentiated harzburgite or lherzolite whose original composition was 70%-80% olivine, 15%-20% pyroxene, and 1%-2% spinel. These rocks are heterogeneous and range from pyroxene-rich peridotite to dunite. The remaining 10% of the peridotite is plagioclase- and spinel-bearing and was originally composed of 50%-70% olivine, 20%-30% pyroxene, 15% plagioclase, and 1%-5% spinel. The coexistence of plagioclase and spinel suggests that these rocks last equilibrated at low pressure, (900-1000 MPa or about 30 km depth). The wide variety of peridotite types and the locally high proportion of plagioclase (up to 40%), suggest that the peridotite may have experienced some melting and even magma mobility. The brecciation ranges from pervasive fracturing and serpentine and carbonate veining to the formation of gravel-sized serpentinized peridotite clasts embedded in a carbonate and serpentine matrix. In some cases, the brecciation shows a well-developed foliation associated with a late-stage shear deformation event. While the peridotites have experienced late, low-temperature deformation, they show almost no signs of high-temperature ductile deformation.

Acoustic formations 1A, 1B, and 2 have been widely recognized in multichannel seismic reflection profiles on the western Iberia margin and have been locally dated by previous drilling. At Site 897, acoustic formation boundaries 1A/1B and 1B/2 correlate with the middle to late Miocene hiatus at 325 mbsf and with the top of middle Eocene claystone and chalk at about 590 mbsf, respectively.

Several tentative magnetostratigraphic correlations have been identified in the Pliocene, and one each in the middle Oligocene and Maastriichtian. Magnetic susceptibility correlates particularly well on a fine scale with the alternating sand and clay units of the terrigenous turbidite sequences in Unit I. Magnetic susceptibility generally is higher in the serpentinized peridotite basement than in the sediments, but decreases with increasing peridotite alteration.

In-situ temperature measurements indicate that the vertical temperature gradient between the seafloor and 215 mbsf is about 43°C/km and that the vertical conductive heat flow is about 54 mW/m².

Physical-property measurements in Units I and II show a steady increase in density, seismic velocity, formation factor, and thermal conductivity, and a concomitant decrease in porosity with depth. Those in Units III and IV are much more variable. In the serpentinized peridotite, density and velocity vary according to the degree of alteration visible in hand specimens and range from 2.3 to 2.5 g/cm³ and 2.8 to 7.1 km/s.

Interstitial-water samples were obtained from Unit I through Subunit IIIA (26-636 mbsf). The pore-water chemistry (sulfate, alkalinity, ammonia, iron, manganese, calcium, magnesium, strontium, potassium, silica, chloride, and sodium) reflects the rapid deposition of the Pliocene-Pleistocene turbidites and the relatively slower deposition of the earlier sediments. The principal result is the surprisingly high sulfate concentration (up to 18 mM) in the sediments below Unit I and Subunit IIA. This is attributed to a low sedimentation rate, low permeability, and an absence of reactive carbon.

Profiles of carbonate content vs. depth reflect a history of generally low biological productivity and deposition of hemipelagic sediment below the CCD, combined with delivery by turbidites of carbonate-rich material initially deposited above the CCD. Elevated organic carbon is found in Units I and IV (0.6 and 0.9%, respectively); Unit IV appears to contain organic material mostly derived from land plant detritus. Relatively high concentrations of biogenic methane were encountered in headspace gas analyses of lithostratigraphic Unit I, but were essentially absent from all deeper sections.

BACKGROUND AND SCIENTIFIC OBJECTIVES

Site 897 (Fig. 1) was one of a series of sites drilled during Leg 149 to elucidate the nature of the top of the crust (acoustic basement) within the ocean/continent transition (OCT) beneath the Iberia Abyssal Plain. The regional background to this and the other Leg 149 sites is presented in the "Introduction" chapter (this volume) and elsewhere (Whitmarsh et al., 1990; Whitmarsh et al., 1993). Site 897 was

chosen to sample the region where the thin oceanic crust to the west merges with the intermediate zone of high magnetization and smooth acoustic basement to the east. The site is located on the easternmost of a series of roughly north-south basement ridges (Figs. 2 and 3). The ridge under Site 897 may have the same tectonic relationship to the OCT as the peridotite ridge drilled at Site 637 during Leg 103 (Beslier et al., 1993). The latter ridge is widely thought to represent the boundary between oceanic and continental rocks off western Galicia Bank (Boillot et al., 1980). Although both sites are situated over linear ridges, which can be followed for tens of kilometers in a north-south direction, the ridges are not continuous but may be linked via two en-echelon sinistral offsets, possibly representing successive stages of south-to-north rifting along this margin (Beslier et al., 1993).

About 680 m of sediment overlies basement. By analogy with Site 398, 145 km to the east of Site 897, the lithologies were expected to be ooze/chalk with turbidites over chalk, mudstone, and claystone. From seismic reflection profiles traced back to Site 398 before Leg 149, the basal sediments were estimated to be as old as Maastrichtian. The Miocene regional unconformity, which resulted from gentle folding that occurred during the Rif-Betic Compressional phase farther south and which is visible clearly in seismic reflection profiles from the Iberia Abyssal Plain, was expected to occur at about 360 mbsf. In the vicinity of Site 897, the unconformity is marked by horizontal sedimentary reflectors that onlap low-angle west-dipping reflectors; this can be seen in the east-west seismic profile across the site (Fig. 3). The sediments thicken to 2.0 s (2.4 km) in a basin west of the site and to 1.4 s (1.5 km) to the east. Although we anticipated that the acoustic basement at Site 897 might contain ultramafic rocks within a few hundred meters of its upper surface, we were not certain that these had ever actually outcropped, so that the uppermost basement was expected to be any mixture of lithology from continental basement rocks to igneous intrusive/extrusive material to tholeiitic lavas of the upper oceanic crust.

OPERATIONS

Ponta Delgada, Azores to Site 897

The *JOIDES Resolution* departed Ponta Delgada, Azores, at 1615 hr (all times are given in Universal Time Coordinated [UTC]), 28 March 1993. We steamed the 631 nmi to Site 897 in 51.25 hr. We started a single-channel seismic reflection and magnetic survey over the proposed Site IAP-4 at 2130, 30 March, to confirm its location (see "Site Geophysics" section, this chapter). During this site survey, a navigation computer program (AGCNAV) proved extremely helpful in providing a real-time display of the ship's track. The seismic survey was completed at 0052 hr, 31 March, and the ship returned to the chosen site location. A Datasonics beacon was deployed at 0145 hr at 40°50.37'N, 12°28.37'W. After the ship was in dynamic positioning (DP) mode, a backup Datasonics beacon was dropped and turned off. The site location had been offset 200 m east-northeast of the approved location to penetrate a thin layer of possible synrift sediments above basement. The precision depth recorder (PDR) indicated a water depth of 5330.2 m below rig floor (mbrf; the rig floor was approximately 11.05 m above sea level).

Hole 897A

Beginning at 0400 hr, 31 March, a rotary core barrel (RCB) bottom-hole assembly (BHA) having a mechanical bit release (MBR) was assembled and run to the seafloor. The bit tagged the bottom at 5331.0 mbrf. Hole 897A was spudded at 1845 hr, 31 March. Cores 149-897A-1R through -6R were cut from 0.0 to 55.2 mbsf, with 17.37 m material recovered (Table 1). A WSTP was used at 55.2 mbsf.

The drawworks brakes were not holding, and several attempts to adjust them were unsuccessful. Sea conditions were causing an occasional 3-m ship's heave and $\pm 40,000$ -lb fluctuations in the 580,000-lb hanging weight of the drill string. The silty/sandy top of the hole was

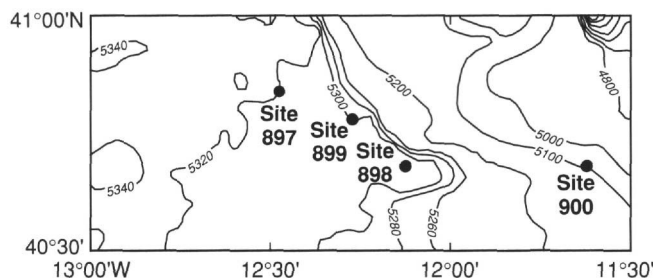


Figure 1. Bathymetry of part of the Iberia Abyssal Plain, based in part on Simrad EM-12 swath bathymetry provided by G. Pautot, IFREMER Centre de Brest, showing the location of Leg 149 sites (except Site 901). Contours are in meters; note irregular contour interval.

potentially unstable, while the hole was only 55 m deep; therefore, we judged it best to terminate operations in Hole 897A. The bit was pulled above the seafloor, and the drawworks brake pads were replaced.

Hole 897B

The ship was not moved; Hole 897B was spudded at 1320 hr, 1 April. The mud line was encountered at 5331.0 mbrf, and the hole was drilled from 0.0 to 52.0 mbsf. Erratic torque was observed in the first 30 m and was assumed to be the result of unstable seafloor sediments that had caved into the hole. A 10.0-m core was cut from 5383.0 to 5393.0 mbrf. Several attempts to retrieve the core barrel were unsuccessful. We pulled the drill pipe out of the hole and found that part of the BHA had been lost.

Hole 897C

A new RCB BHA with a MBR was assembled, and the ship was moved 20 m north. Hole 897C was spudded at 1745 hr, 2 April. The PDR indicated a water depth of 5329.4 mbrf, and the bit encountered the seafloor at 5326.3 mbrf. Cores 149-897C-1R through -73R were cut from 49.9 through 744.9 mbsf (Table 1). A total of 695.0 m was cored with 352.8 m of material recovered. WSTP temperature measurements were taken at 117.9, 166.1, and 214.4 mbsf.

After coring Hole 897C to 744.9 mbsf, the hole appeared to be in good condition, and we judged it prudent to change the drill bit. Because a primary objective of Site 897 was significant basement penetration and the first bit was not fresh enough to complete the hole, we decided to deploy a free-fall funnel (FFF) and retrieve the pipe to replace the bit.

The bit was pulled to 74 mbsf and an FFF was deployed. The vibration-isolation tool (VIT) was deployed with a television camera and a sonar. The FFF and floats were not visible on the seafloor, but the VIT sonar indicated that the funnel was at 4 mbsf. No flow was visible exiting the crater during fluid circulation. The hole was considered to be too valuable to risk losing it on a blind reentry, and additional basement penetration and logging were considered to be important; therefore, we decided to go back to the bottom of the hole and to continue coring for the remaining life of the bit. At this point, however, the drill pipe became stuck. In the process of attempting to free it, the BHA broke off. Hole 897C was terminated, and the drill string pulled out of the hole.

Hole 897D

We decided to drill Hole 897D to acquire additional basement and deep sediment cores and to obtain downhole logs. The ship was offset 100 m west-southwest of Hole 897C to obtain information about the lateral variability within the deep sediments and basement rocks. The PDR indicated a water depth of 5330.2 mbrf. A RCB BHA with an MBR was deployed, and the seafloor was encountered at 5327.0

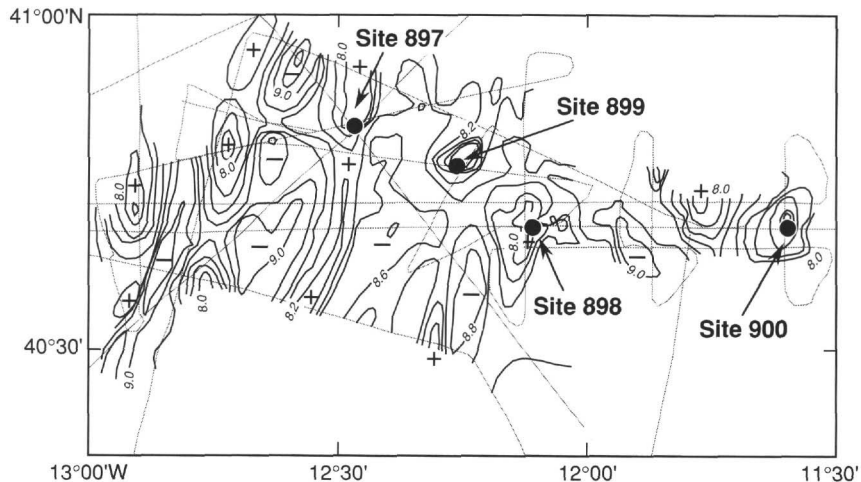


Figure 2. A contoured basement structure map, based on migrated multichannel and unmigrated single-channel seismic reflection profiles, showing the location of Leg 149 sites (except Site 901) with respect to basement relief. Contour interval is 0.25 s (two-way traveltime). Dotted and dashed lines indicate ship's tracks.

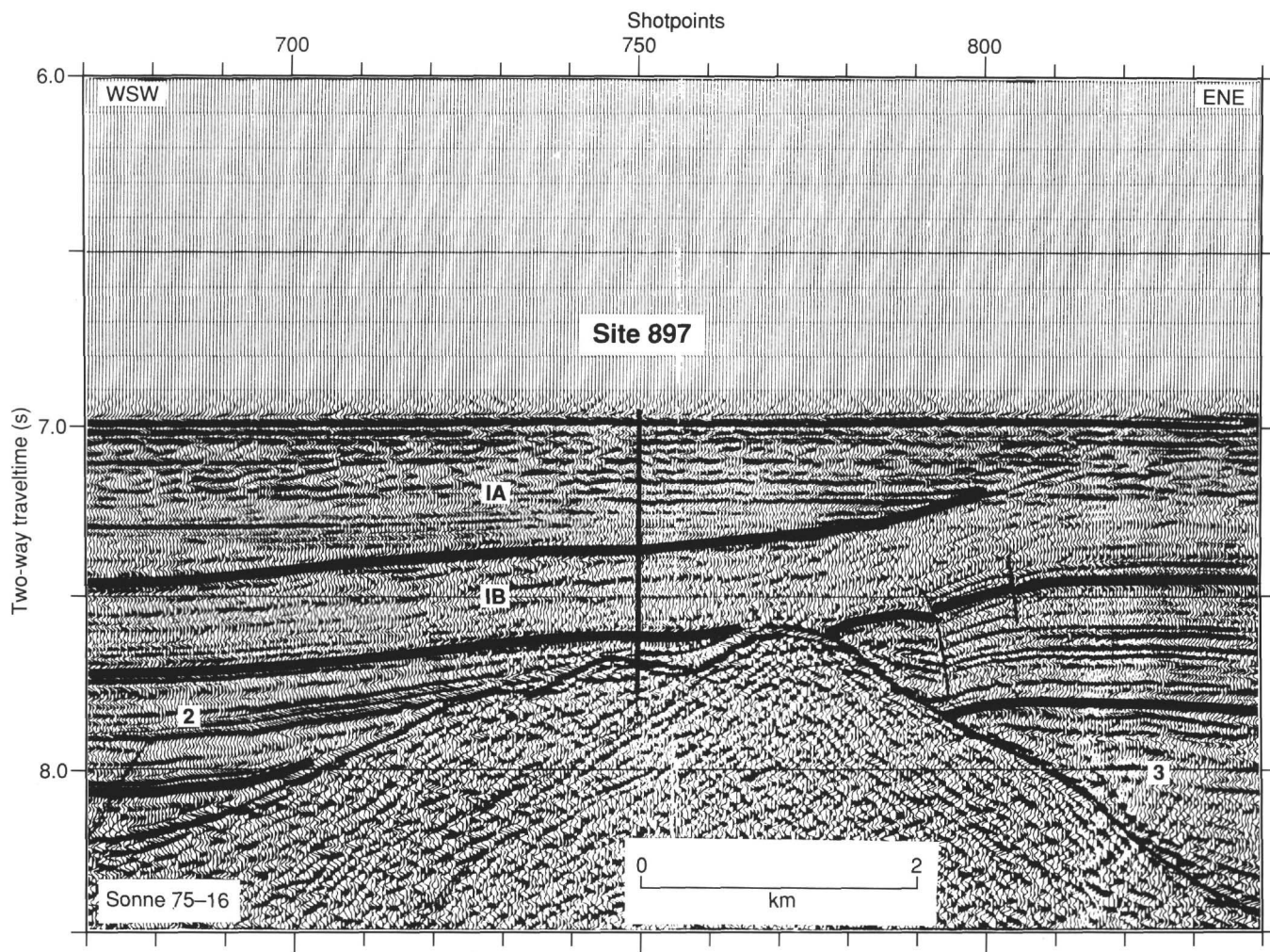


Figure 3. Migrated multichannel seismic reflection profile Sonne 75-16 across Site 897. The thick line indicates the location and penetration of the borehole.

mbrf. Hole 897D was spudded at 0600 hr, 10 April. We drilled from 0 to 596.0 mbsf. The core barrel was recovered at 200-m intervals as a precaution against its becoming stuck by cuttings that might circulate above it. Cores 149-897D-1R to -25R were cut from 596.0 to 837.2 mbsf, an interval of 241.2 m in which we recovered 117.94 m of material (Table 1).

After coring, the hole was flushed, the basement/sediment contact from 5982 to 6164 mbrf was reamed clear, and a short pipe trip was made to 120 mbsf. The bit was dropped at the bottom of the hole, and the pipe was pulled to 120 mbsf again for logging.

A 41-m-long geophysical combination (quad-combo) logging tool (see "Explanatory Notes" chapter, this volume) was run. The tool en-

Table 1. Coring summary for Site 897.

| Core | Date (1993) | Time (UTC) | Depth (mbsf) | Length cored (m) | Length recovered (m) | Recovery (%) | Core | Date (1993) | Time (UTC) | Depth (mbsf) | Length cored (m) | Length recovered (m) | Recovery (%) | | | |
|----------------|-------------|------------|--------------|----------------------------------|----------------------|--------------|----------------|-------------|------------|--------------|------------------|----------------------|-----------------------------------|--------|-------|--|
| 149-897A- | | | | | | | 48R | | | | | | | | | |
| 1R | Mar 31 | 1835 | 0.0–8.7 | 8.7 | 1.32 | 15.2 | 49R | Apr 5 | 1700 | 503.9–513.6 | 9.7 | 8.11 | 83.6 | | | |
| 2R | Mar 31 | 2020 | 8.7–16.7 | 8.0 | 0.03 | 0.4 | 50R | Apr 5 | 1835 | 513.6–523.2 | 9.6 | 6.47 | 67.4 | | | |
| 3R | Mar 31 | 2150 | 16.7–26.3 | 9.6 | 0.65 | 6.8 | 51R | Apr 5 | 2205 | 523.2–532.8 | 9.6 | 4.76 | 49.6 | | | |
| 4R | Mar 31 | 2330 | 26.3–36.0 | 9.7 | 4.37 | 45.0 | 52R | Apr 5 | 2325 | 532.8–542.4 | 9.6 | 4.20 | 43.7 | | | |
| 5R | Apr 1 | 0100 | 36.0–45.6 | 9.6 | 3.73 | 38.8 | 53R | Apr 5 | 2325 | 542.4–552.1 | 9.7 | 4.30 | 44.3 | | | |
| 6R | Apr 1 | 0215 | 45.6–55.2 | 9.6 | 7.27 | 75.7 | 54R | Apr 6 | 0100 | 552.1–561.8 | 9.7 | 3.97 | 40.9 | | | |
| Coring totals: | | | | 55.2 | 17.37 | 31.5 | 55R | Apr 6 | 0205 | 561.8–571.5 | 9.7 | 5.22 | 53.8 | | | |
| | | | | ***** Drilled 0–152.0 mbsf ***** | | | 56R | Apr 6 | 0400 | 571.5–581.1 | 9.7 | 5.88 | 61.3 | | | |
| 149-897B- | | | | | | | 57R | Apr 6 | 0645 | 581.1–590.7 | 9.6 | 9.15 | 95.3 | | | |
| 1R | Apr 1 | 1140 | 52.0–62.0 | 10.0 | 0.00 | 0.0 | 58R | Apr 6 | 0915 | 590.7–600.5 | 9.8 | 7.32 | 74.7 | | | |
| Coring totals: | | | | 10.0 | 0.00 | 0.0 | 59R | Apr 6 | 1130 | 600.5–610.1 | 9.6 | 5.64 | 58.7 | | | |
| | | | | ***** Drilled 0–49.9 mbsf ***** | | | 60R | Apr 6 | 1330 | 610.1–619.7 | 9.6 | 4.69 | 48.8 | | | |
| 149-897C- | | | | | | | 61R | Apr 6 | 1545 | 619.7–629.4 | 9.7 | 4.04 | 41.6 | | | |
| 1R | Apr 2 | 1800 | 49.9–59.9 | 10.0 | 3.99 | 39.9 | 62R | Apr 6 | 1755 | 629.4–639.1 | 9.7 | 5.26 | 54.2 | | | |
| 2R | Apr 2 | 1920 | 59.9–69.6 | 9.7 | 2.01 | 20.7 | 63R | Apr 6 | 1955 | 639.1–648.7 | 9.6 | 4.90 | 51.0 | | | |
| 3R | Apr 2 | 2030 | 69.6–79.2 | 9.6 | 1.31 | 13.6 | 64R | Apr 6 | 2250 | 648.7–658.4 | 9.7 | 2.39 | 24.6 | | | |
| 4R | Apr 2 | 2145 | 79.2–88.9 | 9.7 | 0.71 | 7.3 | 65R | Apr 7 | 0135 | 658.4–668.0 | 9.6 | 4.60 | 47.9 | | | |
| 5R | Apr 2 | 2350 | 88.9–98.5 | 9.6 | 2.53 | 26.3 | 66R | Apr 7 | 0430 | 668.0–677.3 | 9.3 | 2.93 | 31.5 | | | |
| 6R | Apr 2 | 0050 | 98.5–108.2 | 9.7 | 1.05 | 10.8 | 67R | Apr 7 | 0830 | 677.3–686.9 | 9.6 | 3.95 | 41.1 | | | |
| 7R | Apr 3 | 0150 | 108.2–117.9 | 9.7 | 1.18 | 12.1 | 68R | Apr 7 | 1200 | 686.9–696.6 | 9.7 | 3.04 | 31.3 | | | |
| 8R | Apr 3 | 0450 | 117.9–127.5 | 9.6 | 4.35 | 45.3 | 69R | Apr 7 | 1430 | 696.6–706.2 | 9.6 | 0.00 | 0.0 | | | |
| 9R | Apr 3 | 0600 | 127.5–137.2 | 9.7 | 1.80 | 18.5 | 70R | Apr 7 | 1700 | 706.2–710.2 | 4.0 | 1.26 | 31.5 | | | |
| 10R | Apr 3 | 0700 | 137.2–146.8 | 9.6 | 2.37 | 24.7 | 71R | Apr 7 | 2135 | 710.2–715.9 | 5.7 | 3.10 | 54.4 | | | |
| 11R | Apr 3 | 0830 | 146.8–156.6 | 9.8 | 4.37 | 44.6 | 72R | Apr 8 | 0205 | 715.9–725.6 | 9.7 | 3.46 | 35.7 | | | |
| 12R | Apr 3 | 1000 | 156.6–166.1 | 9.5 | 8.54 | 89.9 | 73R | Apr 8 | 0730 | 725.6–735.3 | 9.7 | 2.99 | 30.8 | | | |
| 13R | Apr 3 | 1300 | 166.1–175.8 | 9.7 | 0.00 | 0.0 | Coring totals: | | | | | | 695.0 | 352.81 | 50.8 | |
| 14R | Apr 3 | 1400 | 175.8–185.4 | 9.6 | 5.95 | 62.0 | Drilled: | | | | | | 49.9 | | | |
| 15R | Apr 3 | 1510 | 185.4–195.1 | 9.7 | 5.22 | 53.8 | Total: | | | | | | 744.9 | | | |
| 16R | Apr 3 | 1600 | 195.1–204.7 | 9.6 | 5.21 | 54.3 | | | | | | | ***** Drilled 0–1596.0 mbsf ***** | | | |
| 17R | Apr 3 | 1715 | 204.7–214.4 | 9.7 | 3.55 | 36.6 | 149-897D- | | | | | | | | | |
| 18R | Apr 3 | 2020 | 214.4–224.1 | 9.7 | 0.78 | 8.0 | 1R | Apr 11 | 1130 | 596.0–606.8 | 10.8 | 5.92 | 54.8 | | | |
| 19R | Apr 3 | 2115 | 224.1–233.8 | 9.7 | 5.67 | 58.4 | 2R | Apr 11 | 1445 | 606.8–616.5 | 9.7 | 6.28 | 64.7 | | | |
| 20R | Apr 3 | 2310 | 233.8–243.4 | 9.6 | 3.02 | 31.4 | 3R | Apr 11 | 1735 | 616.5–626.2 | 9.7 | 6.45 | 66.5 | | | |
| 21R | Apr 4 | 0010 | 243.4–253.0 | 9.6 | 1.61 | 16.8 | 4R | Apr 11 | 2005 | 626.2–635.9 | 9.7 | 2.89 | 29.8 | | | |
| 22R | Apr 4 | 0120 | 253.0–262.7 | 9.7 | 6.70 | 69.1 | 5R | Apr 11 | 2245 | 635.9–645.5 | 9.6 | 2.78 | 29.0 | | | |
| 23R | Apr 4 | 0225 | 262.7–272.3 | 9.6 | 4.14 | 43.1 | 6R | Apr 12 | 0055 | 645.5–655.2 | 9.7 | 3.28 | 33.8 | | | |
| 24R | Apr 4 | 0335 | 272.3–282.0 | 9.7 | 2.11 | 21.7 | 7R | Apr 12 | 0330 | 655.2–664.8 | 9.6 | 3.56 | 37.1 | | | |
| 25R | Apr 4 | 0445 | 282.0–291.5 | 9.5 | 2.22 | 23.3 | 8R | Apr 12 | 0830 | 664.8–674.5 | 9.7 | 3.31 | 34.1 | | | |
| 27R | Apr 4 | 0745 | 301.2–310.9 | 9.7 | 0.52 | 5.4 | 9R | Apr 12 | 1100 | 674.5–684.3 | 9.8 | 0.77 | 7.9 | | | |
| 28R | Apr 4 | 0900 | 310.9–320.5 | 9.6 | 6.91 | 72.0 | 10R | Apr 12 | 1400 | 684.3–693.8 | 9.5 | 5.01 | 52.7 | | | |
| 29R | Apr 4 | 1040 | 320.5–330.2 | 9.7 | 8.63 | 88.9 | 11R | Apr 12 | 1740 | 693.8–703.5 | 9.7 | 4.52 | 46.6 | | | |
| 30R | Apr 4 | 1200 | 330.2–339.9 | 9.7 | 9.75 | 100.0 | 12R | Apr 12 | 2110 | 703.5–713.0 | 9.5 | 5.58 | 58.7 | | | |
| 31R | Apr 4 | 1315 | 339.9–349.5 | 9.6 | 8.79 | 91.5 | 13R | Apr 13 | 0220 | 713.0–722.7 | 9.7 | 7.13 | 73.5 | | | |
| 32R | Apr 4 | 1720 | 349.5–359.1 | 9.6 | 0.00 | 0.0 | 14R | Apr 13 | 0630 | 722.7–732.3 | 9.6 | 5.25 | 54.7 | | | |
| 33R | Apr 4 | 1830 | 359.1–368.8 | 9.7 | 9.82 | 101.0 | 15R | Apr 13 | 0930 | 732.3–742.0 | 9.7 | 1.70 | 17.5 | | | |
| 34R | Apr 4 | 2000 | 368.8–378.4 | 9.6 | 10.84 | 112.9 | 16R | Apr 13 | 1315 | 742.0–751.6 | 9.6 | 7.68 | 80.0 | | | |
| 35R | Apr 4 | 2120 | 378.4–388.1 | 9.7 | 9.15 | 94.3 | 17R | Apr 13 | 1700 | 751.6–761.2 | 9.6 | 6.73 | 70.1 | | | |
| 36R | Apr 4 | 2245 | 388.1–397.8 | 9.7 | 9.55 | 98.4 | 18R | Apr 13 | 2140 | 761.2–770.9 | 9.7 | 3.61 | 37.2 | | | |
| 37R | Apr 5 | 0000 | 397.8–407.4 | 9.6 | 7.67 | 79.9 | 19R | Apr 14 | 0245 | 770.9–780.6 | 9.7 | 5.95 | 61.3 | | | |
| 38R | Apr 5 | 0130 | 407.4–417.1 | 9.7 | 9.28 | 95.7 | 20R | Apr 14 | 0800 | 780.6–790.2 | 9.6 | 3.57 | 37.2 | | | |
| 39R | Apr 5 | 0250 | 417.1–426.7 | 9.6 | 6.97 | 72.6 | 21R | Apr 14 | 1245 | 790.2–799.8 | 9.6 | 4.33 | 45.1 | | | |
| 40R | Apr 5 | 0415 | 426.7–436.4 | 9.7 | 9.18 | 94.6 | 22R | Apr 14 | 1835 | 799.8–809.0 | 9.2 | 2.21 | 24.0 | | | |
| 41R | Apr 5 | 0545 | 436.4–446.0 | 9.6 | 4.68 | 48.7 | 23R | Apr 15 | 0050 | 809.0–818.6 | 9.6 | 7.63 | 79.5 | | | |
| 42R | Apr 5 | 0730 | 446.0–455.6 | 9.6 | 7.73 | 80.5 | 24R | Apr 15 | 0730 | 818.6–828.2 | 9.6 | 4.73 | 49.3 | | | |
| 43R | Apr 5 | 0900 | 455.6–465.3 | 9.7 | 7.13 | 73.5 | 25R | Apr 15 | 1200 | 828.2–837.2 | 9.0 | 7.07 | 78.5 | | | |
| 44R | Apr 5 | 1015 | 465.3–475.0 | 9.7 | 5.22 | 53.8 | Coring totals: | | | | | | 241.2 | 117.94 | 48.90 | |
| 45R | Apr 5 | 1130 | 475.0–484.6 | 9.6 | 7.15 | 74.5 | Drilled: | | | | | | 596.0 | | | |
| 46R | Apr 5 | 1245 | 484.6–494.2 | 9.6 | 5.64 | 58.7 | Total: | | | | | | 837.2 | | | |
| 47R | Apr 5 | 1410 | 494.2–503.9 | 9.7 | 8.29 | 85.4 | | | | | | | | | | |

countered a bridge at 228 mbsf and became stuck. The pipe also became stuck, but was freed by circulating seawater at high pressure. The open BHA was carefully washed down over the logging tool from 5447 to 5557 mbsf to recover it. The logging tool became unstuck when we had washed to within 3 m of the bottom of the tool. After recovering the logging tool, the drill string became stuck. Again, the drill string was freed by using the pumps to liquify the formation. Operations at Hole 897D and Site 897 ended at 1515 hr, 17 April, when the BHA was on deck. After a short seismic survey we then steamed to Lisbon, Portugal, to end Leg 149B.

SITE GEOPHYSICS

Geophysical Data near Site 897

Three, high-quality, migrated, multichannel seismic reflection profiles pass near Site 897 (Fig. 4). These are Lusigal Lines 4 (Fig. 5) and

15 (Fig. 6) and Sonne Line 75-16 (Fig. 3), on which Site 897 is located. The profiles show that Site 897 is located over a roughly north- to south-trending basement ridge that rises to within 560 ms two-way traveltimes (510 m) of the seafloor. This ridge is asymmetrical and has a steeper slope on its eastern side. Sedimentary horizons onlap the high on both sides, with most reflectors onlapping higher on the eastern side of the ridge. The troughs adjacent to the ridge contain about 1500 (east) and 2000 (west) m of sediments. Numerous normal faults can be found in the overlying sediments to the east of the top of the ridge. No obvious faults are observed in the sediments to the west of the ridge.

The relationship of Site 897 to the top of the ridge is best seen in Sonne Line 75-16 (Fig. 3). Two local basement highs, to the west of the shallowest point on the ridge, may be offset by west-dipping normal faults. The shape of the highest point on the ridge suggests that it may have been bevelled by erosion, followed by rotation down to the east. We drilled to the west of the main basement high, through an

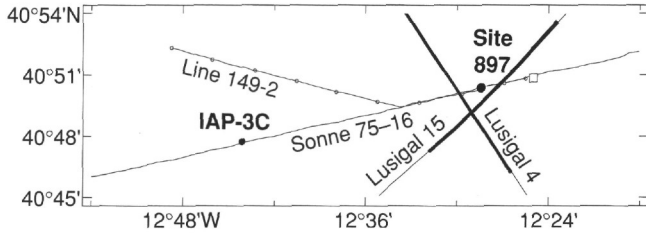


Figure 4. Multichannel seismic reflection and site-approach-survey (Line 149-2) track chart. Bold lines indicate the parts of Lusigal Lines 4 and 15 shown in Figures 5 and 6. The location of the seafloor fault identified in echo-sounder data (Fig. 7) is indicated with an open square.

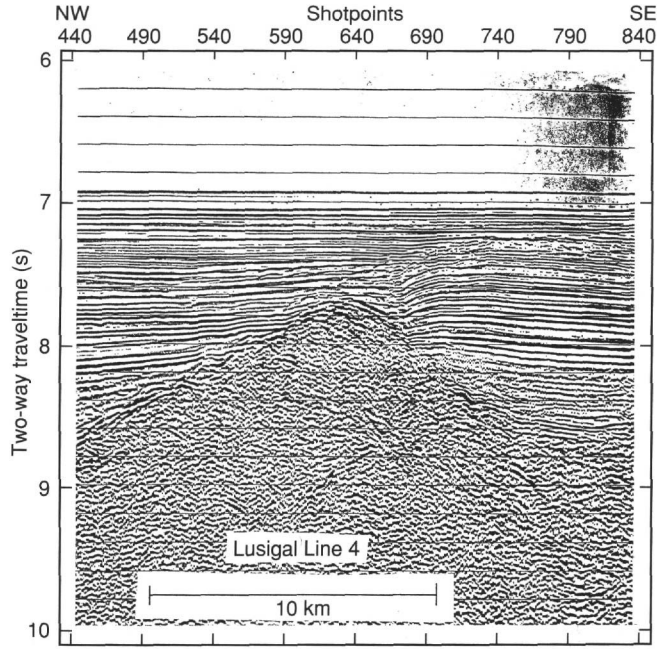


Figure 5. Migrated multichannel seismic profile Lusigal Line 4 near Site 897. The location of this profile is shown in Figure 4.

apparently unconformable and transparent packet of sediments about 60 ms (~55 m) thick, between two of the basement highs. We thought that this was our best chance of encountering at least some synrift sediments. We predicted that basement would be encountered at 680 mbsf at this site.

Magnetic data (see Frontispiece; PR. Miles, J. Verhoef, and R. MacNab, pers. comm., 1993) show that Site 897 is located in a magnetic trough. The magnetic anomalies to the west are lineated roughly north to south and have been interpreted as seafloor-spreading anomalies (Whitmarsh et al., 1990). The anomalies to the east are not lineated and were interpreted as the signature of rifted continental crust. Beslier et al. (1993) interpreted seismic reflection profiles to show that the basement under Site 897 is continental upper mantle that had been exposed during rifting. The basement rocks were predicted to be serpentinized peridotite.

While acquiring the *JOIDES Resolution* seismic profile 149-2, we noted one irregularity in the generally monotonous bathymetry of the Iberia Abyssal Plain. East of Site 897, along Sonne Line 75-16 and the site approach survey track, a 7-m step up to the east was observed in the seafloor (Fig. 7). The seafloor as far as 1 km west of this step is 2 to 3 m lower than typical depths in the area. In Sonne Line 75-16, this feature can be seen as an abrupt step that we had previously

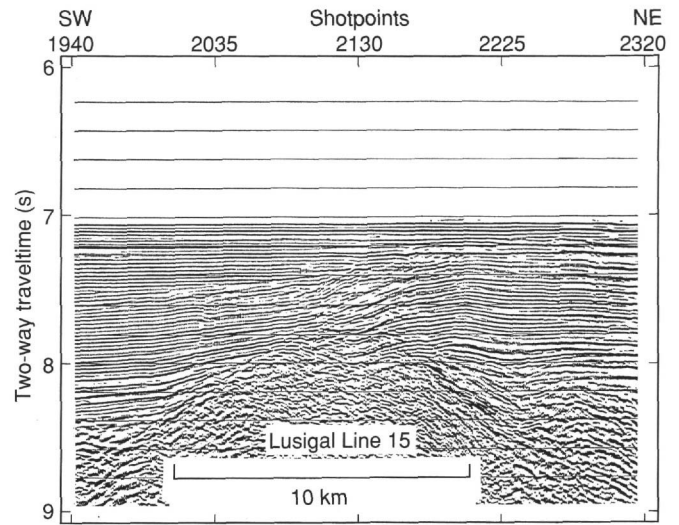


Figure 6. Migrated multichannel seismic profile Lusigal Line 15 near Site 897. The location of this profile is shown in Figure 4.

dismissed as a timing artifact introduced during acquisition or processing. We have now interpreted it as an indication of active faulting in the sedimentary section. The sense of motion of the fault is equivocal and might be a west-dipping normal fault or an east-dipping reverse fault.

LITHOSTRATIGRAPHY

Introduction

The composite sedimentary section recovered at Site 897 (Holes 897A, 897C, and 897D) includes nearly 700 m of Pleistocene to Early Cretaceous sediments and sedimentary rocks, overlying serpentinized peridotite of unknown age (Fig. 8). Pleistocene sediments were recovered at Hole 897A (0-55.2 mbsf), a Pleistocene to Early Cretaceous sedimentary sequence at Hole 897C (49.9-677.5 mbsf), and a middle Eocene to Early Cretaceous sedimentary sequence at Hole 897D (596.0-693.8 m). The lithostratigraphic succession at Site 897 is divided into four lithostratigraphic units on the basis of the degree of lithification and changes in lithology.

Subsequent drilling at Site 900 suggested the regional stratigraphic correlation shown in Figure 9. At Sites 897 through 900, the gross lithostratigraphy consists of a lower carbonate-rich contourite-turbidite-pelagite sequence and an upper turbidite-pelagite sequence. The two sequences contrast sharply in terms of evidence for reworking by contour currents (which is present only in the lower sequence) and in the abundance of siliceous allochems (virtually absent in the upper sequence).

Siliciclastic turbidites facies occur in Unit I and subunit IIA and carbonate-rich turbidites reworked by contour currents in Subunits IIB and IIC. The hemipelagic/pelagic tops of the turbidite sequences are composed of very fine-grained carbonate sediments in Unit I, but are carbonate-poor in Unit II. Subunit IIB is characterized by the presence of brown sediments, whereas Subunits IIA and IIC contain a mixture of gray, green, and brown sediments.

Unit III is exclusively siliciclastic in composition, except for carbonate pebbles and granules in the conglomerates in the lower part of Subunit IIIB. Subunit IIIA is composed entirely of brown terrigenous clay, whereas Subunit IIIB consists of an upward-fining sequence of pebble and gravel conglomerates, coarse sandstones, and sandstones and silty claystones.

Unit IV rests on basement at Holes 897C and 897D and comprises several intervals of serpentinized peridotite (see "Igneous and Meta-

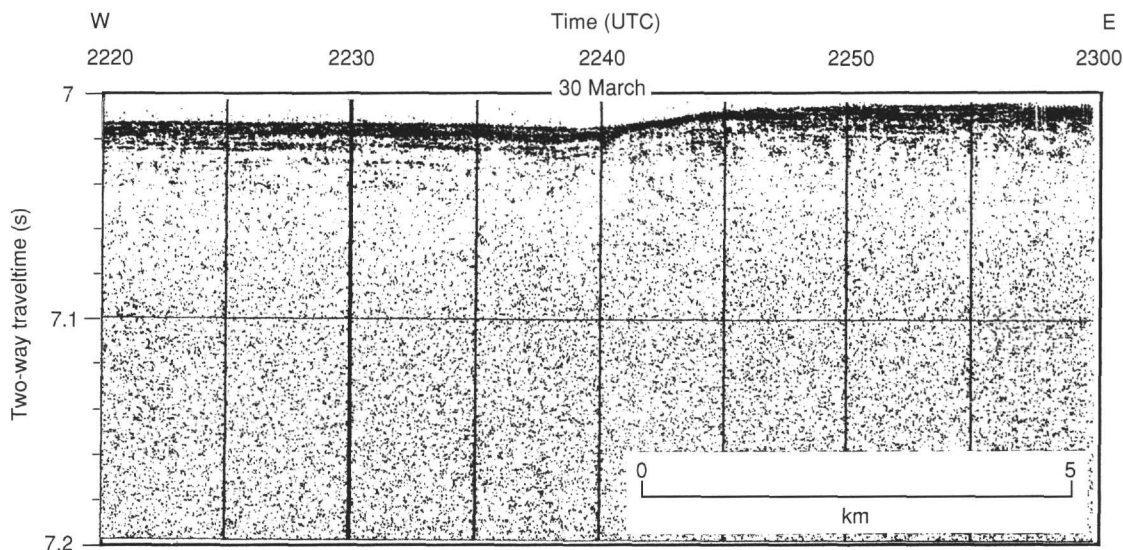


Figure 7. A 3.5-kHz bathymetric profile over an inferred, recently active, fault that offsets the seafloor to the east-northeast of Site 897. The location of the fault is shown in Figure 4.

morphic Petrology and Geochemistry" section, this chapter) between intervals of siliciclastic and carbonate lithologies.

The ages, average lithologic compositions, colors, facies, and depositional environments, boundary depths, and cored intervals of the units are summarized in Table 2. In Table 3, detailed information is given about color variations among lithologies in Units I and II. Colors in Unit III are highly variable and are described in the text; colors in Unit IV are documented in Table 4.

Figure 10 is a plot of age vs. depth data from Table 5 for the sedimentary sequence penetrated at Site 897. Generalized sediment accumulation rates obtained from Figure 10 show variations that exceed an order of magnitude across the units identified at this site: Unit I, 55 m/Ma; Unit II, 8 m/Ma; combined Units III and IV, 0.8 m/Ma.

Unit I

Cores 149-897A-1R through -6R; Cores 149-897C-1R through -26R,
50 cm
Depth: 0-55.2 mbsf (Hole 897A) and 49.9-292.0 mbsf (Hole 897C)
Age: Pleistocene to early Pliocene

General Description

Unit I extends from the seafloor to 292.0 mbsf, where a distinct change in sediment stiffness is seen. All cores in Unit I were split using a wire. Core recovery in the upper part was 10%-25%, but this improved below 150 mbsf to 25%-50%. Increased recovery with depth was accompanied by decreased drilling disturbance in the cores. Recognition of vertical changes in grain sizes in the uppermost cores (149-897A-1R through -5R, and 149-897C-1R) were hampered by extreme drilling disturbance and poor recovery.

Unit I consists of turbidite sequences and associated hemipelagic/pelagic sediments. Individual turbidite-to-pelagite cycles range in thickness from 5 to 60 cm and display a sequence of characteristic textural changes (Fig. 11). A basal, normally graded sand-to-silt interval (1-10 cm thick) usually overlies a sharp erosional contact with underlying fine-grained sediments and grades upwards into a clay-rich and nannofossil-enriched interval, which, locally, then grades into nannofossil ooze. In some individual sequences, the sand-to-silt interval is missing, either because of nondeposition or loss during drilling. Within individual turbidite/pelagite cycles, some lithologic boundaries are highly gradational as a result of depositional processes, bioturbation, and drilling disturbance.

Lighter colors generally are correlated with higher carbonate content. Nannofossil ooze, nannofossil clay, and calcareous clay are mostly very light and medium grays to greenish grays. A few samples of these lithologies range into darker colors, such as greenish black. Nannofossil ooze contains up to 78% carbonate (see "Organic Geochemistry" section, this chapter). Nannofossil clay grades into calcareous clay, depending on the preservation state of the nannofossils and the presence of other carbonate grains, such as foraminifers and carbonate rock fragments. Sedimentary structures in the Unit I nannofossil-rich sediments are limited to minor lamination and mottling from bioturbation.

Darker colors (olive grays, brownish grays, and so forth) are observed in calcareous and nannofossil silty clay to clayey silt and in silty clay to clayey silt. This may reflect higher contents of organic matter or absence of carbonate (e.g., Core 149-897C-23R). Lamination in some silty clay intervals (e.g., in Core 149-897C-8R) may be drilling-induced.

Beds and laminae of silt to fine sand are found throughout Unit I; medium sand is limited to Cores 149-897A-1R and -3R. Silt-to-sand intervals have colors similar to the silty clay to clayey silts. As with the finer-grained lithologies, the darker colors of the silt and sand beds may be related to higher contents of organic matter. Smear-slide analyses show that silt-sized organic matter locally reaches values of 30% (e.g., Core 149-897C-23R), in contrast to the generally low organic content of this unit as a whole (see "Organic Geochemistry" section, this chapter). Pyritized organic material is present (e.g., Core 149-897C-23R) and pyrite-filled burrows are found in Cores 149-897C-1R, -5R, -6R, and -16R.

Petrography

Silt and sand in Unit I are arkosic, being dominated by quartz and feldspar. Applying the classification of Folk (1980), the sands are subarkoses, arkoses, and lithic arkoses. Sand and silt compositions in Unit I, as described below, indicate derivation from a source area that exposed sedimentary, metamorphic, and, possibly, granitic rocks.

Quartz grains are mostly monocrystalline, and some contain inclusions of rutile, tourmaline, and perhaps sillimanite. Polycrystalline quartz is a minor component, characterized by equant subcrystals with mostly straight boundaries. The feldspar assemblage includes both twinned and untwinned plagioclase and K-feldspar. Much of the plagioclase is highly vacuolized, with minor sericite replacement. Much of the K-feldspar is microcline, which shows little alteration.

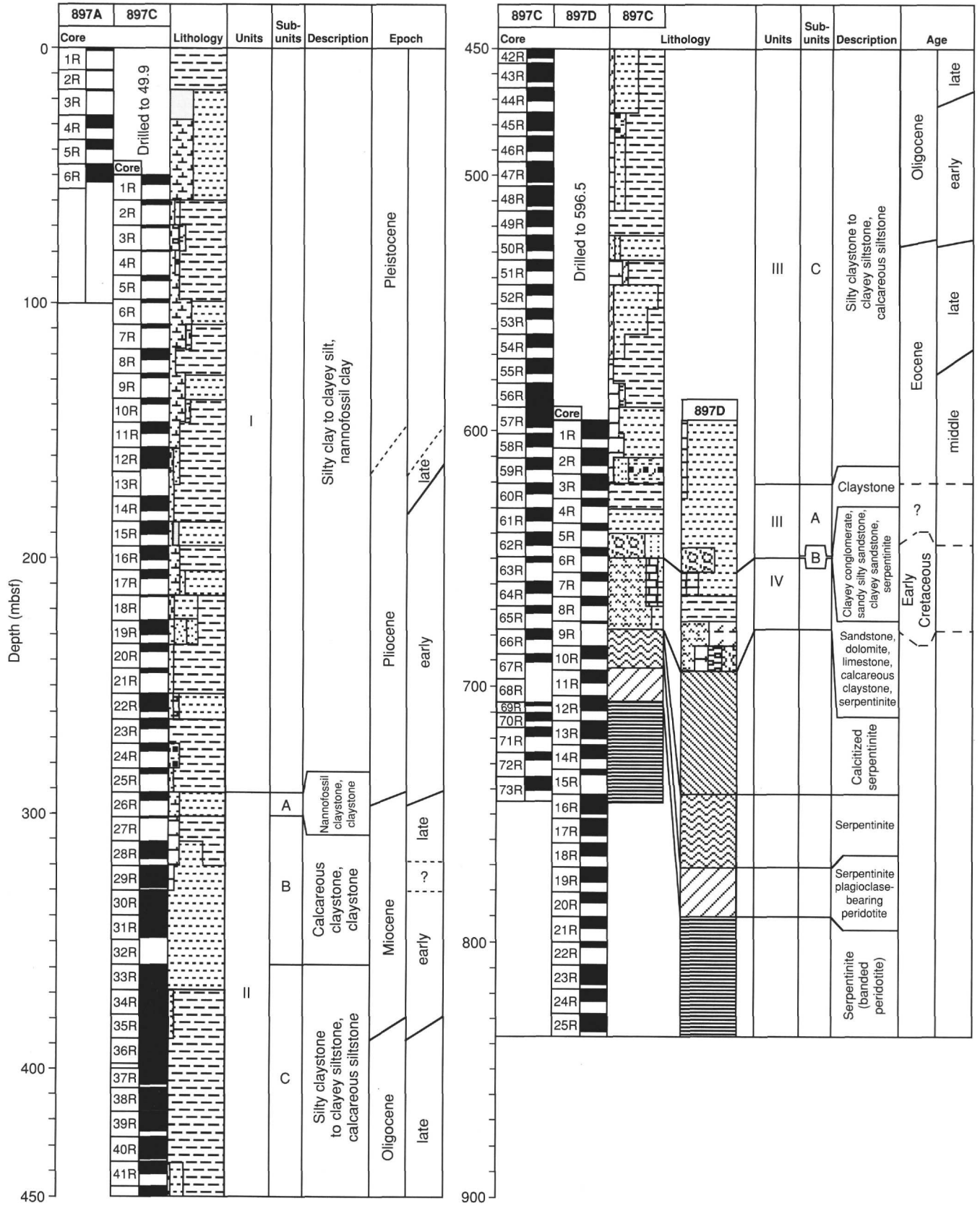


Figure 8. Master column for Site 897.

Table 2. Summary of ages, characteristics, facies, and depositional environments and occurrences of lithostratigraphic units and subunits at Site 897.

| Unit | Age | Thickness (m) | Lithology | Percentage (%) ^a | Color | Facies and <i>environment</i> [total meters described] | Intervals (mbsf) | | Occurrence | |
|------|--------------------------------|------------------------------|----------------------------------------------------------------------------------------------------------------------|-----------------------------|----------------------|--------------------------------------------------------------------------------------|-----------------------------|-----------------------------|-------------------------------|---------------------------------|
| | | | | | | | 897A | 897C | 897A | 897C |
| I | Pleistocene to early Pliocene | (55.2A) ^b 292C | Nannofossil ooze Nannofossil clay Silty clay to clayey silt Silt and fine sand | 3 27 60 10 | Gray/green | Terrigenous turbidites and hemipelagites/pelagites <i>Abyssal plain</i> [97.9] | Top = 0.0 Base = 55.2 | Top = 49.9 Base = 292.0 | 1R-1 at 0 cm 6R-CC | 1R-1 at 0 cm 26R-1 at 50 cm |
| IIA | early Pliocene to late Miocene | 9.2C | Nannofossil claystone Claystone Nanno. silty claystone Siltstones and sandstone | 60 20 15 5 | Gray/green/ brown | Terrigenous turbidites and hemipelagites/pelagites <i>Abyssal plain</i> [2.6] | | Top = 292.0 Base = 301.2 | | 26R-1 at 50 cm 27R-1 at 0 cm |
| IIB | late Miocene to early Miocene | 58.6C | Nannofossil chalk Calcareous claystone Claystone Silty clayst. to clayey siltst. Siltstone and sandstone | 1 45 37 14 1 | Brown | Calcareous turbidites/con-tourites <i>Abyssal plain, below CCD?</i> [35.3] | | Top = 301.2 Base = 359.8 | | 27R-1 at 0 cm 33R-1 at 65 cm |
| | | | | | | | 897D | | 897D | |
| IIc | early Miocene to middle Eocene | 259.9C (30.2D) | Nannofossil chalk Claystone Silty clayst. to clayey siltst. Siltstone and sandstone | <1 3 68 3 | Gray/ brown | Calcareous turbidites/con-tourites <i>Abyssal plain, below CCD?</i> [187.3] | Top = 596.0 Base = 622.9 | Top = 359.8 Base = 619.7 | 1R-1 at 0 cm 3R-5 at 38 cm | 33R-1 at 65 cm 60R-1 at 0 cm |
| IIIA | Uncertain | 19.7C 19.0D | Claystone | 100 | Brown | Pelagite/hemipelagite <i>Abyssal plain, below CCD</i> [15.3] | Top = 622.9 Base = 645.2 | Top = 619.7 Base = 639.4 | 3R-5 at 38 cm 6R-1 at 0 cm | 60R-1 at 0 cm 62R-1 at 30 cm |
| IIIB | Uncertain | 9.3C 10.0D | Clayey conglomerate Clayey sandstone Sandy silty claystone | 40 20 40 | Variiegated | High-density turbidite and debris flow [14.5] | Top = 645.2 Base = 655.2 | Top = 639.4 Base = 648.7 | 6R-1 at 0 cm 7R-1 at 0 cm | 62R-1 at 30 cm 63R-1 at 0 cm |
| IV | late Aptian to Hauterivian | 28.8C 38.6D | (63% basement lithologies 37% sedimentary) Sandstone, dolomite, limestone Calcareous claystone | | Variiegated | Mass flow | Top = 655.2 Base = 693.8 | Top = 648.7 Base = 677.5 | 7R-1 at 0 cm 11R-1 at 0 cm | 63R-1 at 0 cm 66R-1 at 18 cm |

^aHole 897C only.

^b() indicates hole penetrated only a portion of unit/subunit.

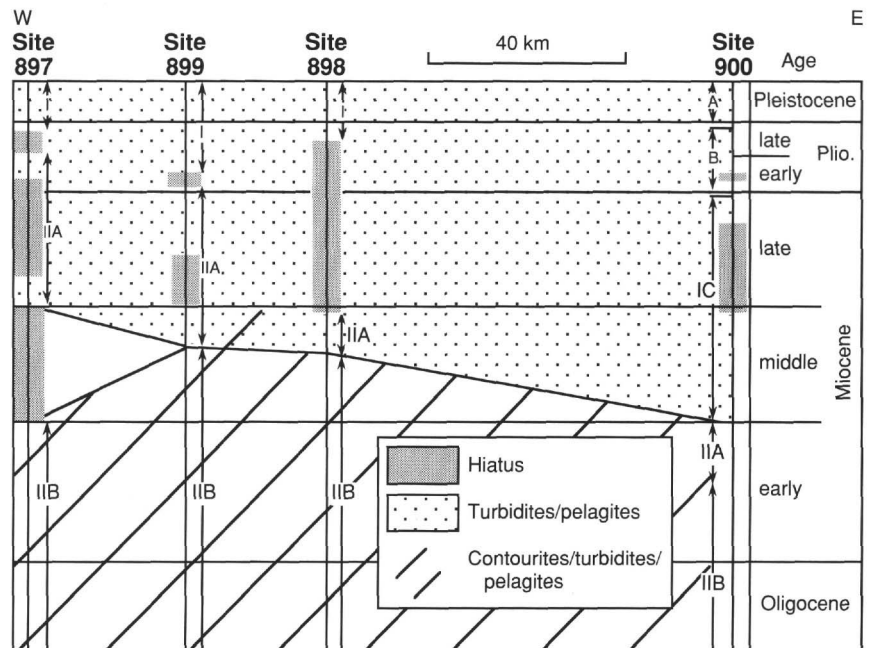


Figure 9. Regional stratigraphic correlation chart for Sites 897 to 900. The lower contourite-turbidite-pelagite sequence contains abundant siliceous allochems and reworked carbonate grains. The upper turbidite-pelagite sequence shows little evidence of reworking.

Carbonate rock fragments (CRFs) and metamorphic rock fragments (MRFs) occur. CRFs are mostly micritic, but a substantial portion of sparry monocrystals also are observed. A minor component of distinctly rhombic particles, mostly in the silt fraction, is probably dolomite. Other sedimentary rock fragments include minor claystone fragments and rare pieces of chert. MRFs are quartz-mica aggregates that derived from low-rank phyllites and schists.

Minor detrital components include abundant micas (muscovite, biotite, and possibly chlorite) that make up to 1% to 2% of the sand-silt fraction. Dense minerals present are mostly ultrastable species, such as zircon and yellow-brown to green tourmaline, with minor epidote, sphene (titanite), apatite, garnet, and green hornblende. Opaque detrital grains include black (magnetite and related minerals) and white (leucosene) varieties.

Most samples contain a proportion (generally less than 10%) of pencontemporaneous calcareous and siliceous marine skeletal debris, including foraminifers, sponge spicules, diatoms, radiolarians, dinoflagellates, and various nannofossils. Locally, siliceous allochems have been partially replaced by pyrite. Sand-sized and coarse silt-sized glauconite is a minor and ubiquitous component. Red-brown organic detritus can be noted occasionally in the coarse silt fraction. All terrigenous clastic materials of Unit I are unconsolidated and contain no obvious post-depositional authigenic phases, except for generally minor framboidal pyrite and partial replacement of wood (e.g., smear slides from Core 149-897C-23R).

Most of the clay-rich lithologies in Unit I contain a significant proportion of clay-sized (<4 μm) carbonate that consists largely of nannofossil debris. The clay-rich lithologies are mostly unconsolidated and disperse readily in distilled water. Clay minerals examined in smear slides are mostly <1 μm in diameter and exhibit no evidence of the crystal elongation and preferred orientation observed in the clay minerals of deeper units (see below). Birefringence of these small particles is low, and clay minerals in these rocks cannot be readily distinguished from clay-sized carbonate, except on the basis of color imparted, presumably, from trace amounts of iron oxides and organic matter. Clay and claystone having the above-described petrographic characteristics are designated "Type 1." Carbonate contents in Type 1 claystones are low (<10%), but at least a small percentage of nannofossil debris is present.

Cursory XRD examination of clay minerals in Unit I suggests the presence of detrital illite, kaolinite, and an expandable clay.

Depositional Processes

During the Pliocene-Pleistocene, deposition on the Iberia Abyssal Plain was dominated by the repeated emplacement of thin- to medium-bedded, fine-grained turbidites. Much of the sediment was probably funneled through submarine canyons that cross the Portuguese continental margin. Unit I includes sediments laid down by both turbidity currents and pelagic to hemipelagic processes.

The structureless to laminated basal sand and silt layers in the turbidites correspond to the Tc-d division of the classic Bouma sequence (Bouma, 1962); however, the Ta-b interval is absent. Clay-rich intervals are bioturbated to laminated, contain significant amounts of reworked nannofossils (see "Biostratigraphy" section, this chapter), and correspond to the turbiditic mud division (Te 1-3) of Piper (1978); this division represents deposition from the low density tail of the turbidity current. The bioturbated nannofossil clay-to-ooze intervals are pelagic deposits. However, visually distinguishing the Te facies from the pelagic interval is difficult because the sediments are fine-grained and have been somewhat mixed by bioturbation and drilling disturbance.

The thicker (up to 50 cm) loosely consolidated and normally graded sand units in the uppermost part of Unit I may be a product of differential grain settling during coring. Low recovery in these sandy intervals precludes any definitive interpretation, but they may possibly have been deposited from one or several turbidity currents, or they may represent sand concentrated by winnowing and reworking.

Structureless, fine-grained units up to 1.5 m thick also occur at several levels in the unit. Given the presence of turbidites, the overall relatively high sedimentation rates (Fig. 10) and the typically low sedimentation rates of carbonate in the deep ocean, it is unlikely that these are pelagic units that accumulated during a prolonged lull in terrigenous sedimentation. Therefore, these intervals may be either a single, thick, massive mud turbidite or a series of amalgamated mud turbidites.

Carbonate-rich layers of well-preserved benthic foraminifers and calcareous nannofossils at the tops of the turbidites suggest deposition above the CCD, although relatively rapid deposition and burial might have aided carbonate preservation.

In Unit I, a maximum 32 turbidites occur in a single core (149-897C-14R). Turbidite frequency in Unit I ranges from about two to seven per meter of core, which suggests that relatively little time elapsed between successive turbidity flows, consistent with the relatively high sediment accumulation rate observed for Unit I. Trace fos-

Table 3. Color variation of lithologies at Site 897.

| Color | Lithologies ^a | | | | | | |
|-----------------------------------|--------------------------|-----------------|------------------------|-------|--------------------------------------------|------------------|------------------|
| | Sand silty sand | Silt sandy silt | Clayey silt silty clay | Clay | Calcareous clay calcareous silty claystone | Nannofossil clay | Nannofossil ooze |
| Dark gray (N4) | | | | | | | |
| Medium gray (N5) | | | | | | | |
| Medium light gray (N6) | ▲ | ▲ | | | ○ | ○ ○ ○ ▲ | ○ + ■ ▲ |
| Light gray (N7) | | | | | | | ○ + ■ |
| Very light gray (N8) | | | | | | | ○ |
| White (N9) | | | | | | | |
| Medium bluish gray (5B 5/1) | | | ▲ | ▲ | ▲ | | |
| Light bluish white (5B 7/1) | | | ▲ | ▲ | | | |
| Bluish white (5B 9/1) | | | + ■ | + ■ ▲ | | + ■ ▲ | + ■ |
| Dark yellowish brown (10YR 4/2) | | | ○ + ■ ▲ | ▲ | ▲ | | |
| Mod. yellowish brown (10YR 5/4) | | | ▲ | ▲ | | | |
| Yellowish brown (10YR 5/2) | | | ▲ | ▲ | ○ | | |
| Pale yellowish brown (10YR 6/2) | | | + ■ ▲ | + ■ ▲ | ▲ | | |
| Moderate brown (5YR 4/4) | | | ▲ | ▲ | | | |
| Brownish gray (5 YR 4/1) | | | ○ | + ■ | ○ | | ▲ |
| Light brownish gray (5 YR 6/1) | | | | + ■ | | | |
| Olive black (5Y 2/1) | ○ + ▲ | ○ + ▲ | ○ | ■ | ○ | ○ | |
| Olive gray (5Y 4/1) | ○ | ○ | ○ | ■ | ○ | | |
| Moderate olive brown (5Y 4/4) | | | ▲ | ▲ | ▲ | | |
| Light olive gray (5Y 5/1) | | | + ■ ▲ | + ■ ▲ | ○ + ■ ▲ | + ■ ▲ | |
| Light olive gray (5Y 6/1) | | | ○ + ■ ▲ | + ■ ▲ | ○ + ■ ▲ | ○ | |
| Yellowish gray (5Y 8/1) | | | | | | | |
| Greenish black (5GY 2/1) | | ▲ | ○ | | ○ | | |
| Dark greenish gray (5GY 4/1) | ○ | ○ | ○ | | ○ | | |
| Greenish gray (5GY 5/1) | ○ | ○ | ○ | | ▲ | ○ | ▲ |
| Greenish gray (5GY 6/1) | + ■ ▲ | + ■ | + ■ ▲ | + ■ ▲ | ▲ | ○ | |
| Light greenish gray (5GY 8/1) | | | | | ▲ | | |
| Greenish black (5G 2/1) | ○ | ○ | ○ | | ▲ | ○ | |
| Dark greenish gray (5G 4/1) | ▲ | | | | ▲ | | |
| Greenish gray (5G 5/1) | | | | | ▲ | | |
| Greenish gray (5G 6/1) | | | + ■ ▲ | + ■ ▲ | + ■ ▲ | | |
| Light greenish gray (5G 7 or 8/1) | + ■ | + ■ | + ■ ▲ | + ■ | | + ■ | |

Note: Subunit I = ○; Subunit IIA = +; Subunit IIB = ■; Subunit IIC = ▲.

^aIncludes lithified equivalents (i.e., -stones, chalk).

Table 4. Summary of the lithologies present in Unit IV at Site 897.

| Lithologic type | Color(s) | Occurrence | | Comments |
|----------------------------------|--------------------------|--------------------------------------------------------------|-----------------------------------------------------------------------------|------------------------------------------------------------------------------------------------------------|
| | | 897C | 897D | |
| Claystones | | | | |
| Nannofossil claystone | 10 YR 7/4, 6/4 | 62R-4, 55–75 cm | 6R-3, 55–58 cm 6R-CC, 0–15 cm | Rounded pieces (~10 cm) may be large clasts. About 60% carbonate (almost a nanno. chalk). |
| Nannofossil claystone | 5Y 2/1 | | 7R-2, 0–101 cm | |
| Claystone | 5Y 6/1 | | 6R-3, 30–63 cm | |
| Claystone | N3 to N5 and 5Y 4/1 | 64R-1, 35–105 cm 64R-2, 50–65 cm | 7R-1, 01–50 cm | |
| Claystone with serpentine clasts | 5Y 4/1 to N3 | 65R-2, 87–130 cm | | |
| Sandy/silty claystone | N4,5; 10YR 4/2 or 5Y 6/4 | 63R-1, 80–95 cm | 7R-3, 0–23 cm 7R-CC, 0–61 cm 8R-2, 0–45 cm 10R-4, 111–150 cm | 63R: Type 1; up to 20% carbonate. 10R: Type 2 at 126–127 cm; Type 1 at 138–139 cm. |
| Siltstones and sandstones | | | | |
| Siltstone | 5Y 6/1 | | 7R-3, 0–25 cm 8R-1, 8–150 cm | Parallel lamination disrupted by slump folds and microfaults. |
| Fine sandstone | N3 | 63R-1, 80–95 cm | 7R-1, 98–105 cm | Subarkose with fragments of shale and limestone; no serpentinite clasts. Ankerite cement. |
| Carbonates | | | | |
| Nannofossil chalk | N3 to N6 or 5Y 6/1 | 63R-2, 0–37 cm | 10R-3, 41–150 cm | ~60% carbonate; serpentinite. |
| Nannofossil foraminiferal chalk | N3 to N4 or 10YR 5/4 | 10R-4, 0–115 cm | | |
| Limestone | N3 to N7 | 63R-CC, 10–20 cm 64R-1, 10–30, 34–35 cm 64R-2, 0–65 cm | 7R-1, 31–40, 47–55, 118–126 cm 8R-2, 46–61 cm 10R-1, 0–52 cm (pieces) | 1–2% serpentine clasts in thin section in samples from 897C. 64R-2: numerous calcispheres in thin section. |
| Limestone | 10YR 7/4 | 63R-1, 56–74 cm | | Clay and carbonate; trace of nannofossils. |
| Brecciated nannofossil limestone | Clasts: N3, clasts: N7 | 7R-1, 80–99 cm | | |
| Limestone | 5GY 6/1 | | 7R-2, 5 and 16 cm | Probable concretions composed of micrite. |
| Dolomite | N3 | | 9R-1, 0–75 cm (pieces) | |

Notes: Type 1 claystones are carbonate-poor and contain unoriented, fine-grained clays. Type 2 claystones are carbonate-poor and contain highly oriented, birefringent coarse clays.

Table 5. Biostratigraphic data for Hole 897.

| Code | Datum | Age and range (Ma) | Depth and range (mbsf) |
|------|----------------------------------------------------------------------------|--------------------|------------------------|
| 1 | B. <i>Emiliana huxleyi</i> and BA. morphogroup 2 <i>Gephyrocapsa</i> spp. | 0.18 ± 0.06 | 1.05 |
| 2 | B. <i>Emiliana huxleyi</i> /B. <i>Emiliana pujosae</i> | 0.31 ± 0.05 | 1.32 |
| 3 | B. <i>Helicosphaera inversa</i> /T. <i>Reticulofenestra</i> sp.A (>6.5 µm) | 0.86 ± 0.05 | 17.00 |
| 4 | T. <i>Helicosphaera sellii</i> | 1.12 | 27.75 – 35.39 |
| 5 | B. <i>Gephyrocapsa</i> spp. (>5.5 µm) | 1.23 | 28.20 – 39.00 |
| 6 | T. <i>Calcidiscus macintyreii</i> (cir., ≥ 10 µm) | 1.47 | 98.50 – 117.90 |
| 7 | B. <i>Gephyrocapsa oceanica</i> (≥ 4.0 µm) | 1.58 | 151.17 – 165.14 |
| 8 | T. <i>Discoaster brouweri</i> | 1.88 | 165.14 – 181.75 |
| 9 | T. <i>Reticulofenestra pseudoumbilica</i> | 3.56 | 165.14 – 181.75 |
| 10 | B. <i>Discoaster tamalis</i> | 3.80 | 294.64 – 301.72 |
| 11 | T. <i>Discoaster bollii</i> | 8.38 | 301.72 – 317.81 |
| 12 | T. <i>Helicosphaera ampliaptera</i> | 16.00 | 329.13 – 339.95 |
| 13 | T. <i>Sphenolithus ciperoensis</i> | 24.60 | 348.69 – 368.92 |
| 14 | T. <i>Helicosphaera recta</i> | 24.70 | 379.64 – 387.55 |
| 15 | T. <i>Shenolithus distentus</i> | 27.60 | 416.68 – 424.07 |
| 16 | T. <i>Reticulofenestra umbilica</i> | 33.70 | 512.01 – 520.07 |
| 17 | T. <i>Discoaster barbadiensis</i> | 35.60 | 520.07 – 527.96 |
| 18 | B. <i>Chiasmolithus oamaruensis</i> | 38.40 | 546.70 – 556.07 |
| 19 | T. <i>Blackites gladius</i> | 44.40 | 598.02 – 606.14 |
| 20 | B. <i>Nannotetrina alata</i> | 48.10 | 613.00 – 622.95 |

Note: T = top; B = bottom; BA = bottom acme; TA = top acme.

sils in the upper parts of the turbidites indicate that periods between successive flows were sufficiently long to enable burrowing organisms to populate the substrate and that oxygen levels in bottom waters were at least dysaerobic.

Unit II

Cores 149-897C-26R-1, 50 cm, through -60R-1, 0 cm
 Cores 149-897D-1R-1, 0 cm, through -3R-5, 38 cm
 Depth: 292.0-619.7 mbsf (Hole 897C) and 596.0-622.9 mbsf (Hole 897D)
 Age: late Miocene to middle Eocene

General Description

In addition to being defined by the first occurrence of carbonate-rich turbidites, the top of Unit II also is marked by a distinct increase in sediment consolidation in Core 149-897C-26R. Soon after passing this boundary (Core 149-897C-29R), a saw was routinely used to split the cores; thus, these are described as "-stones," as opposed to "sediments." In addition, a transitional change from gray/green to brown colors occurs at the Unit I/Unit II boundary.

Core recovery was relatively low in the top 20 m of this unit, but below this level, it increased dramatically, averaging more than 50%. Cores are slightly to moderately fractured (biscuited) throughout.

Subunit IIA

This subunit occurs within a single core (149-897C-26R) in which the first partially lithified sediments occur which are transitional in character between those of Unit I and the remainder of Unit II.

Bedding contacts between the major lithologies in Subunit IIA (nanofossil claystone, nanofossil silty claystone, and claystone) are gradational as a result of the combined effects of drilling disturbance ("biscuits"), splitting the core with a wire, and moderate bioturbation. Three thin (up to 4 cm), graded-to-laminated beds of silty sand are present in the core. Color of the fine-grained lithologies changes down the core from green to brown. The major lithologies are similar to those described below in Subunit IIB; however, the silty sands are more similar in color (dark olive black [5Y 2/1]) to those in Unit I.

Subunit IIB

The lower part of Unit II is divided into two subunits (IIB and IIC) on the basis of the proportion of claystone vs. coarser-grained lithologies, such as silty claystone, siltstone, and sandstone.

Subunit IIB consists predominantly of calcareous/nanofossil claystone and claystone, with minor silty claystone, nanofossil chalk, and clayey-to-silty/fine sand layers occurring as repetitive turbidite/

pelagic sequences. These show a basal calcareous sand-to-silt interval grading upward into nanofossil claystone that is sometimes laminated. In turn, the nanofossil claystone is overlain by silty claystone or claystone that likely represents pelagic sedimentation.

The major component of Subunit IIB is calcareous claystone that exhibits a wide range of colors, mostly browns and grays. The subunit is characterized by intensive color mottling caused by bioturbation. The ichnofauna includes *Zoophycos*, *Chondrites*, and *Planolites*. Apart from bioturbation, the calcareous claystones are structureless.

The minor lithologies include silty claystone and claystone, nanofossil claystone, nanofossil silty claystone, and nanofossil chalk. Lighter shades of gray correlate with higher carbonate contents. The minor lithologies are extensively bioturbated, and the nanofossil silty claystone and nanofossil chalk are locally laminated (Fig. 12). The distinct coloration of several thin, reddish purple laminae in Section 149-897C-30R-1 suggests manganese enrichment.

Layers of calcareous silt-to-fine sand occur in Cores 149-897C-30R and -31R (Fig. 12) and range from 10 to 20 cm thick. These coarse basal units typically are greenish gray and grade upward into nanofossil claystones of the same color.

Subunit IIC

The top of Subunit IIC occurs in Core 49-897C-33R-1 at 65 cm, at the first occurrence of a dominantly yellowish brown claystone succession. This color is in marked contrast to the greenish gray claystones of Subunit IIB. The base of the subunit is defined as the last occurrence of greenish gray claystones interbedded with some brown claystones at the top of 149-897C-60R and at -897D-3R-5, 38 cm. Repeated darkening-upward sequences also occur in Subunit IIC.

The subunit is dominated (about 90%) by claystones and silty claystones to clayey siltstone. These lithologies exhibit a variety of colors, mostly browns and grays.

Carbonate-rich lithologies also are important components of Subunit IIC. These are lighter colored than the fine-grained siliciclastic lithologies and are mostly lighter grays. Carbonate-rich lithologies include calcareous clay, claystone with nanofossils, nanofossil silty claystone, nanofossil claystone, nanofossil foraminiferal chalk, and nanofossil chalk.

The minor siliciclastic lithologies include siltstone and silty sand that contain mixtures of siliciclastic and calcareous grains. Light-colored nanofossil claystones and chalks also occur only sporadically and make up less than 1% of the section measured in Subunit IIC.

Two intervals contain brown claystones and silty claystones: Interval 149-897C-47R-3, 90 cm, to the base of Core 149-897C-52R (thickness, 48.9 m), and Interval 149-897C-55R-1, 0 cm, to the base of Core 149-897C-59R (thickness, 43.3 m).

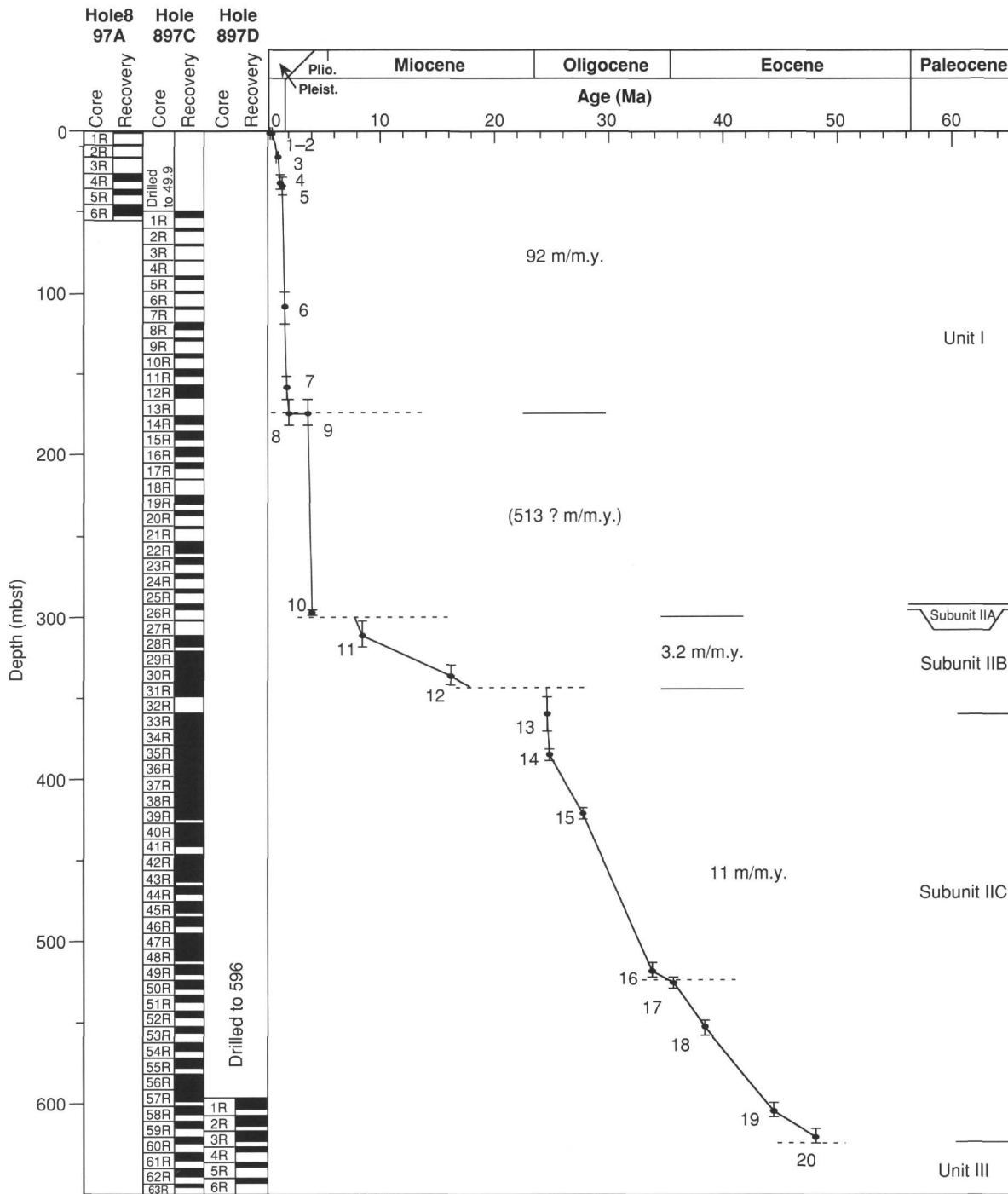


Figure 10. Depth vs. age curve for Site 897, combining nannofossil and foraminifer dates (see "Biostratigraphy" section, this chapter). Each data point is shown with depth and/or age error bars (numbers refer to datums in Table 5). The dashed horizontal lines are unconformities. The horizontal lines are major lithostratigraphic unit boundaries.

All the cores display a series of sharp-based, upward-darkening sequences between 5 and 50 cm thick. In the brownish intervals, these show the following sequence of lithologies, numbered from bottom (1) to top (4):

- | | |
|-------------------------------|---------------------------------|
| 4 Massive silty claystone | Dark yellowish brown (10YR 4/2) |
| 3 Nannofossil silty claystone | Pale yellowish brown (10YR 6/2) |

- | | |
|-------------------------------------|--------------------------------------------|
| 2 Nannofossil silty claystone | Greenish gray (5GY 6/1) |
| 1 Silty fine sandstone or siltstone | Greenish gray (5GY 5/1) or light gray (N7) |

Nannofossil silty claystone and massive silty claystone (Lithologies 1 and 2) are mixed by burrowing, and *Zoophycos*, *Chondrites*, and *Planolites* are commonly observed within the transition between them. This ichnofauna also occurs in silty fine sandstone and nannofossil silty claystone. The massive nature of Lithology 4 was probably

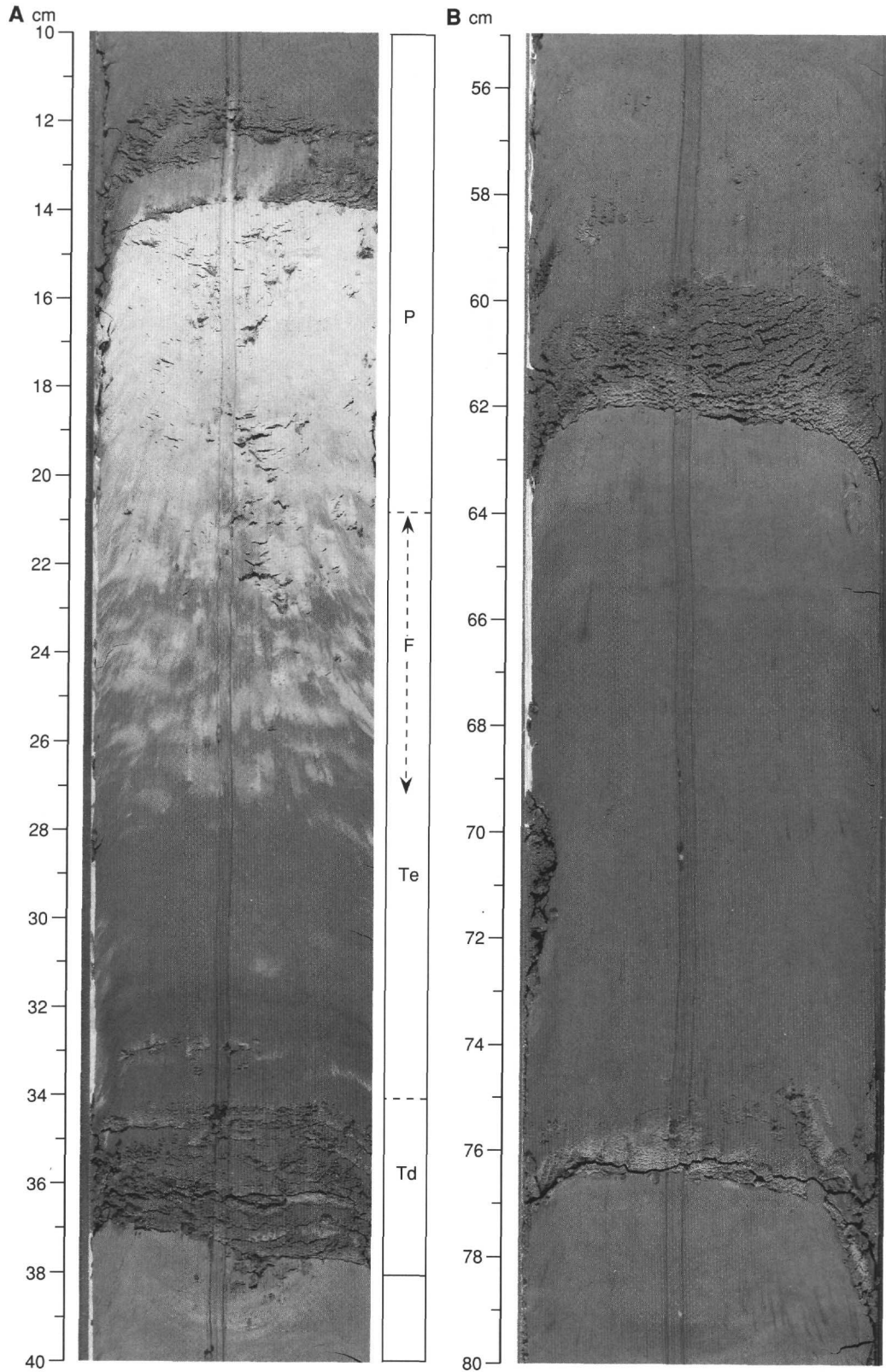


Figure 11. Turbidite sequences in Unit I. **A.** Complete turbidite sequence with a basal layer (34-38 cm) of fine sand (Td) grading upward into silty clay (Te), capped by intensively bioturbated light-colored pelagic nannofossil ooze (P) that is mixed with the underlying turbiditic clay by burrow mottling (F) (Interval 149-897C-14R-3, 10-40 cm). **B.** Two turbidite sequences (at 60-62 cm and 75-76 cm) that lack the upper hemipelagic interval (i.e., showing "top cut-out") as a result of erosion by later turbidity current(s) and/or nondeposition (Interval 149-897C-14R-3, 55-80 cm).

caused by intense bioturbation. Nannofossil silty claystone sometimes shows planar cross lamination, and *Zoophycos* may occur toward the top of it.

In the nonbrownish intervals, the typical lithological sequence (Fig. 13A) is as follows, numbered from bottom (1) to top (3):

| | |
|----------------------------------------------------|-------------------------------------------------------|
| 3 Claystone or silty claystone | Olive gray (5Y 4/10 or dark greenish gray (5GY 4/1) 2 |
| Silty claystone and/or nannofossil silty claystone | Greenish gray (5GY 5/1-6/1) |
| 1 Silty fine sandstone | Dark greenish gray (5GY4/1) |

Burrow mixing occurs commonly between silty claystone and/or nannofossil claystone and claystone or silty claystone. *Planolites*, *Chondrites*, and *Zoophycos* are common in these intervals. In some cases, *Planolites* and *Chondrites* mix Lithologies 1 and 2 into the underlying sequence.

Silty or sandy bases are not always present in either type of upward-darkening sequences (Fig. 13B); however, in some intervals, silty fine sandstone forms the bases of normally graded units, particularly in Cores 149-897C-30R, -40R, -42R, -43R, -50R, -52R, -53R, -54R, and -59R.

The basal interval of some of the sequences is composed of medium sand. It is possible that the sandier basal units are under-represented in the cores and have been lost between the drilling biscuits. A higher proportion of sandy intervals was recovered in Hole 897D at the level equivalent to Core 149-897C-59R, possibly the result of less drilling disturbance.

Sandy layers with possible cross-stratification and sharp tops attest to likely reworking by contour currents (Figs. 14A and 14B).

Petrography

Sand- and silt-sized detritus in Unit II includes components essentially similar to the assemblage observed in Unit I. Some of the better examples of MRFs are not generally observed in Unit II because of the generally finer grain size of the sand, but the general characteristics of the rock fragment assemblage are the same as those in Unit I.

Subunit IIA contains clay-rich lithologies that are similar in most respects to those in Unit I, except for an overall lower carbonate content. The smear slide at Sample 149-897C-27R-CC, 8 cm, in Subunit IIB marks the appearance of a distinctive clay-rich lithology that contains virtually no carbonate. This lithology is designated as "Type 2," in contrast to carbonate-rich claystone varieties called "Type 1" in Unit I.

Clay minerals in the Type 2 claystones and silty claystones are characterized by a larger range of crystal sizes that range up to fine silt. The more coarsely crystalline part of the clay assemblage has higher birefringence (first-order yellow to orange) than that observed in the finer-grained clays in the carbonate-rich claystones of Unit I. Many of the coarser clay minerals are also distinctly elongated, forming small fibers approximately 1 μm wide and up to 20 μm long. Silt-sized particles associated with this coarser clay assemblage are typically coated by 0.5 to 1 μm rims of yellow birefringent clay. Small (<10 μm), near-isotropic flakes of mica(?) coated in this manner produce a distinctive texture in many of the Type 2 claystone smear slides. The minor amount of carbonate that occurs in these claystones is mostly in the form of 10- to 30- μm -thick, rhomb-shaped crystals that may be detrital dolomite. In smear slides, pieces of claystone that have not disaggregated contain coarse yellow birefringent clay minerals having a high degree of preferred orientation.

Both claystone types are present in repeated interbeds and in various shades of browns and green-grays, but in Subunit IIC, Type 1 claystones are lighter in color (mostly greens to grays), whereas Type 2 claystones are red brown (see previous discussion of the two types of upward-darkening sequences).

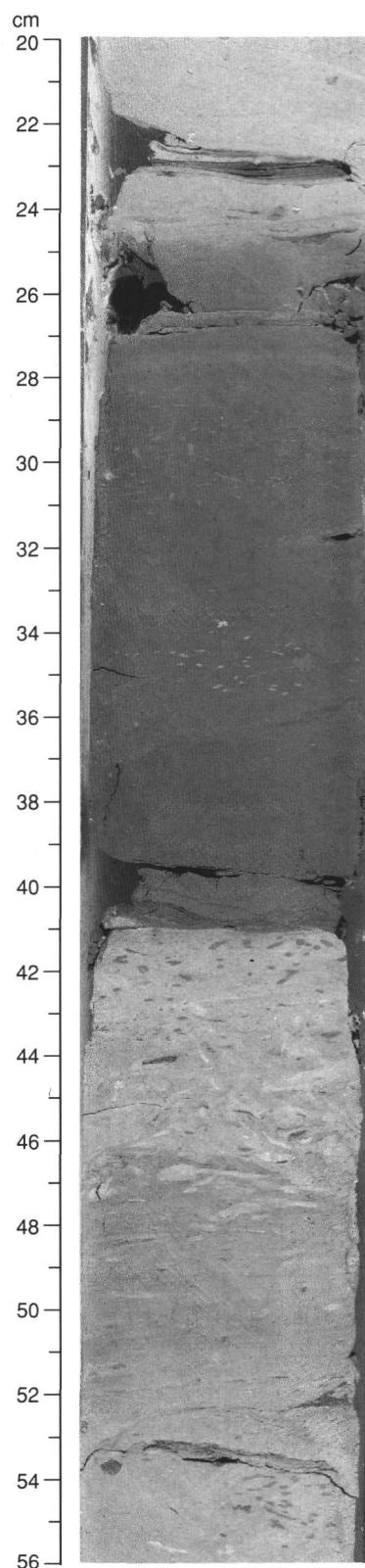


Figure 12. Light- and dark-colored turbidite sequences in Subunit IIB. In the upper sequence, the basal cross-laminated fine sand layer is overlain by a dark bioturbated claystone (27-40 cm). The lower light-colored sequence (41-54 cm) shows more intense bioturbation and mixing with the darker sediment of the overlying turbidite (Interval 149-897C-31R-3, 20-56 cm).

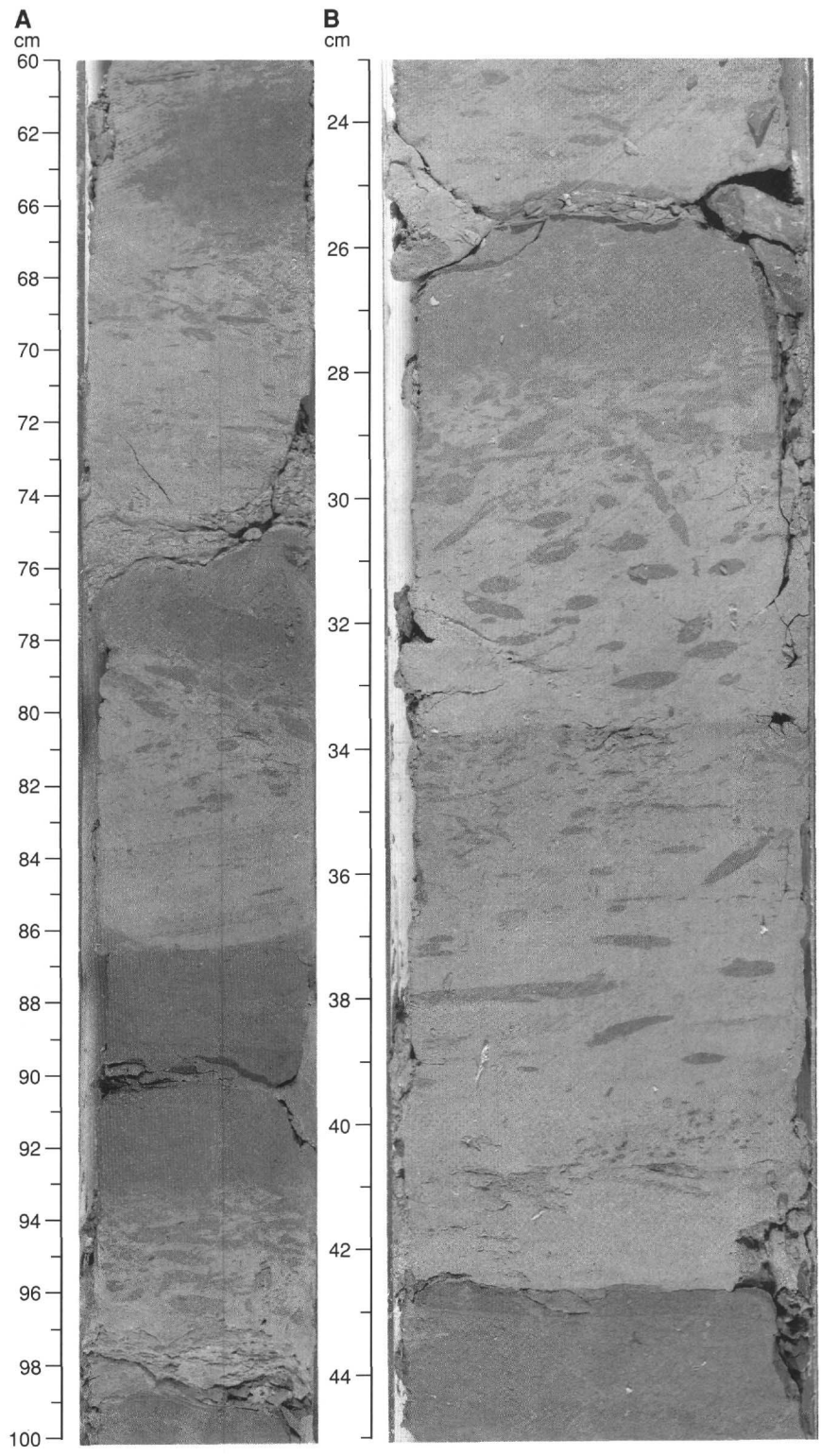


Figure 13. Upward-darkening sequences in Subunit IIC. **A.** Three upward-darkening and -fining sequences separated by fractures between core biscuits. The lower (90-99 cm) and upper (60-74 cm) sequences have thin, calcareous, silty fine sand intervals at the bases. The middle (74-86 cm) and upper sequences exhibit parallel lamination in nannofossil silty claystone. All three sequences show bioturbated intervals having *Planolites* and *Chondrites* overlain by massive, presumably intensely bioturbated, darker-colored hemipelagic/pelagic claystones (Interval 149-897C-40R-6, 60-100 cm). **B.** Core showing partial cut-out at the top and bottom of turbiditic sequences. The lower sequence (34-42.5 cm) shows a thin, sharp-based, silty interval, but no hemipelagic/pelagic sediment (i.e., with top cut out) as this was eroded before the overlying sequence was deposited. The upper sequence (25.5-34 cm) lacks a basal sand ("base cut-out"; Interval 149-897C-39R-5, 23-45 cm).

Cursory XRD examination of clay minerals in Unit II suggests that both types of claystone contain similar clay mineral assemblages, including illite, kaolinite, and a highly expandable clay.

Depositional Processes

The depositional processes for Subunit IIA are similar to those outlined for Unit I, but few of the turbidity flows deposited sand or silt.

Calcareous turbidite facies, according to the classical Bouma sequences (Bouma, 1962), dominate Subunit IIB. These sequences exhibit facies Td through Te, plus a hemipelagic/pelagic interval. The carbonate content of each turbidite in Subunit IIB decreases upward. The relatively high carbonate content of the basal intervals of each individual turbidite sequence reflects the presence of CRFs and locally abundant foraminifers within the silt/sand fraction. The upward

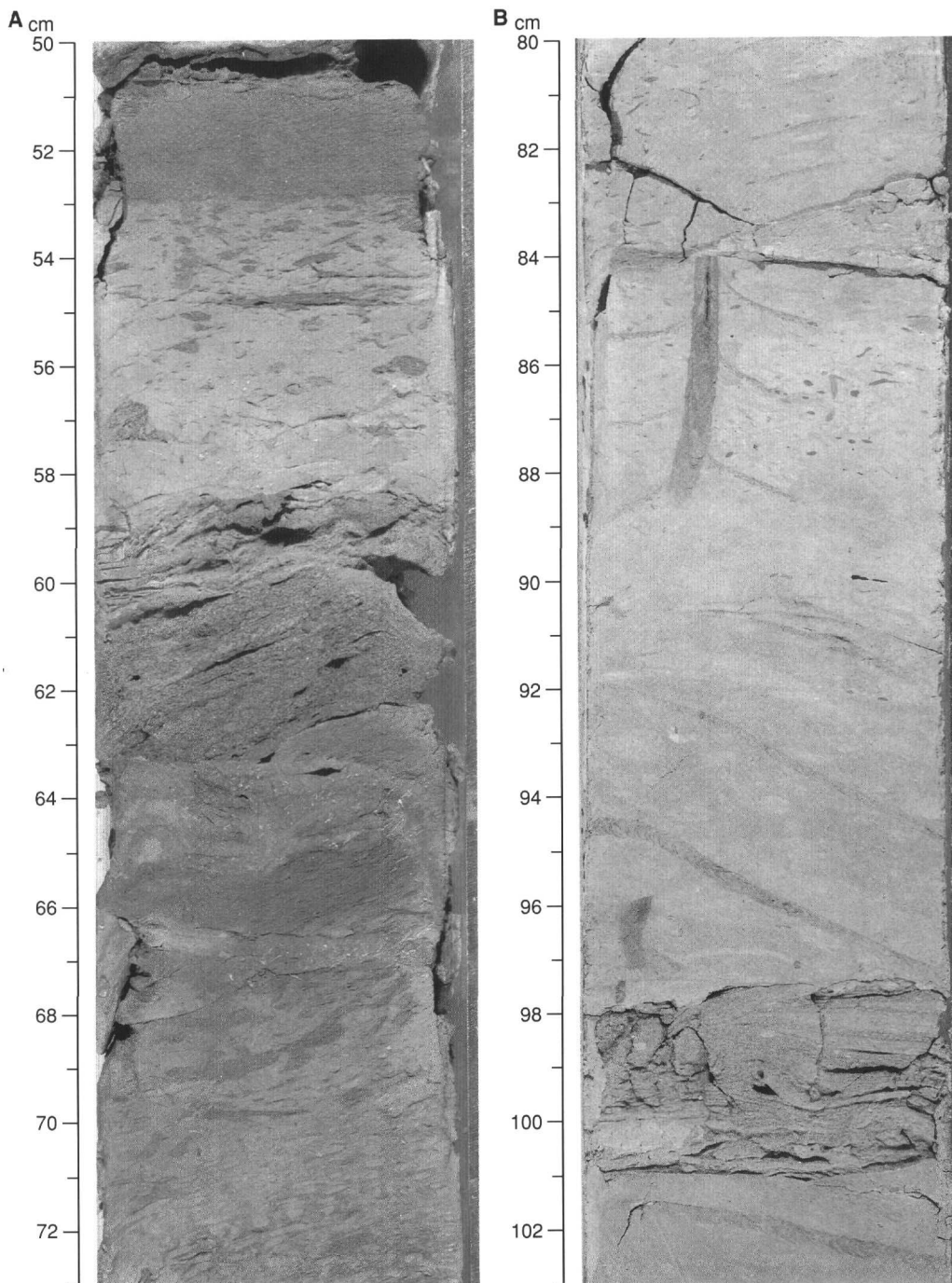


Figure 14. Evidence for reworking of sands by contour currents in Unit IIB. **A.** Possible cross-stratification (60-64 cm). Alternatively, this may be the result of drilling disturbance. Sandstone intervals such as this are probably underrepresented in Unit II because they are friable and easily lost during coring (Interval 149-897C-39R-5, 50-73 cm). **B.** Parallel laminated sandstone (97-101 cm) with sharp base and top. The discrete upper boundary on this bed in particular suggests reworking of sand-sized material by contour currents. Overlying calcareous silty claystone is highly bioturbated: note well-preserved *Zoophycos* (Interval 149-897C-30R, 80-103 cm).

decrease in carbonate content of the upper hemipelagic/pelagic parts of the sequences may have been caused by:

1. Deposition below the CCD, resulting in significant carbonate dissolution in the hemipelagic/pelagic intervals (rapid burial of the basal part of the turbidites would have protected them from dissolution);
2. Low productivity in surface waters reducing the influx of organic carbonate material to the hemipelagic/pelagic intervals;

3. Dilution of the carbonate suspension deposits by influxes of terrigenous clays.

These causes have been linked to cyclical variations in climatic and oceanographic conditions to explain the repeated occurrence of calcareous oozes and terrigenous deposits on the western Iberian margin at DSDP Site 398 (Maldonado, 1976) and ODP Site 637 (Comas and Maldonado, 1988). One or more of the above effects may have

had a part in producing the characteristic turbidites of Subunit IIB at Site 897.

Turbidite, and possibly contourite, facies dominate the sediments of Subunit IIC. Textural and compositional changes within some graded or upward-darkening sequences are similar to those described in Subunit IIB. Individual sequences consist of a basal siltstone or fine sandstone interval that passes upward into silty claystone, claystone, or nannofossil claystone (Td to Te facies; Bouma, 1962). However, some intervals of calcareous siltstone to fine sandstone in Subunit IIC contain features (sharp bases and tops, parallel and cross lamination in siltstones, and parallel silty laminations in claystones) that might reflect deposition by contour currents. Comas and Maldonado (1988) attributed similar facies of the Pliocene-Pleistocene sequence at Site 637 to winnowing and reworking of the substrate by bottom currents. Additional detailed work will be necessary to evaluate the roles of contour currents vs. turbidity currents during the accumulation of Subunit IIC.

Sequences in the lower half of Subunit IIC exhibit upward compositional trends similar to those in Subunit IIB and so also are interpreted as turbidites and carbonate-poor hemipelagic/pelagic sediments that resulted from a combination of conditions, as described for Subunit IIB.

Unit III

Cores 149-897C-60R-1, 0 cm, to the base of -62R
Cores 149-897D-3R-5, 38 cm, to the base of -6R
Depth: 619.7-648.7 mbsf (Hole 897C) and 622.9-655.2 mbsf (Hole 897D)
Age: uncertain

General Description

Unit III contains only a few fossils, all within detrital clasts. The age of this unit can be constrained only on the basis of the ages of the units above and below: middle Eocene to post-Aptian (see "Biostratigraphy" section, this chapter).

The top of Unit III is defined by an abrupt change from the upward-darkening sequences of Unit II to a massive brown claystone to silty claystone (Table 2). In Hole 897C, the change in lithology and color between Units II and III may not have been recovered, as it occurs at a core boundary (the top of Core 149-897C-60R). The contact was recovered at Hole 897D in Core 149-897D-3R, where variegated claystone is overlain by a graded bed of clayey medium-to-coarse sandstone; the contact is placed at the base of this sandstone.

The major lithologies of Unit III are claystone, silty claystone, and sandy silty claystone, with lesser proportions of sandy claystone, matrix-supported sand with dispersed granule-sized lithic clasts, and polymictic, matrix-supported, granule-to-pebble conglomerate.

The unit is divided into two subunits at a lithologic change from massive claystone and silty claystone to coarser-grained clastic sediment. The boundary between Subunits IIIA and IIIB is gradational. The uppermost part of Subunit IIIB (Sections 149-897C-62R-1 and -62R-2) consists of claystone and silty claystone (similar to that of Subunit IIIA) interbedded with thin beds of sandy claystone and clayey sandstone. The Subunit IIIA/IIIB boundary was arbitrarily placed at the top of the first sandstone interval.

Subunit IIIA

Subunit IIIA consists of a monotonous sequence of claystone and minor silty claystone. Colors range from dark reddish brown (10R 5/1) to moderate brown (5YR 3/4) to light brown (5Y 5/6). Round-to-elongate, greenish gray (5GY 6/1) reduction spots are scattered throughout this subunit. Bedding is poorly defined or absent. The clay shows vague color-banding, and bioturbation is not apparent. The core is moderately disturbed and exhibits drilling biscuits.

Subunit IIIB

Subunit IIIB includes sandy-to-silty claystone; fine, medium, and coarse, poorly sorted, matrix-rich sandstones; and matrix-supported, poorly cemented, granule- to pebble-sized, poorly sorted conglomerate. At both Holes 897C and 897D, these lithologies occur within four intervals, each of which constitutes a crudely upward-fining sequence, passing up into the silty claystones of Subunit IIIA.

The four intervals are described below using the facies types defined by Pickering et al. (1986). From top (4) to bottom (1), the sequence is as follows:

4. Highly variegated interval of thin beds of sandy siltstone to sandy claystone within silty claystone and coarse clayey/silty sandstone (Intervals 149-897C-62R-1, 30 cm, to -62R-2, 150 cm, and -6R-1, 0-94 cm; Fig. 15). Sandy beds in this interval exhibit features similar to Facies B1.2 (thin-bedded, coarse-grained sands).

3. Thin-bedded, upward-fining sequence of granule conglomerate and very coarse sandstone that are poorly sorted, matrix-rich, polymictic, and poorly cemented (Intervals 149-897C-62R-3, 0 cm, to -62R-2, 9 cm [Figs. 16B and 16C] and 149-897D-6R-1, 90-110 cm). Within the poorly sorted conglomerate, the sand-silt-clay matrix is similar in composition to the finer-grained sediments within this subunit. This interval exhibits features similar to Facies A2.3 (normally graded gravel).

2. Very poorly sorted, matrix-rich conglomerate (Intervals 149-897C-62R-3, 40 cm, to -62R-4, 50 cm, and 149-897D-6R-1, 0 cm, to -6R-3, 101 cm [Fig. 16A]). Granule- and pebble-sized clasts within the conglomerate framework range from angular to subrounded; maximum clast size is 4 cm. The granule-conglomerate is structure-less, except for a poorly defined imbricate alignment of clasts with bedding. This interval exhibits features similar to Facies A1.1 (disor-ganized gravel).

1. Interval dominated by clasts of yellowish nannofossil claystones and chinks ranging between 2 to 7 cm in diameter, but also including a basalt clast at Interval 149-897D-6R-3, 46 cm, and a fine-grained limestone granule at 149-897C-62R-4, 42-43 cm (Fig. 17). Nanofossil evidence indicates that the claystone/chalk clasts are of different ages (late Hauterivian, Barremian, early Aptian) (see "Biostratigraphy" section, this chapter).

Color in subunit IIIB is extremely variegated and includes moderate reddish to dark reddish brown (10R 4/6; 10R 3/4) and shades of gray, green, and blue (5GY 5/1, 5G 5/1, 5YR 4/1, 5G 6/1, 5B 6/1). Color variations are partly the result of diagenetic effects (e.g., oxidation/reduction) and in part the result of variable clast composition. Parallel lamination, defined by color-banding, characterizes the fine-to-coarse sandstones within the claystones in the upper part of the subunit.

Petrography

Type 2 claystones are the dominant lithology of Subunit IIIA, with a minor silt admixture that includes quartz, feldspars, and MRFs. Coarse-grained sandstones of Unit III are litharenites (classification of Folk, 1980). Many lithic clasts contain, or are coated with, fine-grained and opaque iron oxides (red-brown in reflected light) that obscure their identity. Other opaque grains are white in reflected light, which suggest that fine-grained Ti-oxide is also present as a grain alteration product. Identified lithic types include terrigenous clastic grains (claystones, silty claystones, clayey siltstones, and sandstones), limestones, clayey limestones, possible dolomites, and mafic volcanic grains that have been altered to widely varying degrees (red-brown to green). Black opaque grains are abundant. Some of the carbonate lithologies contain shallow-water allochems.

Several highly lithified pieces of sandstone recovered in Unit IV have been interpreted as caved material from the overlying Unit III and thus are described here. Two sandstone samples were examined in thin section.

A carbonate-cemented moderate brown (5YR 4/4) coarse sandstone from Section 149-897C-64R-1 at 7 cm is an end-member litharenite (classification of Folk, 1980). Rock fragments make up approximately 75% of the volume of total rock and consist of carbonate rock fragments and serpentine clasts. The serpentine fragments are oxidized to varying degrees and vary in color from mottled yellowish brown to green. A few clasts of claystone and clayey siltstone also are present. The carbonate cement is crudely fibrous in part and in part made of equant spar. A portion of the detrital carbonate consists of monocrystals and, hence, the identifying grains from cement is ambiguous in many places.

A sandstone (greenish gray, 5GY 6/1) from Section 149-897C-64R-1 at 34 cm is a medium-sized carbonate-cemented lithic arkose with 40% of mostly monocrystalline quartz. Feldspar (20% of the grains) consists mostly of K-feldspar, including microcline. Minor Ca-plagioclase grains are highly vacuolized and otherwise altered. Rock fragments (40% of the grains) are mostly CRFs. Carbonate lithologies and allochems include micrite, fragments of benthic foraminifers, brachiopods, and red algae. Minor rock fragments include mica schist, basalt, serpentine, and mica. Several biotite grains have expanded fabrics, apparently produced during growth of the authigenic carbonate.

Significant numbers of possibly altered silicate grains are present that have been replaced by one or more authigenic minerals having low, first-order birefringence. Some apparent replacements are microcrystalline with low relief. Another phase has moderate relief and prominent cleavage. Possible minerals corresponding to these phases include various zeolites and clay minerals.

Marly limestone and sandstone pebbles or clasts may be representative of the rocks present in Lower Cretaceous units along the west Iberia margin (Boillot, Winterer, Meyer, et al., 1988; Sibuet, Ryan, et al., 1979). Altered basaltic clasts (see "Igneous and Metamorphic Petrology and Geochemistry" sections, this chapter) are present in the gravel and coarse sandstones of Subunit IIIB. Sand-sized basaltic fragments occur in the thin clayey sandstones in the interval from the top of Subunit IIIB to Interval 149-897C-62R-3, 0-150 cm. These thin sands may represent highly altered ash layers and are evidence of possible contemporaneous volcanic activity.

Cursory examination of the clay mineral assemblage in Unit III reveals the presence of illite, kaolinite, an expandable clay, and possible palygorskite.

Depositional Processes

Subunit IIIA is interpreted as the product of slow accumulation of clay in an oxygenated environment, possibly beneath the CCD. The clay and fine silt are most likely continental material supplied by low-density turbidity flows or by the nepheloid layer of contour currents. Comparison with other DSDP/ODP sites along the northeastern Atlantic continental margin (Laughton, Berggren, et al., 1972; Sibuet, Ryan, et al., 1979; Boillot, Winterer, Meyer, et al., 1988) suggests a probable Eocene-Paleocene age for this subunit, a period when the regional CCD was relatively shallow (Fig. 181, p. 375 in Emery and Uchupi, 1984).

Subunit IIIB is interpreted as being deposited from high-concentration sediment flows that were transported by high-density turbidity currents or as fluidized sand-silt-clay debris flows on relatively gentle slopes. The basal, poorly sorted, conglomerate/gravel interval can be considered as a deposit from a single debris flow. Rounded clasts of different lithologies, ages, and degrees of lithification suggest that the sediment derived from multiple preexisting units that cropped out at seafloor escarpments. Coeval tectonic activity may have affected slope stability, which triggered sediment flow.

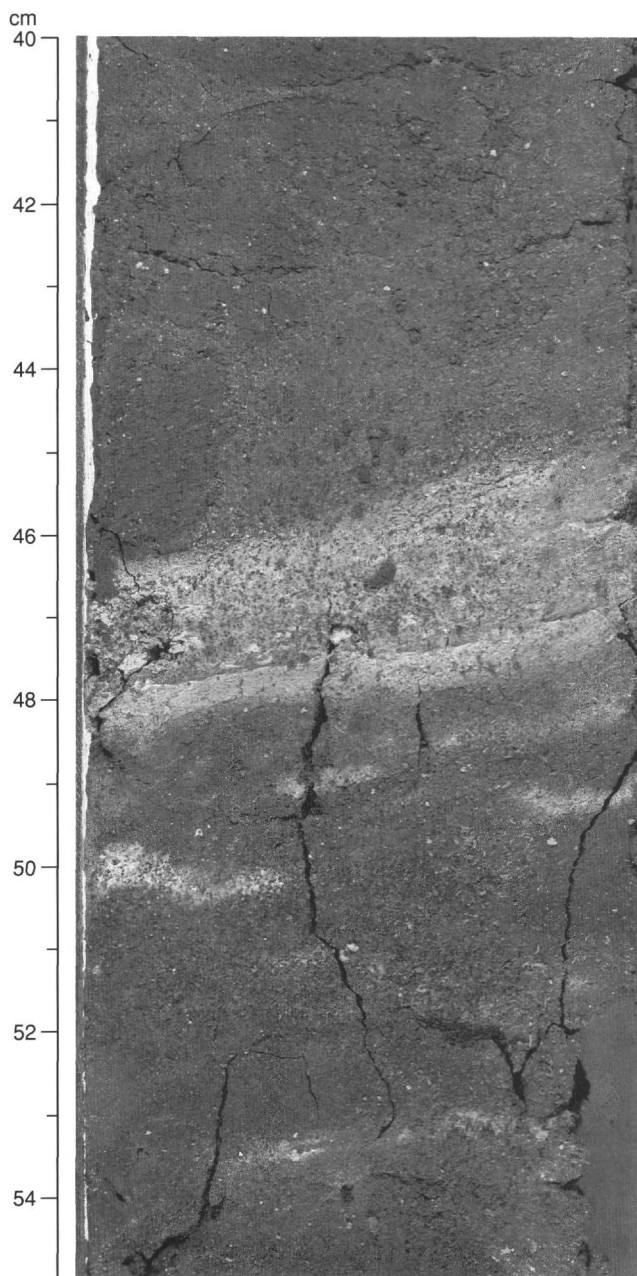


Figure 15. Light-colored sandy siltstone and sandy claystone at the top of Subunit IIIB. The sand-sized fragments in this thin interval include highly altered basaltic clasts, which suggests that it is altered volcanic ash (Interval 149-897C-62R-1, 40-55 cm).

Unit IV

Cores 149-897C-63R-1, 0 cm, to 149-897C-66R-1, 18 cm
Cores 149-897D-7R-1, 0 cm, to 149-897D-11R-1, 0 cm
Depth: 648.7-677.5 mbsf (Hole 897C) and 655.2-693.8 mbsf (Hole 897D)
Age: late Aptian to late Hauterivian(?)

General Description

Unit IV consists of intervals of serpentinized peridotite, ranging from 15 cm to 1.5 m thick, sandwiched between dark gray claystones and a variety of other lithologies including various breccias (Fig. 18). Sedimentary intervals in the unit yield ages that young upward and

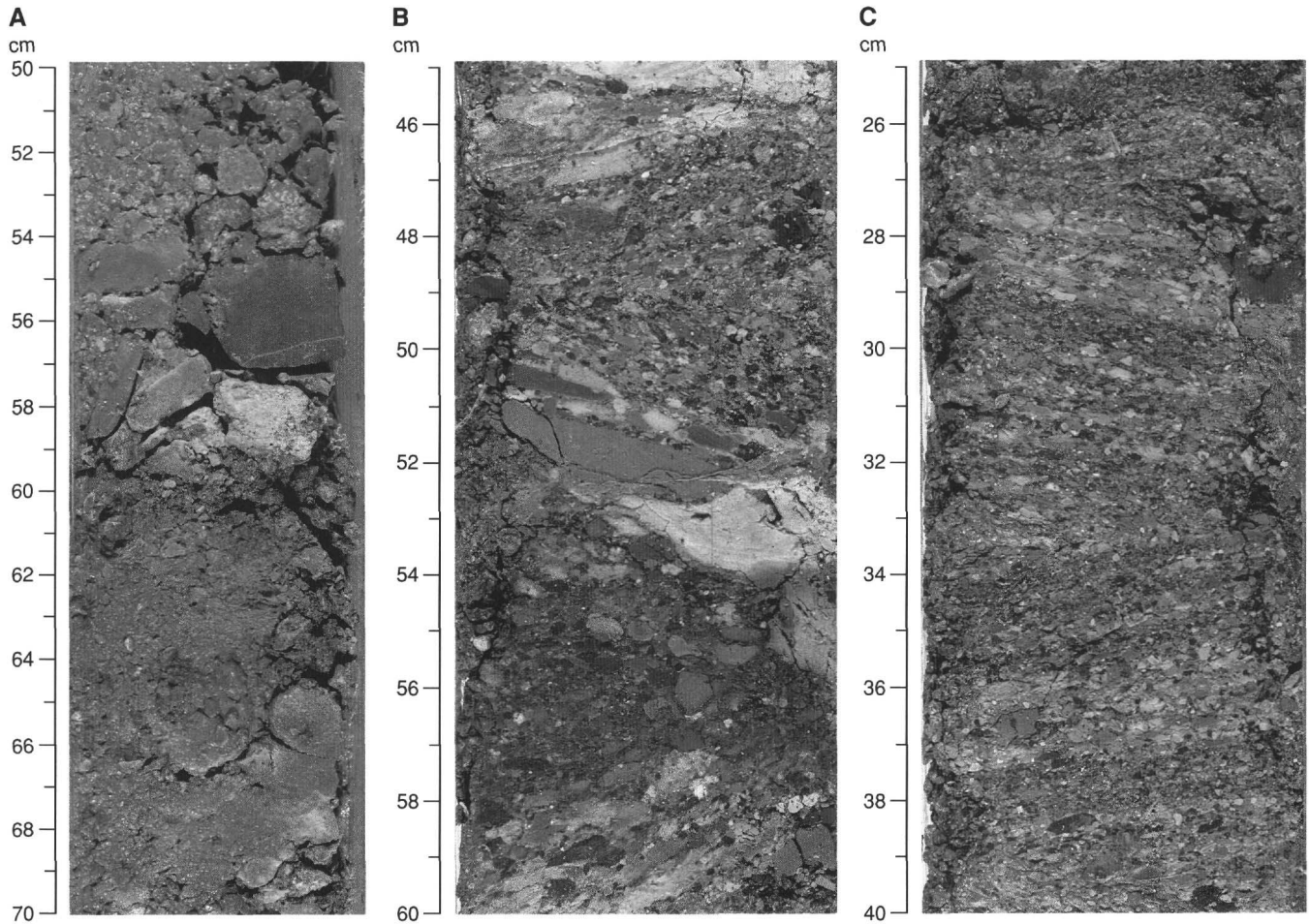


Figure 16. Upward-fining of the polymictic conglomerates at the base of Subunit IIIB. **A.** Very poorly sorted conglomerate with a granule and coarse sand matrix (Interval 149-897D-6R-2, 50-70 cm). **B.** Partially disorganized, poorly sorted granules and pebbles set in a granule-sand matrix; some parallel orientation of the larger clasts is discernible (Interval 149-897C-62R-3, 45-60 cm). **C.** Coarse sand and granules show intervals of inclined layering, which may be current structures or, alternatively, have been produced by slight rotation of core biscuits (Interval 149-897C-62R-3, 25-40 cm).

range from early late Hauterivian to early Aptian (see "Biostratigraphy" section, this chapter).

The top of Unit IV is taken at the top of the first cores beneath the nannofossil claystone/chalk conglomerates of Subunit IIIB.

The base of Unit IV is defined by the first occurrence of serpentinized peridotite uninterrupted by intervals of sedimentary rocks. In Hole 897D, a thick (4.5 m) claystone is present in Sections 149-897D-10R-3 and 10R-4; continuous serpentinized peridotite begins at Section 149-897D-11R-1, 0 cm. However, in Hole 897C, the location of the lower boundary is debatable because of the difficulty of distinguishing genuine sediment intervals from apparent sedimentary material that was introduced by drilling disturbance. The shipboard sedimentologists confidently identified in-situ sediments in Sections 149-897C-64R-1 and -64R-2 immediately above a thick interval of serpentinite that spans Sections 149-897C-64R-3 and -65R-1 and Interval 149-897C-65R-2, 0-98 cm; however, they debated whether the origins of the following four intervals were sedimentary or were caused by drilling disturbance:

1. Interval 149-897C-65R-2, 98-127 cm: medium to dark gray (N3, N5) contorted claystones containing many angular fragments of serpentinite. A smear slide analysis suggests that the sand-sized grains are almost 100% serpentine clasts. The origin of this material might be either sedimentary or a drilling-induced slurry of sedimentary material that caved into the hole from higher up and mixed with

serpentine clasts. The high concentration of organic material (see "Organic Geochemistry" section, this chapter) in this interval argues strongly in favor of a sedimentary origin, however. Nanofossils from this interval indicate a late early Hauterivian age (see "Biostratigraphy" section, this chapter).

2. Interval 149-897C-65R-3, 0-19 cm. Pieces 1 and 2 (see "Igneous and Metamorphic Petrology and Geochemistry" section, this chapter) consist of a breccia of shale, feldspathic diabase, and feldspar phenocrysts.

3. Interval 149-897C-65R-3, 19-51 cm. Pieces 3 and 4 (see "Igneous and Metamorphic Petrology and Geochemistry" section, this chapter) are the only samples in Hole 897C of extensively altered (apparently oxidized and calcitized) serpentine. The pieces of core consist of serpentine breccia in which light greenish gray (5G 8/1) clasts are set in a grayish orange (10 YR 7/4) matrix.

4. Interval 149-897C-66R-1, 0-18 cm: pieces of medium light gray (N6) clayey limestone, are possibly material that caved into the borehole from higher up. The nannofossil assemblage indicates an early Hauterivian age (see "Biostratigraphy" section, this chapter).

The base of Unit IV has been placed immediately below the lowermost interval containing sedimentary rocks (4 above).

The proportion of sedimentary rock intervals recovered from Unit IV in the two holes is different. In Hole 897C, this is about 33% (i.e., about 6.2 m of basement in a total recovery of 9.2 m) and in Hole

897D, is about 85% (i.e., about 1.9 m of basement in a total recovery of 11.4 m).

Figure 19 provides a graphic summary of sedimentary lithologies and serpentinized peridotite recovered from Unit IV in the two holes. Table 4 shows the occurrence, color, grain size and texture, petrographic composition, and internal structures observed in each sedimentary lithology present in the unit.

Several pieces of highly lithified, carbonate-cemented, medium-to-coarse sandstones and granule conglomerates are present in the cores of Unit IV. Occurrences of these lithified materials are within the upper few centimeters of Cores 149-897C-63R to -66R, and Cores 149-897D-7R to -8R. As stated above, these lithologies bear no obvious compositional or textural similarities to other rocks that make up the bulk of Unit IV and may be highly lithified clasts that caved into the hole from the conglomeratic intervals of Unit III.

Tectonic structures within Unit IV are discussed in the "Structural Geology" section (this chapter).

Depositional Processes

When Unit IV was first encountered at Hole 897C, two hypotheses were considered for its origin by the Shipboard Scientific Party: (1) it represents a tectonic melange or megabreccia involving basement rocks and sedimentary cover, or (2) it originated as a mass flow deposit.

A tectonic origin has been discounted because, despite certain brittle deformation within the hard sedimentary rocks, it is unlikely that the soft sediments within Unit IV would have retained primary laminations and slump features had they been subjected to fault brecciation. Therefore, we prefer a mass flow origin for the sequence. Moreover, as the ages obtained from Unit IV indicate that it systematically youngs upward, we postulate that the emplacement of the mass flows occurred during late Hauterivian(?), early Barremian to late Aptian time. If emplacement had occurred later, it would have involved transport of peridotite blocks *and* Early Cretaceous sediments, which should have produced a disordered age pattern, with older intervals overlying younger ones.

The absence of graded deposits within the sediments of Unit IV suggests that the mass flow did not transport material over a great distance. Gravitational transport can occur without major mixing of seawater; thus, fluidized facies, either matrix-rich debris-flow or high-density turbidite deposits, will not necessarily exist. In extremely dense mass flows, mud acts as a mobile phase to permit downslope movement, whereas the rigid blocks of basement are a passive component of the flow. During gravitationally induced movement, the soft sediments suffer ductile deformation.

Indications are that some sediments in Unit IV were in a slightly lithified state during their transport by gravity sliding. For example, the laminated gray siltstone recovered in Interval 149-897D-7R-3, 10-24 cm (Fig. 20) exhibits microfaults that produced millimeter to centimeter offsets, suggesting that lithification had occurred prior to transport. Unlithified sand would probably have undergone complete mobilization.

Deposition of Unit IV possibly occurred at the foot of a fault escarpment that exposed serpentinized peridotite basement during the Early Cretaceous, but the ridge may have been uplifted after the deposition of Unit IV. It is likely that this unit is the same age as the "synrift" sediments in the inter-ridge location imaged in seismic reflection profiles (see "Site Summary" section, this chapter, Fig. 3).

The distinctive sedimentary association observed in Unit IV (i.e., highly varied sedimentary lithologies intermixed with, and overlying, highly calcitized and veined serpentinized peridotite) is not without precedent. For example, one similar succession was described by Tricart and Lemoine (1991) from the Queyras ophiolite of the western Alps. There, pelagic limestones and cherts rest unconformably on a basement-breccia pillow lava assemblage and have been succeeded conformably by pelagic limestones and shales containing ophiolite clasts and olistoliths of continental origin. No equivalents to the basalts and ophicalcite breccias were recovered at Site 897, although altered

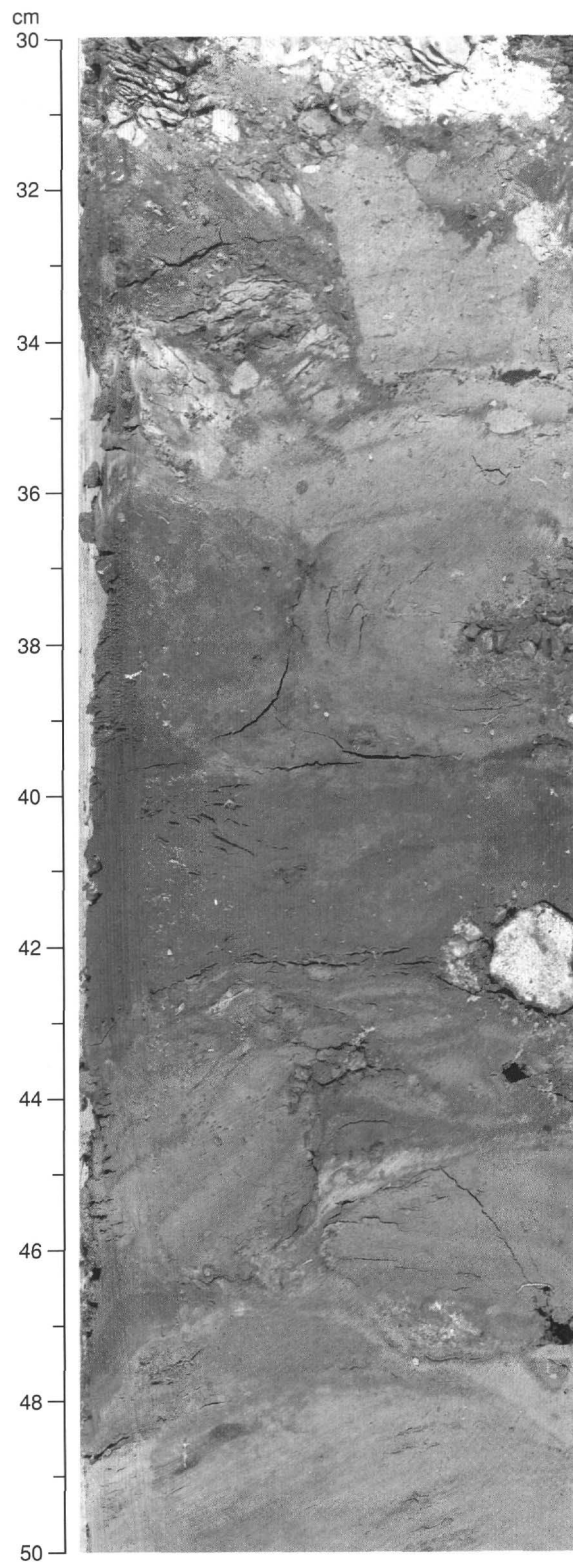


Figure 17. The basal interval of Subunit IIIB. The fractured limestone clast at 31 cm marks the base of the second interval of the upward-fining conglomerate/coarse sandstone sequence illustrated in Figure 16. The orange gray (10YR 7/4,6/4) nannofossil claystone/nannofossil chalk occurs in discrete rounded pieces that are possibly sedimentary clasts (Interval 149-897C-62R-4, 30-50 cm).

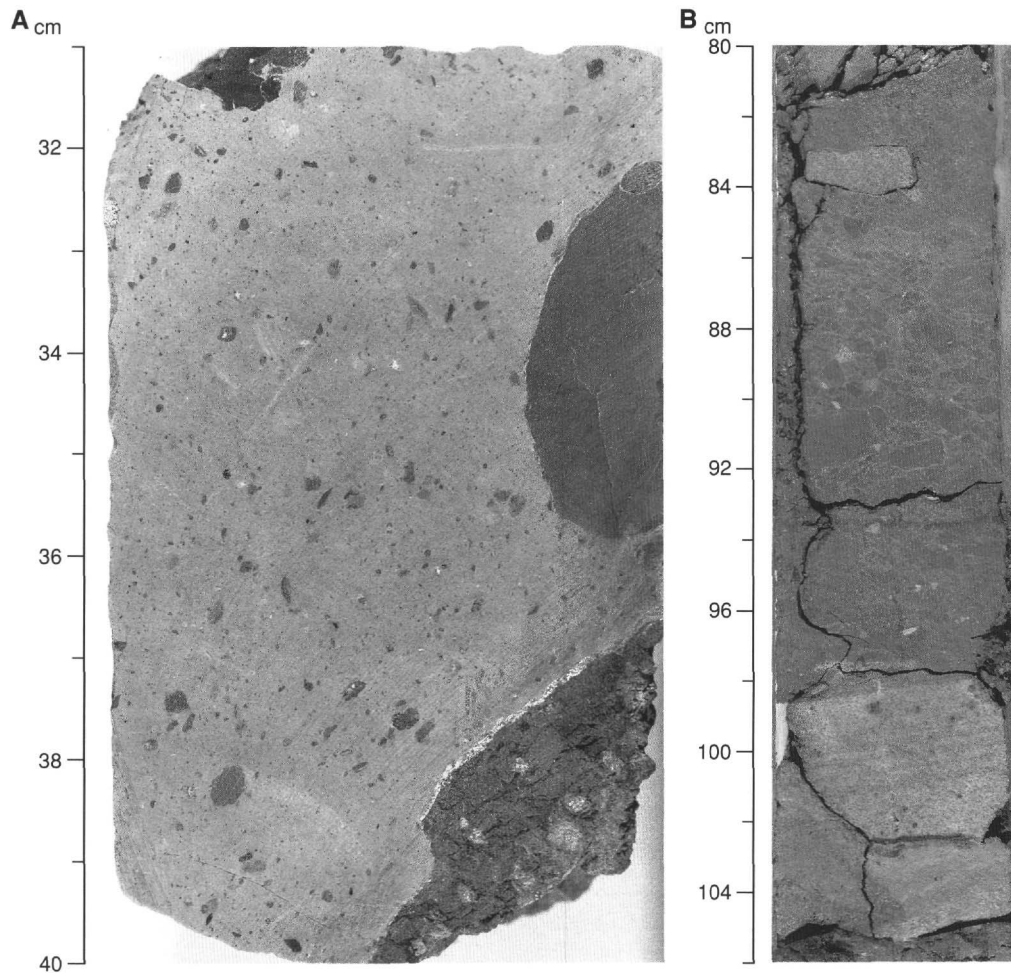


Figure 18. Breccia intervals in Unit IV. **A.** Clayey limestone containing a range of sizes of angular serpentinite clasts that are similar to the serpentinite intervals within Unit IV (Interval 149-897D-10R-1, 31-40 cm). **B.** Brecciated limestone: both the clasts and matrix are nanofossil limestones; the lower part shows inverse grading and the upper part normal grading. The laminated fine sand beneath the breccia is a subarkose (Interval 149-897D-7R-1, 80-106 cm).

basaltic tuffs occur in Subunit IIIB and pieces of altered diabase are present in cores where Unit IV was recovered. More detailed comparison between comparable occurrences of ophiolite-associated sediments and Unit IV of Site 897 await post-cruise studies.

BIOSTRATIGRAPHY

Sediments recovered from the three holes cored at Site 897 provide a discontinuous record for the Pleistocene through the Early Cretaceous (Fig. 21). Present is a thick (310 m) Pliocene-Pleistocene sequence, a much thinner (68 m) Miocene deposit containing two unconformities, a thick (155 m) Oligocene deposit, and middle and upper Eocene sediments (87 m), below which a brown claystone deposit of unknown age overlies an Early Cretaceous deposit. Calcareous nanofossils generally are present throughout the sequence, except for the brown claystone deposit, and provide a well-constrained stratigraphy for the recovered sequence. Planktonic and benthic foraminifers are abundant to common in the Pleistocene and upper Pliocene deposits, but rare to absent throughout most of the remaining cored interval.

Calcareous Nanofossils

Site 897 is situated in the eastern part of the Iberia Abyssal Plain in a water depth of 5320 m. The calcareous nanofossils define a stratigraphic succession from the upper Pleistocene (Zone NN21 of Martini,

1971) to the Lower Cretaceous (Zone CC4 of Sissingh, 1977). Most of the material has been deposited by turbidity currents and part of the section is incomplete (zones NN14 through NN11 are missing) or has been condensed into a short interval (NN10 through NN5). Carbonate-free red-brown claystone, barren of calcareous nanofossils, represents a long interval between the middle Eocene (NP14) and the upper Aptian. About 15 m of pre-Albian (upper lower Hauterivian to the lower upper Aptian) sediment represents the earliest sediment deposited since the rupture of the continental crust. Within this interval, the percentage of shallower water forms of the genera *Lithraphidites*, *Micrantholithus*, and *Nannoconus* decreases progressively from the Hauterivian to the Aptian, indicating a deepening of this site toward a more deep-sea environment. The top of this interval is composed primarily of small debris-flows interbedded with less calcareous claystones that contain a poorly preserved, monospecific assemblage of *Watznaueria* spp. This indicates that subsidence of the margin has occurred to depths near or below the carbonate compensation depth (CCD), which has been estimated as being at 3000 m in the North Atlantic by late Aptian (Tucholke and Vogt, 1979).

Cenozoic Biostratigraphy

Hole 897A

The upper 55.2 m of the sedimentary section from Site 897 was recovered from Hole 897A. The biostratigraphic resolution is limited because of poor core recovery. Calcareous nanofossils are few to very

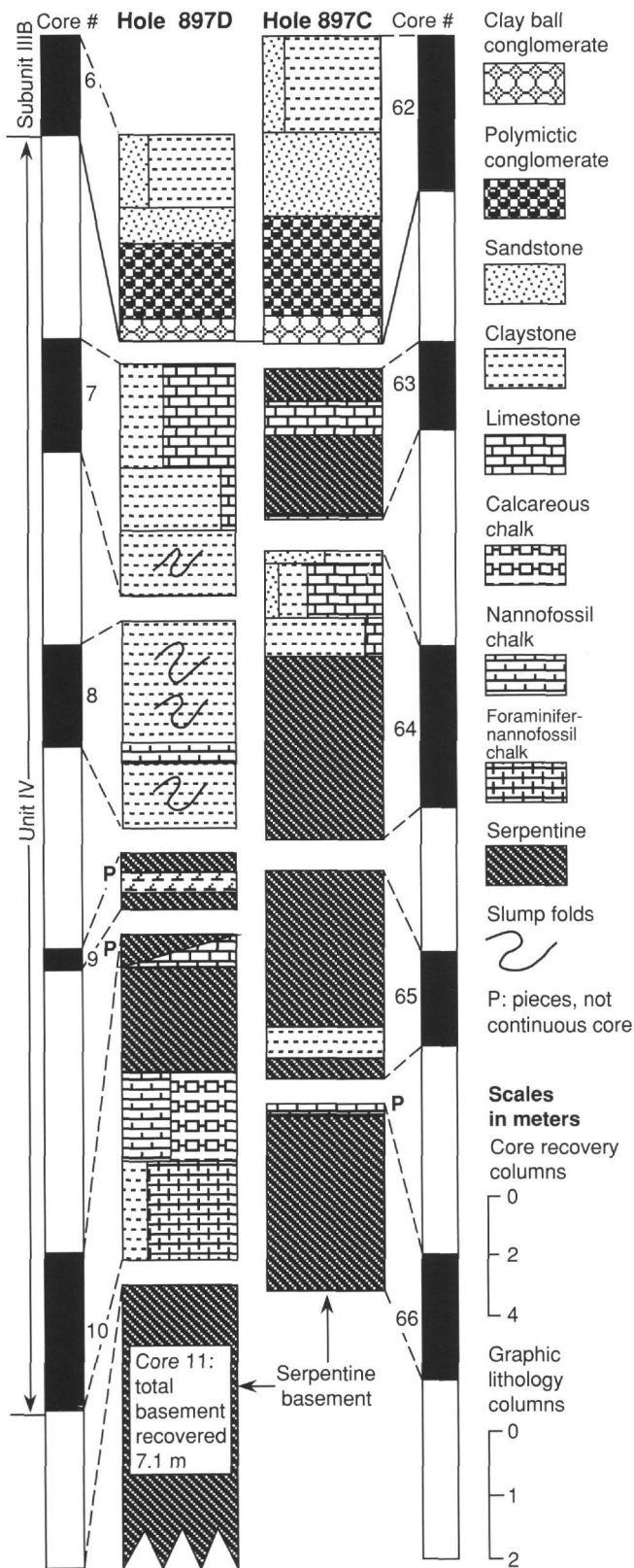


Figure 19. Summary of core recovery through Subunit III B and Unit IV and the lithological succession in Unit IV in Holes 897C and 897D.

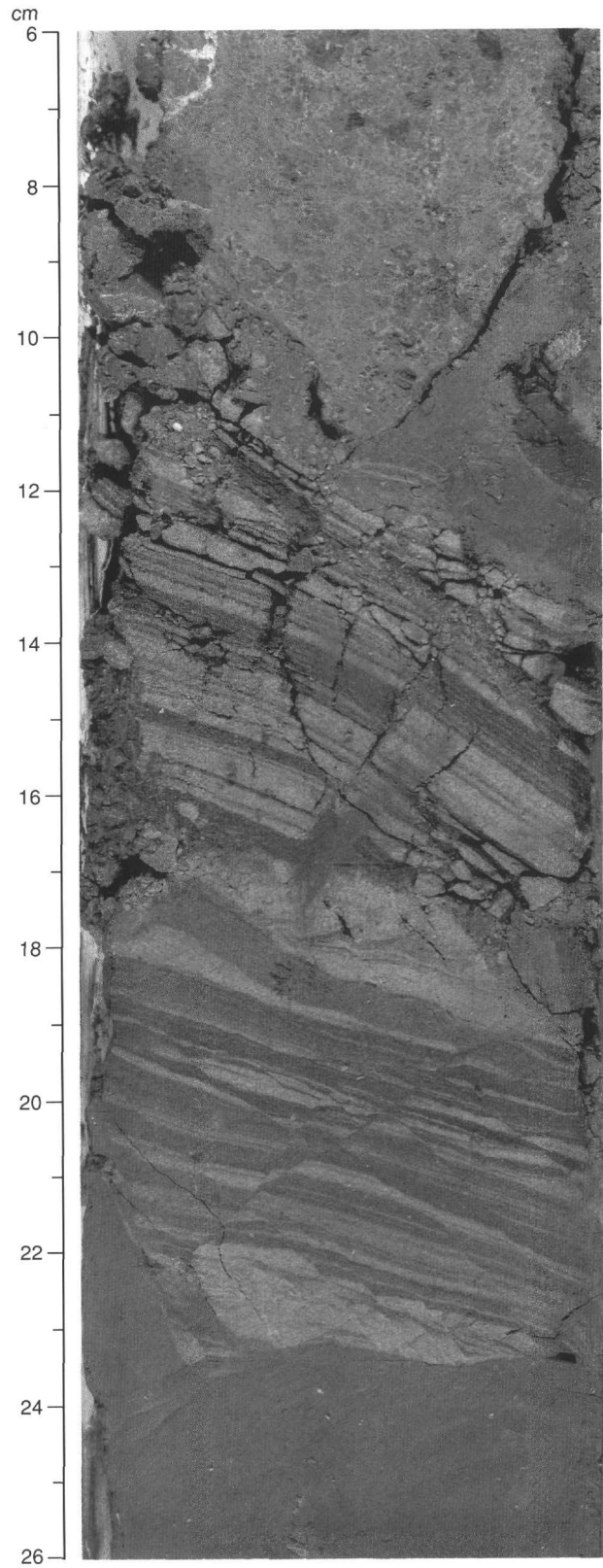


Figure 20. Fine siltstone in Unit IV showing parallel laminae affected by millimeter-scale faulting. Open fractures in the upper part of the interval probably were formed during drilling. A fragment of serpentine occurs at the top of the photograph (Interval 149-897D-7R-3, 6-26 cm).

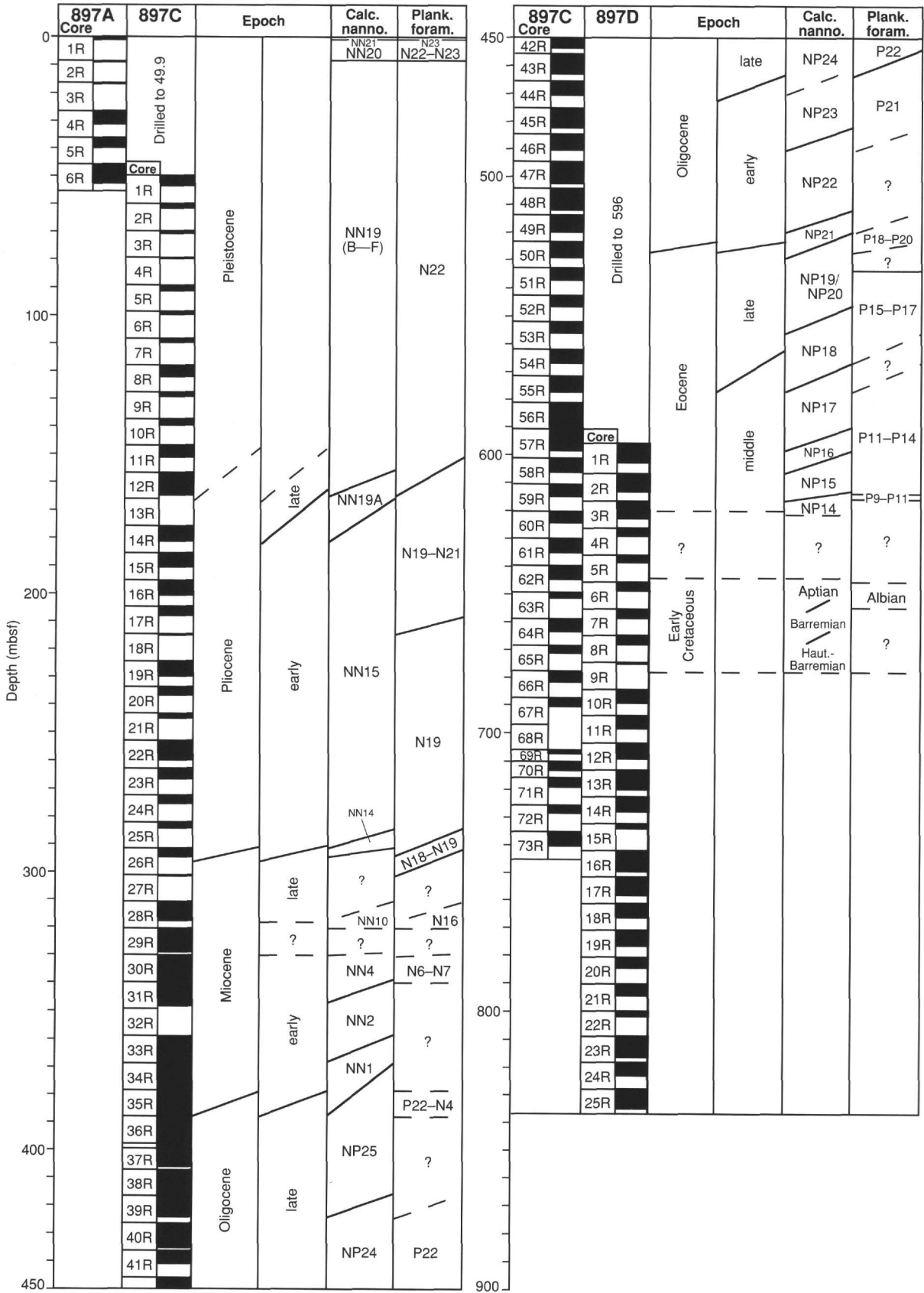


Figure 21. Summary of planktonic microfossil zones from Site 897. Haut. = Hauterivian.

abundant and moderately to well preserved. Few to common specimens of *Emiliania huxleyi* and *Emiliania pujosae* in Samples 149-897A-1R, 55 cm, and 149-897A-1R, 105 cm, indicate Zone NN21 from the upper Pleistocene. In both samples, no shift in dominance between small *Gephyrocapsa* spp. and *Emiliania huxleyi* was observed, and small *Gephyrocapsa* spp. (>2.5 µm) having an open central area dominate the assemblage (morphogroup 1; Gard and Backmann, 1990). This led to an assigned age of 0.186 Ma for the assemblage. In Sample 149-897A-1R-CC, the presence of only *Emiliania pujosae* indicates an age between 0.26 and 0.36 Ma. Sample 149-897A-2R-CC contains rare *Reticulofenestra* sp. A (>5.0-6.0 µm), rare *Reticulofenestra asanoi*, and common *Gephyrocapsa oceanica* (>4.0-5.0 µm). Sample 149-897A-3R-1, 30 cm, has few *Gephyrocapsa oceanica* (>5.0-5.5 µm), very rare *Helicosphaera inversa*, rare *Reticulofenestra* sp. A (>5.0-6.0 µm), very rare *Reticulofenestra* sp. A (>6.5 µm), and rare circular *Pseudoemiliania lacunosa*, which indicate an age from 0.8 to 0.9 Ma. Sample 149-897A-3R-CC contains *Gephyrocapsa oceanica* (>4.0-5.0 µm), *Gephyrocapsa caribbeanica*, and rare elliptical *Pseudoemiliania lacunosa*. The interval from Samples 149-897A-4R-1, 58 cm, to -5R-3, 32 cm, contains abundant *Gephyrocapsa oceanica* (>4.0-5.0 µm), *Gephyrocapsa oceanica* (>5.5 µm), and *Gephyrocapsa caribbeanica*. This indicates an age between 1.10 and 1.37 Ma. Samples 149-897A-5R-CC and -6R-CC contain *Gephyrocapsa oceanica* (>4.0-5.0 µm), which indicates an early Pleistocene age in the middle of Zone NN19 between 1.37 and 1.64 Ma. Most of the core-catcher samples (149-897A-2R-CC to -6R-CC) contain few to very abundant *Coccolithus doronocoides*, scattered occurrences of *Discoaster variabilis*, *Discoaster* sp. (5 rays), and *Discoaster pentaradiatus*, indicating that a large part of the material has been recycled from the Pliocene. Also reworked from the Pliocene are rare *Cladiscus macintyreii*, making the use of this marker difficult. An assignment of the Pleistocene age results from the size of *Gephyrocapsa oceanica* (>4.0 µm). The assemblage of Sample 149-897A-6R-CC has moderately preserved, abundant calcareous nannofossils and contains common *Coccolithus pelagicus*, indicating the presence of cooler water.

Hole 897C

The Cenozoic sediments recovered in Hole 897C from Samples 149-897C-1R-CC to 149-897C-59R-4, 10 cm, cover a long period of time, from the early Pleistocene to the middle Eocene. Below this Cenozoic interval, red-brown claystones barren of calcareous nannofossils were recovered (lithostratigraphic Subunit IIIA and most of Subunit IIIB; see "Lithostratigraphy" section, this chapter). Calcareous nannofossils were found in the majority of the core-catcher samples. The estimated abundances of nannofossil specimens in the core-catcher samples range from barren (Samples 149-897C-7R-CC, -29R-CC, -34R-CC, -40R-CC, -44R-CC, -46R-CC, and -47R-CC) to very abundant. Most core-catcher samples contain rare to few reworked specimens from the Cretaceous. Reworked Cenozoic specimens from the Paleocene to the Pliocene, having a high percentage of Miocene forms, were also observed in Pliocene sediments.

Pleistocene. The Pleistocene sediments extend from Section 149-897C-1R-1 to Sample 149-897C-11R-CC. The nannofossil assemblages mostly are well preserved, and the abundance of nannofossil specimens ranges from barren (Sample 149-897C-7R-CC) to very abundant.

Samples 149-897C-1R-CC to -11R-CC contain rare to few *Gephyrocapsa oceanica* (>4.0-4.2 µm), few *Helicosphaera sellii*, few *Cladiscus macintyreii*, rare to common *Reticulofenestra asanoi*, abundant *Coccolithus doronocoides*, and few to common *Coccolithus pelagicus* (and *Coccolithus crassipons*).

Pliocene. The Pliocene/Pleistocene boundary was placed between Samples 149-897C-11R-CC and 149-897C-12R-CC by the lowest

occurrence (LO) of very rare *Gephyrocapsa oceanica* (≥4.0 µm) in Sample 149-897C-11R-CC. The Pliocene interval extends from Samples 149-897C-12R-CC to -26R-1, 76 cm. The calcareous nannofossils range from few to abundant and are moderately to well preserved. Sample 149-897C-12R-CC was placed in Zone NN19A on the absence of *Discoaster brouweri* and *Gephyrocapsa caribbeanica*. Zones NN18-NN16 are missing. The interval 149-897C-14R-CC to -25R-CC has been assigned to Zone NN15. The highest occurrence (HO) of *Reticulofenestra pseudumbilica* in Sample 149-897C-14R-CC indicated Zone NP15.

In Sample 149-897C-15R-CC, the co-occurrence of rare *Reticulofenestra pseudumbilica* and *Sphenolithus neoabies*, abundant *Pseudoemiliania lacunosa* and *Reticulofenestra ampla* and of very abundant *Coccolithus doronocoides* suggests the top of Zone NN15. Sample 149-897C-17R-CC contains rare *Sphenolithus abies*. Sample 149-897C-25R-CC contains few *Reticulofenestra pseudumbilica*, whereas Sample 149-897C-26R-CC yields few *Pseudoemiliania lacunosa*, few *Discoaster tamalis*, and abundant *Coccolithus doronocoides*. Sample 149-897C-27R-CC contains few *Sphenolithus abies*, common *Sphenolithus neoabies* and *Reticulofenestra pseudumbilica*, rare *Discoaster asymmetricus* and *Discoaster brouweri*, few *Thoracosphaera albatrosiana*, and no *Pseudoemiliania lacunosa*, *Discoaster tamalis*, *Discoaster quinquerramus*, *Amaurolithus* spp., or *Ceratolithus* spp.

Miocene. The Miocene/Pliocene boundary was placed between Samples 149-897C-26R-1, 76 cm and -26R-CC. The Miocene interval extends down to Samples 149-897C-33R-CC and -34R-CC. The interval from Sample 149-897C-26R-CC to -28R-CC was placed in the upper Miocene Zone NN10, and corresponds to the lithostratigraphic Subunit IIA and to the upper part of Subunit IIB. Sample 149-897C-28R-CC contains very abundant and well-preserved assemblages and corresponds to the upper part of lithostratigraphic Subunit IIA (see "Lithostratigraphy" section, this chapter). This sample represents the Miocene Zone NN10, based on the presence of *Discoaster bollii*, *Discoaster loeblichii*, and *Sphenolithus abies* and the absence of *Discoaster quinquerramus* and *Discoaster hamatus*. A hiatus representing part of the lowermost Pliocene and the upper Miocene (Zones NN12 to NN11) lies between Samples 149-897C-26R-1, 76 cm, and -26R-CC. Sample 149-897C-29R-CC is barren of nannofossils. The interval 149-897C-30R-CC to -33R-CC represents the lower Miocene (Zones NN4-NN1). A second major hiatus, or a very condensed section, lies between this interval and Sample 149-897C-28R-CC and may represent the time from Zones NN10 to NN4. Sample 149-897C-30R-CC corresponds to Zone NN4, based on the presence of *Helicosphaera ampliaperata* and *Sphenolithus heteromorphus*. Sample 149-897C-31R-CC was placed in Zone NN2, as suggested by very rare *Cyclicargolithus abisectus* (>10 µm) and the presence of *Discoaster druggii*. Sample 149-897C-33R-CC corresponds to the lowermost Miocene (Zone NN1), as indicated by common *Cyclicargolithus abisectus*, few *Reticulofenestra bisecta*, rare *Sphenolithus ciperoensis*, and very rare *Zygrhabelithus bijugatus*. The HO of *Helicosphaera recta* occurs below this sample.

Oligocene. The Oligocene occurs from Samples 149-897C-34R-CC and -35R-CC to -49R-CC. Sample 149-897C-35R-CC was assigned to Zone NP25 on the presence of *Helicosphaera recta*, *Triquetrorhabdulus carinatus*, and few *Sphenolithus ciperoensis*. Samples 149-897C-36R-CC to -38R-CC are from the same zone. Sample 149-897C-39R-CC has been assigned to Zone NP24 on the presence of *Sphenolithus dissentis*, *Sphenolithus ciperoensis*, and *Helicosphaera compacta*.

Samples 149-897C-40R-CC and -41R-CC are barren of nannofossils. Sample 149-897C-42R-CC has abundant and well-preserved calcareous nannofossils. The presence of *Sphenolithus distentus* and the absence of *Sphenolithus predistentus* indicate the upper Oligo-

cene Zone NP24. Sample 149-897C-45R-CC lies within the base of Zone NP23, as determined by the presence of *Sphenolithus predistentus* and a transitional form of *Sphenolithus predistentus*. Samples 149-897C-46R-CC and -47R-CC are barren of nannofossils. Sample 149-897C-48R-CC has rare and poorly preserved nannofossils. Zone NP21 (lowermost Oligocene) occurs in Sample 149-897C-49R-CC, as indicated by the presence of *Reticulofenestra umbilica*, *Coccolithus formosus*, *Isthmolithus recurvus*, common *Clausicoccus fenestratus*, *Clausicoccus obrutus*, and *Clausicoccus subdistichus*, and by the absence of *Discoaster barbadiensis*.

Eocene. The Eocene is represented by the interval 149-897C-50R-CC to -59R-4, 10 cm. The interval 149-897C-50R-CC to -52R-CC was placed in Zone NP19/NP20 on the presence of *Discoaster barbadiensis*, *Discoaster saipanensis*, *Ericsoniaformosa*, and *Isthmolithus recurvus*. Sample 149-897C-53R-CC contains abundant, well-preserved nannofossils from Zone NP18, as indicated by the presence of *Chiasmolithus oamaruensis* and the absence of *Isthmolithus recurvus* and *Chiasmolithus solitus*. Sample 149-897C-54R-CC has few, poorly preserved nannofossils. Sample 149-897C-55R-CC was assigned to Zone NP17 on the basis of the presence of *Chiasmolithus grandis*, *Discoaster tani*, in the absence of *Chiasmolithus oamaruensis*, and *Chiasmolithus solitus*. Samples 149-897C-56R-CC and -57R-CC have been placed in Zone NP16, as suggested by the presence of *Campylosphaera dela*, *Discoaster tani nodifer*, and *Sphenolithus furcatolithoides*. Samples 149-897C-58R-CC to -59R-4, 9 cm, are in Zone NP15, as indicated by the presence of sporadic *Blackites gladius*, *Discoaster bifax*, sporadic *Chiasmolithus gigas*, *Nannotetrina alata*, and *Sphenolithus furcatolithoides*. Within Zone NP15, the interval 149-897C-59R-3, 97 cm, to -59R-3, 150 cm, is barren.

Hole 897D

The Cenozoic interval recovered in Hole 897D extends from the middle Eocene (NN15) to the lower middle Eocene (NN14). Samples 149-897D-1R-CC and -2R-CC represent the middle Eocene Zone NN15. The calcareous nannofossils have been excellently preserved and are highly diverse. The presence of *Chiasmolithus gigas* in Sample 149-897D-1R-CC indicates the middle of Zone NP15. In Sample 149-897D-2R-CC, the presence of *Nannotetrina alata*, *Discoaster kuepperi*, and *Discoaster lodoensis* in the assemblage characterizes the boundary of Zones NP14/NP15. Sample 149-897D-3R-5, 1 cm, which is 37 cm above the transition between the lower part of lithostratigraphic Subunits IIC and IIIA (brown-red claystone), contains *Discoaster kuepperi*, *Discoaster multiradiatus*, and *Discoaster sublodoensis*, which indicate Zone NP14.

Sediments below Sample 149-897D-3R-CC, situated near the top of lithostratigraphic Subunit IIIA, are barren of nannofossils.

Mesozoic Biostratigraphy

From Holes 897C and 897D, we recovered a thin Mesozoic section of debris flows having calcareous silty claystone (lithostratigraphic Subunit IIIB) and calcareous claystone (lithostratigraphic Subunit IV). Most of these intervals contain moderately to well-preserved nannofossils having moderate-to-abundant species diversity. However, in the upper part of lithostratigraphic Unit IV, a few intervals in Section 149-897C-62R-4 have poorly preserved nannofossils, with a low diversity assemblage composed mostly of the dissolution-resistant form *Watznaueria barnesae* (Sample 149-897C-62R-4, 63 cm). Samples barren of nannofossils include 149-897C-62R-4, 74 cm, and -65R-2, 5-10 cm.

We have applied the zonation of Sissingh (1977: "CC" zones) to the Lower Cretaceous using primary zonal markers and additional events (see "Explanatory Notes," Fig. 8, this volume). In the uppermost part of the Cretaceous succession in Hole 897C (base of Subunit IIIB), the interval 149-897C-62R-4, 38-39 cm, to -64R-CC, 1 cm, was placed in

the Aptian. Sample 149-897C-62R-CC, at the top of lithostratigraphic Unit IV, has an assemblage that contains *Praedicosphaera spinosus*, *Lithastrinus floralis*, *Micrantholithus obtusus*, *Micrantholithus hochulzii*, *Micula infracretacea*, *Nannoconus globulus*, *Nannoconus buckeri*, *Nannoconus steinmanii steinmanii*, and *Rucinolithus terebrodentarius*, which indicate an early late Aptian (CC7) age. Sample 149-897C-65R-2, 114 cm, contains a very rich, well-preserved assemblage from the upper Barremian (CC6) with *Rucinolithus terebrodentarius*, *Calcicalathina* aff. *C. oblongata*, *Chiastozygus* aff. *C. litterarius*, *Reinhardtites praesisyphus*, *Conusphaera rothii*, *Zeugrhabdotus diplogrammus*, *Hayesites radiatus*, *Markalius circumradiates*, *Markalius ellipticus*, *Polypodorhabdus madingleyensis*, *Micrantholithus obtusus*, *Zeugrhabdotus elegans*, *Parhabdololithus infinitus*, *Microstaurus quadratus*, *Microstaurus chiastus*, *Rhagodiscus asper*, *Nannoconus steinmanii steinmanii*, and *Reinhardtites fenestratus*. The oldest sediments recovered at Site 897 were observed in Sample 149-897C-65R, 127 cm. A Hauterivian (CC4) age is indicated by *Crucielipsis cuvillieri*, *Reinhardtites praesisyphus*, *Markalius circumradiatus*, *Micrantholithus hochulzii*, *Nannoconus globulus*, and *Calcicalathina* aff. *C. oblongata*. This assemblage also contains unusually abundant *Zeugrhabdotus embergeri*. Sample 149-897C-70R-3, 26 cm, was placed in the Barremian-late Hauterivian by the presence of *Calcicalathina obongata*, *Calcicalathina* aff. *C. oblongata*, *Ellipsagelosphaera britannica*, *Markalius circumradiatus*, *Nannoconus steinmanii*, *Reinhardtites praesisyphus*, *Retecapsa angustiforata*, and *Rhagodiscus asper*.

Sample 149-897D-6R-CC in the upper part of lithostratigraphic Unit IV has common, fairly well-preserved nannofossils from the middle lower Aptian (CC7), including *Conusphaera mexicana*, *Hayesites irregularis*, *Micrantholithus obtusus*, and *Micrantholithus hochulzii*. Sample 149-897D-7R-1, 38 cm, is lower Aptian (CC7) and consists of an abundant, well-preserved assemblage with *Conusphaera mexicana*, *Micula infracretacea*, and *Vagalapilla matalosa* (muroolith). Sample 149-897D-7R-CC contains *Calcicalathina oblongata*, *Diazomalithus lehmanii*, *Micrantholithus obtusus*, and *Micrantholithus hochulzii*, suggesting an age not younger than late early Barremian. Sample 149-897D-8R-CC has a few, poorly preserved nannofossils and no zonal markers. Samples 149-897D-9R-CC and -10R-CC contained serpentinized peridotite. Sample 149-897D-10R-4, 91 cm, has an abundant, well-preserved assemblage from the lower Barremian with *Calcicalathina* aff. *C. oblongata*, *Conusphaera mexicana*, *Conusphaera rothii*, *Manivitella pemmatoidea*, *Markalius circumradiatus*, *Micrantholithus obtusus*, *Micrantholithus hochulzii*, *Nannoconus steinmanii steinmanii*, *Nannoconus ligius*, *Nannoconus buckeri*, *Nannoconus globulus*, *Reinhardtites praesisyphus*, *Rucinolithus terebrodentarius*, *Tegumentum stradneri*, and *Zygodolites* sp. A.

Foraminifers

Planktonic foraminifers in core-catcher samples from Holes 897A, 897C, and 897D were examined to establish preliminary ages for the sediments. The number of planktonic foraminifers generally was low; most of the samples yielded a low-diversity planktonic foraminiferal assemblage having moderate to poor preservation. More planktonic foraminifers having better preservation were present in Hole 897 A and the upper sections of Hole 897C. Similar patterns were observed in the benthic foraminifer assemblages.

Hole 897A

Planktonic foraminifers identified in Hole 897A are listed in Table 6. Foraminifers of late Pleistocene age were identified in Samples 149-897A-1R-CC and -2R-CC. The presence of *Globorotalia truncatulinoides* in Sample 149-897A-1R-CC allowed us to assign it to Zone N23. The co-occurrence of *Globorotalia tosaensis* and *G. truncatulinoides* in Sample 149-897A-2R-CC enabled us to place it in the upper part of Zone N22 or the lower part of Zone N23. The interval

Table 6. Distribution of planktonic foraminifers in Hole 897A.

| Age | Zone | Core | Abundance | Preservation | <i>Globigerina bulloides</i> | <i>G. ruber alba</i> | <i>G. sacculifer</i> | <i>G. inflata</i> | <i>G. scitula</i> | <i>G. triangula</i> | <i>Globorotalia truncatulinoides</i> | <i>Neogloboquadrina acostaensis</i> | <i>N. pachyderma</i> | <i>Orbulina universa</i> | <i>Globorotalia crassaformis crassaformis</i> | <i>G. tosaensis</i> | <i>Neogloboquadrina ditertei</i> | <i>Globigerinoides fistulosus</i> | <i>Globigerinoides extremus</i> | <i>Neogloboquadrina humerosa</i> | <i>Orbulina suturalis</i> |
|-----------------|------------|------|-----------|--------------|------------------------------|----------------------|----------------------|-------------------|-------------------|---------------------|--------------------------------------|-------------------------------------|----------------------|--------------------------|-----------------------------------------------|---------------------|----------------------------------|-----------------------------------|---------------------------------|----------------------------------|---------------------------|
| 1. Ple. | N23 | 1R | A | G | F | R | R | F | R | F | F | R | F | F | | | | | | | |
| | N22-N23 | 2R | A | G | F | R | | F | R | F | F | F | C | C | R | F | R | | | | |
| 1. Pli.-e. Ple. | N22 (base) | 3R | C | G | F | R | | F | R | F | F | F | C | C | | F | R | R | | | |
| | | 4R | A | G | F | R | | F | R | F | F | F | C | C | R | F | R | | R | | |
| | | 5R | A | G | C | R | | F | R | F | F | F | C | C | | F | | | R | | |
| | | 6R | F | P | | | | | | | | R | R | | | | | | R | R | |

Notes: Age: 1. Pli. = late Pliocene; e. Ple. = early Pleistocene; 1. Ple. = late Pleistocene. Abundance: A = Abundant; C = Common; F = Few. Preservation: G = Good; P = Poor.

149-897A-3R-CC to -5R-CC contains *G. truncatulinoides* and *G. tosaensis* together with *Globigerinoides extremus* and can be assigned to the basal part of Zone N22, which is of latest Pliocene to early Pleistocene age. No age-indicative species were identified in Sample 149-897A-6R-CC. Abyssal and reworked shallow-water benthic foraminifers were identified in all core-catcher samples.

Hole 897C

A late Pliocene to early Pleistocene age sequence (lower Zone N22) was identified in the interval 149-897C-1R-CC to -11R-CC (Table 7). These samples contain *Globorotalia truncatulinoides*, *Globorotalia tosaensis*, and *Globigerinoides extremus*. This interval yielded common to abundant planktonic foraminifers that were moderately to well preserved. Low to moderate numbers of well-preserved abyssal and reworked shallow-water benthic foraminifers also were identified in this interval. Sample 149-897C-5R-CC is barren of planktonic and benthic foraminifers.

Pliocene age sediments (Zones N19 to N21) were identified in the interval 149-897C-12R-CC to -17R-CC. These samples are characterized by the absence of *G. truncatulinoides* and *Sphaeroidinellopsis seminulina*, and, with no zonal markers present, no further age refinement was possible.

Early to early late Pliocene age sediments were identified in the interval 149-897C-18R-CC to -25R-CC. This interval is marked by the presence of *S. seminulina* at the top and *Globorotalia crassaformis* at the base and can be assigned to Zone N19.

Sample 149-897C-26R-CC contains *Globorotalia ronda* and *S. seminulina*. The sample was assigned to Zones N18 and N19, which are of latest Miocene to early late Pliocene age. No zonal marker species were present in Sample 149-897C-27R-CC. Sample 149-897C-28R-CC is characterized by the presence of *Neogloboquadrina acostaensis* and the absence of *Neogloboquadrina humerosa*. The sample can be assigned to Zone N16, which is of late Miocene (Tortonian) age. A hiatus was inferred between Samples 149-897C-26R-CC and -28R-CC, where Zone N17 is missing. No zonal marker species were present in Sample 149-897C-29R-CC. Sample 149-897C-30R-CC contains *Catapsydrax stainforthi* and *Globorotalia johsi peripheroronda* and can be assigned to Zones N6 (upper) and N7, which are of early Miocene age. A hiatus was interpreted between Samples 149-897C-28R-CC and -30R-CC, where Zones N8 to N15, from late early to middle Miocene, are missing. Samples 149-897C-31R-CC, -33R-CC, and -34R-CC are barren.

Sample 149-897C-35R-CC contains *Globigerinoides primordius* and can be assigned to Zones P22 (upper part) to "N4," which are

of late Oligocene to earliest Miocene age. Samples 149-897C-36R-CC and -37R-CC are barren. Sample 149-897C-38R-CC contains no zonal marker species.

The interval 149-897C-39R-CC to -41R-CC is characterized by the absence of *Globigerinoides* spp. and the absence of *Globigerina ciperoensis angulisuturalis*. It was assigned to the upper part of the late Oligocene (Zone P22).

Sample 149-897C-42R-CC contains *Globigerina ciperoensis angulisuturalis* and can be assigned to the lower part of Zone P22, which is also of late Oligocene age. The interval 149-897C-43R-CC to -45R-CC is characterized by the presence of *Globorotalia opima opima* at the top and *Globigerina ciperoensis angulisuturalis* at the base. The interval can be assigned to Zone P21, which is of late early to early late Oligocene age.

Sample 149-897C-46R-CC contains no marker species, and Samples 149-897C-47R-CC and -48R-CC are barren of planktonic and benthic foraminifers. Sample 149-897C-49R-CC is marked by the presence of *Pseudohastigerina micra* and can be assigned to Zones P18 and lower part of P19/20, which are of early Oligocene age. Sample 149-897C-50R-CC is barren of planktonic foraminifers. Samples 149-897C-51R-CC and -52R-CC contain no marker species. Analysis of additional Sample 149-897C-51R-1, 13-15 cm, yielded *Hantkenina* spp., indicating that late Eocene age strata had been reached (Zones P15-P17).

Sample 149-897C-53R-CC contains *Globigerina eoacaena* and was interpreted as late Eocene age, because sediments of this age already were recorded in Sample 149-987C-51R-1, 13-15 cm. Sample 149-897C-54R-CC is barren of planktonic foraminifers. The interval 149-897C-55R-CC to -58R-CC contains a middle Eocene planktonic foraminiferal assemblage (Zones P11(upper)-P14) characterized by the presence of *Truncorotaloides topilensis* and *Truncorotaloides rorhi* at the top and *Globigerinathea index* at the base. Sample 149-897C-59R-CC is characterized by rare specimens of *Morozovella spinulosa* and the absence of *Globigerinathea index*. The sample can be assigned to Zones P9 to P11 (lower), which are of late early to early middle Eocene.

Samples 149-897C-60R-CC and -61R-CC are barren of planktonic foraminifers and contain rare agglutinated benthic foraminifers that are not age-diagnostic and rare ichthyoliths. Samples 149-897C-60R-1, 83-85 cm; -61R-2, 12-14 cm; -61R-2, 17-19 cm; -61R-2, 92-94 cm; and -61R-4, 24-26 cm; also contain agglutinated benthic foraminifers (*Glomospira* spp. and *Recurvoides* spp.), radiolarians, and ichthyoliths. Sample 149-897C-62R-CC is barren of planktonic and benthic agglutinated foraminifers. Samples 149-897C-62R-1,

Table 7. Distribution of planktonic foraminifers in Hole 897C.

| Age | Zone | Core | Abundance | Preservation | <i>Globigerina bulloides</i> | <i>Globigerinoides extremus</i> | <i>G. ruber alba</i> | <i>Globorotati crassaformis crassaformis</i> | <i>G. inflata</i> | <i>G. scitula</i> | <i>G. tosaensis</i> | <i>G. triangula</i> | <i>G. truncatulinoides</i> | <i>Neoglobobulimina acostaensis</i> | <i>N. duterlei</i> | <i>N. humerosa</i> | <i>N. pachyderma</i> | <i>Orbulina universa</i> | <i>Globigerinoides obliquus</i> | <i>Globorotalia crassula</i> | <i>Globigerinita naparimaensis</i> | <i>Sphaeroidinellopsis seminulina</i> | <i>Sphaeroidinellopsis paenedehiscens</i> | <i>Orbulina suturalis</i> | <i>Globorotalia ronda</i> | <i>Globobulimina vancouveriana</i> | <i>Globorotalia tumida</i> | <i>G. merotumida</i> | <i>Catapsydrax stainforthi</i> | <i>Globorotalia fohsi peripheroronda</i> | <i>Globorotalia meyeri</i> | <i>Globorotalia praescitula</i> | <i>Catapsydrax unicavus</i> | | | | | |
|-------------------|---------|------|-----------|--------------|------------------------------|---------------------------------|----------------------|----------------------------------------------|-------------------|-------------------|---------------------|---------------------|----------------------------|-------------------------------------|--------------------|--------------------|----------------------|--------------------------|---------------------------------|------------------------------|------------------------------------|---------------------------------------|-------------------------------------------|---------------------------|---------------------------|------------------------------------|----------------------------|----------------------|--------------------------------|------------------------------------------|----------------------------|---------------------------------|-----------------------------|---|---|---|--|--|
| l. Pl. to e. Ple. | N22 | 1R | A | G | F | R | F | F | F | F | R | F | F | R | R | R | C | C | | | | | | | | | | | | | | | | | | | | |
| | | 2R | A | G | F | R | F | F | F | F | R | F | F | F | R | R | R | F | C | R | R | | | | | | | | | | | | | | | | | |
| | | 3*R | R | M | | | | | | | | | | | | | | | | | | | | | | | | | | | | | | | | | | |
| | | 4R | A | G | F | R | F | | F | R | | | F | R | R | | | F | R | R | R | | | | | | | | | | | | | | | | | |
| | | 5R | B | | | | | | | | | | | | | | | | | | | | | | | | | | | | | | | | | | | |
| | | 6R | F | G | R | | | R | R | | | | R | R | | | | R | R | | | | | | | | | | | | | | | | | | | |
| | | 7R | C | G | | | | R | | | | | | | | | | | | R | | | | | | | | | | | | | | | | | | |
| | | 8R | C | G | R | | | | | R | | | | | | | | | R | R | | | | | | | | | | | | | | | | | | |
| | | 9R | C | G | F | | | R | R | R | | R | R | R | R | | | | F | R | | | | | | | | | | | | | | | | | | |
| | | 10R | C | M | | | | R | R | | R | F | R | | | | | | F | | | | | | | | | | | | | | | | | | | |
| | | 11R | A | G | F | C | R | | | | | F | | R | F | R | | R | C | | | R | | | | | | | | | | | | | | | | |
| Pliocene | N19-N21 | 12R | F | M | | | | | | | | | | | | | | | | | | | | R | | | | | | | | | | | | | | |
| | | 13R | X | | | | | | | | | | | | | | | | | | | | | | | | | | | | | | | | | | | |
| | | 14R | A | M | R | | | | R | | | R | | | | | | | R | R | | | | | | | | | | | | | | | | | | |
| | | 15R | C | G | R | | | | | | | | | | | | | | R | | | | | | | | | | | | | | | | | | | |
| | | 16R | C | M | | | | | | R | | | R | | | | | | | | | | | | | | | | | | | | | | | | | |
| | N19 | 18R | C | M | R | | | | | | | | | | | | | | F | R | | | R | | | | | | | | | | | | | | | |
| | | 19R | C | M | | | | | | | | | | | R | | | | R | | | | | R | | | | | | | | | | | | | | |
| | | 20*R | F | M | | | | | | | | | | | | | | | | | | | | | | | | | | | | | | | | | | |
| | | 21*R | F | M | | | | | | | | | | | | | | | | | | | | | | | | | | | | | | | | | | |
| | | 22R | C | M | R | | R | | | | | | | | | | | | | | | | | | | | | | | | | | | | | | | |
| | | 23*R | C | M | | | | | | | | | | | | | | | | | | | | | | | | | | | | | | | | | | |
| 24R | A | M | | | R | | R | | | | | | | | | | | | | | | | | | | | | | | | | | | | | | | |
| 25R | A | G | F | | | R | R | | | | | | | | | | R | F | | | | | | | | | | | | | | | | | | | | |
| I. M-P | N18-N19 | 26R | C | M | | | | | | | | | | | | | | | | | | | | R | | | | | | | | | | | | | | |
| ? | ? | 27*R | R | M | | | | | | | | | | | | | | | | | | | | | | | | | | | | | | | | | | |
| I. Mio. | N16 | 28R | C | M | | | | | | | | | | F | | | F | R | | | | | | | R | R | R | R | | | | | | | | | | |
| ? | ? | 29*R | R | P | | | | | | | | | | | | | | | | | | | | | | | | | | | | | | | | | | |
| e. Mio. | N6-N7 | 30R | C | M | | | | | | | | | | | | | | | | | | | | | | | | | | | | | R | R | R | R | | |
| ? | ? | 31R | B | | | | | | | | | | | | | | | | | | | | | | | | | | | | | | | | | | | |
| 32R | X | | | | | | | | | | | | | | | | | | | | | | | | | | | | | | | | | | | | | |
| 33R | B | | | | | | | | | | | | | | | | | | | | | | | | | | | | | | | | | | | | | |
| 34R | B | | | | | | | | | | | | | | | | | | | | | | | | | | | | | | | | | | | | | |
| I. O.-e. M. | P22-N4 | 35R | A | M | | | | | | | | | | | | | | | | | | | | | | R | | | | | | F | | R | | | | |
| ? | ? | 36R | B | | | | | | | | | | | | | | | | | | | | | | | | | | | | | | | | | | | |
| 37R | B | | | | | | | | | | | | | | | | | | | | | | | | | | | | | | | | | | | | | |
| 38R | R | P | | | | | | | | | | | | | | | | | | | | | | | | R | | | | | | | | | | | | |
| late Oli. | P22 | 39R | F | M | | | | | | | | | | | | | | | | | | | | | | | | | | | | | | | | | | |
| 40*R | R | M | | | | | | | | | | | | | | | | | | | | | | | | | | | | | | | | | | | | |
| 41R | F | M | | | | | | | | | | | | | | | | | | | | | | | | | | | | | | | | | | | | |
| 42R | F | M | | | | | | | | | | | | | | | | | | | | | | | | | | | | | | | | | | | | |
| Oli. | P21 | 43R | A | G | | | | | | | | | | | | | | | | | | | | | | | | | | | | | | | | | | |
| 44*R | R | P | | | | | | | | | | | | | | | | | | | | | | | | | | | | | | | | | | | | |
| 45R | F | M | | | | | | | | | | | | | | | | | | | | | | | | | | | | | | | | | | | | |
| ? | ? | 46*R | R | P | | | | | | | | | | | | | | | | | | | | | | | | | | | | | | | | | | |
| 47R | B | | | | | | | | | | | | | | | | | | | | | | | | | | | | | | | | | | | | | |
| 48 | B | | | | | | | | | | | | | | | | | | | | | | | | | | | | | | | | | | | | | |
| e. Oli. | P18-P20 | 49 | F | M | | | | | | | | | | | | | | | | | | | | | | | | | | | | | | | | | | |
| ? | ? | 50 | B | | | | | | | | | | | | | | | | | | | | | | | | | | | | | | | | | | | |
| I. Eoc. | P15-P17 | 51 | R | M | | | | | | | | | | | | | | | | | | | | | | | | | | | | | | | | | | |
| 52* | R | M | | | | | | | | | | | | | | | | | | | | | | | | | | | | | | | | | | | | |
| 53 | R | M | | | | | | | | | | | | | | | | | | | | | | | | | | | | | | | | | | | | |
| ? | ? | 54 | B | | | | | | | | | | | | | | | | | | | | | | | | | | | | | | | | | | | |
| mid. Eoc. | P11-P14 | 55 | C | G | | | | | | | | | | | | | | | | | | | | | | | | | | | | | | | | | | |
| 56 | C | M | | | | | | | | | | | | | | | | | | | | | | | | | | | | | | | | | | | | |
| 57 | R | M | | | | | | | | | | | | | | | | | | | | | | | | | | | | | | | | | | | | |
| 58 | F | M | | | | | | | | | | | | | | | | | | | | | | | | | | | | | | | | | | | | |

Table 7 (continued).

SITE 897

| Age | Zone | Core | <i>Globigerina ciperensis angustiumblicata</i> | <i>Globigerinoides primordius</i> | <i>Catapsydrax stainforthi</i> | <i>Globorotalia nana/continua</i> transition | <i>Globoquadrina dehiscens</i> | <i>Globorotaloides suteri</i> | <i>Catapsydrax dissimilis</i> | <i>Globigerina ciperensis ciperensis</i> | <i>Globorotalia optima nana</i> | <i>G. optima optima</i> | <i>G. ciperensis angulituralis</i> | <i>Pseudohaastergina micra</i> | <i>Globigerina tripartita</i> | <i>G. eocaena</i> | <i>Morozovella spinulosa</i> | <i>Truncorotaloides rohri</i> | <i>T. topilensis</i> | <i>Turborotalia cerroazulensis</i> | <i>T. increbescens</i> | <i>Globigerina semii</i> | <i>Globigerinatheka index</i> | <i>Morozovella spinulosa coronata</i> | <i>M. lehnerti</i> | <i>M. aragonensis</i> | <i>Truncorotaloides pseudotopilensis</i> | | |
|--------------------|---------|------|------------------------------------------------|-----------------------------------|--------------------------------|----------------------------------------------|--------------------------------|-------------------------------|-------------------------------|------------------------------------------|---------------------------------|-------------------------|------------------------------------|--------------------------------|-------------------------------|-------------------|------------------------------|-------------------------------|----------------------|------------------------------------|------------------------|--------------------------|-------------------------------|---------------------------------------|--------------------|-----------------------|------------------------------------------|--|--|
| l. Pli. to e. Ple. | N22 | 1R | | | | | | | | | | | | | | | | | | | | | | | | | | | |
| | | 2R | | | | | | | | | | | | | | | | | | | | | | | | | | | |
| | | 3*R | | | | | | | | | | | | | | | | | | | | | | | | | | | |
| | | 4R | | | | | | | | | | | | | | | | | | | | | | | | | | | |
| | | 5R | | | | | | | | | | | | | | | | | | | | | | | | | | | |
| | | 6R | | | | | | | | | | | | | | | | | | | | | | | | | | | |
| | | 7R | | | | | | | | | | | | | | | | | | | | | | | | | | | |
| | | 8R | | | | | | | | | | | | | | | | | | | | | | | | | | | |
| | | 9R | | | | | | | | | | | | | | | | | | | | | | | | | | | |
| | | 10R | | | | | | | | | | | | | | | | | | | | | | | | | | | |
| | | 11R | | | | | | | | | | | | | | | | | | | | | | | | | | | |
| Pliocene | N19-N21 | 12R | | | | | | | | | | | | | | | | | | | | | | | | | | | |
| | | 13R | | | | | | | | | | | | | | | | | | | | | | | | | | | |
| | | 14R | | | | | | | | | | | | | | | | | | | | | | | | | | | |
| | | 15R | | | | | | | | | | | | | | | | | | | | | | | | | | | |
| | | 16R | | | | | | | | | | | | | | | | | | | | | | | | | | | |
| 17*R | | | | | | | | | | | | | | | | | | | | | | | | | | | | | |
| l. M-P | N18-N19 | 18R | | | | | | | | | | | | | | | | | | | | | | | | | | | |
| | | 19R | | | | | | | | | | | | | | | | | | | | | | | | | | | |
| | | 20*R | | | | | | | | | | | | | | | | | | | | | | | | | | | |
| | | 21*R | | | | | | | | | | | | | | | | | | | | | | | | | | | |
| | | 22R | | | | | | | | | | | | | | | | | | | | | | | | | | | |
| | | 23*R | | | | | | | | | | | | | | | | | | | | | | | | | | | |
| ? | ? | 24R | | | | | | | | | | | | | | | | | | | | | | | | | | | |
| | | 25R | | | | | | | | | | | | | | | | | | | | | | | | | | | |
| ? | ? | 26R | | | | | | | | | | | | | | | | | | | | | | | | | | | |
| l. Mio. | N16 | 28R | | | | | | | | | | | | | | | | | | | | | | | | | | | |
| ? | ? | 29*R | | | | | | | | | | | | | | | | | | | | | | | | | | | |
| e. Mio. | N6-N7 | 30R | | | | | | | | | | | | | | | | | | | | | | | | | | | |
| l. O.-e. M. | P22-N4 | 31R | | | | | | | | | | | | | | | | | | | | | | | | | | | |
| | | 32R | | | | | | | | | | | | | | | | | | | | | | | | | | | |
| | | 33R | | | | | | | | | | | | | | | | | | | | | | | | | | | |
| ? | ? | 34R | | | | | | | | | | | | | | | | | | | | | | | | | | | |
| ? | ? | 35R | R | R | | | | | | | | | | | | | | | | | | | | | | | | | |
| late Oli. | P22 | 36R | | | | | | | | | | | | | | | | | | | | | | | | | | | |
| | | 37R | | | | | | | | | | | | | | | | | | | | | | | | | | | |
| | | 38R | | | | | | | | | | | | | | | | | | | | | | | | | | | |
| | | 39R | | | | | | | | | | | | | | | | | | | | | | | | | | | |
| Oli. | P21 | 40*R | | | | | | | | | | | | | | | | | | | | | | | | | | | |
| | | 41R | | | | | | | | | | | | | | | | | | | | | | | | | | | |
| | | 42R | R | | | | | | | | | | | | | | | | | | | | | | | | | | |
| ? | ? | 43R | | | | | | | | | | | | | | | | | | | | | | | | | | | |
| | | 44*R | | | | | | | | | | | | | | | | | | | | | | | | | | | |
| | | 45R | | | | | | | | | | | | | | | | | | | | | | | | | | | |
| e. Oli. | P18-P20 | 46*R | | | | | | | | | | | | | | | | | | | | | | | | | | | |
| | | 47R | | | | | | | | | | | | | | | | | | | | | | | | | | | |
| | | 48 | | | | | | | | | | | | | | | | | | | | | | | | | | | |
| ? | ? | 49 | | | | | | | | | | | | | | | | | | | | | | | | | | | |
| ? | ? | 50 | | | | | | | | | | | | | | | | | | | | | | | | | | | |
| l. Eoc. | P15-P17 | 51 | | | | | | | | | | | | | | | | | | | | | | | | | | | |
| | | 52* | | | | | | | | | | | | | | | | | | | | | | | | | | | |
| | | 53 | | | | | | | | | | | | | | | | | | | | | | | | | | | |
| ? | ? | 54 | | | | | | | | | | | | | | | | | | | | | | | | | | | |
| mid. Eoc. | P11-P14 | 55 | | | | | | | | | | | | | | | | | | | | | | | | | | | |
| | | 56 | | | | | | | | | | | | | | | | | | | | | | | | | | | |
| | | 57 | | | | | | | | | | | | | | | | | | | | | | | | | | | |
| | | 58 | | | | | | | | | | | | | | | | | | | | | | | | | | | |

Table 7 (continued).

| Age | Zone | Core | Abundance | Preservation | |
|----------|--------|------|-----------|--------------|--|
| em. Eoc. | P9-P11 | 59 | R | P | |
| | | 60 | B | | |
| | | 61 | B | | |
| ? | ? | 62 | B | | |
| | | 63 | B | | |
| | | 64 | XX | | |
| | | 65 | B | | |

32-34 cm; -62R-1, 69-71 cm; -62R-3, 54-56 cm; and -62R-4, 11-13 cm; contain no foraminifers, radiolarians, diatoms, or ichthyoliths. Sample 149-897C-62R-2, 48-50 cm, contains a single specimen of *Glomospira* spp., while radiolarians, diatoms, and ichthyoliths are absent. Sample 149-897C-62R-4, 54-56 cm, contains very small hedbergellids (*Hedbergella delrioensis*) and globigerinoidinids, indicating an Aptian to Albian age. A single specimen of a cone-shaped radiolarian was found in this sample. Samples 149-897C-63R-CC and -65R-CC are barren of planktonic and benthic foraminifers, radiolarians, diatoms, and ichthyoliths.

Hole 897D

The interval 149-897D-1R-CC to -2R-CC contains a middle Eocene (Zones P11-lower P12) planktonic foraminiferal assemblage characterized by the co-occurrence of *Acarinina pentacamerata* and *Globigerinatheka index*. The interval 149-897D-3R-CC to -5R-CC is barren of planktonic foraminifers. Sample 149-897D-3R-CC contains rare ichthyoliths. Samples 149-897D-4R-CC and -5R-CC contain rare agglutinated benthic foraminifers (*Glomospira* spp. and *Recurvoides* spp.) and rare ichthyoliths. Sample 149-897D-6R-CC is characterized by the presence of a diverse assemblage of very small hedbergellids and globigerinelloids, indicating an Aptian to Albian age. The species *Hedbergella simplex*, found in this core, would restrict the age of this core to the Albian, as the first evolutionary appearance of this species is in lower Albian sediments (Tourmakine and Luterbacher, 1985). Also characteristic of this sample are the relatively few cone-shaped radiolarians. Sample 149-897D-7R-CC contains pyritized radiolarians and diatoms. Sample 149-897D-8R-CC is completely barren of any microfauna.

PALEOMAGNETISM

Archive-half sections of cores from Holes 897A, 897C, and 897D were measured using the cryogenic magnetometer. Most sections were alternating-field (AF)-demagnetized at 10-cm intervals using a peak field intensity of 15 mT. When time permitted, sections of lithostratigraphic Unit IV were demagnetized progressively at 5-cm intervals using peak fields of 2, 5, 10, and 15 mT. A total of 31 discrete samples, taken from the working halves of cores recovered from the three holes, were AF demagnetized progressively up to a peak field of 50 mT, and 12 microwires from Holes 897C and 897D were thermally demagnetized to determine directional stability and to verify magnetostratigraphic results from the cryogenic magnetometer. Magnetic susceptibility was measured at 3- to 5-cm intervals on most of the recovered cores from Holes 897A, 897C, and 897D.

Demagnetization Behavior

Whole-core Pass-through Measurements

One of the major experimental requirements in paleomagnetic research is to isolate the characteristic remanent magnetization by selective removal of secondary magnetization. In Figure 22, we show the natural remanent magnetization (NRM) intensities and inclinations before and after 15-mT AF demagnetization observed in Cores 149-897D-4R and -5R. The NRM inclinations are strongly biased toward high positive inclinations (65° to 87°). AF demagnetization to 15 mT removes a soft, possibly drilling-induced component, as indicated by a change in inclination to values ranging from 10° to 60°. The expected normal inclination at Site 897 is about 60°. That the NRM inclinations are biased toward the vertical (+90°) in most cores suggests that drilling-induced magnetization is present.

In several cores, we observed a dramatic decrease in magnetic intensity by one or two orders of magnitude from the upper to the lower part of a single core. Examples of this phenomenon are found in Cores 149-897C-8R (117.9 mbsf), -12R (156.6 mbsf), -19R (228.6 mbsf), and -35R (379.0 mbsf). The magnetic susceptibility data of these cores also show extremely high-amplitude spikes (with values exceeding 1.88×10^{-3} SI units). We suspect that this is also related to drilling. It may have been caused by rust flakes that fell into the uppermost portions of each core and/or exposure to a strongly magnetized core barrel.

AF and Thermal Demagnetization of Discrete Samples

Oriented samples (6-cm³ plastic cubes or 10-cm³ minicores) were collected from almost every core: (1) to verify the magnetostratigraphic results from the cryogenic magnetometer and (2) to understand the magnetic behavior of the sediments during stepwise demagnetization. Thirty-one of these samples were measured using the Mol-spin magnetometer, with progressive AF demagnetization steps to 50 mT on a Schonstedt GSD-1 AF-demagnetizer. During AF demagnetization of the discrete samples with this instrument, we noticed that several samples acquired spurious magnetizations above 50 mT (e.g., Fig. 23). Tests, conducted after demagnetization along each positive and negative axis, suggest that these spurious magnetizations were mainly an anhysteretic remanent magnetization (ARM), produced along the axis of demagnetization. Thus, the determination of the magnetization carried by high-coercivity magnetic grains was hindered, and higher demagnetization steps will have to be made in shore-based studies on a triaxial tumbling AF demagnetizer.

Progressive thermal demagnetization was performed on 12 minicores from representative lithified cores in Holes 897C and 897D to

Table 7 (continued).

| Age | Zone | Core | |
|----------|--------|------|---|
| em. Eoc. | P9-P11 | 59 | R |
| | | 60 | |
| | | 61 | |
| ? | ? | 62 | |
| | | 63 | |
| | | 64 | |
| | | 65 | |

Notes: Age: em. Eoc. = early to middle Eocene; mid. Eoc. = middle Eocene; l. Eoc. = late Eocene; e. Oli. = early Oligocene; Oli. = Oligocene; late Oli. = late Oligocene; l. O.-e. M. = late Oligocene to early Miocene; e. Mio. = early Miocene; l. Mio. = late Miocene; l. M.-P. = late Miocene to Pliocene; l. Pli. to e. Ple. = late Pliocene to Pleistocene. A "*" in the "Core" column indicates that core-catcher sample contained only juvenile planktonic foraminifers or no marker species. Abundance: A = Abundant; C = Common; F = Few; R = Rare; B = Barren; X = no core recovery; XX = core-catcher was rock. Preservation: G = Good; M = Moderate; P = Poor.

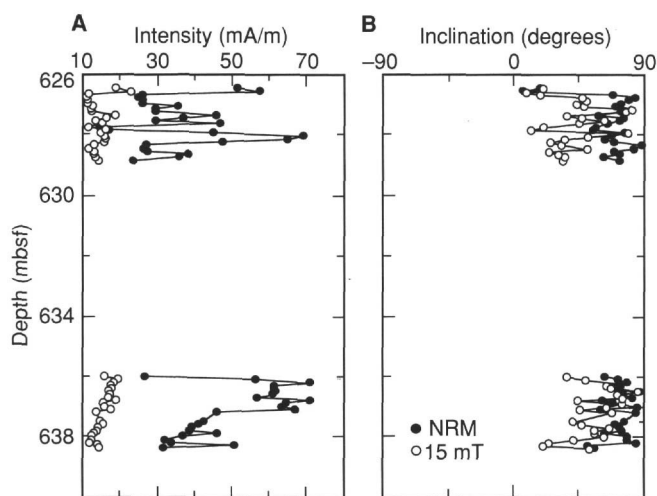


Figure 22. Downhole variation of intensity (A) and inclination (B) of NRM and stable magnetization after AF demagnetization at 15 mT for Cores 149-897D-4R (upper part) and -5R (lower part). NRM inclinations are strongly biased toward high positive inclinations, suggesting that drilling-induced magnetization is present. AF demagnetization to 15 mT generally can remove this drilling-induced magnetization, as indicated by changes in inclination and intensity.

test the stability of the magnetization vs. temperature and to help identify the magnetic minerals. We found that removal of secondary magnetization was better accomplished through thermal demagnetization than through AF demagnetization (Fig. 24). A secondary magnetic component of magnetization was removed at low temperatures (300°C), and a component of magnetization having higher unblocking temperatures (up to 620°C) could be identified. Despite the apparent stability of the magnetization of these samples, the absence of core orientation and information about the attitude of the bedding planes precluded a more detailed interpretation of the paleomagnetic data.

Magnetic Results

Hole 897A

In Hole 897A, paleomagnetic results were obtained from only three cores because of poor recovery. Evidence for remagnetization

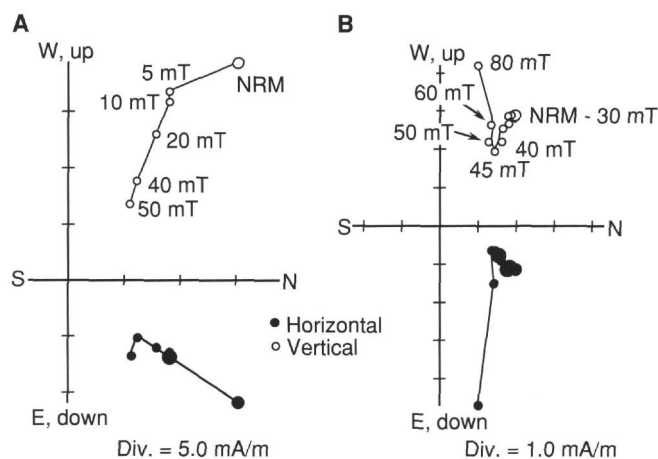


Figure 23. Representative vector end-point diagram showing the results of AF demagnetization for discrete Samples 149-897C-15R-4, 24-26 cm (A) and -20R-2, 64-71 cm (B). Open and solid circles represent vector end points projected onto the vertical and horizontal planes, respectively.

imparted by coring was observed. Clayey silts appear to be more easily affected by this type of remagnetization than the turbidite units recovered in Hole 897C. We observed only normal magnetic polarity.

Holes 897C and 897D

The paleomagnetic properties of material recovered from Holes 897C and 897D reflect the observed lithologic variations. Thus, the paleomagnetic data from these two holes are discussed according to the major lithologic changes and are summarized below:

1. Lithostratigraphic Unit I (0.0-292.0 mbsf; see "Lithostratigraphy" section, this chapter). NRM intensities range from 10^{-1} to 10 mA/m. AF demagnetization of seven discrete samples indicates that, in most cases, stable magnetization can be identified, although the demagnetization curves did not reach the origin of the vector plots (because of the ARM problem with the AF demagnetizer mentioned above). Polarity reversals occur in several intervals in this unit, and magnetostratigraphy is discussed below. The polarity sequence deter-

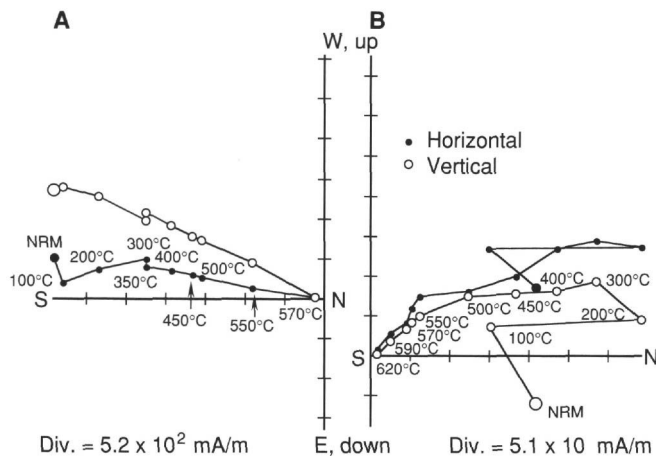


Figure 24. Representative vector end-point diagram showing the results of thermal demagnetization for discrete Samples 149-897C-66R-4, 15-17 cm (A) and -897D-11R-4, 71-73 cm (B). Open and solid circles represent vector end points projected onto the vertical and horizontal planes, respectively.

mined from measurements in the cryogenic magnetometer was confirmed by progressive AF demagnetization of discrete samples.

2. Lithostratigraphic Unit II (292.0-619.7 mbsf in Hole 897C, and 596.0-622.9 mbsf in Hole 897D; see "Lithostratigraphy" section, this chapter). The average NRM intensities were approximately 2 mA/m, with many intervals having magnetization of less than 5×10^{-1} mA/m. Intensity generally decreased by a factor of one-third or more after AF demagnetization at 15 mT. Four discrete samples were AF-demagnetized with the Schonstedt AF demagnetizer and were measured using the Molspin magnetometer. The Molspin magnetometer apparently lacked the sensitivity necessary to measure these weakly magnetized samples accurately. Thus, five samples from this unit in Hole 897D were selected to be demagnetized and were measured in the 2G cryogenic magnetometer. Unfortunately, because of the limit to the applied demagnetization field (20 mT) in the on-line AF demagnetizer, stable magnetization was not clearly resolved. The viscous magnetic properties of sediments from this unit will necessitate that discrete samples be measured ashore in a zero magnetic field.

3. Lithostratigraphic Unit III (619.7-648.7 mbsf in Hole 897C and 622.9-655.2 mbsf in Hole 897D; see "Lithostratigraphy" section, this chapter). The conglomerate and coarse sandstone layers in this unit do not provide reliable magnetic signals. On the other hand, the NRM intensity of the brown claystone is strong (about 15 mA/m) and presents an interesting magnetic signal. As shown in Figure 25, the NRM inclinations observed from Section 149-897C-61R-1 are biased toward positive values, indicating the presence of a drilling-induced remagnetization and/or a normal component of viscous magnetization. Upon demagnetization to 15 mT, we observed a shift toward a negative inclination and a significant decrease in intensity. The reversed polarity of magnetization was also confirmed by progressive AF demagnetization in three discrete samples from this section (squares in Fig. 25). The significance of this reversal is discussed in the "Magnetostratigraphy" section (see below).

4. Lithostratigraphic Unit IV (648.7-671.0 mbsf in Hole 897C and 655.2-693.8 mbsf in Hole 897D; see "Lithostratigraphy" section, this chapter). As in lithostratigraphic Unit III, a probable overprinting caused by drilling is present that generally can be removed by demagnetization at 10 mT. Thermal and AF demagnetizations for five discrete samples suggest that the magnetization in these rocks is complex and will need to be interpreted with caution.

Below 677.5 mbsf in Hole 897C and below 693.8 mbsf in Hole 897D, all cores are extensively serpentinized peridotites. Pervasive

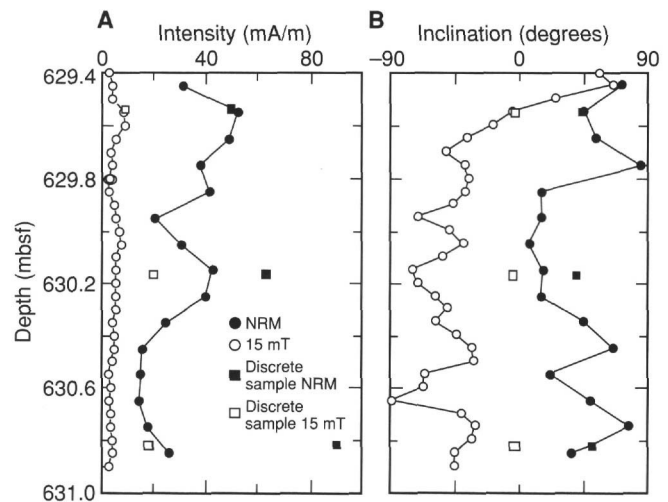


Figure 25. Remanent magnetization before and after 15-mT AF demagnetization as a function of sub-bottom depth. Intensities (A) and inclinations (B) of archive halves and discrete samples from Section 149-897C-61R-1 are shown.

brittle deformation with serpentinite and calcite veining has affected the entire section (see "Structural Geology" section, this chapter). AF and thermal demagnetizations in nine discrete samples revealed an apparently stable component of magnetization. Information is lacking about core orientation and bedding attitude of these rocks, which precludes a more detailed interpretation of the paleomagnetic data at present. It may be possible after further work to investigate whether a component of viscous remagnetization parallel to the present-day magnetic field has been recorded in these rocks that may be used to reorient these cores. Rotary coring often disrupts the core by breaking it into several pieces that rotate independently of each other within the core liner. These effects can sometimes be removed using magnetic declination data, assuming that each segment having a constant declination is a homogeneous drilling biscuit. Several sections in Cores 149-897C-71R and -73R, and in Core 149-897D-23R exhibit drilling-induced rotations. The orientations of the veins in different parts of these sections suggest that these can be divided into two groups, with a difference in orientation of about 90° . Paleomagnetic declinations measured between the groups are also about 90° apart, suggesting that they rotated about 90° with respect to each other during drilling.

Magnetostratigraphy

Age control in the sediments at Site 897 is primarily from nanno-fossil and planktonic foraminiferal biostratigraphy. Preliminary magnetostratigraphic interpretation mostly agrees with biostratigraphic ages (Table 8). The normal polarity of Cores 149-897A-1R through -3R suggests that these sediments were deposited during the Brunhes Chron (i.e., age <0.78 Ma), which agrees well with the biostratigraphic age estimate (see "Biostratigraphy" section, this chapter). Although dates (based on foraminifers) suggest that Cores 149-897A-4R through -6R were deposited within the Matuyama reversed Chron, we observed no evidence for a reversed polarity in these cores. However, most sections of these cores were highly disturbed by drilling, making the polarity record less reliable. The Brunhes/Matuyama boundary was not observed in Hole 897C. The first evidence for a reversed magnetization occurs in Core 149-897C-10R (137.2-138.7 mbsf), which may correspond to the Olduvai (1.81 Ma), assuming that the biostratigraphic ages (Table 8) are correct. Samples between 137.2 and 181.8 mbsf (Cores 149-897C-1 OR to -14R) tentatively have been assigned to the late Pliocene on the basis of preliminary biostratigraphic data. Thus, the reversal sequence found in this interval suggests that these

Table 8. Preliminary paleomagnetic and biostratigraphic datums at Site 897.

| Magnetic datum (Chron or Subchron) | Biostratigraphic datums | Code/Zones (N, F) | Age (Ma) Magnetism | Age (Ma) Biostratigraphy | Depth range (mbsf) Magnetism | Depth range (mbsf) Biostratigraphy |
|---------------------------------------|----------------------------|----------------------|------------------------|-----------------------------|------------------------------------|------------------------------------------|
| Lower Olduvai Reunion (?) | 8 | NN18, N22 | 1.88 2.06–2.09 | 1.81 | 137.2–138.7 138.7–146.8 | 130.5–134.2 |
| Gauss Gilbert | 10-11 | NN15, N19 | 2.45–2.91 3.40–3.87 | 3.56–3.8 | 175.8–198.1 224.1–262.7 | 185.4–291.5 |
| Upper Cochiti Nunivak | 12 | NN15, N16 ? | 3.87–3.99 4.12–4.26 | 4.1 | 264.2–265.7 310.9–312.4 | 291.4–301.2 |
| C9 + C10 (?) | 17-19 | NP24-NP25, P22? | 28.1–29.6 | 24.7–29.4 | 418.6–449.0 | 388.1–487.9 |

Note: See "Biostratigraphy" section (this chapter) for explanation of the codes.

sediments were deposited within the Gauss Chron (2.6-3.55 Ma). The next reversal was found in Cores 149-897C-19R through -23R (224.1-262.7 mbsf). Preliminary biostratigraphic evidence suggests that sediments from these cores are of early Pliocene age (NN15). Therefore, the shift in polarity from normal to reversed at Core 149-897C-19R (224.1 mbsf) may represent the Gauss/Gilbert boundary (3.55 Ma). A transition from normal to reversed polarity in Core 149-897C-28R (310.9-312.4 mbsf) might record the Nunivak Subchron (4.12-4.26 Ma); this is supported by the calcareous nannofossils found in this core (see Table 8).

The absence of a distinctive polarity sequence in cores of Oligocene age precludes independent correlation of polarity sequences with the geomagnetic polarity time scale. Based on the nannofossil and foraminiferal biostratigraphy, however, the polarity intervals found in cores from lithostratigraphic Unit II (see "Lithostratigraphy" section, this chapter) can be tentatively assigned ages. The reversed polarity found in Core 149-897C-39R at 418.6 mbsf may contain the lower part of reversed Chron C9 (corresponding to nannofossil Zone NP24), and the polarity change in Core 149-897C-43R (455.6 mbsf) may correspond to the boundary between Chrons C9 and C10. The magnetostratigraphy for the entire Eocene and Paleocene is unknown at this site. The next reversed polarity interval was found in Core 149-897C-61R. The brown clays in the upper part of the core (Section 149-897C-61R-1) exhibit reversed magnetization on the basis of both pass-through and discrete sample measurements (Fig. 25). The dark brown clays in the middle and lower parts of the core (Sections 149-897C-61R-2 to -4) exhibit normal polarity. Hence, the evidence for reversed magnetization occurs over less than one section.

Cores from lithostratigraphic Unit IV (see "Lithostratigraphy" section, this chapter) and from the basement did not provide any reliable polarity results; and no magnetostratigraphic interpretation is possible for these cores at present.

Although the preliminary magnetic polarity reversals in Hole 897C, summarized in Table 8, are prominent, more detailed paleomagnetic and biostratigraphic studies will be needed to construct a definitive magnetostratigraphy.

Magnetic Susceptibility

The downhole profile of magnetic susceptibility at Site 897 is shown in Figure 26. Poor core recovery and drilling disturbance in Hole 897A resulted in an incomplete record of susceptibility that is difficult to interpret. The magnetic susceptibility of Unit I in Hole 897C ranges from 1.25 to 8.79×10^{-4} SI units, with four large spikes (exceeding 1.88×10^{-3} SI units) in Cores 149-897C-8R (~120 mbsf), -12R (~160 mbsf), -19R (~230 mbsf), and -35R (~380 mbsf), respectively. These susceptibility spikes may have been caused by rust flakes from the drill pipes. The mixture of terrigenous sands and pelagic clays in this interval also produces a distinctive pattern of alternating high and low susceptibilities, which correlates well with turbidite layering (see Fig. 27 for an example). This characteristic susceptibility response might be useful for identifying turbidites using a magnetic susceptibility logging tool. Below 300 mbsf, susceptibility values gradually

decrease, corresponding to a decreasing NRM intensity and with a change in color from brown pelagic claystone to green and gray pelagic claystone (e.g., Cores 149-897C-29R and -30R), observed in Unit II. The color change and decrease in susceptibility are consistent with a transition from oxidized iron phases in the Miocene brown clays to reduced iron phases in the late Oligocene age green and gray clays. The suggested boundary between oxidized and reduced iron phases corresponds to the top of a region of high concentration of sulfate, which is apparent in interstitial water analyses (see "Inorganic Geochemistry" section, this chapter). Besides the big spike (3.14×10^{-3} SI units) near 380 mbsf, which is probably an artifact resulting from rust flakes, several smaller-scale susceptibility maxima were observed between 400 and 600 mbsf. These correspond to the clay-rich intervals of the pelagic host sediments and to the bioturbated zones at the tops of the calcareous turbidites in lithostratigraphic Subunit IIC.

Magnetic susceptibility increases from 1.26×10^{-4} (SI units) in Subunit IIIA to 6.28×10^{-3} (SI units) in Subunit IIIB, a trend that reflects the increasing abundance of opaque minerals observed in smear-slides (see "Lithostratigraphy" section, this chapter). A distinctive peak in susceptibility occurs at about 640 mbsf in Holes 897C and 897D (Fig. 27B; Cores 149-897C-62R and -897D-6R). Susceptibility peaks found in both holes exhibit similar magnitudes, and susceptibility plots are similar. Significant changes in rock type, magnetic polarity, and other physical properties at this depth suggest the need for a detailed study of this interval and for regional correlation with the other sites that were drilled during Leg 149.

Sharp increases in susceptibility occur at approximately 640 mbsf in Hole 897C and at 645 mbsf in Hole 897D. These increases correspond to the boundary between Subunits IIIA and IIIB and coincide with the appearance of conglomeratic material. The serpentized peridotite basement (see "Igneous and Metamorphic Petrology and Geochemistry" section, this chapter) has much higher susceptibility values (averaging 1.88×10^{-2} SI units) than the sedimentary section. The variability of susceptibility below 640 mbsf in Hole 897C reflects differences in the degree of alteration of the original peridotite. Two distinct groups of altered peridotite are indicated (Fig. 28). Moderately low susceptibility values (less than 1.26×10^{-2} SI units) are associated with highly altered serpentized peridotite, in which nearly all of the olivine and pyroxene have been replaced by serpentine with a clay texture. The least-altered peridotite has the highest susceptibility values (4.2×10^{-2} SI units; see Fig. 28). A similar multimodal pattern was observed in the acoustic velocity, in which samples having different degrees of alteration fall into distinct groups with very different velocities (see "Physical Properties" section, this chapter). Susceptibility measurements in cores from Hole 897D do not follow this trend; instead, they indicate a monotonically decreasing susceptibility, with increasing alteration of the basement rock.

IGNEOUS AND METAMORPHIC PETROLOGY AND GEOCHEMISTRY

The ocean/continent boundary of the West Iberia passive continental margin is characterized along its northern part, west of the Galicia

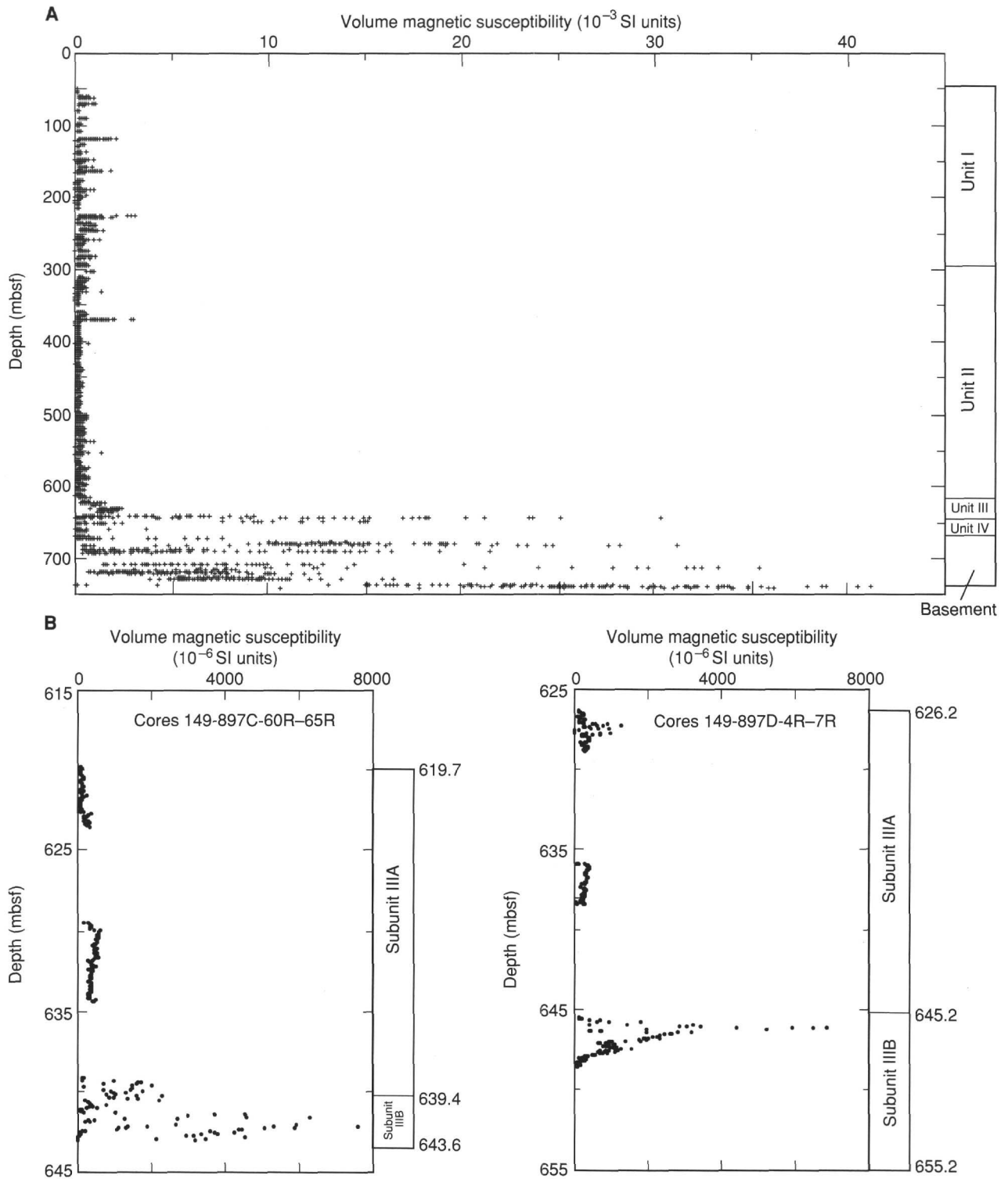


Figure 26. **A.** Plot of magnetic susceptibility as a function of sub-bottom depth from Hole 897C. **B.** Susceptibility variations in Subunits IIIA and IIIB, within Holes 897C and 897D.

Bank, by a 100-km-long peridotite ridge. This ridge was emplaced during Mesozoic continental rifting (Boillot, Girardeau, et al., 1988; Boillot, Comas, et al., 1988). Geophysical data suggest that this ridge extends southward beneath the sedimentary cover of the Iberia Abyssal Plain (Whitmarsh et al., 1990; Beslier et al., 1993). Site 897 is located in a small basin on the top of this basement ridge and was drilled to deter-

mine the nature of the basement and to test geophysical predictions. Two holes (897C and 897D), separated by 100 m, were drilled through a 678- to 694-m-thick sedimentary cover of Pleistocene to Hauterivian age. Drilling recovered basement cores composed of serpentinized peridotite (Fig. 29). In Hole 897C, 97.4 m of basement was drilled with 33.8% recovery, and in Hole 897D, 143.4 m with 54% recovery.

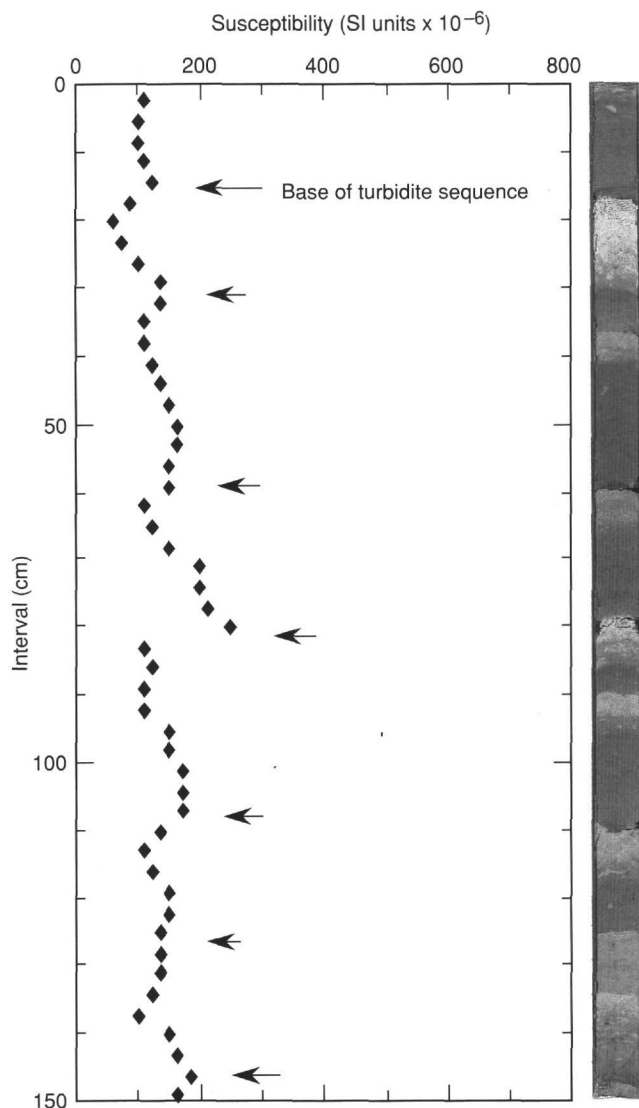


Figure 27. Correlation of magnetic susceptibility with turbidite layering in Section 149-897C-17R-2.

General Lithologic Description

Three sedimentary intervals are bounded by altered peridotite in the lowest sedimentary unit (Unit IV) encountered in Hole 897C (Intervals 149-897C-63R-1, 55 cm, through -63R-2, 40 cm; -897C-64R-1 through -64R-2; and -897C-65R-2, 88 cm, through -897C-65R-3, 20 cm), and one interval in the lowest part of the Unit IV at Hole 897D (Interval 149-897D-10R-3, 40 cm, through -10R-4, 115 cm; Fig. 29). Interval 149-897C-65R-3, 0-12 cm, is a breccia of uncertain origin, either sedimentary or volcanic, that contains diverse lithic fragments, including highly altered diabase. The other intervening hard-rock sections are highly altered peridotite, except the lowest one in Hole 897C, which contains harzburgite, pyroxenite, and serpentinized peridotite breccias. The serpentinite intervals have been tentatively interpreted as large blocks within the base of the sedimentary section (Unit IV).

The basement in both Holes 897C and 897D is composed of lithologically heterogeneous peridotite. The dominant lithology (about 85%) is serpentinized peridotite that originally contained 70%-80% olivine, 15%-20% pyroxene, and 1%-2% spinel. About 10% of this serpentinized peridotite is brecciated. Although relicts of clinopyroxene were recognized in most cores, extensive serpentinization inhibits

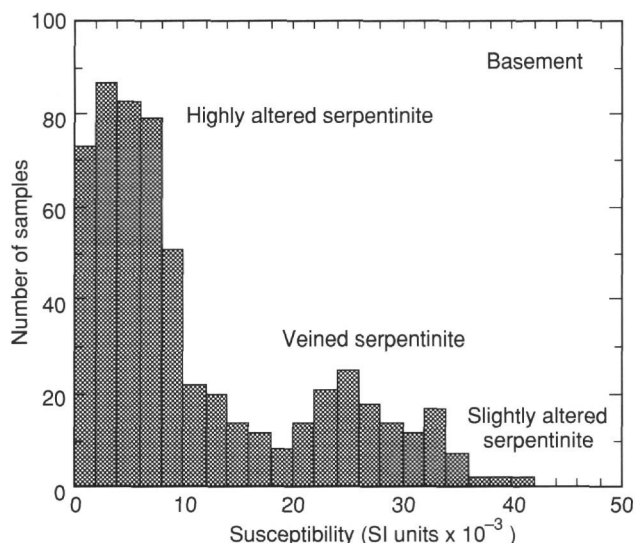


Figure 28. Histogram of susceptibility measurements from serpentinized peridotite basement in Hole 897C.

the precise determination of the proportion of clinopyroxene, and the peridotite was either harzburgite or lherzolite.

Approximately 10% of the recovered rocks is plagioclase-bearing peridotite; one-third of these rocks is brecciated. The proportion of plagioclase is highly variable (averaging 15%), but ranges up to 35%-40%. This facies is also pyroxene-rich (20%-30%), with 20%-70% olivine and 1%-5% spinel. A thick (30 cm) pyroxenitic zone was encountered in Hole 897C (Interval 149-897C-70R-1, 110-135 cm).

The remaining 5% of the serpentinized peridotite is a friable serpentinite breccia found at the top of the basement in Hole 897C (Sections 149-897C-66R-1 to -66R-3), in the largest block immediately above the top of basement in Hole 897D (Intervals 149-897D-10R-2, 0-150 cm, and -10R-3, 0-39 cm), and deeper in the basement (Intervals 149-897D-18R-2, 30-70 cm, -18R-4, 0-18 cm, and -25R-6, 52-104 cm).

Two facies may be distinguished in the serpentinized harzburgitic/lherzolitic rocks, depending on the abundance and distribution of pyroxene (Fig. 29): (1) a variety in which the pyroxene is homogeneously distributed (Fig. 30), and (2) a banded variety where pyroxene-rich areas and pyroxene-poor, or even dunitic, areas alternate (Fig. 31). The transition between these two facies generally is sharp. No plagioclase was recognized in these rocks, but the extensive serpentinization makes identification of this mineral difficult. Locally, a pyroxene-rich or a pyroxenite facies occurs as a thin (1-5 cm) diffuse band or as parallel bands or dykelets. Primary zonation within the dykelets is preserved. Despite complete serpentinization, the borders are clearly visible as zones of bastite derived from pyroxenes (Fig. 32).

The plagioclase-rich peridotite is a banded facies of pyroxene- and plagioclase-rich zones (Fig. 33), with a sharp transition between the two types. The Interval 149-897C-64R-5, 20-65 cm, displays a primary banding marked by four parallel pyroxenitic bands (2 cm thick). Plagioclase is particularly abundant (35%-40%) in the Interval 149-897C-66R-4 at 53-70 cm.

The entire ultramafic section in both holes has been extensively serpentinized. In addition, the upper part of basement in Hole 897D has been pervasively calcitized and altered, and is yellow to brown (Sections 149-897D-10R-3 to -15R-2 and -16R-4 to -16R-7). Elsewhere, the harzburgitic or lherzolitic rocks generally are pale green or black; the plagioclase-bearing peridotite is usually gray or black, depending on the abundance of plagioclase.

Tectonic breccias occur throughout the cores from both holes. Two main types of breccia are distinguished: (1) angular blocks of ser-

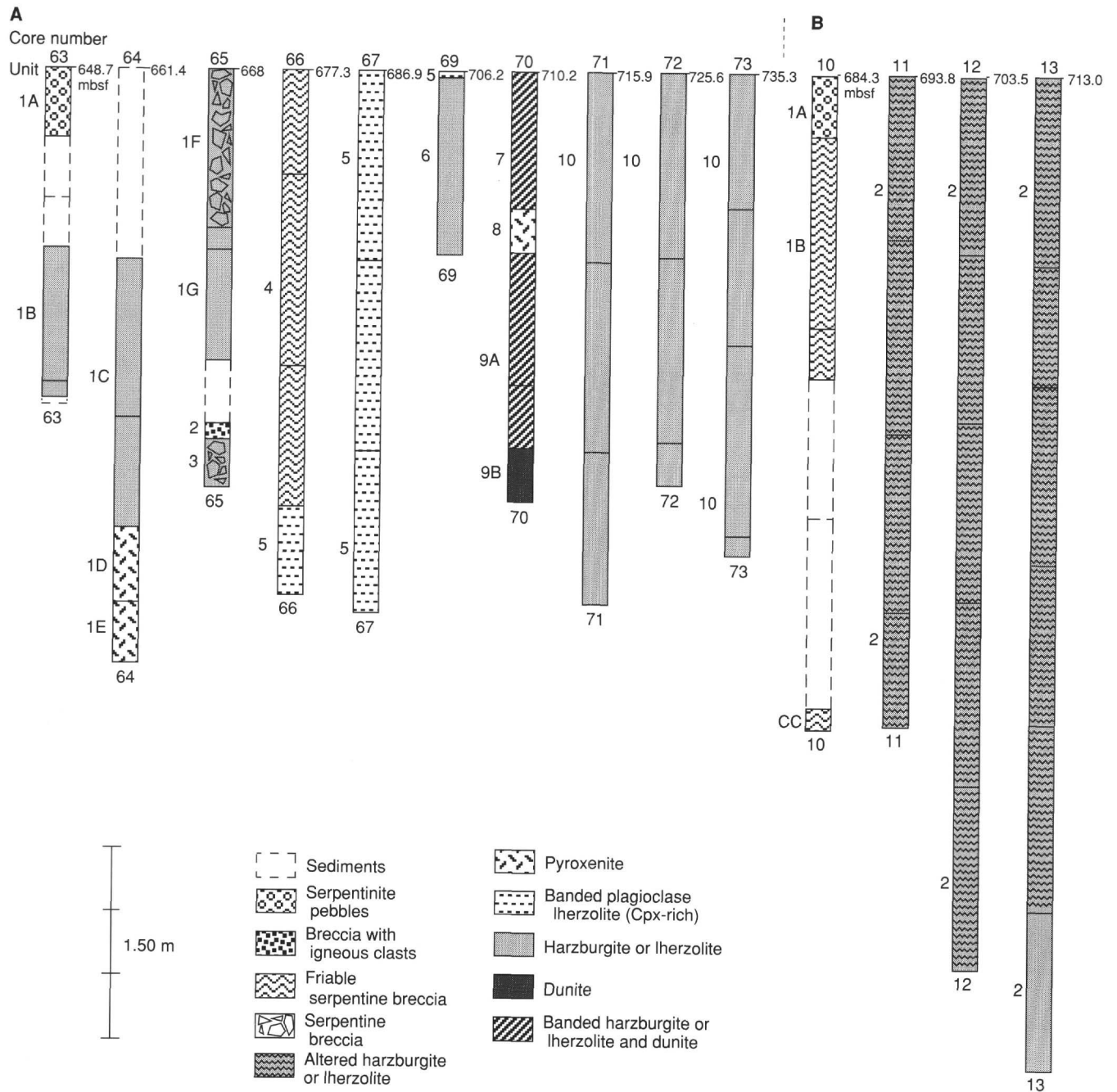


Figure 29. Lithologic column of the basement rocks recovered. **A.** Hole 897C. **B.** Hole 897D. Thicknesses of the intercalated sediments are not shown to scale.

pentinitized peridotite embedded in a network of fractures filled with calcite and/or serpentine; the proportion of calcite and/or serpentine depends on the intensity of fracturing (e.g., Interval 149-897C-64R-5, 0-65 cm; Sections 149-897C-65R-1 and -19R-4); (2) more rounded, smaller blocks of serpentine embedded in a matrix of calcite and/or serpentine; these breccias are locally sheared or fractured (Sections 149-897D-17R-4 to -6). When the latter variety is altered, the matrix is friable with thin blue-gray or white layers (Sections 149-897D-10R-2 and -3; 149-897D-18R-3 to -18R-4; and Interval 149-897D-25R-6, 52-104 cm). In Sections 149-897C-66R-1 to -3, the unconsolidated matrix of green serpentine containing a few fragments of serpentinite may be such an altered breccia, but it is also comparable to serpentine sediments described from the Izu-Bonin-Mariana forearc (Fryer, Pearce, Stokking, et al, 1990).

The serpentinized peridotite has an equant texture and displays almost no high-temperature ductile deformation. However, this primary texture has been overprinted in many places by later low-temperature deformation. Features associated with this deformation include (1) the development of fractures and brecciation of the serpentinized peridotites; (2) a shear deformation marked by foliation planes and shear bands, and (3) a penetrative deformation of the serpentine mesh, either in the serpentinized rocks or in the breccias (see "Structural Geology" section, this chapter).

The late deformation is heterogeneous, and the relative timing of the development of these different features is not obvious; they appear to be more or less co-eval. However, structural relationships show that the calcite-filled fractures cross-cut serpentinite breccias (Section 149-897D-17R-5).

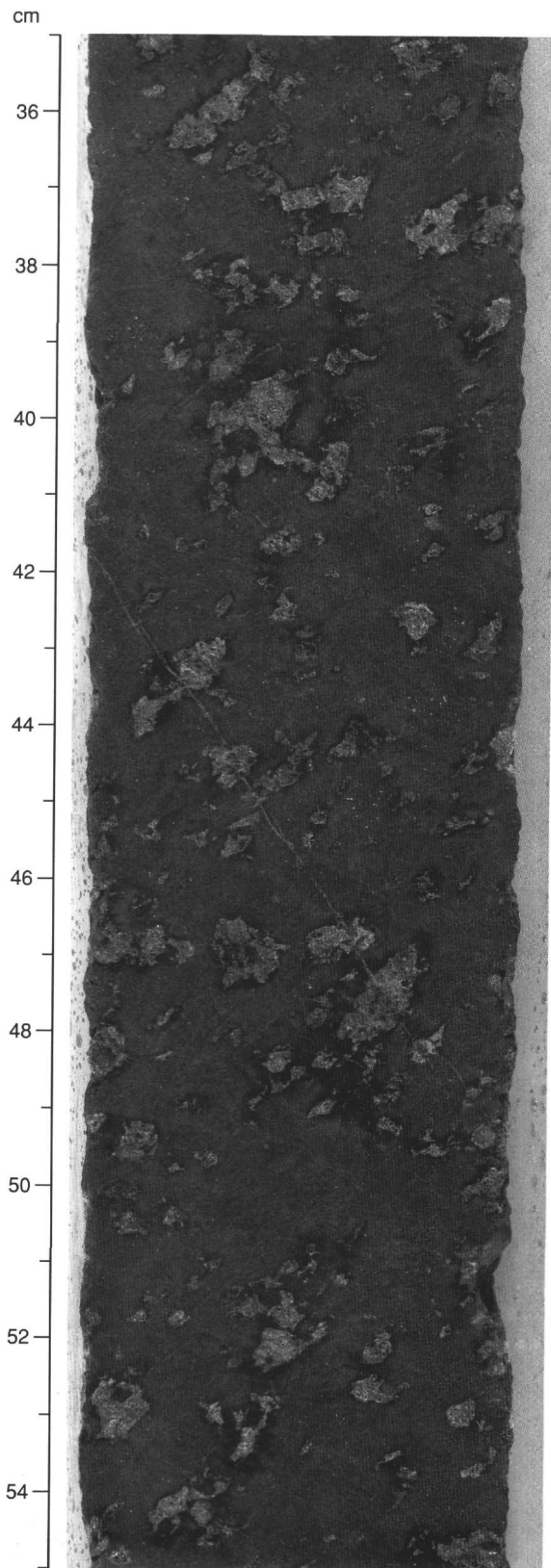


Figure 30. Lherzolite or harzburgite facies in which the pyroxene is homogeneously distributed (Interval 149-897C-72R-1, 35-55 cm).

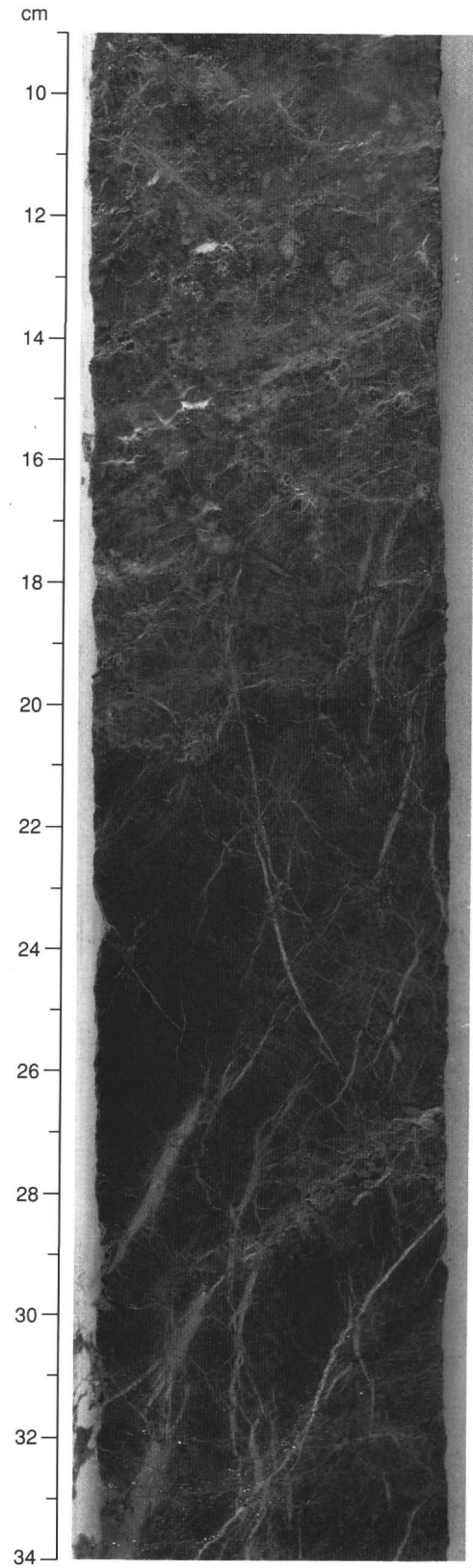


Figure 31. Banded variety of harzburgite or lherzolite with alternating pyroxene-rich, pyroxene-poor, and dunitic areas in Interval 149-897C-70R-1, 9-34 cm.

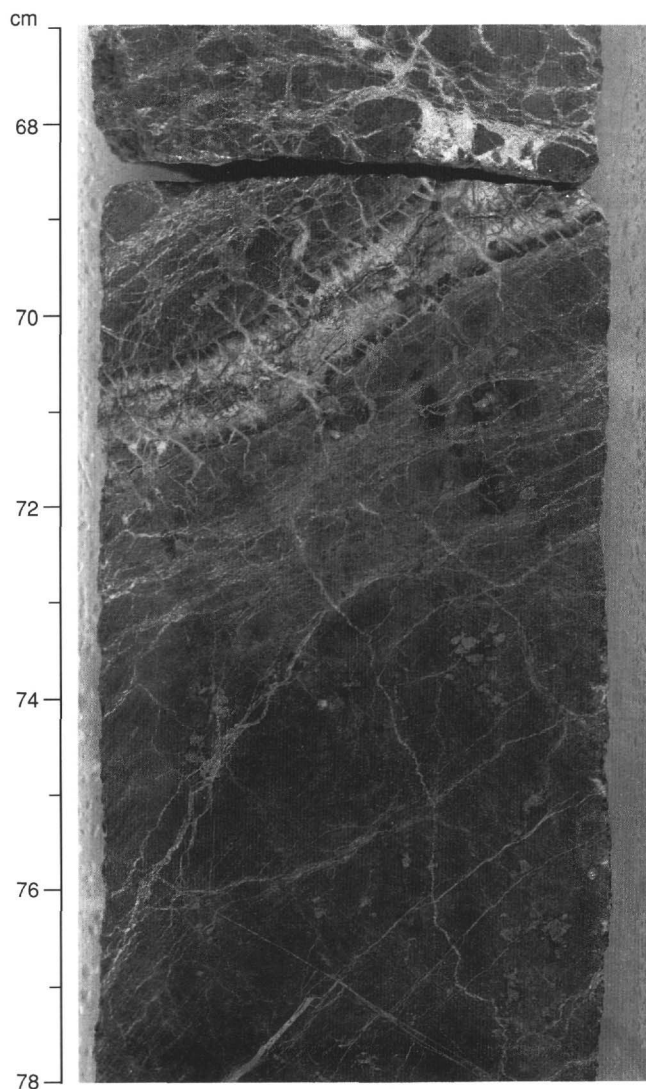


Figure 32. Pyroxenitic dikelet in Interval 149-897D-16R-2, 67-78 cm, displaying a preserved primary zonation despite complete serpentinization; the borders are clearly visible as zones of bastite derived from pyroxenes.

equant crystals (from 0.5 to 10 mm) that were clustered at the periphery of orthopyroxene grains in connection with exsolution. In the pyroxene-rich facies, primary banding is sometimes outlined by clinopyroxene crystals with their associated curved enstatite exsolution lamellae. The modal abundance of the clinopyroxene is highly variable: from 0% in dunitic facies to 50% in some pyroxenite dikes.

Spinel crystals usually have embayed, irregular shapes (like a holly leaf), that range in size from 0.5 to 3 mm. Frequently fractured, sometimes they are broken into pieces as small as 0.1 mm without being altered. A brown chrome-rich spinel is the most abundant variety. It becomes opaque as it is altered and invaded by pervasive exsolved-magnetite. The pyroxene- and plagioclase-rich facies contain green elongate spinel grains, perhaps with a lower iron and chromium content.

Plagioclase makes up to 40% of the whole rock in the pyroxene and green spinel-bearing facies. Most of this plagioclase has been completely altered. It normally rims corroded spinel crystals or forms irregular veinlets that pervasively invade the lherzolite and constitute from 0% to 15% of the whole rock (Fig. 35).

The primary texture of the peridotites has often been overprinted by serpentinization, calcitization, and late deformation. Primary tex-

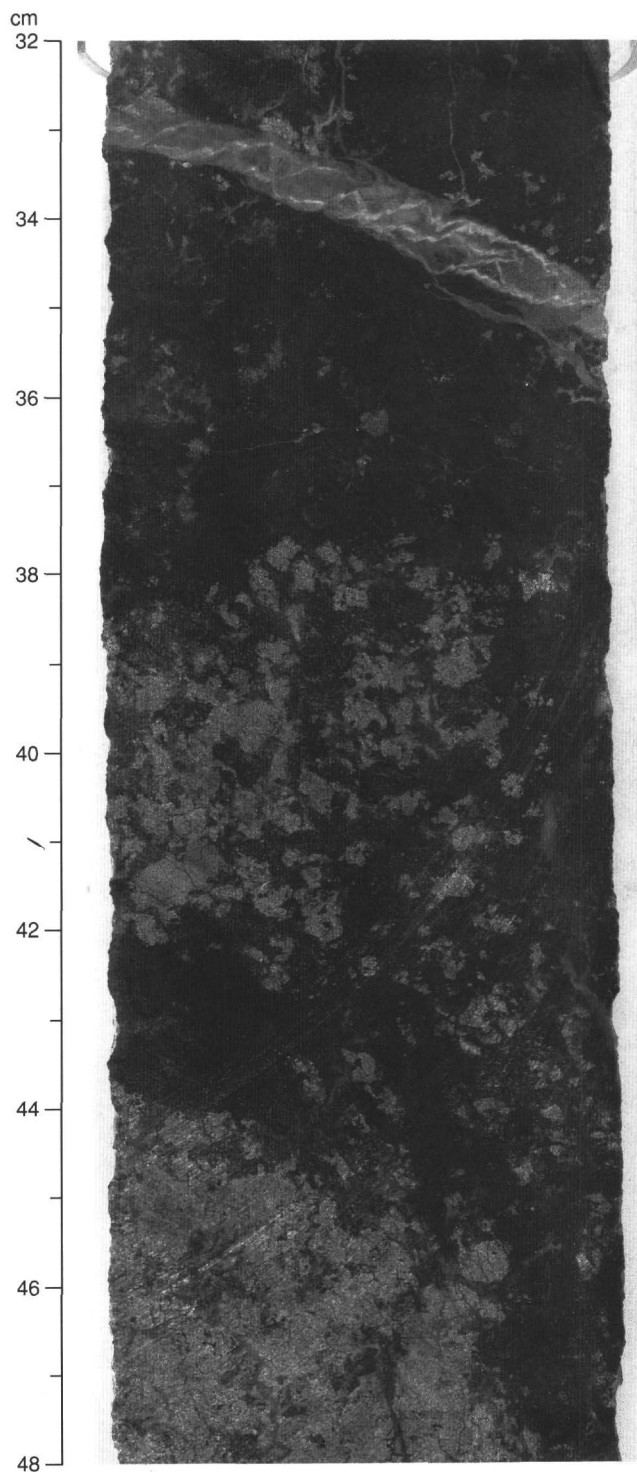


Figure 33. Banded plagioclase-rich peridotite in Interval 149-897C-67R-2, 32-48 cm; the transition between pyroxene-poor and pyroxene-rich zones is sharp.

tures, however, have been identified tentatively in some of the less altered samples. Two main types were recognized: coarse-grained equant and porphyroclastic. The majority of the rocks are coarse-grained equant, with neither macroscopic nor microscopic evidence of high-temperature deformation. Porphyroclastic textures (70% porphyroclasts on average) and locally high-temperature mylonitic textures were observed only in well-preserved pyroxenite or plagioclase-bearing lherzolitic rocks.

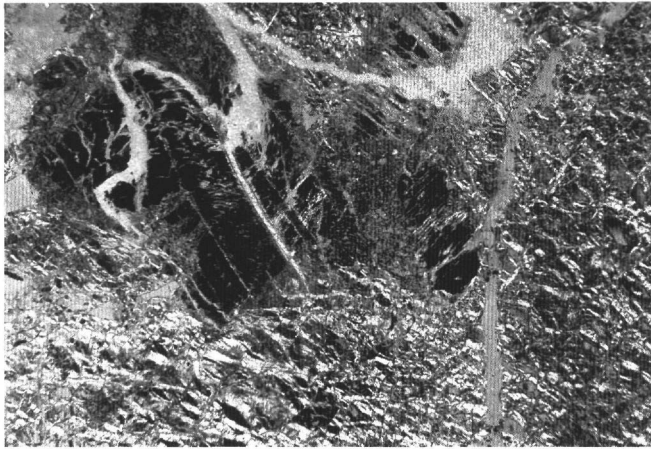


Figure 34. Kinked orthopyroxene that has been darkened by magnetite in the serpentinized peridotite (Interval 149-897C-67R-2, 59-61 cm). Crossed-plane polarized light (polarizers slightly uncrossed). The longer dimension of the photomicrograph represents 5.2 mm.

Alteration Mineralogy

Secondary minerals usually constitute 80% to 100% of the rock. The freshest material occurs in Hole 897C, whereas samples from Hole 897D are both serpentinized and altered, and few primary minerals are preserved. The secondary minerals include lizardite and chrysotile, opaque minerals (magnetite, hematite, amorphous oxide phases, and sulfides), scarce amphibole and chlorite, iowaite, calcite, brucite, and, locally, quartz.

Several generations of serpentine formation can be inferred from the textural relationships in these rocks. The peridotite is mostly a mesh of thin serpentine veinlets derived from the alteration of olivine. Orthopyroxene crystals have been partly or completely serpentinized. The original crystal shapes of orthopyroxene grains usually have been preserved, making it possible to assess the original abundance of orthopyroxene. Several types of cross-cutting serpentine veins can be distinguished, including thin parallel lenses (1 × 20 mm) filled with massive serpentine and thicker (5-20 mm) veins filled with a very fine-grained cream to black near-translucent variety, and greenish gray fibers (1-10 mm × 30-50 mm). All these varieties have the serpentine mesh texture of lizardite and/or chrysotile. In addition, several zones, resembling contorted pervasive veins having a faint bluish to purple color, display the XRD pattern of iowaite.

Secondary opaque minerals are mainly magnetite and pyrite. Magnetite, a by-product of the serpentinization, is observed in the serpentine mesh and darkens the deeply altered pyroxene crystals. Magnetite also was produced by the alteration of primary spinels, pseudomorphing the original crystal. Pyrite, the most common sulfide encountered, occurs as scattered grains or forms small veinlets in the fractures filled by massive serpentine (e.g., Interval 149-897C-67R-1, 38-43 cm).

Few occurrences of amphibole were observed. Some orthopyroxenes have been replaced by fibrous amphibole and are rimmed by bastite (Interval 149-897D-16R-2, 68-71 cm). The highly deformed lherzolite displays acicular amphibole (probably tremolite) (0.2-1 mm long), associated with chlorite (1.5 mm in size) in veinlets parallel to the foliation (Interval 149-897C-67R-3, 62-65 cm).

The color of the serpentinized peridotite is related to the extent of calcite alteration. The peridotite having the least amount of calcite is black or dark green. Yellow to orange-brown colors are associated with the presence of large amounts of calcite and ferric hydroxides. Calcite replacement and vein formation apparently was the last alteration stage of these rocks; calcite veins crosscut, brecciate, or replace preexisting structures related to serpentinization (Fig. 36). Extensive replacement by serpentine has sometimes induced crystallization of

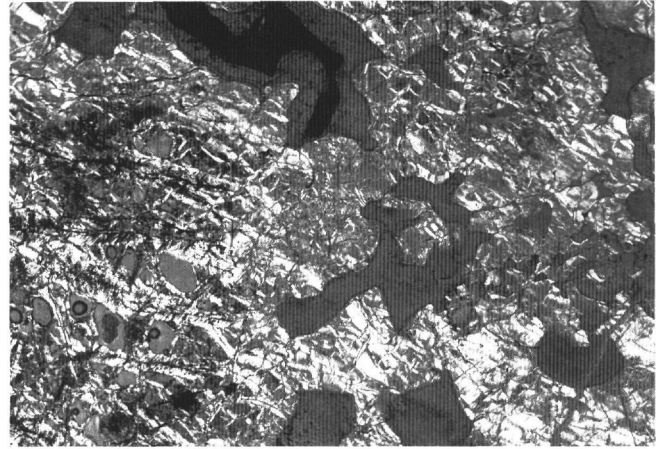


Figure 35. Irregular veinlets of former plagioclase (dark gray) rimming spinel (black) in the plagioclase-bearing serpentinized peridotite (Interval 149-897C-66R-4, 50-54 cm). Crossed-plane polarized light (polarizers slightly uncrossed). The longer dimension of the photomicrograph represents 5.2 mm.



Figure 36. Fibrous serpentine vein (S) cut into sections by late veins of calcite (C) in the serpentinized peridotite (Interval 149-897D-13R-1, 73-76 cm). Crossed-plane polarized light. The longer dimension of the photomicrograph represents 1.2 mm.

small pockets of chalcedony or quartz (Interval 149-897D-12R-5, 83-85 cm). Calcite alteration becomes less pervasive downhole and is essentially absent beneath 677 mbsf in Hole 897C and beneath 753 mbsf in Hole 897D. Extensive calcitization did not occur in the basement of Hole 897C, but only in the serpentinite blocks in the lowest part of the sedimentary section (Cores 149-897C-63R to -65R). However, calcitization is extensively developed in Hole 897D in the upper 60 m of the basement section.

Brucite occurs in one 1-cm-thick vein (Sample 149-897D-17R-6, 1-2 cm) and as scattered crystals (Interval 149-897D-23R-1, 59-62 cm) associated with fractures. This mineral usually is considered to be hydrothermal in origin and is characteristic of low-temperature/low-pressure conditions. The rock has been stained by purple crystals of iowaite near this vein of brucite.

Igneous and Metamorphic Geochemistry

Major Element Geochemistry

Geochemical results of major elements from X-ray fluorescence (XRF) analysis of 15 serpentinized peridotite samples, taken from

Table 9. Major element composition (wt%) and Cr and Ni content (ppm) of serpentinized peridotites from of Holes 897C and 897D.

| Core, section: Interval (cm): | SiO ₂ | TiO ₂ | Al ₂ O ₃ | Fe ₂ O ₃ | MnO | MgO | CaO | Na ₂ O | K ₂ O | P ₂ O ₅ | Total | LOI | Cr | Ni | |
|----------------------------------|------------------|------------------|--------------------------------|--------------------------------|------|-------|-------|-------------------|------------------|-------------------------------|--------|-------|------|------|--------------------------------------------|
| 149-897C- | | | | | | | | | | | | | | | |
| 64R-3, 56-60 | 40.39 | 0.00 | 0.65 | 8.64 | 0.19 | 38.08 | 10.22 | 0.10 | 0.00 | 0.00 | 98.27 | 17.48 | 2084 | 2040 | Green serpentinized peridotite |
| 64R-3, 56-60 | 49.78 | 0.02 | 11.85 | 6.56 | 0.01 | 20.82 | 9.49 | 0.10 | 0.01 | 0.00 | 98.64 | 3.87 | 3072 | 1421 | Green serpentinized plagioclase peridotite |
| 66R-4, 8-12 | 41.72 | 0.07 | 4.57 | 9.36 | 0.16 | 43.00 | 0.10 | 0.10 | 0.00 | 0.00 | 99.08 | 14.31 | 3768 | 1947 | Gray serpentinized peridotite |
| 67R-2, 68-73 | 42.11 | 0.03 | 2.77 | 10.83 | 0.14 | 43.79 | 0.10 | 0.10 | 0.00 | 0.00 | 99.87 | 15.68 | 1390 | 2285 | Gray serpentinized peridotite |
| 67R-3, 51-55 | 43.87 | 0.12 | 7.76 | 9.62 | 0.16 | 34.00 | 4.45 | 0.10 | 0.00 | 0.00 | 100.08 | 7.68 | 3240 | 1560 | Gray serpentinized plagioclase peridotite |
| 69R-1, 92-95 | 41.66 | 0.00 | 0.51 | 8.80 | 0.10 | 47.35 | 0.12 | 0.10 | 0.00 | 0.00 | 98.64 | 16.36 | 1564 | 2159 | Gray serpentinized peridotite |
| 70R-2, 19-22 | 41.91 | 0.00 | 0.18 | 9.16 | 0.12 | 46.96 | 0.10 | 0.10 | 0.00 | 0.00 | 98.53 | 15.49 | 673 | 2429 | Gray serpentinized peridotite |
| 71R-3, 115-118 | 41.05 | 0.00 | 0.50 | 8.65 | 0.15 | 48.07 | 0.09 | 0.10 | 0.00 | 0.00 | 98.61 | 16.62 | 1177 | 2047 | Gray serpentinized peridotite |
| 72R-1, 55-58 | 41.54 | 0.00 | 0.42 | 8.72 | 0.15 | 47.39 | 0.06 | 0.10 | 0.00 | 0.00 | 98.38 | 15.67 | 1113 | 2117 | Gray serpentinized peridotite |
| 12R-2, 85-89 | 8.76 | 0.00 | 0.55 | 8.41 | 0.09 | 2.83 | 73.30 | 0.10 | 0.01 | 0.08 | 94.13 | 36.79 | 1572 | 607 | Yellow-brown carbonated serpentine |
| 13R-2, 14-18 | 19.36 | 0.00 | 0.52 | 8.05 | 0.11 | 12.57 | 56.13 | 0.10 | 0.01 | 0.04 | 96.89 | 33.09 | 1715 | 1110 | Yellow-brown carbonated serpentine |
| 16R-2, 91-94 | 45.76 | 0.00 | 1.18 | 9.19 | 0.09 | 37.09 | 6.71 | 0.10 | 0.00 | 0.00 | 100.12 | 13.20 | 2144 | 2138 | Green serpentinized peridotite |
| 16R-6, 116-119 | 19.50 | 0.00 | 0.59 | 9.88 | 0.06 | 1.64 | 63.25 | 0.10 | 0.08 | 0.07 | 95.17 | 34.40 | 1158 | 645 | Yellow-brown carbonated serpentine |
| 20R-1, 84-87 | 43.18 | 0.00 | 0.94 | 9.62 | 0.14 | 44.68 | 0.18 | 0.10 | 0.00 | 0.00 | 98.84 | 13.44 | 1426 | 2202 | Green serpentinized peridotite |
| 25R-5, 58-62 | 42.50 | 0.00 | 0.56 | 8.76 | 0.14 | 46.38 | 0.27 | 0.10 | 0.00 | 0.00 | 98.71 | 14.70 | 1903 | 2215 | Gray serpentinized peridotite |

Table 10. Analyses of minor elements (ppm) and carbonate content of serpentinized peridotites from Hole 897C.

| Core, section, interval (cm) | Depth (mbsf) | Nb | Zr | Y | Sr | Rb | Zn | Cu | Ni | V | Cr | Ba | CaCO ₃ (wt%) |
|---------------------------------|-----------------|----|----|----|-----|----|----|-----|------|-----|------|----|----------------------------|
| 149-897C- | | | | | | | | | | | | | |
| 63R-2, 72-75 | 650.4 | 1 | 7 | 0 | 84 | 4 | 45 | 6 | 1527 | 31 | 2338 | 34 | 39 |
| 64R-3, 40-43 | 660.5 | 1 | 6 | 0 | 41 | 4 | 43 | 3 | 2001 | 22 | 2608 | 11 | 16 |
| 64R-3, 56-60 | 660.7 | 2 | 7 | 0 | 37 | 5 | 38 | 4 | 2040 | 25 | 2084 | 2 | |
| 64R-4, 31-34 | 661.7 | 1 | 7 | 0 | 68 | 4 | 37 | 5 | 1680 | 16 | 1844 | 33 | 31 |
| 64R-5, 42-45 | 662.7 | 0 | 7 | 0 | 70 | 4 | 45 | 8 | 1678 | 41 | 762 | 39 | 32 |
| 64R-5, 66-70 | 662.9 | 2 | 12 | 12 | 121 | 4 | 58 | 110 | 1421 | 223 | 3072 | 23 | |
| 65R-1, 38-41 | 668.4 | 1 | 8 | 4 | 54 | 4 | 25 | 13 | 613 | 108 | 1235 | 28 | 26 |
| 65R-1, 53-56 | 668.5 | 0 | 7 | 3 | 63 | 4 | 48 | 6 | 1420 | 72 | 929 | 20 | 30 |
| 65R-2, 48-51 | 669.9 | 1 | 6 | 1 | 27 | 3 | 46 | 5 | 2196 | 17 | 2038 | 0 | 9 |
| 65R-3, 41-43 | 671.2 | 0 | 8 | 1 | 107 | 4 | 67 | 9 | 1379 | 40 | 1903 | 66 | 56 |
| 66R-4, 4-12 | 680.8 | 2 | 8 | 0 | 9 | 4 | 50 | 6 | 1947 | 75 | 3768 | 0 | |
| 67R-2, 68-73 | 689.0 | 1 | 7 | 0 | 9 | 5 | 59 | 31 | 2285 | 47 | 1390 | 0 | |
| 67R-3, 51-55 | 690.3 | 2 | 11 | 0 | 63 | 5 | 53 | 2 | 1560 | 108 | 3240 | 8 | |
| 69R-1, 41-43 | 706.6 | 1 | 7 | 0 | 8 | 5 | 41 | 24 | 2116 | 17 | 1706 | 0 | 1 |
| 69R-1, 92-95 | 707.1 | 2 | 7 | 0 | 8 | 6 | 42 | 13 | 2159 | 19 | 1564 | 2 | |
| 70R-1, 62-64 | 710.8 | 1 | 7 | 0 | 8 | 5 | 43 | 2 | 1766 | 47 | 6126 | 11 | 1 |
| 70R-2, 19-22 | 711.8 | 2 | 7 | 0 | 8 | 7 | 38 | 2 | 2429 | 2 | 673 | 0 | |
| 70R-3, 57-60 | 713.2 | 1 | 6 | 0 | 8 | 5 | 45 | 5 | 2699 | 0 | 1176 | 3 | 1 |
| 71R-1, 58-61 | 716.5 | 1 | 6 | 0 | 8 | 5 | 41 | 2 | 2280 | 7 | 1441 | 4 | 1 |
| 71R-3, 57-59 | 719.5 | 1 | 6 | 0 | 7 | 5 | 41 | 16 | 2284 | 6 | 1122 | 0 | 1 |
| 71R-3, 115-118 | 720.1 | 1 | 7 | 0 | 8 | 6 | 38 | 10 | 2047 | 8 | 1177 | 0 | |
| 72R-1, 55-58 | 726.2 | 1 | 6 | 0 | 7 | 4 | 39 | 6 | 2117 | 18 | 1113 | 0 | |
| 72R-1, 64-66 | 726.2 | 1 | 6 | 0 | 9 | 4 | 39 | 4 | 2151 | 7 | 1320 | 0 | 1 |
| 73R-1, 50-52 | 735.8 | 1 | 6 | 0 | 9 | 4 | 42 | 6 | 2280 | 13 | 1922 | 0 | 1 |
| 73R-3, 50-52 | 737.6 | 1 | 6 | 0 | 8 | 4 | 36 | 17 | 2237 | 7 | 1388 | 0 | 1 |

both Holes 897C and 897D, are presented in Table 9. These results are for ignited samples and thus are water- and carbonate-free. The loss-on-ignition values also are included; however, the ratio of ferric to ferrous iron was not determined. The quoted iron concentrations are "total iron" expressed as Fe₂O₃.

The results confirm the ultramafic, magnesium-rich nature of the rocks. Concentrations of Na₂O, K₂O, and P₂O₅ are low, at or below the detection limit for the XRF analytical procedures used. As expected, concentrations of Al₂O₃, TiO₂, and MnO also are low, and concentrations of CaO are less than 1.3%, except in samples that have suffered extensive calcite alteration.

The most obvious primary variation in the major-element geochemical data is in the concentration of MgO. The most alumina-rich samples (Samples 149-897C-64R-5, 66-70 cm and -67R-3, 51-55 cm) originally contained relatively high concentrations of plagioclase and spinel, and these results confirm the relatively undepleted nature of some of the peridotites, as suggested by thin-section studies. Abundances of all major oxides, except Fe₂O₃, decrease during calcitization; the reason why Fe₂O₃ is not affected is not clear. Alteration effects dominate the analyses.

Trace Element Geochemistry

To help characterize both the primary chemical variation within the serpentinite and the chemical effects of varying amounts of car-

bonate alteration, a relatively large number of samples was analyzed for the elements Nb, Zr, Y, Ba, Rb, Sr, Cu, Zn, Cr, Ni, and V. Calcium carbonate concentrations and grain densities also were measured. The results for 66 samples, taken from Holes 897C and 897D, are presented in Tables 10 and 11. Considerable care was taken to sample the core in a representative fashion to ensure that all the different primary and secondary facies were represented. Although the calcium carbonate alteration is the youngest of the processes which have modified the chemistry of the rocks, it is discussed first because it dominates, and is superimposed on, an initial relatively homogeneous ultramafic parental material.

The pervasive nature of the carbonate alteration is apparent from the results presented in Tables 10 and 11, which shows that some "serpentine" samples now contain more than 80% CaCO₃. Results clearly show that this alteration is most pronounced in the upper part of Hole 897D and that the bottom 60 m is largely unmodified by carbonate alteration (Fig. 37).

Abundances of Sr and Ba, but not Rb, increase directly in proportion to the intensity of carbonate alteration. In contrast, the low abundances of refractory elements such as Nb, Y, and Zr are unmodified. The concentrations of the relatively abundant transition metals Cr and Ni were reduced with the introduction of carbonate. All these results are compatible with carbonate being introduced as a result of interaction with seawater at relatively low temperatures, a model supported by the preferential alteration of the upper parts of the serpentinite in both Holes 897C and 897D.

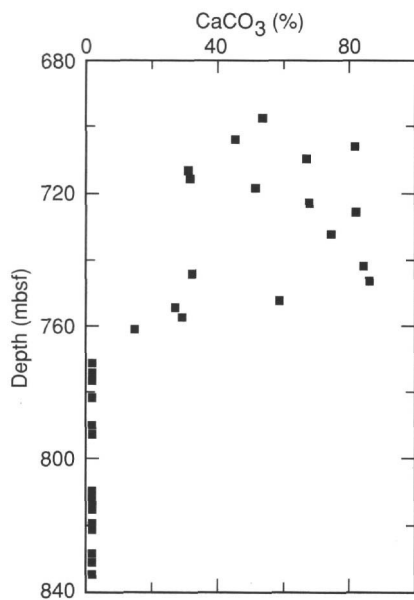


Figure 37. Carbonate content of serpentinites from Hole 897D showing the relatively sharp lower boundary of the carbonate-rich zone near 760 mbsf.

Abundances of trace elements in the sections of serpentinite not modified by carbonate alteration are typical of dunite to lherzolitic rocks from the seafloor and from ophiolite complexes. Abundances of the elements Ba, Nb, and Y generally are less than 5 ppm; abundances of Sr and Zr are about 10 ppm or less. Concentrations of the transition metals Cr and Ni correlate negatively; these reflect varying relative modal abundances of olivine and pyroxene in the original peridotite (Fig. 38).

To make quantitative statements about, and model, the relative degree of depletion and the extent of mantle melting involved in the formation of these rocks requires microprobe analyses and an extensive trace elements data set, which were not available on board the ship.

Discussion

Only a few mantle outcrops at the ocean/continent boundary of passive margins are known at present. These are important windows into the deep lithosphere beneath a continental rift. Investigating these rocks may help to constrain the mechanisms of uplift, emplacement and exposure on the sea-floor during crustal thinning.

The occurrence of mantle rocks at Site 897 demonstrates that the Galicia Bank peridotite ridge, drilled during Leg 103, is not an isolated occurrence, but a major feature of this margin along the ocean/continent boundary. Geophysical and geologic data show that this ridge forms at least two segments that are offset eastward from north to south. The first segment extends continuously for more than 100 km along the Galicia Bank margin (Boillot, Girardeau, et al., 1988; Boillot, Comas, et al., 1988; Boillot et al., 1992). The southern segment continues for another 200 km beneath the sediments of the Iberia Abyssal Plain (Whitmarsh et al., 1990; Whitmarsh et al., 1993; Beslier et al., 1993). Preliminary Site 897 petrographic and mineralogical studies indicate that the mantle cores are plagioclase- and spinel-bearing peridotites. The presence of plagioclase rimming spinel in some of the rocks attests to late equilibration at low pressures (0.9-1 GPa \approx 30 km below surface; Ringwood, 1975), near the transition between plagioclase- and spinel-peridotite stability fields. This is compatible with adiabatic decompression beneath a rift zone.

Another striking feature of Site 897 is the variety of rocks encountered, which range from plagioclase- and pyroxene-rich varieties to lherzolite or harzburgite and dunite. Although less than 150 m of

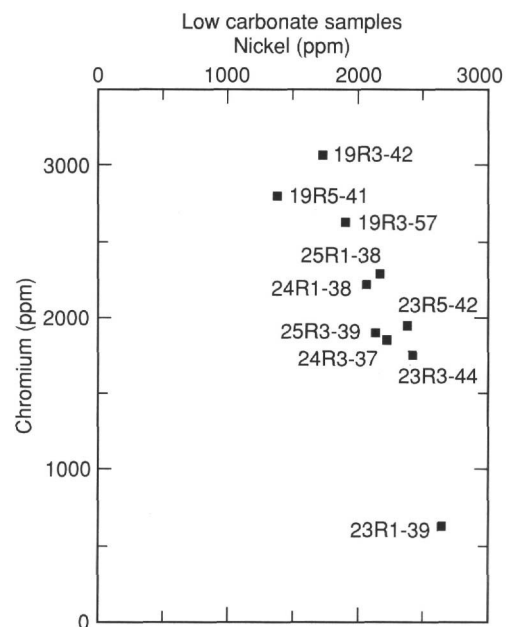


Figure 38. Selected low-carbonate serpentinites from Hole 897D showing a negative linear correlation of Ni and Cr. High Cr rocks are relatively enriched in pyroxene and spinel, and high-Ni rocks are dunitic. 19R3-42 indicates Sample 149-897D-19R-3, 42 cm, etc.

basement was drilled at each hole, the succession of rock types is similar in both holes: the depleted rocks occur below the enriched ones. The high proportion of plagioclase, and its distribution within the plagioclase facies, suggest partial melting in the mantle and upward melt migration. The wide range of compositions is unusual for abyssal peridotite occurrences (Dick, 1989).

Eventually, geochemical and petrological studies of the Site 897 peridotites will give an estimate of the degree of melting that took place in the rocks and the genetic relations of the different facies. This will help to constrain the processes of mantle emplacement.

The Site 897 serpentinitized peridotites typically display an equant primary texture, with a porphyroclastic, or locally mylonitic, texture limited to some fresh plagioclase- and pyroxene-rich facies. Two late deformation fabrics have been heterogeneously developed throughout the recovered section. The chronology of formation of the different features associated with this late deformation is not obvious. The features may have developed during the last rift-related deformation events at the margin, when the peridotites were already near, or at, the surface and already partially serpentinitized (see "Structural Geology" section, this chapter).

Comparison with the Galicia Bank Peridotites

The peridotites of the Galicia Bank margin were emplaced at the end of continental rifting and/or at the very beginning of oceanic accretion (Girardeau et al., 1988; Féraud et al., 1988; Boillot et al., 1989). These rocks were sampled by drilling during ODP Leg 103 (Site 637) and with the French submersible *Nautille* at five sites along the ridge (Boillot, Comas, et al., 1988). These rocks are serpentinitized plagioclase-bearing harzburgite and lherzolite. During their ascent beneath the continental rift, they experienced limited melting (<10%) and high-temperature/low-stress ductile deformation, followed by intense mylonitization in a rotational regime accompanied by decreasing temperature (1000°-850°C) and increasing deviatoric stress (>102 MPa), thereby suggesting lithospheric conditions (Girardeau et al., 1988; Evans and Girardeau, 1988; Beslier et al., 1990). This mylonitization formed in a normal shear zone gently dipping toward the conti-

Table 11. Analyses of minor elements (ppm), carbonate content, and grain density of serpentinized peridotites from Hole 897D.

| Core, section, interval (cm) | Depth (mbsf) | Nb | Zr | Y | Sr | Rb | Zn | Cu | Ni | V | Cr | Ba | CaCO ₃ (wt%) | Grain density (g/cm ³) |
|---------------------------------|-----------------|----|----|---|-----|----|----|----|------|----|------|-----|----------------------------|------------------------------------------|
| 149-897D- | | | | | | | | | | | | | | |
| 11R-1, 39-42 | 694.2 | 0 | 8 | 2 | 141 | 4 | 48 | 15 | 1089 | 37 | 899 | 72 | 68 | 2.81 |
| 11R-3, 55-58 | 697.3 | 1 | 8 | 1 | 113 | 5 | 6 | 7 | 1341 | 30 | 1449 | 69 | 53 | 2.74 |
| 12R-1, 48-51 | 704.0 | 1 | 7 | 0 | 86 | 5 | 37 | 5 | 1604 | 24 | 1233 | 46 | 44 | 2.78 |
| 12R-2, 85-89 | 705.8 | 1 | 8 | 0 | 118 | 5 | 77 | 11 | 607 | 43 | 1572 | 100 | | |
| 12R-3, 39-42 | 706.7 | 0 | 8 | 0 | 178 | 6 | 40 | 7 | 403 | 52 | 748 | 85 | 80 | 2.88 |
| 12R-5, 41-44 | 709.6 | 0 | 8 | 1 | 131 | 5 | 77 | 10 | 1168 | 39 | 1295 | 75 | 66 | 2.77 |
| 13R-1, 38-41 | 713.4 | 1 | 7 | 0 | 70 | 5 | 34 | 6 | 1876 | 23 | 1926 | 28 | 30 | 2.72 |
| 13R-2, 14-18 | 714.6 | 1 | 9 | 0 | 115 | 5 | 78 | 8 | 1110 | 25 | 1715 | 81 | | |
| 13R-3, 40-43 | 715.8 | 1 | 7 | 0 | 73 | 4 | 37 | 5 | 1850 | 24 | 1659 | 35 | 31 | 2.69 |
| 13R-5, 39-42 | 718.5 | 1 | 8 | 0 | 158 | 5 | 30 | 4 | 1422 | 18 | 1245 | 57 | 51 | 2.75 |
| 14R-1, 39-42 | 723.1 | 0 | 7 | 0 | 121 | 6 | 61 | 8 | 1018 | 39 | 1009 | 89 | 67 | 2.80 |
| 14R-3, 38-41 | 725.9 | 0 | 8 | 2 | 125 | 4 | 58 | 11 | 636 | 50 | 1147 | 120 | 81 | 2.82 |
| 15R-1, 38-41 | 732.7 | 1 | 7 | 0 | 110 | 6 | 94 | 29 | 976 | 91 | 1665 | 78 | 74 | 2.85 |
| 16R-1, 38-41 | 742.4 | 0 | 11 | 0 | 517 | 3 | 15 | 11 | 419 | 4 | 307 | 104 | 83 | 2.80 |
| 16R-2, 91-94 | 743.3 | 1 | 8 | 0 | 42 | 4 | 40 | 9 | 2138 | 23 | 2144 | 6 | | |
| 16R-3, 39-42 | 744.1 | 0 | 7 | 0 | 94 | 3 | 35 | 11 | 1766 | 29 | 1682 | 47 | 31 | 2.72 |
| 16R-5, 38-41 | 747.0 | 1 | 7 | 5 | 138 | 5 | 63 | 18 | 497 | 50 | 1244 | 100 | 86 | 2.83 |
| 16R-6, 116-119 | 749.2 | 1 | 8 | 3 | 96 | 6 | 83 | 37 | 645 | 77 | 1158 | 60 | | |
| 17R-1, 26-32 | 751.9 | 0 | 8 | 0 | 131 | 4 | 49 | 5 | 1244 | 19 | 1474 | 85 | | |
| 17R-1, 40-43 | 752.0 | 0 | 7 | 0 | 91 | 6 | 72 | 9 | 1598 | 43 | 1747 | 79 | 58 | 2.80 |
| 17R-1, 73-78 | 752.3 | 0 | 8 | 1 | 150 | 5 | 18 | 6 | 117 | 15 | 176 | 124 | | |
| 17R-3, 39-41 | 755.0 | 0 | 7 | 0 | 68 | 3 | 40 | 3 | 2660 | 6 | 1529 | 22 | 26 | 2.70 |
| 17R-5, 38-40 | 757.4 | 0 | 6 | 0 | 58 | 4 | 35 | 3 | 1500 | 13 | 1340 | 29 | 28 | 2.64 |
| 18R-1, 39-41 | 761.6 | 1 | 6 | 0 | 27 | 4 | 37 | 9 | 1754 | 15 | 1592 | 13 | 13 | 2.64 |
| 19R-1, 68-70 | 771.6 | 1 | 6 | 0 | 10 | 5 | 42 | 7 | 2296 | 23 | 1347 | 12 | 1 | 2.67 |
| 19R-3, 42-44 | 773.7 | 1 | 8 | 0 | 11 | 4 | 40 | 10 | 1732 | 42 | 3062 | 7 | 1 | 2.60 |
| 19R-3, 57-63 | 773.9 | 1 | 9 | 1 | 11 | 4 | 43 | 8 | 1890 | 36 | 2620 | 6 | 1 | 2.67 |
| 19R-5, 41-43 | 776.3 | 1 | 8 | 1 | 13 | 4 | 36 | 6 | 1385 | 51 | 2799 | 3 | 1 | 2.66 |
| 20R-1, 38-41 | 781.0 | 0 | 6 | 0 | 12 | 4 | 44 | 5 | 2130 | 10 | 1881 | 12 | 1 | 2.68 |
| 20R-1, 84-87 | 781.4 | 1 | 7 | 0 | 8 | 4 | 44 | 6 | 2202 | 19 | 1426 | 0 | | |
| 21R-1, 43-46 | 790.6 | 1 | 7 | 0 | 10 | 4 | 41 | 12 | 2169 | 7 | 2283 | 2 | 1 | 2.57 |
| 21R-3, 38-41 | 792.5 | 1 | 6 | 0 | 10 | 4 | 38 | 9 | 2215 | 14 | 1847 | 0 | 1 | 2.61 |
| 23R-1, 39-42 | 809.4 | 1 | 6 | 0 | 8 | 3 | 40 | 6 | 2653 | 0 | 625 | 0 | 1 | 2.63 |
| 23R-3, 44-47 | 812.2 | 1 | 6 | 0 | 10 | 4 | 35 | 3 | 2413 | 7 | 1743 | 4 | 1 | 2.59 |
| 23R-5, 42-45 | 815.0 | 1 | 6 | 0 | 10 | 4 | 39 | 7 | 2383 | 7 | 1941 | 3 | 1 | 2.62 |
| 24R-1, 38-41 | 819.0 | 1 | 7 | 0 | 10 | 4 | 38 | 11 | 2049 | 23 | 2227 | 3 | 1 | 2.68 |
| 24R-3, 37-40 | 821.1 | 1 | 6 | 0 | 10 | 4 | 39 | 15 | 2207 | 14 | 1845 | 7 | 1 | 2.60 |
| 25R-1, 38-40 | 828.6 | 1 | 6 | 0 | 10 | 3 | 39 | 9 | 2053 | 24 | 2353 | 5 | 1 | 2.62 |
| 25R-3, 39-41 | 830.7 | 1 | 6 | 0 | 10 | 4 | 39 | 4 | 2127 | 9 | 1992 | 9 | 1 | 2.61 |
| 25R-5, 58-62 | 833.7 | 1 | 7 | 0 | 11 | 4 | 39 | 6 | 2215 | 14 | 1903 | 5 | | |
| 25R-5, 64-66 | 833.7 | 1 | 6 | 0 | 10 | 4 | 39 | 12 | 2246 | 6 | 1599 | 11 | 1 | 2.61 |

ment. Serpentinization occurred mainly below 300°C as a consequence of the introduction of seawater as the rocks were intensely fractured during a late brittle deformation (Agrinier et al., 1988).

The preliminary studies of the Site 897 peridotites allow for only preliminary comparison with the peridotites at Site 637. It is clear, however, that these peridotites display some similar features, with the occurrence of (1) plagioclase- and spinel-bearing peridotites; (2) textures suggestive of partial melting; (3) extensive late serpentinization; (4) intense late brittle deformation that formed fractures filled with calcite and/or serpentine, and local brecciation.

In contrast, the Galicia Bank margin peridotites of Site 637 differ from those of Site 897 in that no evidence can be observed at Site 897 of extensive intense high-temperature mylonitization. Instead, the Site 897 peridotites underwent a late shear deformation event, leading to the development of foliation and shear bands in the serpentinite and local brecciation of the serpentinite. This suggests that the structural evolution of the mantle rocks during their uplift differed at the two places. Similarly, the absence of high-temperature amphibole in the serpentinite at Site 897 suggests different retrometamorphic conditions. Other striking differences observed at Site 897 are (1) the higher proportion of plagioclase in the plagioclase peridotite and (2) the occurrence of dunite indicative of the wide variety of rocks types encountered in this site.

STRUCTURAL GEOLOGY

Introduction

Site 897 is located on the top of a basement ridge of serpentinized peridotite bounding the western Iberia passive margin (see "Igneous and Metamorphic Petrology and Geochemistry" section, this chapter)

that is buried under a 677- to 694-m-thick sedimentary sequence of Pleistocene to Hauterivian age. Holes 897C and 897D were drilled 100 m apart and penetrated 67.4 and 143.4 m, respectively, of serpentinized peridotites. Sediments and basement rocks display evidence for several episodes of deformation associated with pre-rift, synrift, or post-rift events. Deformational structures identified in the recovered sedimentary section included large- and small-scale folds, microfaults, and sheared clays. Basement ultramafic rocks mainly exhibit evidence of late heterogeneous deformation of already serpentinized material, with shearing and fracturing that leads locally to complete brecciation of the rocks.

Sediment Deformation

The sediments overlying the basement high at Site 897 can be divided into two domains based on their deformational histories. Domain I consists of lithologic Units I, II, and III (49.9-648.7 mbsf in Hole 897C, 596.0-655.2 mbsf in Hole 897D; see "Lithostratigraphy" section, this chapter), in which the sediments are generally undisturbed except for an ambiguous record of stratigraphic dip. Domain II corresponds to lithologic Unit IV (648.7-677.5 mbsf in Hole 897C, 655.2-693.8 mbsf in Hole 897D), which displays abundant evidence for soft sediment folding, microfaulting, and shearing.

Domain I

Deformation structures in Domain I include soft sediment features, such as dewatering structures and small slump folds at the centimeter scale. An irregular downhole increase in bedding dip in Hole 897C between 320 (Core 149-897C-29R) and 640 (Core 149-

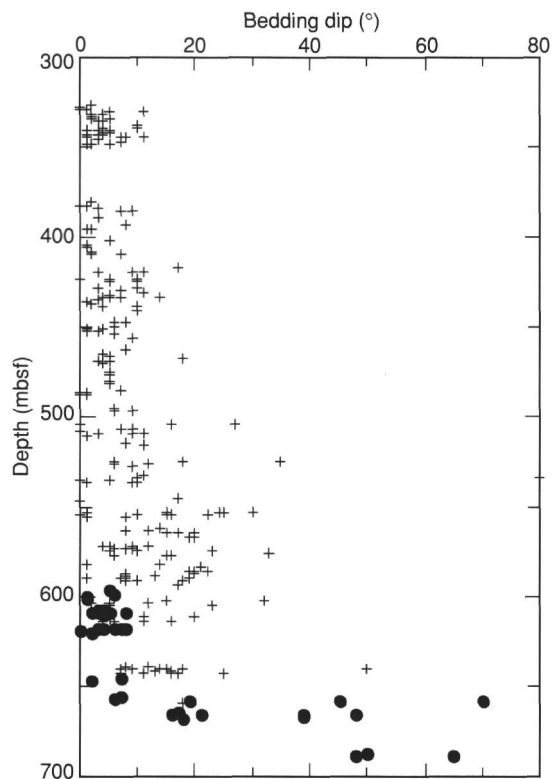


Figure 39. Apparent dips in bedding vs. depth for Holes 897C (crosses) and 897D (circles).

897C-62R) mbsf is the only observation that hints at pervasive, possibly tectonic, deformation within structural Domain I.

Bedding dips were determined from core photographs by measuring the apparent dips within rotated drilling biscuits. We assumed that over a given interval of core, a range of apparent bedding dips would be observed within the randomly rotated and split drill biscuits and that the maximum apparent dip should approximate the true dip angle. The inferred true dip angles for Hole 897C, plotted in Figure 39, reach a maximum of about 25° between 552.1 (Core 149-897C-53R) and 600.5 (Core 149-897C-58R) mbsf. The maximum dips observed between 596.0 (Core 149-897D-1R) and 655.2 (Core 149-897D-6R) mbsf were close to 8° (Fig. 39). Without reliable paleomagnetic measurements from the rotated biscuits, we were unable to determine the dip direction. Bedding within cores from Hole 897D did not display such a range of dips; however, the core records a much shorter interval. If these measured dips are real, this indicates some structural disruption (i.e., faulting or folding) of the strata within the 100 m distance between Holes 897C and 897D.

It is possible that the apparent dips are artifacts of drilling and recovery, either due to tilting of drill biscuits within the core liner or to the deflection of the drill hole from vertical. The lack of correspondence between bedding dips and biscuit thickness, however, discounts drilling-induced rotation of the biscuits. Downhole measurement of hole deflection was not possible at Site 897, but hole deviations of up to 8° at Site 900 (see "Site 900," chapter, this volume) suggest that some of this apparent dip may be an artifact.

Domain II

Structural Domain II, lithostratigraphic Unit IV (9.3 m in Hole 897C and 10.0 m in Hole 897D), contains many different sedimentary lithologies, as well as large blocks of serpentized peridotite. Nearly all of the sediments exhibit evidence of deformation, except those

clearly identified as sedimentary clasts. Deformation structures identified in Unit IV at Site 897 included folded and dipping strata, microfaults, sheared clays, and structural contacts between sediments and serpentized peridotites. The expression and distribution of deformation are variable, particularly between the two holes. The modes of deformation in the sediment appear to correlate well with both sediment composition and lithification state, which may provide a first-order explanation for their distribution.

Dipping Beds

Steeply dipping beds (up to 50°, Interval 149-897C-63R, 80-91 cm) were observed within structural Domain II (Fig. 39); these are commonly associated with folded strata or allochthonous sedimentary clasts. No systematic trend was observed in the distribution of dips in bedding in either hole.

Folded Strata

Folded strata were observed within Unit IV in Hole 897D within fairly uniform sediment packages. The clearest examples were observed in Section 149-897D-7R-3, and Sample 149-897D-7R-CC, and Core 149-897D-8R, which were predominantly composed of relatively unconsolidated, carbonate-poor (15%-20%), black clayey siltstones, with fine light-colored, silty laminations. These defined, broad folds extending beyond the diameter of the core, which provide important evidence for soft sediment deformation, possibly resulting from slumping. This unit is still soft. The fine silt laminations are commonly offset by normal microfaults, which often truncate against the more uniform black siltstone (Fig. 40); the largest example occurs at Interval 149-897D-7R-3, 11-24 cm (Fig. 20, "Lithostratigraphy" section, this chapter). This brittle response within the ductily deformed unit points to variations in rheology associated with composition or porosity.

Smaller and more isolated folding occurs at 687.4 mbsf (Interval 149-897D-10R-4, 99-107 cm), within a yellow-orange calcareous claystone. Dips in bedding reach 45° near the top of this unit (Interval 149-897D-10R-3, 3-10 cm), but folds here are poorly defined. This calcareous claystone is bounded by clay-rich units that exhibit high shear (Fig. 41), but it is not clear if these folds pre-dated or accompanied shearing.

No examples of soft-sediment folding were identified in Unit IV in Hole 897C. Although this may be an artifact of the core recovery in the two holes, it may indicate that sediments at the two locations deformed through different mechanisms, possibly controlled by variations in the stress regimes.

Microfaulting

Microfaults were identified within several different lithologies having relatively high contents of carbonate (50%-65%) in Holes 897C and 897D; the best example was found in limestones within Sections 149-879C-64R-1 and -64R-2. These faults are evident as fine dark lines, apparently caused by concentrations of clay minerals along the slip surfaces (Fig. 42). The rock tends to break preferentially along fault planes to reveal slickensides (Fig. 43). Several fault sets are evident; however, evidence for the relative timing of these sets is ambiguous. At 659.1 mbsf (Interval 149-897C-64R-1, 65-75 cm), the dominant set has a strike of 180° and dip of 47°, with respect to the archive-half reference frame (see "Explanatory Notes" chapter, this volume). Slickenlines suggest a slip direction that trends 223° and plunges 37°, with apparently normal displacements of millimeters (Fig. 42). Preliminary paleomagnetic determinations suggest a true northwest strike for these features.

Minor microfaults also were observed within sheared clay fragments at 687.3 mbsf (Interval 149-897D-10R-3, 100-150 cm), suggesting that microfaulting and shearing may occur on a continuum of scales.

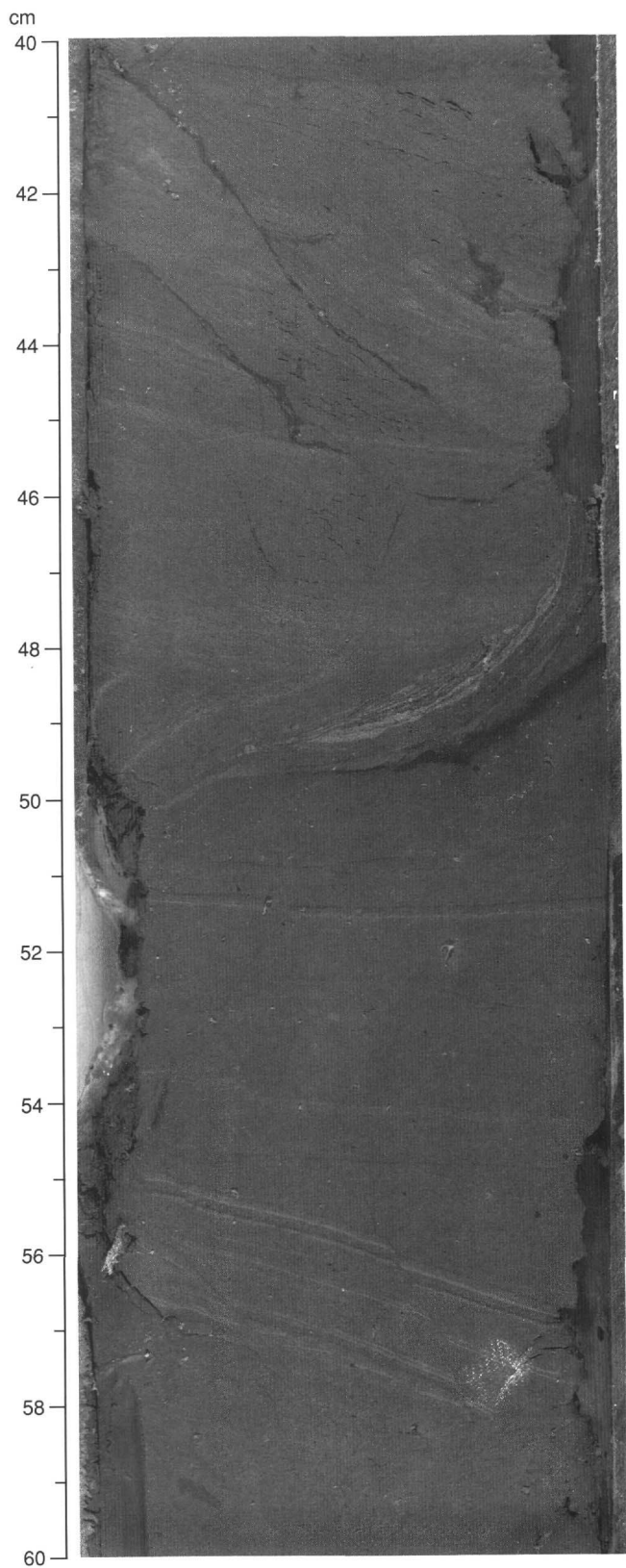


Figure 40. Microfaults offsetting light and dark silt layers within folded laminated siltstones. The faults are truncated at the lower boundary (Interval 149-897D-8R-3, 40-60 cm).

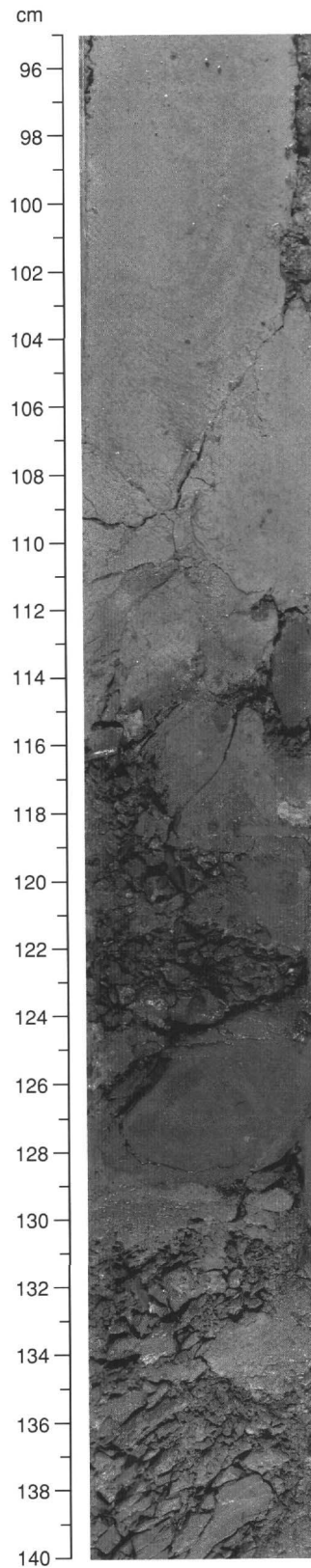


Figure 41. Fold within calcareous claystone (Interval 149-897D-10R-4, 95-140 cm). Highly sheared clays can be recognized below this feature.

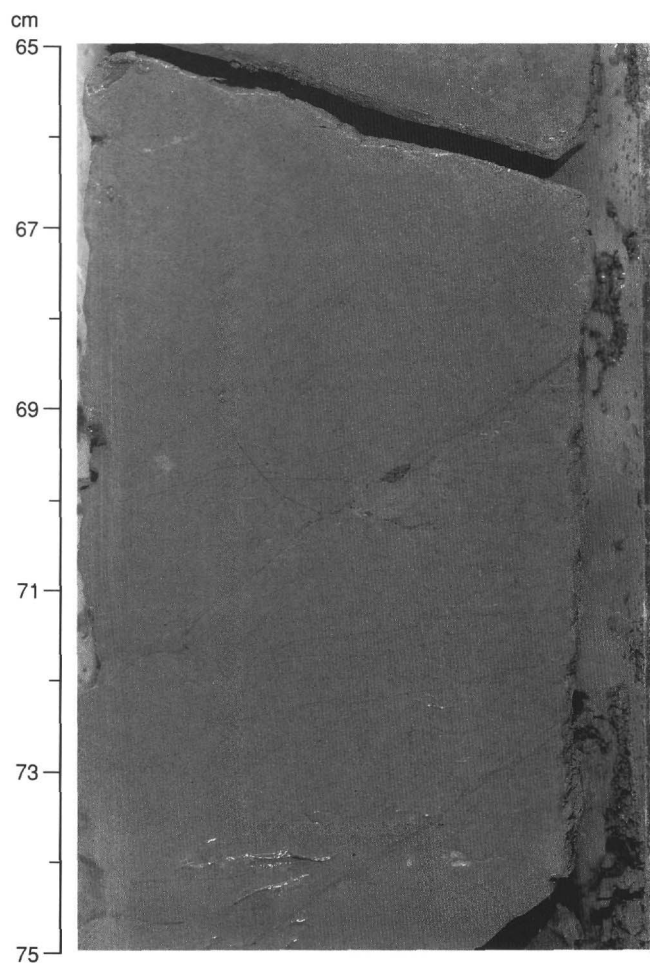


Figure 42. Highly faulted limestone in Interval 149-897C-64R-1, 65-75 cm. Primary normal(?) faults dip about 47° to the left and displace minor faults having shallower and more variable dips.

Sheared Clays

Zones of distributed shear were recognized in the form of fragmented and highly sheared lenticular fragments of claystone bounded by slickensided surfaces. Claystones associated with the folded and tilted calcareous claystone mentioned above (Sections 149-897D-10R-3 and -10R-4) are pervasively sheared (Fig. 41), as are many other clay-rich units in Domain II. These features resemble the scaly clays that distinguish fault zones in submarine accretionary prisms and thus may mark zones that have accommodated significant displacement (Lundberg and Moore, 1986). The ubiquitous presence of these sheared claystones throughout this domain is the strongest evidence for syn- or post-emplacement, in-situ deformation within Unit IV.

Several unique claystones displayed extreme shear deformation. Interval 149-897D-7R-2, 20-66 cm, at the top of Unit IV, contained very disturbed and folded fissile claystone having highly polished surfaces indicative of slip that grades into moderately deformed claystones below. A similar, highly disturbed, organic-rich clay unit at Interval 149-897C-65R-2, 90-110 cm (late early Hauterivian age) displayed polished and striated surfaces that define a folded mesoscopic fabric (Fig. 44). This unit also contains several centimeter-scale clasts of serpentinized peridotite that had been incorporated into the fabric of the clay unit, demonstrating a significant association between the clasts and sediments during deformation (see below).

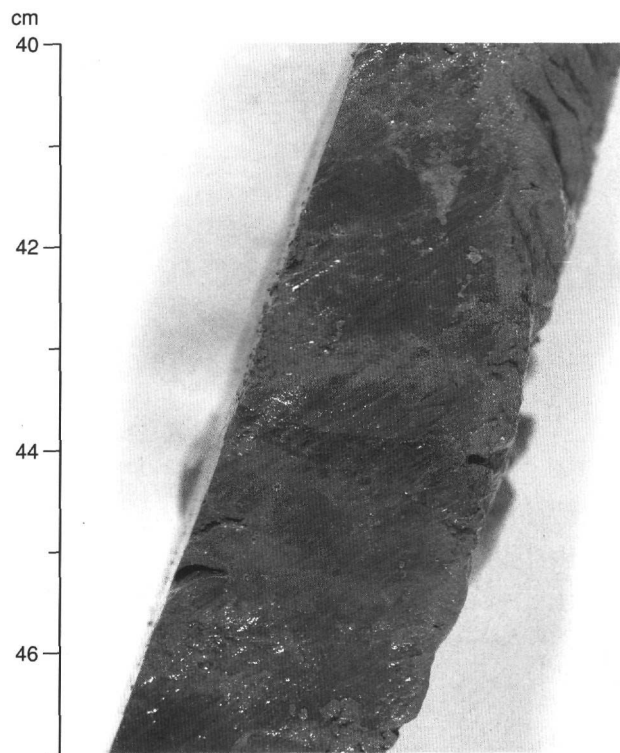


Figure 43. Slickenlines along the primary fault surfaces of Interval 149-897C-64R-1, 40-47 cm.

Sediment Peridotite Contacts

The occurrence of serpentinized peridotite within sediments in structural Domain II (i.e., Unit IV) might arise from either tectonic or sedimentary emplacement. Contacts between various sedimentary lithologies and the common serpentinized peridotite units provide contradictory evidence regarding their relationships. Several limestone cobbles found in Interval 149-897D-10R-1, 10-50 cm, contain clasts of serpentinized peridotite up to 4 cm wide. These contacts are loci for calcite veins that penetrate both lithologies, apparently overprinting earlier generations of calcite in the serpentinized peridotite (Fig. 45). This suggests that the two lithologies suffered a common history of burial, lithification, and diagenesis prior to the deposition of Unit IV. By contrast, a dolomitic limestone cobble at the base of Sample 149-897D-9R, 75-77 cm, within highly weathered serpentinite, displays slickensides at the contact, which suggests a deformational contact.

Most of the serpentinite clasts within Unit IV exhibit little evidence for penetrative deformation, such as was observed in basement rocks at Site 897, suggesting that they were passive elements during syndepositional or post-depositional deformation. One clast, at Interval 149-897D-10R-1, 45-52 cm, although highly sheared, also displays a very sharp contact with the surrounding sediment, which was interpreted to be depositional.

In contrast, intensely sheared clays at Interval 149-897C-65R-2, 90-100 cm, are in direct contact with highly altered serpentinite and have entrained rounded, elongate, serpentinized peridotite clasts during shearing. The uppermost contact is relatively sharp and oblique to the foliation of the serpentinite (Fig. 44); granular fragments of serpentinite in the claystone near the boundary decrease in size away from the contact, suggesting a weathered depositional contact. Within the fissile claystone, the elongate clasts are aligned with the tightly folded clay. In places, the serpentinized peridotite clasts appear to have been sheared with the claystone, although the foliation within the clasts is

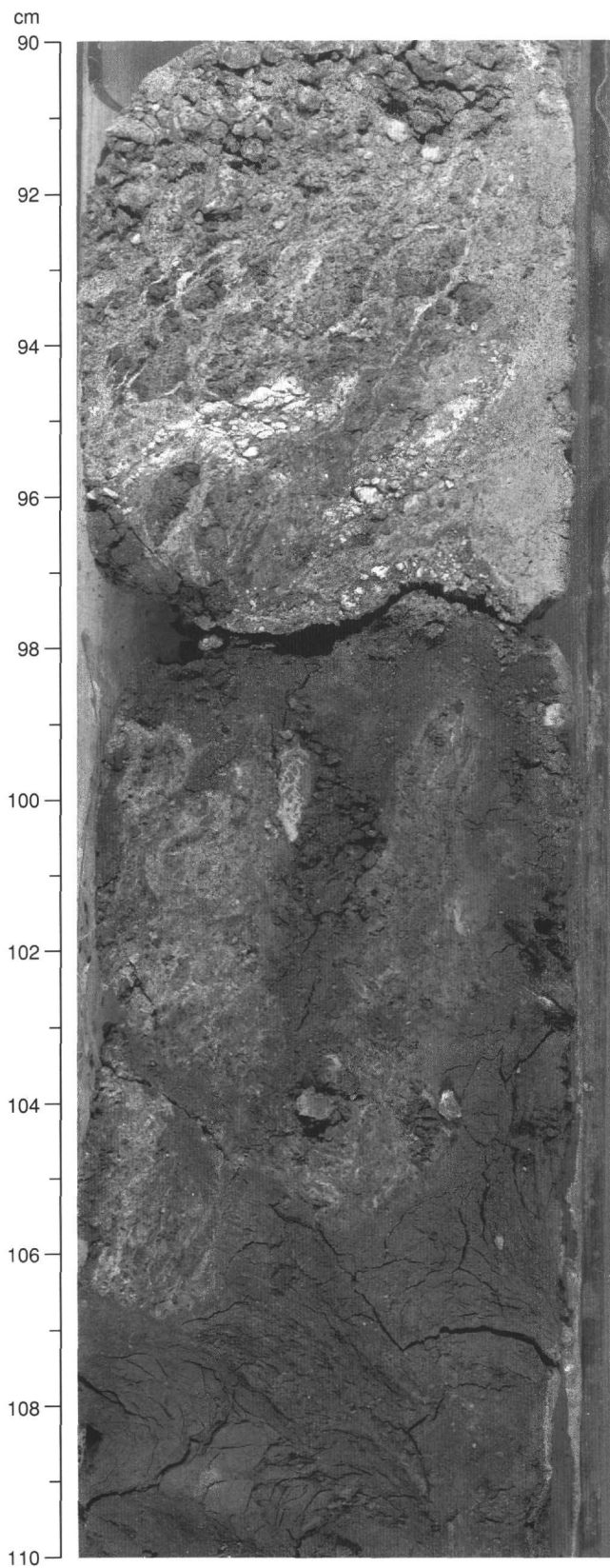


Figure 44. Intensely sheared claystone (Interval 149-897C-65R-2, 90-110 cm). The fissile clay fabric is folded around elongate and sheared clasts of serpentinized peridotite.

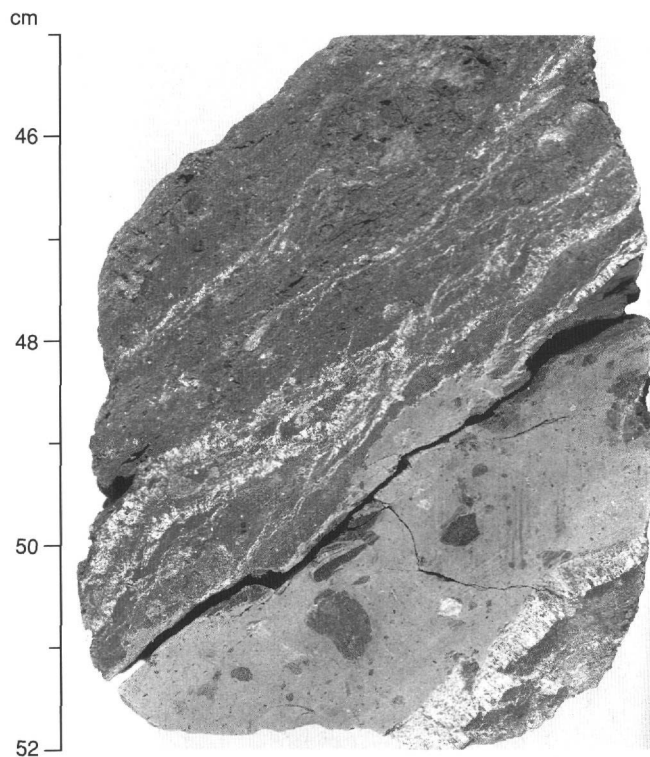


Figure 45. Cobble from Interval 149-897D-10R-1, 45-52 cm, displaying a contact between altered serpentinized peridotite and limestone and late-stage calcite veins that penetrated both lithologies.

locally discordant with the clay fabric. Elsewhere, nearly equant serpentinized peridotite fragments appear to be relatively undisturbed. These observations appear to document the involvement of serpentine in the deformation of Unit IV, but possibly only as small clasts.

Discussion

The general absence of structural features within Domain I is consistent with the accumulation of sediments in a post-rift margin setting, although locally high dips in bedding (documented in Hole 897C) may indicate some structural disruption between the two holes. By contrast, evidence does exist for pervasive sediment deformation in Domain II, although the modes and distributions are heterogeneous. Differences between holes also are striking. Hole 897C contains a much lower proportion of sediment than Hole 897D in Unit IV, and soft sediment deformation is volumetrically more important within Hole 897D.

First-order explanations for the different types of deformation feature are provided by contrasts in lithology, consolidation state, and carbonate content, which will control the mechanism of deformation. Most of the soft-sediment deformation was observed in relatively unconsolidated, carbonate-poor, clayey siltstones. Discrete brittle fractures can be detected most clearly in relatively lithified carbonate-rich claystones and limestones. Zones that exhibit distributed shear contain slickensided fragments having high contents of clay and generally low contents of carbonate.

One model favored for the origin of Unit IV is debris-flow emplacement (see "Lithostratigraphy" section, this chapter), which may account for some of the structures observed in structural Domain II (e.g., soft-sediment folds and faults). The uncemented sheared clays and microfaulted limestones are less easily explained by this model as they are likely to break up during transport. This suggests that most

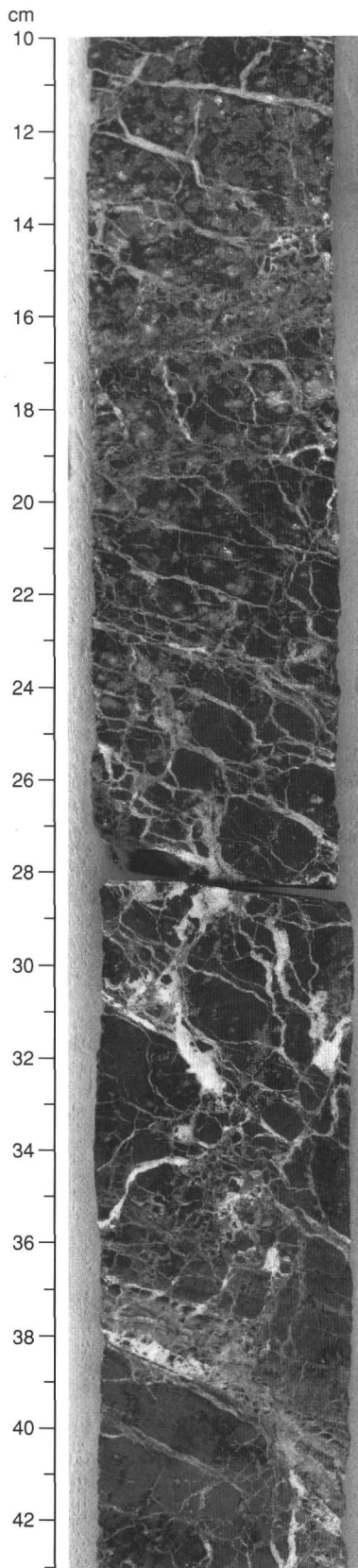


Figure 46. Calcite and/or pale serpentine veins in Interval 149-897D-16R-2, 10-43 cm.

of the brittle features formed in situ. It is possible that stress concentrations within the load-bearing clasts resulted in localized brittle deformation. Alternatively, all of the deformation features recognized in Unit IV may document deformation involving basement during the last stages of rifting, which may have trapped sediments within zones of shear. The differences between the two holes may result from lateral structural variations.

Basement Rock Deformation

Two main types of structure can be distinguished in the serpentinized peridotite basement, although a continuum may exist. These are

(1) textures acquired by the mantle rocks at depth at high temperature prior to serpentinization and (2) later structures developed at low temperatures during or after the main serpentinization event of the peridotite, at or near the surface.

High-temperature Deformation of the Peridotites

Primary high-temperature textures in the peridotites have been tentatively identified in several of the less altered samples. However, the primary fabric has been extensively overprinted by later serpentinization, calcite alteration, and late deformation. Undeformed, coarse-grained equant fabrics, deformed porphyroclastic fabrics, and, locally, mylonitic fabrics were recognized. Most of the recovered peridotites display coarse-grained equant textures with relict, 5- to 10-mm-diameter pyroxenes and no macroscopic or microscopic evidence of deformation.

Porphyroclastic textures were observed only in some well-preserved plagioclase-bearing lherzolitic or pyroxenitic samples (Samples 149-897C-64R-5, 63 cm; -65R-1, 45 cm; -66R-4, 56 cm; -66R-4, 68 cm; -67R-3, 32 cm; -67R-3, 63 cm). Dynamic recrystallization is suggested by strained porphyroclasts (50%-90%) of pyroxenes, olivine, plagioclase, and spinel surrounded by recrystallized grains of reduced size (0.1-0.2 mm). A more intense deformation can be observed in Sample 149-897C-64R-5, 86 cm, and, locally, in Samples 149-897C-67R-3, 63 cm, and -64R-5, 60 cm, which display a mylonitic texture that contains very fine recrystallized grains within thin anastomosing bands.

Low-temperature Structures in the Serpentinized Peridotite

Deformation of the serpentinized peridotite is heterogeneous, both spatially and in style. Three main types of structural features can be recognized: (1) filled fractures associated with brittle deformation, (2) narrow shear zones characterized by foliation planes and shear bands (C-S fabric), and (3) breccias.

Fractures and Veins

The most obvious structural features are fractures that are observed throughout the serpentinized peridotites. Four types of fractures can be distinguished on the basis of the composition, color, and habit of the infilling material:

1. Veins, 1- to 15-mm-thick, composed of white calcite and/or pale serpentine (Fig. 46) and, locally, of dark serpentine, which are continuous over the width of the core (Sections 149-897C-67R-1 and -67R-2; Fig. 47). In both Holes 897C and 897D, the dominant vein-filling mineral progressively changes downward from calcite to serpentine. Textural evidence suggests that the calcite crystallization follows serpentine formation. The intensity of fracturing is highly variable and extensively developed in the upper parts of both Holes 897C and 897D. This fracturing is absent below 710 mbsf in Hole 897C and 780 mbsf in Hole 897D.

The general vein patterns suggest that the fractures show two sets of conjugate directions, with one set preferentially developed. Their

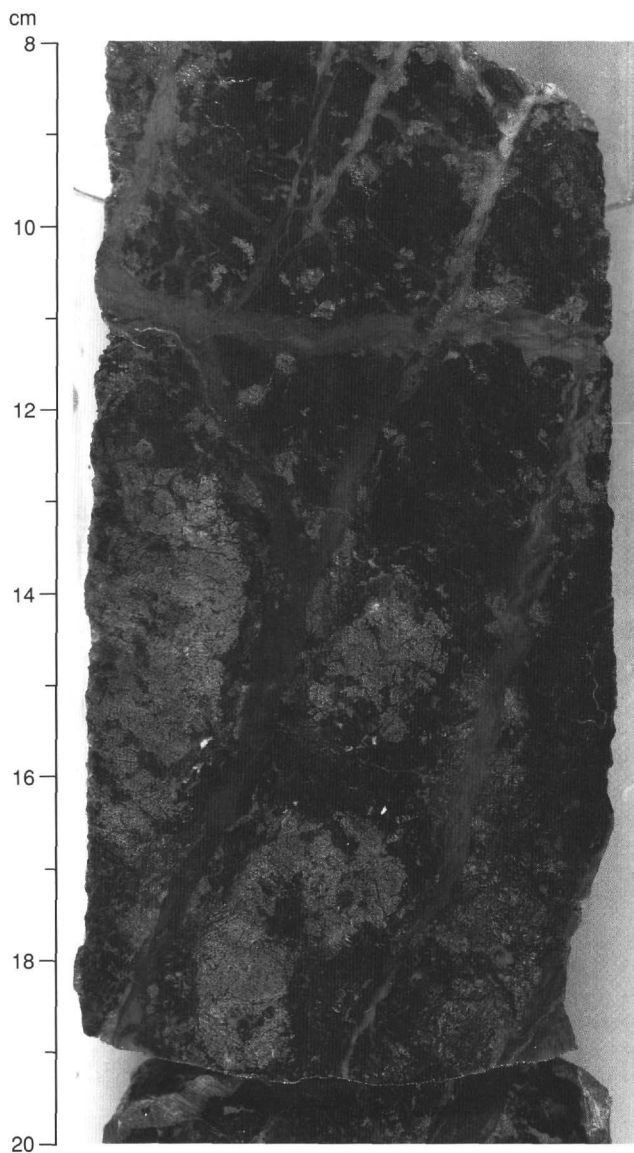


Figure 47. Dark serpentine veins in Interval 149-897C-67R-2, 8-20 cm. The geometry of these veins is representative of the general attitude of these fractures (i.e., a conjugate system with the preferential development of one set; horizontal fractures are scarce).

dips vary from 30° to 75° . Locally, the dip of successive fractures progressively decreases down to 0° (Interval 149-897C-64R-3, 60-100 cm); some subvertical fractures are also observed. In intensely fractured zones, anastomosing veins isolate small (1-2 cm) elements of rock. However, initial heterogeneities may disturb this general framework. For example, in Section 149-897D-19R-4, fractures tend to be localized around pyroxene-rich areas, which appear to be the precursors of many of the small blocks within the breccias.

2. Small discontinuous veins (1-2 mm thick, 5-40 mm long) of white massive serpentine. This fracturing, observed only in the deeper part of both basement sections (below 710 mbsf in Hole 897C and below 780 mbsf in Hole 897D), is unevenly distributed: some areas are apparently free of deformation (e.g., Intervals 149-897C-72R, 1-90 cm, and -897D-20R, 20-95 cm; Sections 149-897D-23R-1 to -23R-3 and 149-897D-25R-4 and -25R-5) and alternate with zones of varying fracture intensity. In slightly deformed areas, small parallel fractures cross-cut pyroxene crystals along cleavage planes (Interval 149-897D-20R-1, 20-95 cm). With increasing deformation, small

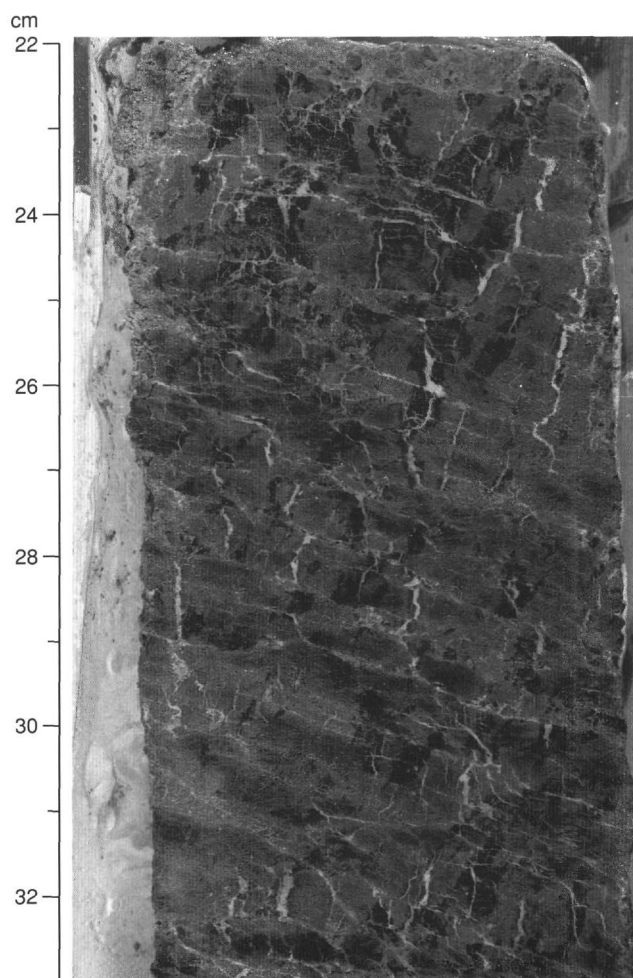


Figure 48. Fracture cleavage along thin serpentinite-filled fractures in serpentinized peridotite (Interval 149-897C-71R-2, 22-33 cm).

fractures radiate from individual pyroxene crystals or clusters (e.g., Interval 149-897D-21R-2, 20-38 cm) or connect pyroxene crystals along a preferential dipping plane (35° - 50° ; e.g., Section 149-897C-73R-4). En-echelon sigmoidal veinlets (e.g., Section 149-897D-23R-6) also were observed and have been interpreted as tension gashes whose geometries are in accordance with horizontal extension. Locally (e.g., Section 149-897C-71R-2), deformation appears to grade into penetrative deformation, leading to fracture cleavage (Fig. 48) and into foliation (Fig. 49) or brecciation (Fig. 50).

3. Diffuse, irregular sinuous veins of pale-green fibrous serpentine occur in the deeper half of both holes (below 700 mbsf in Hole 897C and below 780 mbsf in Hole 897D) and, locally, coexist with Type 2 veins. The distribution of these veins, particularly visible in dark dunitic zones, is not uniform. They are abundant in Core 149-897C-70R, Sections 149-897C-72R-1 and -72R-2, and Cores 149-897D-21R to -23R. They usually display sigmoidal shapes characteristic of tension gashes (Interval 149-897C-70R-2, 50-90 cm). With increasing density, the veins form an anastomosing pattern that outlines rhomboidal elements of serpentinized peridotite (Fig. 51) and, locally, is transitional into brecciation (Fig. 52). When they coexist, veins of Types 2 and 3 appear to be co-eval, as no vein offsets were observed. However, in cross-cutting zones, the Type 2 veins seem to be slightly obscured by the Type 3 ones.

4. Thin, irregular (1-mm-thick) veinlets of green to blue gray serpentine and/or iowaite. These veins, well-expressed in Interval 149-897D-18R-1, 25-150 cm, display an unusual contorted habit and per-

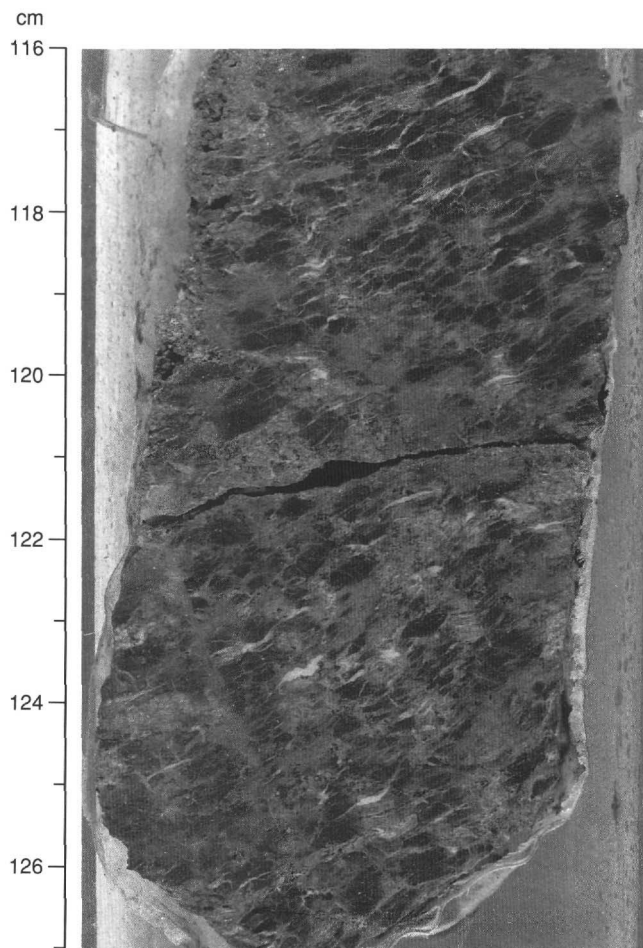


Figure 49. Foliation developed in Interval 149-897C-71R-2, 116-127 cm.

meate the rock suggesting that hydrothermal fluid circulation may have aided the deformation. Where vein density is high, small rounded elements are isolated (Interval 149-897D-18R-2, 30-50 cm). Locally, thicker veins display a foliation associated with shear bands (C-S fabric) marked by alternating colored layers (e.g., Interval 149-897D-18R-1, 95-110 cm).

Shear Zones

In the upper part of Holes 897C and 897D, shear deformation can be observed only in friable breccias (see below). In the deeper part of both holes (below 780 mbsf in Hole 897C and below 800 mbsf in Hole 897D), narrow shear zones are unevenly distributed and usually are characterized by a C-S fabric. The material involved in these zones is highly friable, and their relative scarcity may result from poor core recovery in these intervals. The shear deformation features are marked either by a foliation derived from an intense fracture cleavage of white serpentine veins (Type 2; Interval 149-897C-71R-2, 115-125 cm; Fig. 49), or by preferential orientation of numerous, anastomosing, serpentine veins of Types 2 and 3 (e.g., Intervals 149-897D-21R-2, 105-114 cm; -22R-1, 50-55 cm, and -18R-1, 95-110 cm; Fig. 52). The occurrence of a C-S fabric implies a rotational regime for this deformation (Figs. 52 and 53; Interval 149-897C-70R-1, 105-110 cm; Sections 149-897D-19R-1 and -19R-2; Intervals 149-897D-21R-2, 105-114 cm, and -22R-1, 49-54 cm). Figure 52 (Interval 149-897D-22R-1, 49-54 cm) shows that this shear deformation develops significant brecciation into small rounded blocks. The deformation generally is more developed in the brecciated rocks having a serpentine matrix. In

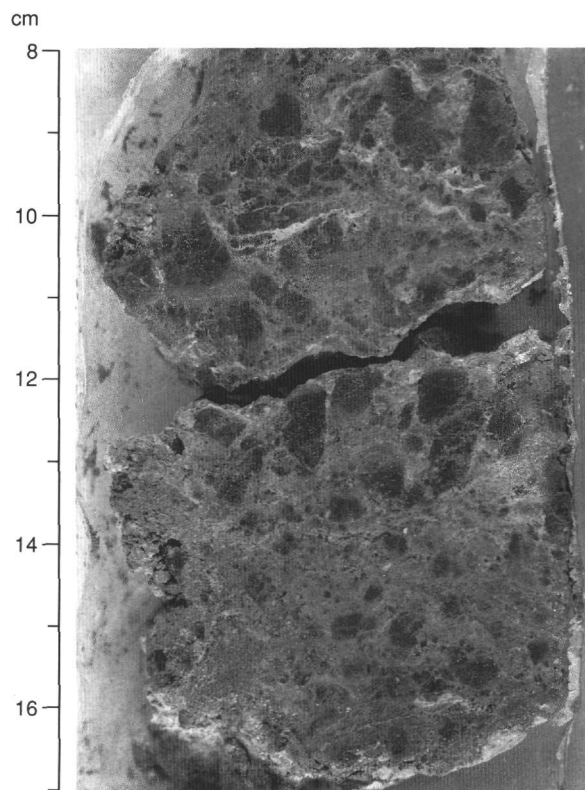


Figure 50. Brecciation of serpentinized peridotite in Interval 149-897C-71R-2, 8-17 cm.

Sections 149-897D-17R-4 to -17R-5, the foliation is marked in the matrix by (1) alternating layers of variously colored serpentine and thin white calcite layers, (2) the alignment and/or flattening of blocks, (3) a concordant layer of creamy yellow serpentine (see below; Fig. 53). The occurrence of rolling structures (Van den Driessche and Brun, 1987) around some of the blocks and of shear bands clearly indicates that this foliation developed in a rotational shear regime.

Brecciation

Three major types of breccia can be distinguished on the basis of block shape, matrix type, and the relative proportion of blocks to matrix:

1. Breccias having angular serpentinized peridotite blocks, 1 cm to more than 40 cm in diameter, embedded in a calcite and/or serpentine matrix. The proportion of blocks varies from 50% to 90%. In a high proportion of the blocks, the individual fragments appear to retain their approximate initial orientation (e.g., Sections 149-897C-65R-1 and -897D-19R-4; Interval 149-897C-64R-4, 55-65 cm; Fig. 54). Deeper in the recovered sections, the blocks are embedded in a variably colored serpentine matrix that shows disorganized folds and convolutions, attesting to high ductility (Section 149-897D-19R-3, 75-105 cm). In some intervals, a subtype was identified by breccias associated with the development of an intense fracture cleavage and shear deformation; the serpentine blocks display a penetrative deformation expressed by the flattening of the serpentine mesh texture (e.g., Intervals 149-897D-22R-1, 48-54 cm; -897C-71 R-2, 5-20 cm, and 130-145 cm). These Type 1 breccias, which result from intense fracturing or shearing, are unevenly distributed in both holes and make up 30% of the serpentinized peridotites.

2. Breccias, containing small (about 10 mm) rounded blocks of serpentine in a variably colored serpentine matrix, occur as a thick

layer in Sections 149-897D-17R-4 to -17R-6 and in Interval 149-897D-18R-1, 0-20 cm. In Figure 53, one can see a 5-cm-thick layer of creamy yellow serpentine matrix that contains a few small blocks. Two types of deformation clearly affect this breccia: (1) a heterogeneously distributed shearing and (2) a later episode of heterogeneous fracturing expressed as thin, parallel-dipping veins of calcite or brucite; these breccias have been consolidated by late calcitization.

3. Type C friable breccias, which contain blocks that make up about 70% of the rock, with a matrix comparable to that in the Type 2 breccias (Sections 149-897D-10R-2 and -10R-3). This may be the same material that has been pervasively altered. These breccias are locally foliated and display a shear deformation. Friable breccias also were observed in Sections 149-897C-66R-1, -66R-2, and -66R-3; 149-897D-18R-2, -18R-3, and -18R-4. However, in these instances, the proportion of soft serpentine matrix was much larger (up to 90%) and the blocks varied in size.

Discussion

Ductile high-temperature deformation of the peridotites was observed rarely at Site 897 and is unevenly distributed. This high-temperature deformation is mainly characterized by thin bands containing very fine recrystallized grains, which indicates that recrystallization occurred under high deviatoric stress and relatively low temperatures (<1000°C). Similar thin zones of extremely reduced grains have been identified as shear bands in the Galicia Bank margin peridotites (Girardeau et al., 1988; Beslier et al., 1990).

The intense fracturing, shearing, and brecciation that overprint the primary textures indicate extensive late-stage and low-temperature deformation. These structures are unevenly distributed throughout the cores. The dominant vein-filling mineral progressively changes downward from calcite to serpentine.

The fractures tend to be localized around preexisting heterogeneities that are at a variety of scales (e.g., around isolated pyroxene crystals and pyroxene-rich dikes, bands, or diffuse pyroxene-rich areas). With increasing deformation intensity, the fracturing evolves into brecciation. This brecciation exhibits little, if any, displacement of the angular blocks. The attitude and geometry of tension gashes is compatible with a horizontal principal extensional stress direction.

Shear zones are characterized by a C-S fabric. Foliation is marked by an intense fracture cleavage, or it is developed in thick or parallel thin serpentine veins associated with a penetrative deformation of the serpentine mesh. This attests to a late deformation, when the peridotite was already at least partly serpentinized. Because serpentine usually is a ductile material, shear zones occur preferentially in serpentine-rich levels and, in particular, in breccias containing a serpentine matrix. The presence of veins of iowaite and brucite, as well as the contorted shape of some veins, suggest that hydrothermal fluids also may have aided deformation. Textural evidence and relationships between the different structural features suggest (1) that the high- and low-temperature deformations may represent stages along a continuum during the uplifting of the mantle rocks, (2) that the low-temperature shear deformation occurred during and/or after the main serpentinization event, and (3) that the different features associated with the late-stage deformation represent a continuum, with late calcite veining.

Further structural, paleomagnetic, and petrologic studies may help define the conditions during the deformation events, the sequence of the different types of late-stage structures, the kinematics of the deformation (sense of shear), and the attitude of the foliation in the geographic reference frame.

Comparison with the Galicia Bank Margin Peridotites

The petrostructural evolution of the Galicia Bank margin peridotites is summarized in the "Igneous and Metamorphic Petrology

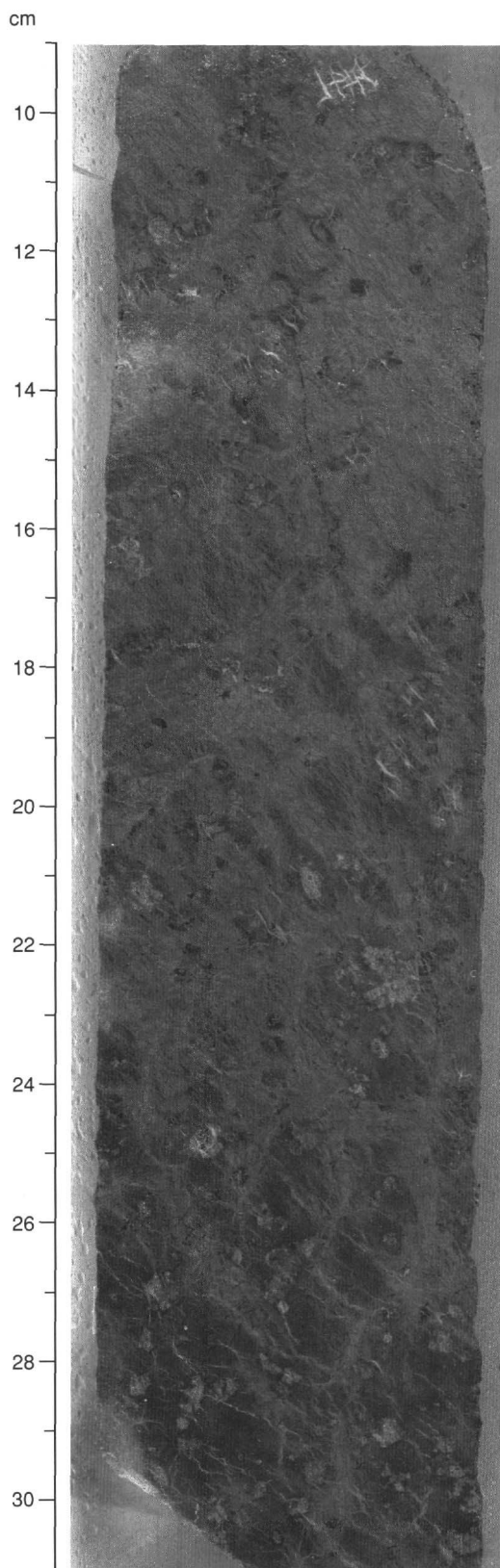


Figure 51. Anastomosing pale green fibrous serpentine veins in Interval 149-897D-21R-4, 9-31 cm.

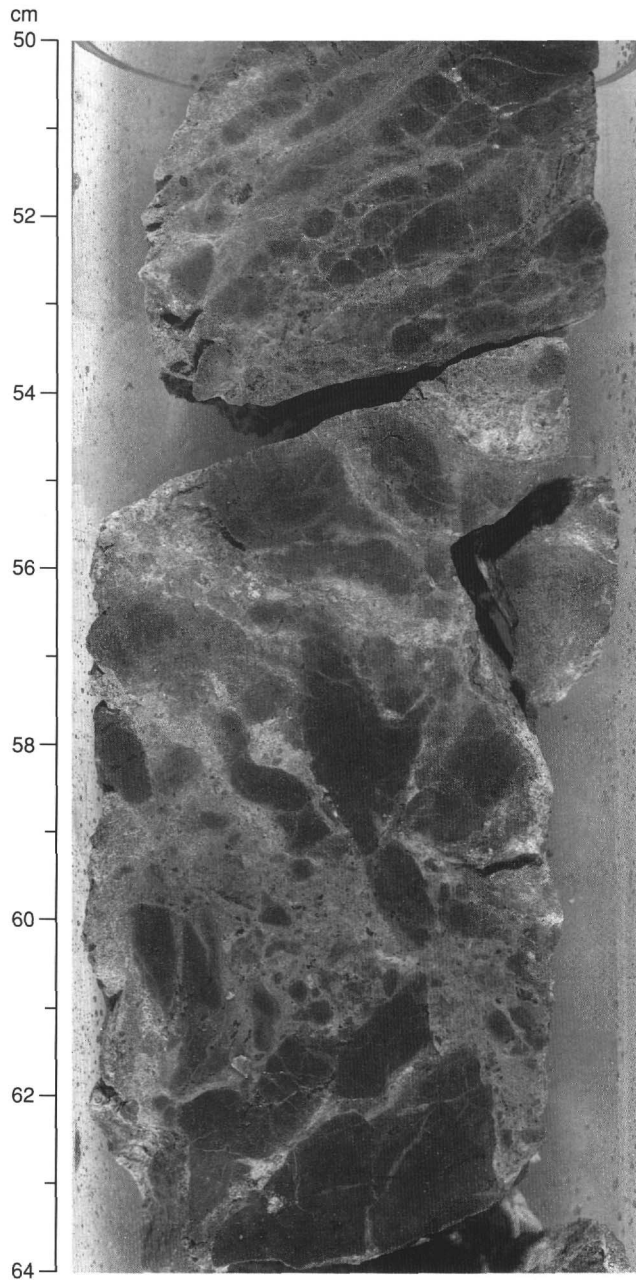


Figure 52. Anastomosing pale green fibrous serpentine veins that mark a dipping foliation associated with shear bands and that locally evolve into brecciation (Interval 149-897D-22R-1, 50-64 cm).

and Geochemistry" section (this chapter). At this time, the preliminary studies of the Site 897 peridotites allow us to tentatively compare the peridotites sampled at the two sites. Some striking differences in the texture and tectonic evolution of the mantle rocks arise from previous observations:

1. The high-temperature ductile deformation, which developed a well-marked foliation in the Galicia Bank peridotites during their uplifting, was not observed in the Site 897 peridotites. This indicates that the structural evolution of the mantle rocks beneath these two portions of the continental rift was different. The only comparable ductile deformation at Site 897 is the relatively low-temperature

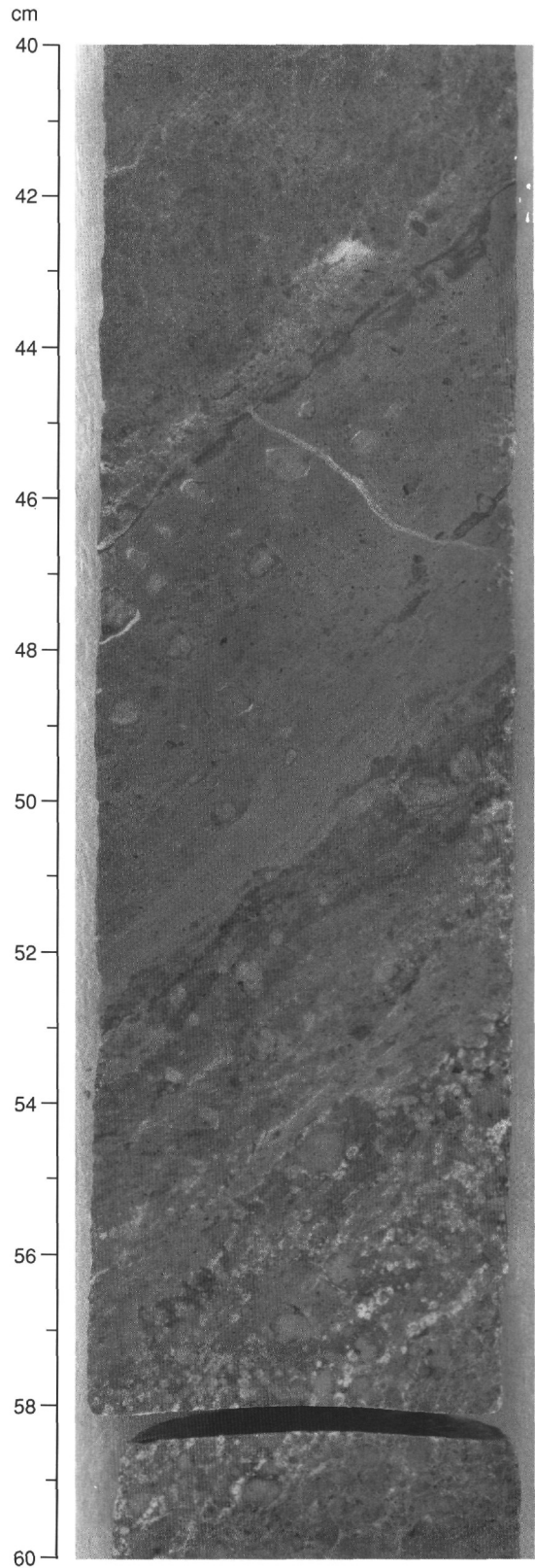


Figure 53. Sheared breccias containing subrounded blocks of serpentine in a serpentine matrix (Interval 149-897D-17R-4, 40-60 cm). A highly sheared layer, composed of a few serpentine clasts in a creamy yellow serpentine matrix, is interbedded.

deformation characterized by fine-grained shear bands. Petrological studies have shown that on the Galicia Bank margin such ductile deformation probably occurred at about 850°C at shallow depths (<7 km: Girardeau et al, 1988).

2. The late-stage shear deformation of the Site 897 serpentinized rocks was not observed in the Galicia Bank peridotites. This suggests that the top of the mantle was sheared during or after the main serpentinization event (i.e., in the latest stages of rifting at the ocean/continent transition of the Iberia Abyssal Plain margin). However, extensive late fracturing, serpentinization, and calcite alteration are present at both sites.

ORGANIC GEOCHEMISTRY

Concentrations of calcium carbonate and organic carbon were measured in samples obtained regularly at selected intervals from Holes 897A, 897C, and 897D. Results of organic-matter atomic C/N ratios and pyrolysis were employed to determine the type of organic matter contained within the sediments. Routine monitoring of head-space gas contents (done for drilling safety) yielded interesting information about the evolution and migration of biogenic gas in these passive margin sediments.

Concentrations of Inorganic and Organic Carbon

Concentrations of carbonate carbon vary between a high of 9.4% to essentially 0% in sediments and rocks from Site 897 (Table 12). These concentrations of carbonate carbon are equivalent to 78% to 0% CaCO₃ in the sediment, assuming that all of the carbonate is present as pure calcite. Lithologic Unit III is uniformly low in carbonate carbon; the other three units are highly variable. This variability reflects a history of generally low biological productivity and deposition of hemipelagic sediments below the CCD, combined with delivery of carbonate-rich turbiditic sediments initially deposited in shallower waters.

Concentrations of organic carbon are relatively high in several parts of the Site 897 lithologic column (Table 12). Unit I, a Pleistocene to upper Pliocene turbidite-containing sequence, averages 0.6% organic carbon, and Unit IV, a Cretaceous sandstone-claystone-clast sequence, averages 0.9% (Fig. 55). Both units contain substantially more organic carbon than the average of 0.2% that was calculated from DSDP Legs 1 through 31 by McIver (1975). The two principal sources of organic matter in oceanic sediments are marine algal production and land plant detritus supplied by rivers and winds. Algal organic matter typically is oxidized and largely recycled during and shortly after settling to the seafloor (e.g., Suess, 1980; Emerson and Hedges, 1988). The land-derived organic matter that is delivered to deep-sea sediments generally is the less-reactive material that remains after transport to the ocean. Consequently, the elevated organic carbon concentrations found in Units I and IV result from special depositional conditions. Both units are dominated by sediments displaced from shallower locations (see "Lithostratigraphy" section, this chapter), and downslope transport and rapid burial participated in delivering and preserving the organic matter.

Characterizations of Organic Matter Sources

The source of organic matter in Site 897 samples was determined two ways: by organic C/N ratios and GHM pyrolysis. Algal organic matter generally has C/N ratios of between 5 and 10, whereas organic matter derived from land plants has values between 20 and 100 (e.g., Emerson and Hedges, 1988; Meyers, in press). C/N ratios for samples from Unit I averaged 6.7 (Table 12; Fig. 56), suggesting a predominantly marine source for the organic matter in these sediments. The C/N values of samples from Units II and III are highly variable,

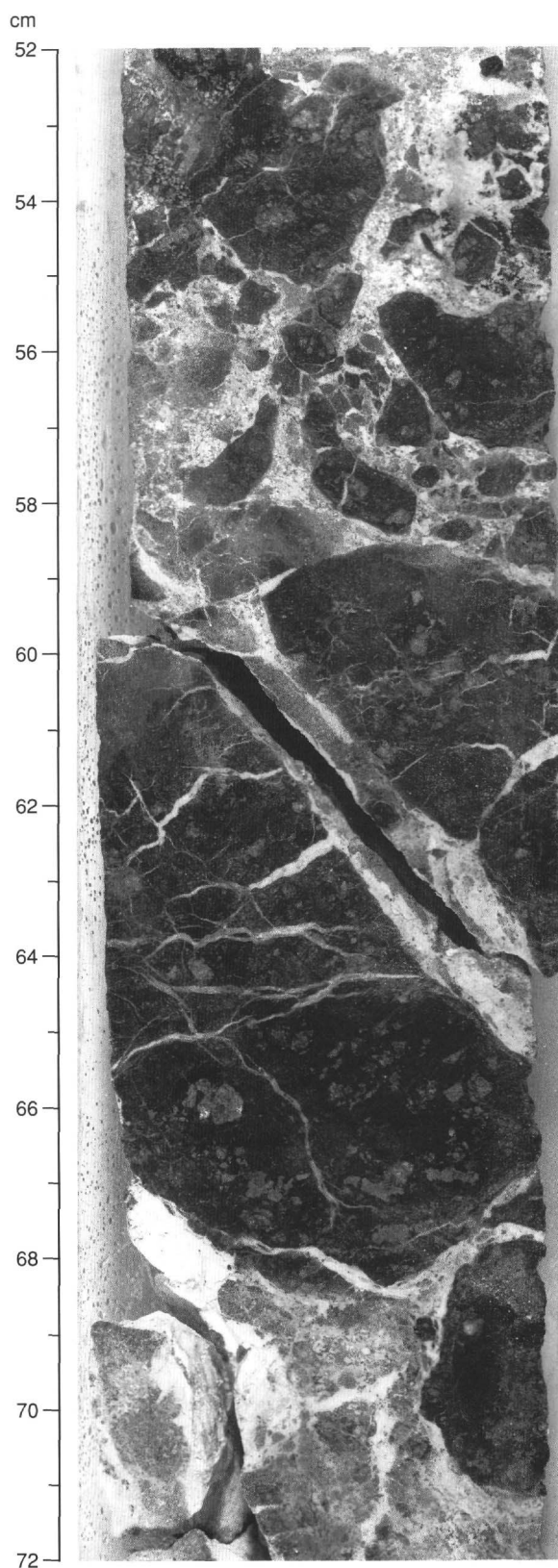


Figure 54. Breccias derived from intense fracturing (Interval 149-897C-65R-1, 52-72 cm). Angular blocks of serpentinized peridotite are embedded in a calcite and/or serpentine matrix.

Table 12. Concentrations of total, inorganic, and organic carbon in sediments and rocks from Holes 897A, 897C, and 897D.

| Hole | Core, section, interval (cm) | Depth (mbsf) | Total C (%) | Inorg. C (%) | Org. C (%) | CaCO ₃ (%) | Org. C/N | Org. C/S | Lithologic unit |
|----------|------------------------------|--------------|-------------|--------------|------------|-----------------------|----------|----------|-----------------------------------------------------------|
| 149-897- | | | | | | | | | |
| A | 1R-1, 58-60 | 0.58 | 2.30 | 1.65 | 0.65 | 13.7 | 8.1 | 0.5 | Unit I - nannofossil clay and silty clay with sand layers |
| A | 3R-1, 40-41 | 17.10 | 4.65 | 4.36 | 0.29 | 36.3 | 4.8 | 1.1 | |
| A | 3R-CC, 1-2 | 17.21 | 2.97 | 2.39 | 0.58 | 19.9 | 7.2 | 1.5 | |
| A | 4R-1, 58-60 | 26.88 | 3.43 | 2.70 | 0.73 | 22.5 | 10.0 | 1.4 | |
| A | 4R-1, 121-122 | 27.51 | 4.23 | 3.89 | 0.34 | 32.4 | 5.6 | 1.5 | |
| A | 4R-2, 5-6 | 27.85 | 4.14 | 3.64 | 0.50 | 30.3 | 7.1 | 0.7 | |
| A | 4R-2, 60-62 | 28.40 | 8.24 | 7.84 | 0.40 | 65.3 | 6.6 | | |
| A | 5R-1, 29-30 | 36.29 | 4.85 | 4.23 | 0.62 | 35.2 | 8.8 | 1.8 | |
| A | 5R-2, 21-22 | 37.71 | 7.12 | 6.59 | 0.53 | 54.9 | 8.8 | 2.8 | |
| A | 5R-2, 45-46 | 37.95 | 8.15 | 7.65 | 0.50 | 63.7 | 8.3 | 2.8 | |
| A | 5R-2, 122-123 | 38.72 | 4.92 | 4.45 | 0.47 | 37.1 | 7.8 | 0.8 | |
| C | 1R-1, 30-31 | 50.20 | 4.98 | 4.49 | 0.49 | 37.4 | 3.2 | 0.3 | |
| A | 6R-4, 104-105 | 51.14 | 4.07 | 3.61 | 0.46 | 30.1 | 5.1 | 0.1 | |
| C | 1R-2, 11-12 | 51.51 | 5.61 | 4.74 | 0.87 | 39.5 | 7.9 | 0.4 | |
| A | 6R-5, 2-3 | 51.62 | 5.12 | 4.87 | 0.25 | 40.6 | | | |
| A | 6R-5, 36-37 | 51.96 | 2.73 | 2.17 | 0.56 | 18.1 | 5.6 | 0.5 | |
| C | 1R-2, 112-113 | 52.52 | 4.88 | 4.30 | 0.58 | 35.8 | 5.8 | 0.3 | |
| C | 2R-1, 58-59 | 60.48 | 0.84 | 0.41 | 0.43 | 3.4 | 3.9 | | |
| C | 2R-1, 129-130 | 61.19 | 8.52 | 8.15 | 0.37 | 67.9 | 5.3 | | |
| C | 3R-1, 12-13 | 69.72 | 2.89 | 2.70 | 0.19 | 22.5 | 3.1 | 0.0 | |
| C | 3R-1, 56-58 | 70.16 | 6.25 | 5.78 | 0.47 | 48.1 | 5.2 | 7.8 | |
| C | 4R-1, 17-18 | 79.37 | 5.60 | 5.03 | 0.57 | 41.9 | 5.7 | 1.1 | |
| C | 4R-1, 45-46 | 79.65 | 4.27 | 2.90 | 1.37 | 24.2 | 9.8 | 0.6 | |
| C | 4R-1, 54-55 | 79.74 | 2.23 | 1.73 | 0.50 | 14.4 | 4.5 | 0.2 | |
| C | 5R-1, 59-60 | 89.49 | 4.14 | 3.40 | 0.74 | 28.3 | 6.7 | 0.4 | |
| C | 5R-2, 15-16 | 90.55 | 3.53 | 3.09 | 0.44 | 25.7 | 7.3 | 0.1 | |
| C | 5R-2, 61-62 | 91.01 | 3.66 | 3.33 | 0.33 | 27.7 | 4.1 | 0.8 | |
| C | 6R-1, 53-54 | 99.03 | 4.72 | 4.08 | 0.64 | 34.0 | 7.1 | 2.9 | |
| C | 6R-1, 101-102 | 99.51 | 4.30 | 3.84 | 0.46 | 32.0 | 6.6 | 1.6 | |
| C | 7R-1, 34-35 | 108.54 | 2.55 | 1.95 | 0.60 | 16.2 | 6.0 | 30.0 | |
| C | 7R-1, 59-60 | 108.79 | 1.84 | 1.60 | 0.24 | 13.3 | 6.0 | 0.2 | |
| C | 7R-1, 113-114 | 109.33 | 2.86 | 2.04 | 0.82 | 17.0 | 7.4 | 0.7 | |
| C | 8R-1, 49-50 | 118.39 | 4.36 | 2.84 | 1.52 | 23.7 | 9.5 | 0.2 | |
| C | 8R-2, 19-20 | 119.59 | 2.56 | 2.04 | 0.52 | 17.0 | 6.5 | 0.3 | |
| C | 8R-2, 113-114 | 120.53 | 4.91 | 4.54 | 0.37 | 37.8 | 4.6 | 12.0 | |
| C | 8R-3, 57-58 | 121.47 | 8.69 | 8.52 | 0.17 | 71.0 | 3.4 | | |
| C | 9R-1, 23-24 | 127.73 | 3.24 | 2.26 | 0.98 | 18.8 | 9.8 | 1.2 | |
| C | 9R-2, 1-2 | 128.51 | 1.80 | 1.46 | 0.34 | 12.2 | 3.4 | 3.4 | |
| C | 10R-1, 56-57 | 137.76 | 3.39 | 2.6 | 0.79 | 21.7 | 7.9 | 11.0 | |
| C | 10R-1, 103-104 | 138.23 | 9.56 | 9.28 | 0.28 | 77.3 | 9.3 | | |
| C | 11R-2, 65-66 | 147.74 | 3.76 | 3.37 | 0.39 | 28.1 | 4.3 | | |
| C | 11R-2, 71-72 | 147.80 | 2.13 | 1.66 | 0.47 | 13.8 | 4.7 | 3.1 | |
| C | 11R-2, 74-75 | 147.83 | 3.36 | 1.61 | 1.75 | 13.4 | | | |
| C | 11R-4, 29-30 | 150.09 | 0.49 | 0.24 | 0.25 | 2.0 | 2.5 | 1.1 | |
| C | 11R-4, 92-93 | 150.72 | 6.23 | 5.85 | 0.38 | 48.7 | 4.7 | | |
| C | 12R-5, 44-45 | 163.04 | 2.84 | 2.28 | 0.56 | 19.0 | 11.0 | 0.3 | |
| C | 12R-5, 138-139 | 163.98 | 9.50 | 9.34 | 0.16 | 77.8 | 4.0 | | |
| C | 12R-6, 13-14 | 164.23 | 7.87 | 7.76 | 0.11 | 64.6 | 2.2 | 1.2 | |
| C | 12R-6, 34-35 | 164.44 | 2.10 | 1.47 | 0.63 | 12.2 | 7.0 | 0.7 | |
| C | 14R-2, 84-85 | 178.14 | 7.01 | 6.93 | 0.08 | 57.7 | 1.0 | 0.1 | |
| C | 14R-3, 16-17 | 178.96 | 7.77 | 7.56 | 0.21 | 63.0 | 4.2 | | |
| C | 14R-3, 30-31 | 179.10 | 1.31 | 1.24 | 0.07 | 10.3 | 1.0 | 1.0 | |
| C | 14R-3, 36-37 | 179.16 | 2.09 | 1.47 | 0.62 | 12.2 | 10.0 | 2.0 | |
| C | 14R-4, 64-65 | 180.94 | 3.66 | 2.45 | 1.21 | 20.4 | 10.1 | 1.8 | |
| C | 15R-1, 3-4 | 185.43 | 6.52 | 6.08 | 0.44 | 50.6 | 4.9 | 0.9 | |
| C | 15R-1, 23-24 | 185.63 | 2.75 | 1.96 | 0.79 | 16.3 | 7.9 | 2.2 | |
| C | 15R-1, 37-38 | 185.77 | 2.35 | 1.78 | 0.57 | 14.8 | 9.5 | 0.8 | |
| C | 15R-2, 119-120 | 188.09 | 6.6 | 6.28 | 0.32 | 52.3 | 5.3 | | |
| C | 16R-1, 69-70 | 195.79 | 4.13 | 3.68 | 0.45 | 30.7 | 5.6 | 3.7 | |
| C | 16R-1, 75-76 | 195.85 | 3.52 | 2.32 | 1.20 | 19.3 | 10.0 | 1.5 | |
| C | 16R-1, 107-108 | 196.17 | 4.17 | 4.04 | 0.13 | 33.7 | 2.1 | 4.3 | |
| C | 17R-1, 39-40 | 205.09 | 4.44 | 4.10 | 0.34 | 34.2 | 5.6 | 3.4 | |
| C | 17R-1, 52-53 | 205.22 | 5.03 | 4.05 | 0.98 | 33.7 | 8.9 | 2.8 | |
| C | 17R-1, 125-126 | 205.95 | 9.58 | 9.38 | 0.20 | 78.1 | 5.0 | 0.8 | |
| C | 19R-1, 10-11 | 224.20 | 2.61 | 1.84 | 0.77 | 15.3 | 8.5 | 8.5 | |
| C | 19R-1, 71-72 | 224.81 | 2.46 | 2.13 | 0.33 | 17.7 | 4.1 | | |
| C | 19R-3, 61-62 | 227.71 | 2.31 | 1.54 | 0.77 | 12.8 | 9.6 | 1.8 | |
| C | 20R-1, 10-11 | 233.90 | 1.90 | 1.10 | 0.80 | 9.2 | 8.0 | 7.3 | |
| C | 20R-1, 110-110 | 234.90 | 3.45 | 2.91 | 0.54 | 24.2 | 11.0 | 1.0 | |
| C | 20R-1, 134-135 | 235.14 | 7.01 | 6.65 | 0.36 | 55.4 | 7.2 | | |
| C | 21R-1, 107-108 | 244.47 | 1.77 | 0.92 | 0.85 | 7.7 | 12.0 | 7.1 | |
| C | 21R-1, 124-125 | 244.64 | 4.44 | 1.70 | 2.74 | 14.2 | 11.9 | 4.5 | |
| C | 21R-1, 134-135 | 244.74 | 1.24 | 0.67 | 0.57 | 5.6 | 11.0 | 1.0 | |
| C | 22R-2, 73-74 | 255.23 | 3.53 | 3.22 | 0.31 | 26.8 | 3.9 | | |
| C | 22R-2, 99-100 | 255.49 | 4.57 | 3.67 | 0.90 | 30.6 | 9.0 | 3.6 | |
| C | 22R-4, 30-31 | 257.80 | 8.43 | 8.22 | 0.21 | 68.5 | 5.2 | | |
| C | 23R-1, 69-70 | 263.39 | 3.38 | 1.57 | 1.81 | 13.1 | 2.8 | 3.4 | |
| C | 23R-1, 106-107 | 263.76 | 4.57 | 4.23 | 0.34 | 35.2 | 5.6 | | |
| C | 23R-1, 140-141 | 264.10 | 2.98 | 1.95 | 1.03 | 16.2 | 14.7 | | |
| C | 24R-1, 85-86 | 273.15 | 1.36 | 0.72 | 0.64 | 6.0 | 7.1 | 16.0 | |
| C | 25R-1, 11-12 | 282.11 | 1.74 | 1.23 | 0.51 | 10.2 | 7.3 | 5.6 | |
| C | 25R-1, 85-86 | 282.85 | 2.18 | 1.53 | 0.65 | 12.7 | 11.0 | 3.4 | |
| C | 25R-1, 122-123 | 283.22 | 1.69 | 1.13 | 0.56 | 9.4 | 14.0 | 0.5 | |
| C | 25R-1, 128-129 | 283.28 | 1.81 | 1.33 | 0.48 | 11.1 | 6.8 | 9.6 | |

Table 12 (continued).

| Hole | Core, section, interval (cm) | Depth (mbsf) | Total C (%) | Inorg. C (%) | Org. C (%) | CaCO ₃ (%) | Org. C/N | Org. C/S | Lithologic unit |
|------|------------------------------|--------------|-------------|--------------|------------|-----------------------|----------|----------|---------------------------------------------------|
| C | 26R-1, 66-67 | 292.16 | 2.79 | 2.75 | 0.04 | 22.9 | 1.0 | | Unit II - nannofossil claystone and silty clay |
| C | 26R-1, 99-100 | 292.49 | 4.78 | 4.58 | 0.20 | 38.2 | 6.6 | | |
| C | 26R-2, 60-61 | 293.60 | 6.54 | 6.41 | 0.13 | 53.4 | 6.5 | | |
| C | 26R-2, 77-78 | 293.77 | 2.02 | 1.91 | 0.11 | 15.9 | 2.7 | | |
| C | 26R-2, 134-135 | 294.34 | 3.67 | 3.56 | 0.11 | 29.7 | 2.7 | 0.3 | |
| C | 27R-1, 14-15 | 301.34 | 0.09 | 0.05 | 0.04 | 0.4 | 0.8 | | |
| C | 27R-CC, 13-14 | 301.62 | 9.15 | 8.93 | 0.22 | 74.4 | 1.1 | 2.2 | |
| C | 28R-1, 105-106 | 311.95 | 2.46 | 2.31 | 0.15 | 19.2 | 5.0 | | |
| C | 28R-2, 29-30 | 312.69 | 0.16 | 0.13 | 0.03 | 1.1 | 0.7 | | |
| C | 28R-2, 80-81 | 313.20 | 0.23 | 0.15 | 0.08 | 1.2 | 2.0 | | |
| C | 28R-4, 140-141 | 316.80 | 7.26 | 7.23 | 0.03 | 60.2 | 1.0 | | |
| C | 28R-5, 30-31 | 317.20 | 8.20 | 5.67 | 2.53 | 47.2 | | | |
| C | 28R-CC, 3-4 | 317.72 | 8.77 | 6.36 | 2.41 | 53.0 | 60.2 | | |
| C | 29R-1, 22-23 | 320.72 | 2.96 | 2.81 | 0.15 | 23.4 | 5.0 | 7.5 | |
| C | 29R-3, 48-49 | 323.98 | 1.45 | 1.27 | 0.18 | 10.6 | 4.5 | 3.0 | |
| C | 29R-4, 120-121 | 326.20 | 4.09 | 4.00 | 0.09 | 33.3 | 2.0 | | |
| C | 29R-5, 21-22 | 326.71 | 4.26 | 4.09 | 0.17 | 34.1 | 2.8 | | |
| C | 30R-1, 60-61 | 330.80 | 5.13 | 5.07 | 0.06 | 42.2 | 3.0 | | |
| C | 30R-1, 70-71 | 330.90 | 5.27 | 4.74 | 0.53 | 39.5 | 8.8 | 10.0 | |
| C | 30R-1, 92-93 | 331.12 | 0.33 | 0.23 | 0.10 | 1.9 | 1.6 | 1.6 | |
| C | 30R-6, 24-25 | 337.94 | 8.55 | 8.49 | 0.06 | 70.7 | 2.0 | | |
| C | 31R-1, 86-87 | 340.76 | 5.00 | 4.95 | 0.05 | 41.2 | 1.0 | | |
| C | 31R-1, 116-117 | 341.06 | 1.56 | 1.42 | 0.14 | 11.8 | | | |
| C | 31R-1, 129-130 | 341.19 | 5.11 | 4.45 | 0.66 | 37.1 | 8.2 | 13.0 | |
| C | 31R-2, 32-33 | 341.72 | 6.84 | 6.80 | 0.04 | 56.6 | 1.0 | 1.0 | |
| C | 33R-1, 75-76 | 359.85 | 0.67 | 0.62 | 0.05 | 5.2 | 1.0 | 1.0 | |
| C | 33R-6, 137-138 | 367.97 | 0.29 | 0.21 | 0.08 | 1.7 | 1.0 | 4.0 | |
| C | 33R-7, 59-60 | 368.69 | 0.44 | 0.33 | 0.11 | 2.7 | 2.2 | 1.4 | |
| C | 34R-1, 113-114 | 369.93 | 1.63 | 1.46 | 0.17 | 12.2 | 3.4 | | |
| C | 34R-1, 115-116 | 369.95 | 0.88 | 0.55 | 0.33 | 4.6 | 6.6 | | |
| C | 34R-4, 35-36 | 373.45 | 4.56 | 3.47 | 1.09 | 28.9 | 12.1 | 2.3 | |
| C | 35R-2, 41-42 | 380.31 | 0.24 | 0.16 | 0.08 | 1.3 | 2.0 | | |
| C | 35R-2, 74-75 | 380.64 | 3.33 | 3.26 | 0.07 | 27.2 | 2.0 | | |
| C | 35R-6, 51-52 | 386.41 | 4.55 | 3.83 | 0.72 | 31.9 | 12.0 | 2.2 | |
| C | 36R-1, 55-56 | 388.65 | 2.12 | 1.97 | 0.15 | 16.4 | 3.7 | 2.5 | |
| C | 36R-1, 71-72 | 388.81 | 2.49 | 1.92 | 0.57 | 16.0 | 11.0 | 3.8 | |
| C | 36R-2, 78-79 | 390.38 | 3.87 | 3.66 | 0.21 | 30.5 | 5.2 | | |
| C | 36R-5, 75-76 | 394.85 | 0.28 | 0.25 | 0.03 | 2.1 | 1.0 | | |
| C | 36R-5, 134-135 | 395.44 | 4.39 | 4.33 | 0.06 | 36.1 | 3.0 | | |
| C | 37R-1, 109-110 | 398.89 | 0.12 | 0.04 | 0.08 | 0.3 | 2.0 | | |
| C | 37R-5, 18-19 | 403.98 | 1.04 | 1.02 | 0.02 | 8.5 | 1.0 | | |
| C | 37R-6, 37-38 | 405.17 | 7.42 | 7.25 | 0.17 | 60.4 | 17.0 | | |
| C | 38R-2, 17-18 | 409.07 | 2.34 | 2.26 | 0.08 | 18.8 | | | |
| C | 38R-3, 79-80 | 411.19 | 2.64 | 2.60 | 0.04 | 21.7 | 2.0 | | |
| C | 38R-6, 22-23 | 415.12 | 0.73 | 0.72 | 0.01 | 6.0 | 0.5 | | |
| C | 39R-1, 133-134 | 418.43 | 2.45 | 2.36 | 0.09 | 19.7 | | | |
| C | 39R-2, 63-64 | 419.23 | 2.59 | 2.42 | 0.17 | 20.2 | 5.6 | | |
| C | 39R-3, 133-134 | 421.43 | 3.31 | 3.22 | 0.09 | 26.8 | 0.6 | | |
| C | 40R-2, 14-15 | 428.34 | 1.90 | 1.76 | 0.14 | 14.7 | 14.0 | | |
| C | 40R-3, 4-5 | 429.74 | 0.19 | 0.12 | 0.07 | 1.0 | 2.0 | 2.0 | |
| C | 40R-4, 73-74 | 431.93 | 5.27 | 5.00 | 0.27 | 41.7 | 9.0 | 27.0 | |
| C | 41R-1, 100-101 | 437.4 | 0.27 | 0.17 | 0.10 | 1.4 | 2.0 | 1.6 | |
| C | 41R-2, 81-82 | 438.71 | 7.67 | 7.55 | 0.12 | 62.9 | 4.0 | 1.7 | |
| C | 41R-4, 18-19 | 440.58 | 0.34 | 0.24 | 0.10 | 2.0 | 2.0 | 1.2 | |
| C | 42R-1, 108-109 | 447.08 | 3.16 | 3.07 | 0.09 | 25.6 | 2.0 | 4.0 | |
| C | 42R-2, 30-31 | 447.8 | 1.08 | 1.02 | 0.06 | 8.5 | 1.0 | 1.0 | |
| C | 42R-3, 59-60 | 449.59 | 7.21 | 7.09 | 0.12 | 59.1 | 4.0 | | |
| C | 43R-1, 38-39 | 455.98 | 0.54 | 0.51 | 0.03 | 4.2 | 1.0 | 1.0 | |
| C | 43R-4, 81-82 | 460.91 | 2.86 | 2.20 | 0.66 | 18.3 | 22.0 | 33.0 | |
| C | 44R-1, 128-129 | 466.58 | 0.69 | 0.64 | 0.05 | 5.3 | 1.0 | 0.6 | |
| C | 45R-2, 89-90 | 477.39 | 3.32 | 3.29 | 0.03 | 27.4 | 0.7 | 1.0 | |
| C | 46R-2, 43-44 | 486.53 | 7.66 | 7.61 | 0.05 | 63.4 | 2.0 | | |
| C | 46R-2, 68-69 | 486.78 | 0.90 | 0.73 | 0.17 | 6.1 | 4.2 | 8.5 | |
| C | 46R-4, 64-65 | 489.74 | 3.99 | 3.90 | 0.09 | 32.5 | 3.0 | | |
| C | 47R-2, 41-42 | 496.11 | 0.23 | 0.17 | 0.06 | 1.4 | 1.0 | 2.0 | |
| C | 47R-3, 75-76 | 497.95 | 4.14 | 4.03 | 0.11 | 33.6 | 3.6 | 11.0 | |
| C | 47R-4, 25-26 | 498.95 | 5.39 | 5.36 | 0.03 | 44.6 | 1.0 | | |
| C | 47R-5, 144-145 | 501.64 | 0.36 | 0.24 | 0.12 | 2.0 | 3.0 | | |
| C | 48R-1, 48-50 | 504.38 | 3.65 | 3.41 | 0.24 | 28.4 | 12.0 | 12.0 | |
| C | 48R-1, 68-69 | 504.58 | 5.76 | 5.57 | 0.19 | 46.4 | 6.3 | | |
| C | 48R-2, 43-44 | 505.83 | 0.10 | 0.06 | 0.04 | 0.5 | 1.0 | 4.0 | |
| C | 48R-3, 56-57 | 507.46 | 4.89 | 4.69 | 0.20 | 39.1 | 10.0 | | |
| C | 49R-1, 51-52 | 514.11 | 0.35 | 0.18 | 0.17 | 1.5 | 4.2 | 8.5 | |
| C | 49R-2, 5-6 | 515.15 | 0.13 | 0.00 | 0.13 | 0.0 | 3.2 | 6.5 | |
| C | 49R-4, 33-34 | 518.43 | 6.27 | 6.13 | 0.14 | 51.1 | 7.0 | | |
| C | 50R-1, 5-6 | 523.25 | 5.77 | 5.44 | 0.33 | 45.3 | 11.0 | | |
| C | 50R-3, 29-30 | 526.49 | 5.80 | 5.32 | 0.48 | 44.3 | 48.0 | | |
| C | 50R-4, 12-13 | 527.32 | 0.23 | 0.20 | 0.03 | 1.7 | 1.0 | | |
| C | 51R-1, 14-15 | 532.94 | 6.48 | 6.41 | 0.07 | 53.4 | 7.0 | | |
| C | 51R-2, 25-26 | 534.55 | 0.15 | 0.11 | 0.04 | 0.9 | 2.0 | | |
| C | 52R-1, 102-103 | 543.42 | 3.07 | 2.98 | 0.09 | 24.8 | 9.0 | | |
| C | 52R-3, 57-58 | 545.97 | 2.47 | 2.44 | 0.03 | 20.3 | | | |
| C | 53R-3, 80-81 | 555.9 | 5.10 | 4.98 | 0.12 | 41.5 | | | |
| C | 54R-3, 3-4 | 564.83 | 5.62 | 5.53 | 0.09 | 46.1 | 9.0 | | |
| C | 55R-1, 118-119 | 572.68 | 2.82 | 2.74 | 0.08 | 22.8 | 8.0 | | |
| C | 55R-3, 49-50 | 574.99 | 5.57 | 5.40 | 0.17 | 45.0 | 17.0 | | |
| C | 55R-4, 105-106 | 577.05 | 2.33 | 2.22 | 0.11 | 18.5 | 11.0 | | |
| C | 56R-1, 125-126 | 582.35 | 6.72 | 6.70 | 0.02 | 55.8 | 1.0 | | |

Table 12 (continued).

| Hole | Core, section, interval (cm) | Depth (mbsf) | Total C (%) | Inorg. C (%) | Org. C (%) | CaCO ₃ (%) | Org. C/N | Org. C/S | Lithologic unit |
|------|------------------------------|--------------|-------------|--------------|------------|-----------------------|----------|----------|----------------------------------------------------------------------|
| C | 56R-6, 90-91 | 589.50 | 6.74 | 6.67 | 0.07 | 55.6 | 3.0 | | |
| C | 56R-7, 54-55 | 590.14 | 3.69 | 3.48 | 0.21 | 29.0 | 7.0 | 7.0 | |
| C | 57R-1, 103-104 | 591.73 | 7.29 | 7.16 | 0.13 | 59.6 | 6.5 | | |
| C | 57R-1, 123-124 | 591.93 | 3.25 | 3.19 | 0.06 | 26.6 | 2.0 | 0.2 | |
| C | 57R-2, 130-131 | 593.50 | 6.76 | 6.7 | 0.06 | 55.8 | 3.0 | | |
| C | 57R-4, 84-85 | 596.04 | 6.97 | 6.75 | 0.22 | 56.2 | 11.0 | | |
| D | 1R-1, 34-35 | 596.34 | 1.57 | 1.51 | 0.06 | 12.6 | 1.0 | | |
| D | 1R-1, 145-146 | 597.45 | 6.74 | 6.68 | 0.06 | 55.6 | 2.0 | | |
| D | 1R-2, 41-42 | 597.91 | 2.61 | 2.43 | 0.18 | 20.2 | 4.5 | 6.0 | |
| D | 1R-3, 81-82 | 599.81 | 0.39 | 0.31 | 0.08 | 2.6 | 1.0 | 8.0 | |
| D | 1R-4, 40-41 | 600.90 | 5.99 | 5.72 | 0.27 | 47.6 | 9.0 | | |
| D | 1R-CC, 3-4 | 601.77 | 4.56 | 4.45 | 0.11 | 37.1 | 3.6 | 5.5 | |
| C | 58R-1, 145-146 | 601.95 | 6.61 | 6.48 | 0.13 | 54.0 | 4.3 | | |
| C | 58R-2, 114-115 | 603.14 | 7.19 | 7.04 | 0.15 | 58.6 | 15.0 | | |
| C | 58R-3, 97-98 | 604.47 | 6.54 | 6.38 | 0.16 | 53.1 | | | |
| D | 2R-3, 49-50 | 610.29 | 5.10 | 5.07 | 0.03 | 42.2 | 1.0 | | |
| C | 59R-1, 126-127 | 611.36 | 2.78 | 2.68 | 0.10 | 22.3 | 5.0 | 2.5 | |
| C | 59R-2, 63-64 | 612.23 | 4.48 | 4.35 | 0.13 | 36.2 | 4.3 | | |
| D | 2R-4, 117-118 | 612.28 | 0.34 | 0.31 | 0.03 | 2.6 | 0.7 | 3.0 | |
| C | 59R-3, 71-72 | 613.81 | 3.38 | 3.27 | 0.11 | 27.2 | 2.7 | 3.6 | |
| D | 3R-2, 111-112 | 619.11 | 5.51 | 5.40 | 0.11 | 45.0 | 5.5 | | |
| D | 3R-3, 64-65 | 620.14 | 7.17 | 7.00 | 0.17 | 58.3 | 5.6 | | Unit III - claystone and silty claystone |
| D | 3R-3, 110-111 | 620.60 | 3.68 | 3.59 | 0.09 | 29.9 | 2.0 | 4.0 | |
| C | 60R-1, 122-123 | 620.92 | 0.24 | 0.23 | 0.01 | 1.9 | 0.2 | 0.5 | |
| C | 60R-2, 40-42 | 621.60 | 0.14 | 0.08 | 0.06 | 0.7 | 1.0 | 3.0 | |
| C | 60R-3, 29-30 | 623.06 | 0.14 | 0.15 | 0.00 | 1.2 | 0.0 | | |
| D | 4R-1, 50-51 | 626.70 | 0.08 | 0.08 | 0.00 | 0.7 | 0.0 | | |
| D | 4R-2, 50-51 | 628.20 | 0.16 | 0.09 | 0.07 | 0.7 | 2.0 | 3.0 | |
| C | 61R-1, 48-49 | 629.88 | 0.11 | 0.05 | 0.06 | 0.4 | | | |
| C | 61R-3, 133-134 | 633.73 | 0.05 | 0.04 | 0.01 | 0.3 | 0.2 | | |
| D | 5R-1, 25-26 | 636.15 | 0.07 | 0.05 | 0.02 | 0.4 | 0.5 | | |
| D | 5R-2, 92-93 | 638.32 | 0.05 | 0.04 | 0.01 | 0.3 | 0.2 | 1.0 | |
| C | 62R-4, 53-54 | 643.63 | 6.68 | 6.47 | 0.21 | 53.9 | 10.0 | | Unit IV - sandstone, limestone, and claystone with peridotite clasts |
| D | 6R-1, 12-13 | 645.62 | 0.08 | 0.08 | 0.00 | 0.7 | 0.0 | | |
| D | 6R-CC, 7-8 | 648.68 | 7.97 | 7.85 | 0.12 | 65.4 | 6.0 | | |
| C | 63R-1, 70-71 | 649.40 | 9.05 | 8.63 | 0.42 | 71.9 | | | |
| C | 63R-1, 94-95 | 649.64 | 4.17 | 2.93 | 1.24 | 24.4 | 17.7 | | |
| C | 63R-2, 28-30 | 650.00 | 8.54 | 7.79 | 0.75 | 64.9 | 37.0 | | |
| D | 7R-1, 39-40 | 655.59 | 8.06 | 7.46 | 0.60 | 62.1 | 15.0 | 0.8 | |
| D | 7R-1, 124-125 | 656.44 | 9.11 | 7.97 | 1.14 | 66.4 | 22.8 | 114.0 | |
| D | 7R-2, 8-9 | 656.78 | 1.14 | 0.67 | 0.47 | 5.6 | 9.4 | 12.0 | |
| D | 7R-2, 76-77 | 657.46 | 6.75 | 5.47 | 1.28 | 45.6 | 16.0 | 2.3 | |
| D | 7R-3, 60-61 | 658.30 | 3.25 | 1.77 | 1.48 | 14.7 | 16.4 | 2.3 | |
| C | 64R-1, 13-14 | 658.53 | 7.33 | 6.55 | 0.78 | 54.6 | 39.0 | | |
| C | 64R-1, 56-57 | 658.96 | 8.44 | 7.44 | 1.00 | 62.0 | 50.0 | | |
| C | 64R-1, 96-97 | 659.36 | 8.02 | 7.35 | 0.67 | 61.2 | 33.0 | | |
| C | 64R-2, 3-4 | 659.48 | 9.59 | 8.38 | 1.21 | 69.8 | | | |
| D | 8R-1, 30-31 | 665.10 | 3.26 | 1.96 | 1.30 | 16.3 | 16.2 | 1.2 | |
| D | 8R-2, 30-31 | 666.60 | 3.26 | 2.24 | 1.02 | 18.7 | 17.0 | 1.2 | |
| D | 8R-2, 55-56 | 666.85 | 7.35 | 6.61 | 0.74 | 55.1 | 18.0 | | |
| D | 8R-CC, 3-4 | 667.93 | 2.79 | 1.69 | 1.10 | 14.1 | 13.7 | 5.5 | |
| D | 10R-1, 25-26 | 684.55 | 7.22 | 6.96 | 0.26 | 58.0 | 8.6 | 8.6 | |
| D | 10R-3, 68-69 | 687.00 | 7.48 | 6.80 | 0.68 | 56.6 | 22.0 | 9.7 | |
| D | 10R-3, 142-143 | 687.74 | 6.54 | 6.36 | 0.18 | 53.0 | 9.0 | | |
| D | 10R-4, 90-91 | 688.72 | 7.85 | 6.90 | 0.95 | 57.5 | 47.0 | | |
| D | 10R-4, 141-142 | 689.23 | 3.28 | 3.18 | 0.10 | 26.5 | 5.0 | | |

Notes: Concentrations of calcium carbonate have been estimated from the inorganic carbon values, assuming all of the inorganic carbon is present as CaCO₃. Concentrations of organic carbon have been estimated from the difference between total and inorganic carbon values. Atomic C/N and C/S ratios were calculated from concentrations of organic carbon, total nitrogen, and total sulfur, respectively.

largely because the low concentrations of organic carbon and nitrogen in these units introduced large uncertainties in the measurement. Many samples that contain little organic carbon have relatively high C/N ratios; others have very low ratios (<5). The latter probably are an artifact of the low carbon contents, combined with the tendency of clay minerals to absorb ammonium ions that were generated during the degradation of organic matter (Müller, 1977). Consequently, the extreme C/N ratios in Units II and III are not accurate indicators of the source of organic matter. Samples from Unit IV are relatively rich in organic carbon and have elevated C/N ratios that average 23.5, indicating that the organic matter in this unit is mostly derived from land plant detritus.

Pyrolysis of samples rich in organic carbon from Units I and IV provided verification of the characterizations of the source of organic carbon inferred from the C/N ratios. Unit I samples yielded small S₁ peaks, but substantial S₂ peaks, as expected from thermally immature marine organic matter. The small S₁ peaks imply that the organic

matter has experienced considerable microbial degradation, which is consistent with an inferred history of downslope transport from a shallower site of initial sedimentation. Samples from Unit IV differed significantly from those in Unit I: these completely lack S₁ peaks and have small-to-absent S₂ peaks. The organic matter in this unit is virtually geochemically inert and, evidently, has undergone extensive degradation prior to sedimentation. This characteristic is consistent with a continental source.

Headspace Gases

Concentrations of headspace methane measured in Hole 897C are displayed in Figure 57. These were high in Unit I, reaching values of more than 100,000 ppm before decreasing to near-background levels in Units II, III, and IV. C₁/C₂ ratios were high in Unit I (Table 13). Two sources of the gas in Unit I are possible. First, gas from some deeper origin may have migrated into the unit, which consists of turbiditic

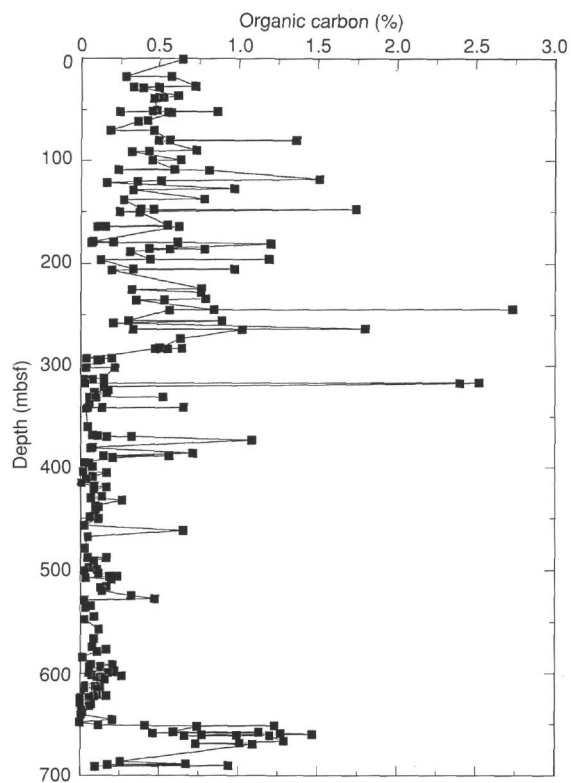


Figure 55. Concentrations of organic carbon in sediments from Holes 897A, 897C, and 897D.

sand, silt, and clay layers. The location of Site 897 on a basement high makes this an especially reasonable possibility. Evidence of migration of methane into porous sediments from deeper sources was found at Sites 762 and 763 on the Exmouth Plateau (Snowdon and Meyers, 1992). In the latter case, however, a known source existed in underlying Jurassic rocks; a suitable deeper source for the methane at Site 897 is unknown. A second possibility is in-situ formation by methanogenic bacteria. The high values occurred in the upper Pliocene sediments having elevated concentrations of marine organic matter (Table 12; Fig. 55), which is prone to microbial utilization. High C_1/C_2 ratios indicate that the gas is biogenic, as opposed to thermogenic (Table 13). The source of the methane may be from in-situ microbial fermentation of the marine organic matter present in this turbiditic unit. Similar in-situ microbial production of methane from marine organic matter has been inferred from high biogenic gas concentrations in Pliocene-Pleistocene sediments from Site 532 on the Walvis Ridge (Meyers and Brassell, 1985), although at a shallower depth (100 mbsf) than at Site 897 (292 mbsf). The generally low amounts of organic matter in Units II and III and its inert character in Unit IV evidently preclude methanogenesis. Furthermore, Claypool and Kvenvolden (1983) observed that the presence of pore-water sulfate inhibits methanogenesis in marine sediments, and concentrations of sulfate are anomalously high in Units II and III (see "Inorganic Geochemistry" section, this chapter). Consequently, head-space methane concentrations are low in sediments below Unit I.

INORGANIC GEOCHEMISTRY

Twenty-seven interstitial-water samples were collected at Site 897 from cores ranging from 26 to 636 mbsf. Samples were collected at approximately 10-m intervals in the top 50 m and in the 50 m above basement (when core recovery permitted). Samples were collected at

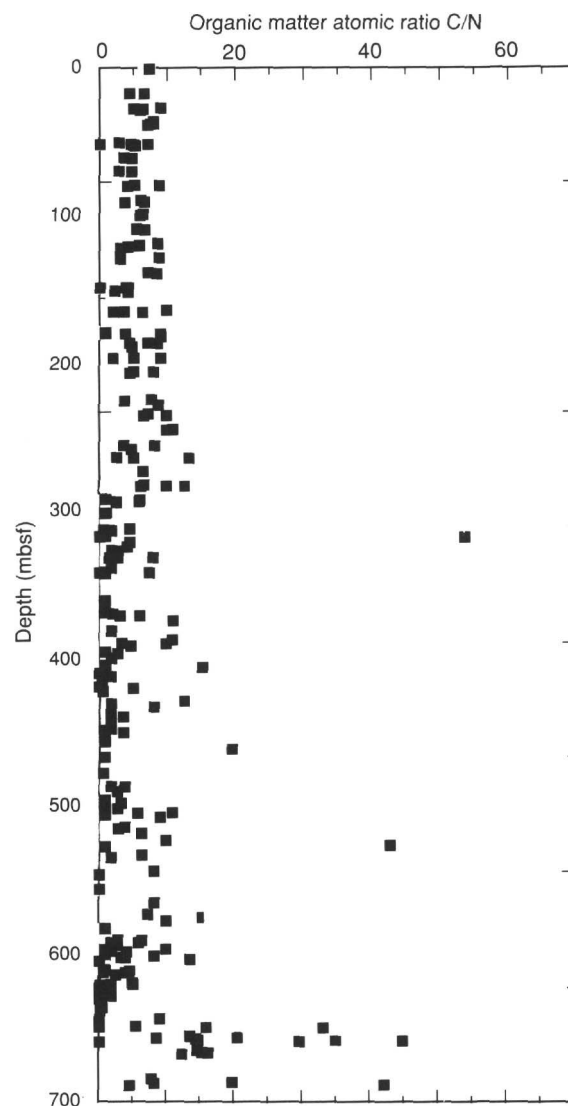


Figure 56. Atomic ratios of organic C/N in sediments from Holes 897A, 897C, and 897D.

30-m intervals between 50 and 580 mbsf. Results from the shipboard interstitial-water analyses are presented in Table 14.

Interstitial-water samples spanned lithostratigraphic Unit I through Subunit IIIA. The most significant changes in interstitial-water chemistry occurred at the boundary between Unit I and Subunit IIA. These changes coincide with a major increase in sedimentation rate that occurred at about the Miocene/Pliocene boundary.

The Pleistocene and Pliocene sediments are dominated by turbidite sequences relatively rich in organic carbon. In contrast, the Miocene through Eocene sediments are depleted of reactive carbon (see "Organic Geochemistry" section, this chapter).

The concentration of sulfate decreases from bottom-water concentration (approximately 29 mM) to near zero by 100 mbsf, thereby driving the diffusion of bottom-water sulfate into the sediment (Fig. 58A). Sulfate concentrations remain low until 300 mbsf, where the concentration of sulfate increases to a maximum at 500 mbsf. The depletion of sulfate, in the sequence between 100 and 300 mbsf, is indicative of the presence of reactive organic carbon. The increase in concentration of sulfate below 300 mbsf indicates upward diffusion

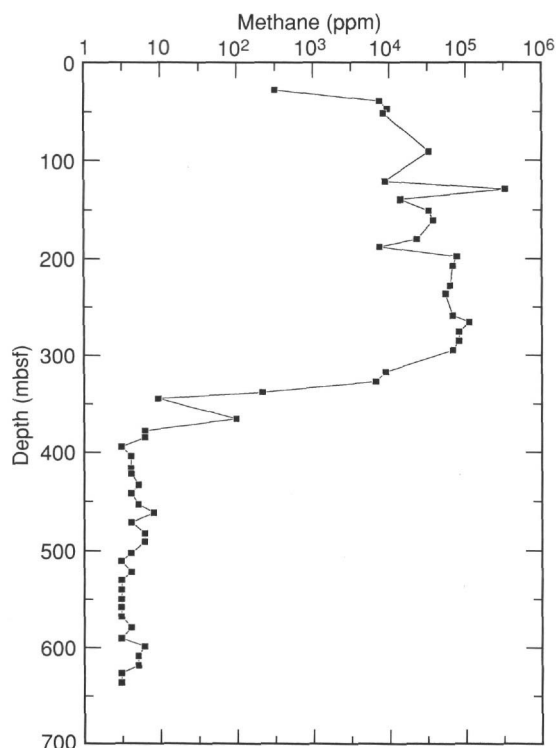


Figure 57. Profile of headspace methane concentration in samples from Site 897.

of sulfate from a deep reservoir into the Pleistocene and Pliocene sequences. This deep reservoir contains sulfate that has been preserved as a result of the relatively slow accumulation rates of the Miocene to late Oligocene sequence (see "Lithostratigraphy" section, this chapter). A gradient is seen between the deep sulfate maximum (~490 mbsf) and the near-basement sediments, which indicates greater demand for oxidant in the Late Cretaceous age sediments (albeit not large enough to deplete the sulfate reservoir) compared to that for the Eocene sediments.

The alkalinity profile reflects variations in the rate of organic carbon degradation through sulfate reduction (Fig. 58B). Alkalinity is normally produced at a rate that is charge equivalent to the rate of sulfate reduction (Gieskes, 1974, 1983). At this site, the alkalinity profile in part mirrors the sulfate profile, but the increase in alkalinity does not reach levels that one would predict from the decrease in sulfate concentration. Alkalinity reaches values greater than 15 mM in the top 150 m of the sediment column and decreases to about 10 mM by 300 m. Alkalinity may have been reduced by means of precipitation of a carbonate phase in the upper 150 mbsf. Below 350 mbsf, alkalinity decreases to a minimum of about 1 mM near basement.

The production of ammonia in sediments results from anoxic carbon degradation; thus, the ammonia profile at this site mirrors the sulfate profile (Fig. 58C). The highest concentrations of ammonia were observed in the Pleistocene and Pliocene sediments of Unit I. Ammonia concentrations decrease from a maximum greater than 4500 μM at 250 mbsf to near constant concentrations of about 200 μM by 400 mbsf. In the Oligocene to Eocene sediments, the relatively low and constant ammonia concentrations confirm the premise that reactive organic carbon is absent.

Dissolved iron concentrations are elevated with respect to the normal range of seawater values in the organic-rich Pleistocene and Pliocene sediment sequence (0-300 mbsf, Fig. 58D). The concentration of iron decreases below 270 mbsf to values of less than 10 μM and remains low through the Miocene to Eocene sequence. The

Table 13. Results of headspace-gas analyses from Holes 897A and 897C.

| Core, section, interval (cm) | Depth (mbsf) | C ₁ | C ₂ | C ₁ /C ₂ |
|------------------------------|--------------|----------------|----------------|--------------------------------|
| 149-897A- | | | | |
| 4R-2, 0-5 | 27.8 | 309 | | |
| 5R-3, 0-5 | 39 | 7536 | | |
| 6R-2, 0-5 | 47.1 | 9471 | | |
| 149-897C- | | | | |
| 1R-2, 0-5 | 51.4 | 8,401 | | |
| 5R-2, 0-5 | 90.4 | 33,180 | | |
| 8R-3, 0-5 | 120.9 | 8,918 | | |
| 9R-2, 0-5 | 128.5 | 338,115 | | |
| 10R-2, 0-5 | 138.7 | 14,088 | | |
| 11R-4, 0-5 | 149.8 | 33,310 | | |
| 12R-3, 0-5 | 159.6 | 38,691 | | |
| 14R-3, 0-5 | 178.8 | 23,257 | | |
| 15R-2, 0-5 | 186.9 | 7,612 | | |
| 16R-2, 0-5 | 196.6 | 78,397 | 2 | 40,000 |
| 17R-2, 0-5 | 206.2 | 69,615 | 2 | 35,000 |
| 19R-3, 0-5 | 227.1 | 64,099 | | |
| 20R-2, 0-5 | 235.3 | 55,486 | 1 | 55,000 |
| 22R-4, 0-5 | 257.5 | 69,736 | | |
| 23R-2, 0-5 | 264.2 | 115,805 | | |
| 24R-2, 0-5 | 273.8 | 83,809 | | |
| 25R-2, 0-5 | 283.35 | 83,997 | | |
| 28R-2, 0-5 | 293 | 69,802 | | |
| 29R-4, 0-5 | 315.4 | 9,101 | | |
| 30R-4, 0-5 | 325 | 6,724 | | |
| 31R-5, 0-5 | 336.2 | 213 | | |
| 32R-3, 0-5 | 342.9 | 9 | | |
| 33R-4, 0-5 | 363.6 | 97 | | |
| 34R-6, 0-5 | 376.1 | 6 | | |
| 35R-4, 0-5 | 382.9 | 6 | | |
| 36R-4, 0-5 | 392.6 | 3 | | |
| 37R-4, 0-5 | 402.3 | 4 | | |
| 38R-6, 0-5 | 414.9 | 4 | | |
| 39R-3, 0-5 | 420.1 | 4 | | |
| 40R-4, 0-5 | 431.2 | 5 | | |
| 41R-3, 0-5 | 439.4 | 4 | | |
| 42R-4, 0-5 | 450.5 | 5 | | |
| 43R-3, 0-5 | 458.6 | 8 | | |
| 44R-3, 0-5 | 468.3 | 4 | | |
| 45R-4, 0-5 | 479.5 | 6 | | |
| 46R-3, 0-5 | 487.6 | 6 | | |
| 47R-4, 0-5 | 498.7 | 4 | | |
| 48R-3, 0-5 | 506.9 | 3 | | |
| 49R-4, 0-5 | 518.1 | 4 | | |
| 50R-3, 0-5 | 526.2 | 3 | | |
| 51R-3, 0-5 | 535.8 | 3 | | |
| 52R-3, 0-5 | 545.4 | 3 | | |
| 53R-2, 0-5 | 553.6 | 3 | | |
| 54R-2, 0-5 | 563.3 | 3 | | |
| 55R-3, 0-5 | 574.5 | 4 | | |
| 56R-4, 0-5 | 585.6 | 3 | | |
| 57R-3, 0-5 | 593.7 | 6 | | |
| 58R-3, 0-5 | 603.5 | 5 | | |
| 59R-3, 0-5 | 613.1 | 5 | | |
| 60R-2, 0-5 | 621.2 | 3 | | |
| 61R-2, 0-5 | 630.9 | 3 | | |

Notes: Concentrations of methane (C₁) and ethane plus ethylene (C₂) are given in parts per million.

elevated concentrations can be attributed to the release of iron as a result of its reduction by sulfide to the soluble Fe²⁺ state.

In contrast to those of iron, concentrations of manganese remain relatively low (<6 μM) in the Pleistocene and Pliocene sediments (above 300 mbsf, Fig. 59A). However, concentrations increase to values greater than 12 μM (maximum 38 μM) in the deep Miocene to Eocene sequence (below 300 mbsf), indicating a zone of manganese release. The low concentrations of manganese above 300 mbsf probably are the result of precipitation of an authigenic carbonate phase. Release of manganese from the older sediments might be the result of manganese reduction, but the apparent absence of reactive carbon (see "Organic Geochemistry" section, this chapter) would argue against such a mechanism. The dissolution of a manganese-bearing carbonate phase or phases may be the mechanism of release.

Concentrations of calcium show depletion (30%-40%) with respect to present bottom-water concentrations in the Pleistocene/Pliocene sequence (to about 280 mbsf), but become enriched (> 100%) below 280 mbsf (Fig. 59B). This depletion in calcium is coincident

Table 14. Interstitial-water data for Site 897.

| Core, section, interval (cm) | Top of core (mbsf) | Depth (mbsf) | Strontium (μM) | Chloride (mM) | Sulfate (mM) | Sodium (mM) | Potassium (mM) | Magnesium (mM) | Calcium (mM) | Alkalinity (mM) | Iron (μM) | Manganese (μM) | Ammonia (μM) | Silica (μM) |
|------------------------------|--------------------|--------------|-----------------------------|---------------|--------------|-------------|----------------|----------------|--------------|-----------------|------------------------|-----------------------------|---------------------------|--------------------------|
| 149-897A- | | | | | | | | | | | | | | |
| 4R-1, 145-150 | 26.3 | 27.78 | 78.2 | 562 | 6.52 | 493 | 10.90 | 42.8 | 5.15 | 13.70 | 49.00 | 5.8 | 2443.0 | 465.0 |
| 5R-2, 145-150 | 36.0 | 38.98 | 89.4 | 559 | 4.22 | 497 | 11.20 | 40.6 | 5.68 | 12.40 | 3.90 | 4.0 | 1525.0 | 444.0 |
| 149-897C- | | | | | | | | | | | | | | |
| 1R-1, 145-150 | 49.9 | 51.38 | 92.4 | 665 | 3.67 | 505 | 10.90 | 43.7 | 6.75 | 15.30 | | | 2262.0 | 747.0 |
| 5R-1, 145-150 | 88.9 | 90.38 | | 675 | 0.83 | 501 | 10.10 | 39.5 | 7.03 | 16.10 | | | 4180.0 | 691.0 |
| 8R-2, 145-150 | 117.9 | 120.9 | 99.8 | 546 | 1.26 | 500 | 9.75 | 37.9 | 7.06 | 14.70 | 56.00 | 2.3 | 3596.0 | 822.0 |
| 11R-4, 145-150 | 146.8 | 152.8 | 113.0 | 547 | 1.82 | 491 | 9.60 | 37.2 | 7.07 | 16.20 | 30.00 | 1.2 | 3554.0 | 321.0 |
| 14R-2, 145-150 | 175.0 | 178.0 | 121.0 | 548 | 0.67 | 496 | 9.50 | 36.2 | 7.60 | 15.60 | 55.00 | 2.4 | 3499.0 | 737.0 |
| 17R-1, 145-150 | 204.7 | 206.2 | 136.0 | 541 | 1.90 | 489 | 8.40 | 37.3 | 8.17 | 13.90 | 47.00 | 2.3 | 4625.0 | 826.0 |
| 22R-3, 145-150 | 253.0 | 257.5 | 178.0 | 556 | 2.27 | 491 | 8.22 | 38.8 | 8.72 | 11.60 | 57.00 | 1.1 | 3513.0 | 317.0 |
| 25R-1, 130-135 | 282.0 | 283.3 | 209.0 | 554 | 2.81 | 496 | 7.93 | 43.1 | 12.80 | 9.77 | 46.00 | 1.7 | 2139.0 | 270.0 |
| 28R-3, 145-150 | 310.9 | 315.4 | | 535 | 3.12 | 469 | 5.55 | 43.7 | 12.40 | | | | 894.6 | 544.0 |
| 29R-3, 140-150 | 320.5 | 325.0 | 313.0 | 534 | 5.38 | 482 | 6.09 | 41.7 | 13.50 | 10.20 | 4.50 | 18.0 | 1096.0 | 634.0 |
| 31R-2, 140-150 | 339.9 | 342.9 | 322.0 | 556 | 8.09 | 485 | 7.20 | 41.0 | 16.90 | 9.13 | 6.20 | 3.9 | 1068.0 | 1170.0 |
| 34R-2, 140-150 | 368.8 | 371.7 | 334.0 | 551 | 12.10 | 485 | 6.45 | 42.6 | 22.40 | 13.00 | 5.10 | 32.0 | 519.3 | 1125.0 |
| 37R-3, 140-150 | 397.8 | 402.2 | 350.0 | 537 | 14.50 | 472 | 4.70 | 43.7 | 25.20 | | | | 365.2 | 1014.0 |
| 40R-3, 135-150 | 426.7 | 431.1 | 402.0 | 538 | 16.50 | 477 | 4.54 | 44.1 | 26.30 | 12.00 | | 26.0 | 387.4 | 1023.0 |
| 43R-2, 135-150 | 455.6 | 458.5 | 406.0 | 543 | 17.00 | 478 | 4.85 | 43.2 | 24.90 | 6.20 | 0.97 | 14.0 | 354.1 | 638.0 |
| 46R-2, 138-150 | 484.6 | 487.5 | 452.0 | 540 | 17.80 | 475 | 4.34 | 45.2 | 27.30 | 6.30 | 1.40 | 24.0 | 316.5 | 469.0 |
| 49R-3, 135-150 | 513.6 | 518.0 | 492.0 | 550 | 16.60 | 477 | 3.61 | 43.3 | 27.80 | 4.60 | 0.32 | 38.0 | 311.0 | 527.0 |
| 52R-2, 135-150 | 542.4 | 545.3 | 570.0 | 515 | 16.50 | 432 | 2.55 | 47.6 | 29.40 | | | | 212.3 | 476.0 |
| 55R-2, 135-150 | 571.5 | 574.4 | | 537 | 15.10 | 475 | 3.22 | 41.3 | 26.60 | 1.36 | 2.70 | 6.7 | 262.3 | 326.0 |
| 58R-2, 135-150 | 600.5 | 603.4 | 518.0 | | | 494 | 3.67 | 39.7 | 26.60 | 0.99 | 2.70 | 12.0 | 191.4 | 309.0 |
| 149-897D- | | | | | | | | | | | | | | |
| 1R-3, 130-150 | 596.0 | 600.4 | | 586 | 13.10 | 483 | 3.43 | 39.7 | 27.30 | 1.03 | | | 217.8 | 277.4 |
| 2R-3, 111-131 | 606.8 | 611.0 | | 585 | 13.00 | 485 | 3.48 | 38.1 | 26.60 | 0.90 | | | 351.3 | 320.3 |
| 3R-3, 0-20 | 616.5 | 619.6 | | 575 | 13.10 | 491 | 3.38 | 37.8 | 27.70 | 1.30 | | | 251.2 | 310.8 |
| 4R-1, 0-20 | 626.2 | 626.3 | | 590 | 14.60 | 494 | 3.56 | 39.3 | 27.60 | 1.78 | | | 430.5 | 386.9 |
| 5R-1, 130-150 | 635.9 | 637.3 | | 572 | 12.90 | 477 | 2.41 | 40.0 | 30.10 | 1.79 | | | 288.7 | 322.2 |

with the zone of maximum alkalinity and probably reflects precipitation of a carbonate phase. The enrichment (26-28 mM) between 280 and 400 mbsf probably reflects a region of silicate mineral alteration and/or carbonate dissolution. The profile below 400 mbsf exhibits only minor changes in the gradient, indicating minimal dissolution or precipitation of carbonate.

Concentrations of magnesium show some depletion with respect to bottom water throughout the sediment column having the greatest depletion (~30%) coincident with the zone of calcium depletion (Fig. 59C). Magnesium concentrations increase slightly from 300 to 545 mbsf, similar to calcium concentrations.

Concentrations of strontium generally increase with depth from a minimum of about 80 μM near the sediment surface to a maximum of about 580 μM near basement (Fig. 59D). The strontium profile is concave up between the surface and 300 mbsf, indicating some removal in the Pleistocene sediments, with a zone of release in the late Miocene sequence. The concentration maximum at 550 mbsf indicates a second significant zone of strontium release to the interstitial waters. The release of strontium probably is associated with recrystallization of carbonate phases (Gieskes, 1974).

In general, concentrations of potassium decrease through the sediment column, with some narrow zones of release and removal that produce fluctuations in the profile (Fig. 60A). Concentrations of potassium decrease from a maximum of 11 mM near the seafloor to values slightly higher than 2 mM below about 550 mbsf. Unfortunately, the potassium concentration may depend on the temperature at the time of squeezing (Waterman, 1973). Possible artifacts in potassium concentrations as a result of this problem could not be verified because of failure of the in-situ WSTP sampler at this site.

Concentrations of silica show three maxima between 50 and 100 mbsf, between 170 and 200 mbsf, and between 320 and 400 mbsf, all of which indicate alternating zones of silica release and removal (Fig. 60B). Silica concentrations are elevated (up to 800 μM) with respect to bottom water through much of the Pleistocene and Pliocene sequences. Silica has been removed from the interstitial water at the boundary between Units I and IIA (~290 mbsf), a sequence dominated by claystones. Silica concentrations show release through the Miocene to the late Oligocene sequence, resulting in a maximum that approaches 1200 μM . Below 450 mbsf, silica has been removed from

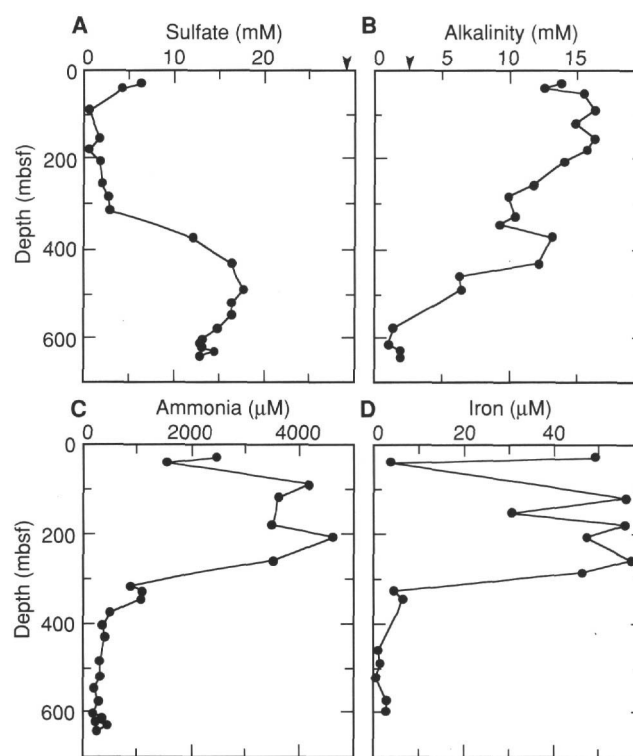


Figure 58. Interstitial-water profiles for Site 897. Arrows indicate typical bottom-water values. A. Sulfate. B. Alkalinity. C. Ammonia. D. Iron.

the interstitial water, producing a negative gradient that extends to 580 mbsf.

Concentrations of chloride show anomalous enrichment with respect to seawater from 50 to 100 mbsf, but then return to values near those of bottom water below (Table 14). This chloride peak represents a greater than 20% enrichment, which is greater than one usually

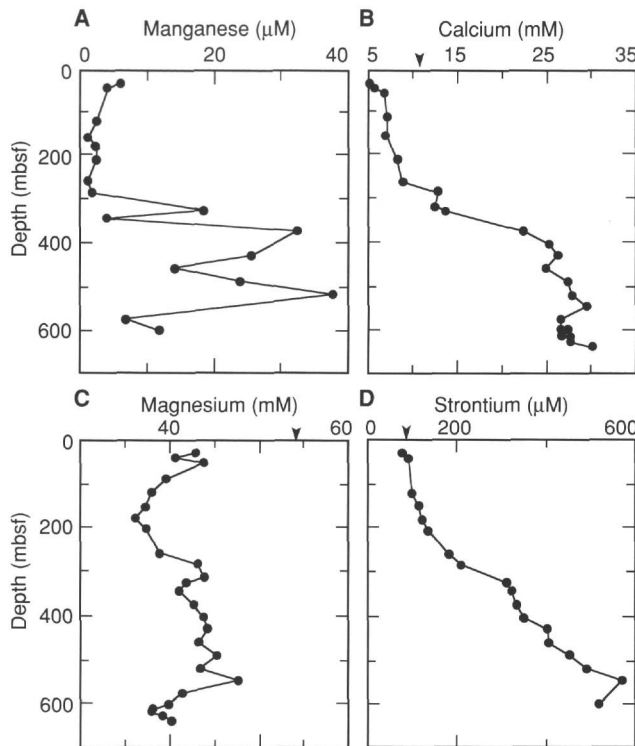


Figure 59. Interstitial-water profiles for Site 897. Arrows indicate typical bottom-water values. A. Manganese. B. Calcium. C. Magnesium. D. Strontium.

associates with changes in paleosalinity. The absence of a comparable increase in concentrations of sodium suggests either contamination or an analytical problem. The chloride values determined by the Dionix chromatograph were found to be less reliable than the titration method. The variation in chloride concentrations below 100 mbsf typically is less than 5% with respect to present-day bottom water and may be associated with mineral hydration. The marked increase in chloride below 600 mbsf probably results from water removal through hydration of basement rock.

The concentration of sodium varies with that of chloride below 100 mbsf, with the exception of a slight negative gradient between 100 and 500 mbsf (Table 14). At 530 mbsf, concentration of sodium is anomalously low, but shows slight enrichment below, similar to that of chloride.

PHYSICAL PROPERTIES

Introduction

Physical properties measured on whole cores at Site 897 included magnetic susceptibility, Gamma-Ray Attenuation Porosity Evaluator (GRAPE) bulk density, and thermal conductivity. Measurements of split cores included Digital Sound Velocimeter (DSV) velocity in unlithified sediments and resistivity. Measurements in discrete samples included wet and dry masses and wet and dry volumes for determining index properties and acoustic velocities using the Hamilton Frame Velocimeter.

Despite slight differences in the depths of the lithostratigraphic units among Holes 897A, 897C, and 897D (see "Lithostratigraphy" section, this chapter), the physical properties from all holes have been plotted together and are discussed as a single section representative of Site 897. These data show several systematic trends that correlate with downhole lithostratigraphic and chemical changes and may point to important variations in hydrologic and mechanical conditions.

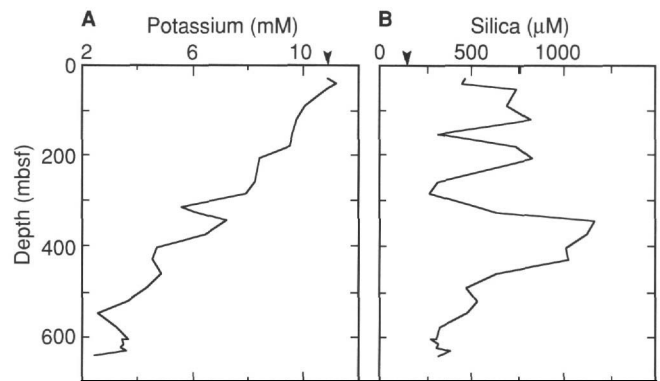


Figure 60. Interstitial-water profiles for Site 897. Arrows indicate typical bottom-water values. A. Potassium. B. Silica.

Index Properties

Bulk densities, porosities, and grain densities were determined in discrete samples recovered from Holes 897A, 897C, and 897D using gravimetric methods (Table 15; Fig. 61). Uncertainties when determining these quantities can be estimated from the precision of the mass and volume measurements (see "Explanatory Notes" chapter, this volume) and have been estimated as $\pm 0.02 \text{ g/cm}^3$ for densities, and $\pm 2\%$ for porosities. Probably less reliable data points near the top of Hole 897C are attributed to instrument difficulties early in the measurement program. The suspect data points are circled in Figure 61. The overall plots of bulk density and porosity vs. depth indicate a general downhole decrease in the water content. The trends are marked by several distinct offsets and changes in slope, some of which coincide with lithostratigraphic unit boundaries.

Bulk densities generally increase from about 1.6 g/cm^3 near the seafloor to about 2.45 g/cm^3 within basement at a depth of 830 mbsf in Hole 897D. Porosities decrease from about 60% near the seafloor to 10%-20% in basement rock.

Between 600 and about 650 mbsf, bulk density decreases from about 2.3 to 1.9 g/cm^3 . Porosity increases from 40% to 60% across the same interval. A similar downhole inversion also is visible in the GRAPE bulk density and thermal conductivity data (discussed below). The base of this zone corresponds to the contact between lithostratigraphic Units III and IV (debris flow). Overlying this contact is a 23-m-thick section of very fissile, relatively uniform reddish-brown claystone (lithostratigraphic Subunit IIIA). The reversals in trends of downhole density and porosity originate above this section.

At 650 mbsf, one observes a sharp offset in bulk density and porosity. Bulk density increases from about 1.9 to 2.4 g/cm^3 , while porosity decreases from 60% to less than 40%. This step coincides with the contact between lithostratigraphic Units III and IV, at the top of the debris flow overlying the basement. Index properties show significant scatter within Unit IV, which reflects the variable lithologies sampled in the debris flow.

Crystalline basement rock composed of serpentinized peridotite (see "Igneous and Metamorphic Petrology and Geochemistry" section, this chapter) was encountered at 677.5 mbsf in Hole 897C, and at 693.8 mbsf in Hole 897D. Bulk densities within this material generally are higher than in the sedimentary section and range from 2.3 to 2.5 g/cm^3 . Porosities cluster between 15% and 20%. Grain densities within the basement range from 2.5 to 2.75 g/cm^3 , with a slight decrease downward. These grain densities are lower than those in the sedimentary sequence, which maintain a nearly constant value of about 2.8 g/cm^3 . The downward decrease in grain density in the basement was interpreted as a consequence of decreasing calcite content in the serpentinized peridotite with depth (see "Igneous and Meta-

morphic Petrology and Geochemistry" section, this chapter). The decrease in grain density with depth appears to stabilize near 2.6 g/cm³ in the deepest rocks, which is consistent with the density of serpentine (chrysotile) of about 2.55 g/cm³ (Deer et al., 1966).

Several measurements were performed to test the grain density calculations for representative lithologies using a flask pycnometer. Results generally corroborated the grain densities determined using the helium pycnometer, producing values within 0.05 g/cm³ of the measured value.

GRAPE Measurements

Bulk densities also were estimated using whole-core GRAPE measurements performed on most sections recovered from Holes 897A, 897C, and 897D. Densities were corrected for the composition of the pore fluids (Boyce, 1976) and for shorter gamma-ray paths in the incompletely filled RCB core liners (Evans and Cotterell, 1970; see "Explanatory Notes" chapter, this volume). Following the methods of Boyce (1973) and Gealy (1971), the maximum values for GRAPE densities were assumed to provide the best estimates of bulk density. The curve describing the maximum GRAPE density was estimated visually and is shown in Figure 61.

The gravimetrically and GRAPE-derived determinations of bulk density show a close correlation throughout the sedimentary section (Fig. 61). The GRAPE-determined bulk densities increase slightly downhole in the sedimentary section, from about 1.8 g/cm³ at 45 mbsf to 2.1 g/cm³ at 600 mbsf. Between 600 and 640 mbsf, GRAPE bulk density decreases from 2.1 to 1.9 g/cm³. This decrease is corroborated by the estimates of gravimetric bulk density and correlates with a sudden increase in porosity near the interface between lithostratigraphic Units II and III. Bulk densities within the basement serpentinized peridotites exhibit a mean value of 2.7 g/cm³, which varies with the visually observed degree of alteration. This value is about 0.15 g/cm³ higher than the bulk density that was obtained gravimetrically. One cause of this discrepancy is the Fe/Mg-rich minerals in the Serpentinized peridotite. These have a higher gamma-ray attenuation coefficient than quartz, which was the standard assumed during data processing (Peterson, Edgar, et al., 1970). Consequently, an artificially high density was computed for the serpentinized peridotite during data reduction.

Electrical Resistivity

Electrical resistivities were measured at intervals of 0.5 to 0.75 m in split cores taken from between 110 and 690 mbsf. Resistivity was used to calculate the formation factor, which is the ratio of the electrical resistivity of the sediment to that of the interstitial water (see "Explanatory Notes" chapter, this volume). The formation factor commonly correlates with porosity, but the relationships must be determined empirically for individual lithologies (Boyce, 1980). Formation factor was calculated using the resistance of seawater at room temperature.

The plotted values indicate a general increase in formation factor with depth (Fig. 61). Because resistivity measurements are obtained within the uppermost few millimeters of the surface of the split core and are sensitive to changes in near-surface water content, the computed formation factors must be treated cautiously.

Acoustic Velocities

Acoustic velocity was measured in each core recovered in Holes 897C and 897D (Table 16). The DSV was used to measure compressional-wave velocity in split cores containing unconsolidated sediment from Cores 149-897C-1R through -29R. Below Core 149-897C-29R, sediments were sufficiently lithified to allow us to cut dis-

crete samples from the split core, and velocity was measured using the Hamilton Frame Velocimeter. The quality of the RCB core was inadequate for measurement of acoustic velocity using the MST (see "Explanatory Notes" chapter, this volume).

Discrete samples taken from the sedimentary units were trimmed to a roughly cubic shape, and velocity was measured in three mutually orthogonal directions, one of which was parallel to the long axis of the core. Below Cores 149-897C-63R and 149-897D-11R, 25-mm-diameter minicores were cut from basement units. The minicores were oriented perpendicular to the split face of the core, and velocity was measured along the axis of the minicore. Sample spacing within the basement cores was varied to sample representative lithologies. The accuracy of the velocity measurements taken with the DSV and the Hamilton Frame Velocimeter was estimated as 2% to 3% on the basis of repeated measurements of numerous samples and calibration standards.

Measured vertical Hamilton Frame Velocimeter velocities are remarkably uniform throughout the sedimentary section and increase only slightly from about 1700 m/s at 324 mbsf to about 2000 m/s at 689 mbsf (Fig. 62). Acoustic anisotropy throughout most of the sedimentary section is less than 5% (Fig. 62; see "Explanatory Notes" chapter, this volume). On the basis of the accuracy of the velocity measurements, anisotropy was estimated to be accurate to within 2% to 3%.

In contrast to the cores from the Cenozoic sedimentary section, those from basement and lithostratigraphic Subunit IIIB and Unit IV (see "Lithostratigraphy" section, this chapter) have highly variable velocities that range from about 1950 to 7100 m/s (Fig. 62). The slowest velocities in these cores were measured in Cretaceous(?) clays within lithostratigraphic Unit IV in Hole 897C. Velocities greater than 2700 m/s are from serpentinized peridotite (see "Igneous and Metamorphic Petrology and Geochemistry" section, this chapter). Velocities within the ultramafic rocks segregate into distinct groups that strongly correlate with the degree of alteration estimated from visual inspection (Fig. 63). The least-altered samples (well-indurated, with dark green to black color and lacking common veining) have velocities greater than 6000 m/s. Well-indurated samples containing common serpentine and calcite veins have velocities ranging from 4200 to 5300 m/s. The most highly altered ultramafic rocks have velocities that range from 2800 to 3800 m/s. These rocks are poorly indurated, with common calcite and serpentine veins and clayey texture.

Magnetic Susceptibility

Magnetic susceptibility was measured at 3- to 5-cm intervals in all cores collected at Site 897. Results are discussed within the "Paleomagnetism" section (this chapter).

Thermal Conductivity

Thermal conductivity was measured on all cores recovered from Site 897 at a frequency of two measurements per section in the sedimentary sequence and one measurement per section in the basement cores. The mean error associated with these measurements was estimated as 0.2 W/(m·K). Above about 650 mbsf, values of thermal conductivity range between 1.1 and 1.6 W/(m·K) (Fig. 64; Table 17). The data suggest a slight increase with depth, which most likely results from a decrease in porosity (Fig. 61). Below 650 mbsf, within lithostratigraphic Unit IV and the crystalline basement, consistently higher values were obtained for thermal conductivity that range between 1.7 and 2.3 W/(m·K). The high scatter in thermal conductivity values in the deeper rocks may be related to varying concentrations of calcite and serpentine veins (see "Igneous and Metamorphic Petrology and Geochemistry" section, this chapter).

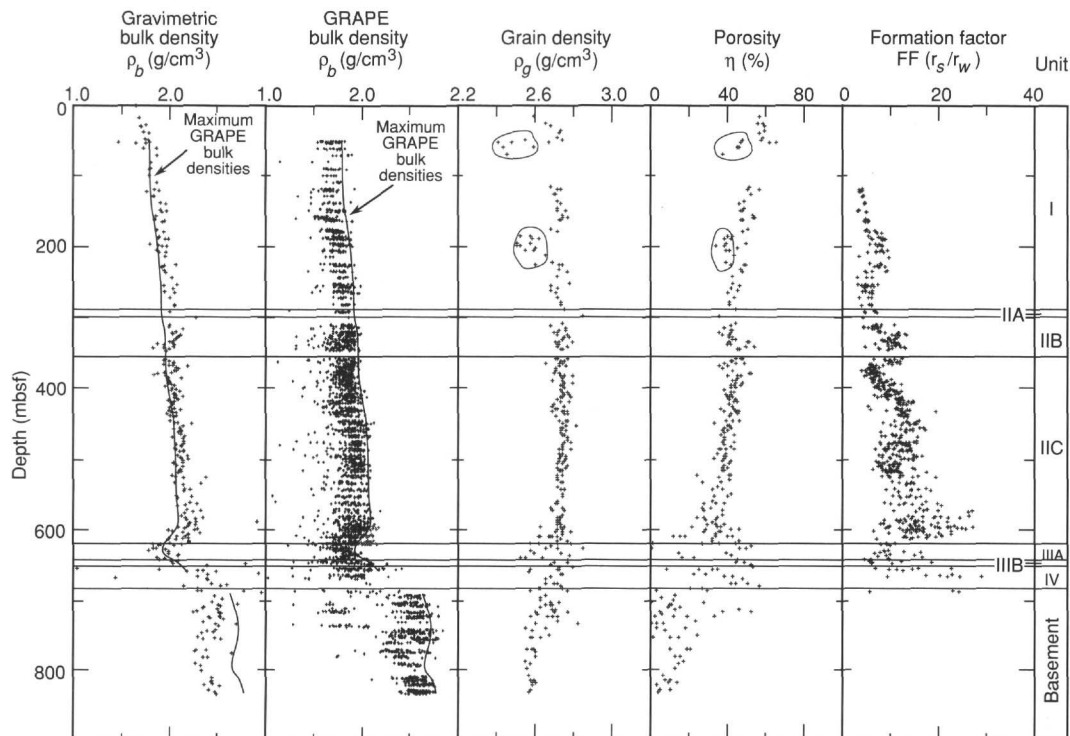


Figure 61. Gravimetrically determined and GRAPE-estimated bulk densities, grain density, porosity, and formation factor measurements in cores from Holes 897A, 897C, and 897D. The lines on the bulk density graphs are the visually estimated maximum GRAPE bulk density.

The following correlations were done using the computed depths of the reflectors and are summarized in Table 18.

1. Many reflectors are seen in the uppermost 300 m of the section (e.g., R_1 in Fig. 66) from which cores containing sand, silty sand, and silt were obtained. These lithologies are associated with the bases of numerous turbidites, and it is likely that the contrasts in acoustic impedance at the bases of the turbidites contribute substantially to the reflection of sound. The reflectors are more likely to correspond to the net acoustic interference pattern produced by the series of turbidites than to individual turbidites that are much less than a seismic wavelength thick.

2. Reflector R_2 (associated with the acoustic formation 1A/1B unconformity computed to be at 340 mbsf), which is recognized in the vicinity of the site as a surface onto which numerous reflectors onlap, correlates with the onset at this site of a 10.5-Ma middle Miocene-late Miocene hiatus defined by the virtual absence of the nannofossil Zones NN4 to NN10. Measurements of physical properties do not suggest a physical cause for this acoustic event; it is evident principally from the angular relationship between the tilted underlying, and horizontal onlapping, reflectors.

3. Reflector R_3 has been computed to be at a depth of 420 mbsf and may correspond to the onset of claystone in cores below 440 mbsf, which is accompanied by a significant increase in density.

4. Reflector R_4 (associated with the acoustic formation 1B/2 boundary) is computed to lie at about 590 mbsf, which associates it with beds that are predominantly claystone and chalk of middle Eocene age. These beds exhibit alternating high and low velocity layers on a scale of 10 to 20 m, with the higher values exceeding velocities in the beds above 590 mbsf. This led to rapidly changing reflection coefficients, which probably explain the observed reflector.

5. The thin unreflective zone immediately above basement (Fig. 3), which may correspond to the deposits of lithostratigraphic Unit IV, can just be discerned on the expanded seismic section between 0.675 s and basement (Fig. 66).

6. The basement reflector was computed to lie at 670 mbsf. This places it in the lower part of lithostratigraphic Unit IV close to the depth below which no more sediment was cored.

IN-SITU TEMPERATURE MEASUREMENTS

The WSTP tool was deployed to collect in-situ temperature data at 55.2 mbsf in Hole 897A and at 117.9, 166.1, and 214.4 mbsf in Hole 897C (WSTP depth is based on the depth of penetration of the bottom of the previous core barrel). We did not use the measurement at 117.9 mbsf because the probe was apparently inserted into fill at the bottom of the hole. The tool deployed at 166.1 mbsf experienced an electronic failure. We judged that only the data from 55.2 and 214.4 mbsf warranted further analysis.

Interpretations of data from the tool deployed at 55.2 mbsf yielded a bottom-water temperature of $3.6^\circ \pm 0.1^\circ\text{C}$ and an in-situ temperature of $7.3^\circ \pm 0.8^\circ\text{C}$ (error estimates for bottom-water and in-situ temperatures are informed guesses; Fig. 67). The bottom-water temperature was obtained by averaging temperature readings between 2900 and 3100 s, when the tool was stopped at the seafloor. The in-situ temperature was extrapolated using 4753 s as the insertion time and modeling the data over the interval from 4770 to 4982 s. The recorded temperatures indicate that the tool was inserted at least twice, originally at about 4400 s and again at about 5900 s. The tool also may have been moving during the measurements, which may have introduced errors because of frictional heating of the probe. We chose to model the data over the interval prior to the second penetration, when motion apparently had stopped. Because of these problems, we have assumed that a larger than normal error range is appropriate for this in-situ temperature measurement.

Analyses of the measurements at 214.4 mbsf yielded a bottom-water temperature of $3.6^\circ \pm 0.1^\circ\text{C}$ and an in-situ temperature of $13.1^\circ \pm 0.1^\circ\text{C}$ (Fig. 68). The bottom-water temperature was obtained by averaging temperature readings between 2200 and 2400 s, when the tool had stopped at the seafloor. The in-situ temperature was extrapo-

Table 16. Hamilton Frame velocity data from Holes 897C and 897D.

| Core, section, interval (cm) | Depth (mbsf) | Velocity (m/s) | | | Core, section, interval (cm) | Depth (mbsf) | Velocity (m/s) | | |
|---------------------------------|-----------------|----------------|-------|-------|---------------------------------|-----------------|----------------|-------|-------|
| | | V | H_x | H_y | | | V | H_x | H_y |
| 149-897C- | | | | | 73R-3, 62-64 | 737.70 | | | 3307 |
| 29R-3, 53-55 | 324.03 | 1721 | 1746 | 1711 | 149-897D- | | | | |
| 29R-6, 40-43 | 328.41 | 1780 | 1618 | 1580 | 1R-2, 102-104 | 598.52 | 2015 | 2070 | 2062 |
| 30R-6, 61-64 | 338.42 | 1535 | | 1711 | 2R-1, 35-37 | 607.15 | 2028 | 2312 | 2256 |
| 31R-2, 122-125 | 342.15 | 1744 | 1829 | 1719 | 3R-2, 104-106 | 619.04 | 1982 | 1961 | 1990 |
| 31R-1, 78-81 | 349.80 | 1712 | 1753 | 1698 | 3R-4, 80-82 | 621.80 | 1819 | 1841 | 1882 |
| 34R-1, 29-31 | 369.10 | 1617 | 1763 | 1654 | 4R-1, 97-99 | 627.17 | 1665 | 1937 | 1867 |
| 35R-5, 63-65 | 385.04 | 1618 | 1609 | 1608 | 5R-2, 6-8 | 637.10 | 1687 | 1715 | 1708 |
| 36R-5, 106-108 | 395.17 | 1760 | | | 6R-1, 81-84 | 646.31 | 1676 | 1737 | 1696 |
| 37R-3, 76-78 | 401.57 | 1697 | 1673 | 1647 | 7R-3, 39-41 | 658.16 | 1836 | 1863 | 1920 |
| 38R-4, 33-35 | 412.24 | 1730 | 1760 | 1713 | 8R-1, 95-97 | 665.75 | 1905 | 1916 | 1926 |
| 39R-5, 78-80 | 423.89 | 1715 | 1873 | 1799 | 10R-4, 92-94 | 688.76 | 2009 | 1978 | 2088 |
| 40R-6, 60-62 | 434.81 | 1753 | | 1739 | 11R-1, 73-75 | 694.53 | | | 3607 |
| 41R-2, 134-136 | 439.24 | 1778 | 1755 | 1722 | 11R-4, 32-34 | 698.46 | | | 4380 |
| 42R-5, 138-140 | 453.38 | 1789 | 1853 | 2106 | 12R-5, 51-53 | 709.69 | | | 4623 |
| 43R-3, 18-20 | 458.78 | 1848 | 1879 | 1804 | 12R-3, 49-51 | 706.81 | | | 5436 |
| 44R-1, 37-39 | 465.67 | 1787 | 1771 | 1828 | 12R-1, 39-41 | 703.89 | | | 4208 |
| 45R-4, 11-14 | 479.61 | 1735 | 1742 | 1714 | 12R-4, 4-6 | 707.75 | | | 3909 |
| 46R-4, 48-51 | 489.58 | 1781 | 1866 | 1802 | 13R-5, 61-63 | 718.68 | | | 4106 |
| 47R-3, 17-19 | 497.37 | 1783 | 1795 | 1818 | 13R-1, 61-63 | 713.61 | | | 4129 |
| 48R-5, 57-59 | 510.15 | 1779 | 1727 | 1742 | 13R-4, 53-54 | 717.33 | | | 3792 |
| 49R-1, 106-108 | 514.66 | 1758 | 1792 | 1805 | 14R-1, 137-139 | 724.07 | | | 4505 |
| 50R-2, 48-50 | 525.18 | 1770 | 1730 | 1694 | 14R-2, 84-86 | 724.97 | | | 4555 |
| 51R-1, 63-64 | 533.43 | 1771 | | 1729 | 14R-3, 78-80 | 726.32 | | | 3555 |
| 52R-3, 59-61 | 545.99 | 1762 | 1849 | 1818 | 15R-2, 81-83 | 734.48 | | | 4122 |
| 53R-1, 90-92 | 553.00 | 1790 | 1780 | 1757 | 15R-1, 43-45 | 732.73 | | | 3369 |
| 54R-3, 102-104 | 565.82 | 1731 | 1872 | 1832 | 16R-2, 76-78 | 747.03 | | | 4408 |
| 55R-1, 102-104 | 572.52 | 1786 | 1820 | 1799 | 16R-3, 65-67 | 748.18 | | | 3452 |
| 56R-3, 50-52 | 584.64 | 1942 | 2072 | 2013 | 16R-6, 47-49 | 752.41 | | | 3034 |
| 57R-4, 75-78 | 595.95 | 1786 | 1826 | 1814 | 16R-5, 66-68 | 751.10 | | | 4273 |
| 58R-2, 24-26 | 602.24 | 1748 | 1749 | 1718 | 17R-5, 3-5 | 757.05 | | | 4142 |
| 59R-4, 18-20 | 614.28 | 1692 | 1706 | 1640 | 17R-2, 40-42 | 753.50 | | | 3701 |
| 60R-1, 62-64 | 620.32 | 1707 | 1750 | 1689 | 17R-3, 28-30 | 754.88 | | | 3332 |
| 63R-2, 138-140 | 651.10 | | | 3539 | 18R-1, 54-56 | 761.76 | | | 3156 |
| 64R-1, 64-66 | 659.04 | 2233 | 2014 | 1924 | 19R-2, 62-63 | 772.73 | | | 2638 |
| 64R-3, 37-39 | 660.47 | | | 3664 | 19R-3, 39-40 | 773.69 | | | 2540 |
| 64R-5, 74-76 | 662.99 | | | 6660 | 20R-1, 121-123 | 781.81 | | | 3194 |
| 65R-2, 57-59 | 670.03 | | | 3472 | 20R-2, 39-41 | 782.46 | | | 2993 |
| 65R-2, 57-59 | 670.03 | | | 3409 | 21R-2, 12-14 | 791.06 | | | 2800 |
| 65R-3, 33-35 | 671.26 | | | 4274 | 21R-4, 23-25 | 793.81 | | | 2990 |
| 66R-3, 106-108 | 680.70 | | | 2200 | 22R-2, 71-73 | 801.18 | | | 3160 |
| 66R-4, 27-29 | 681.02 | | | 4561 | 23R-2, 87-89 | 811.17 | | | 3477 |
| 67R-1, 74-76 | 687.64 | | | 5184 | 23R-6, 47-49 | 816.36 | | | 3311 |
| 67R-3, 5-7 | 689.79 | | | 7132 | 23R-5, 74-76 | 815.27 | | | 3658 |
| 69R-1, 60-62 | 706.80 | | | 2327 | 24R-1, 81-83 | 819.43 | | | 3775 |
| 70R-1, 36-38 | 710.56 | | | 2836 | 24R-4, 59-61 | 822.77 | | | 3668 |
| 70R-2, 65-67 | 712.27 | | | 1946 | 24R-3, 62-64 | 821.34 | | | 3819 |
| 71R-1, 73-75 | 716.63 | | | 2949 | 25R-1, 17-19 | 828.37 | | | 3816 |
| 71R-3, 100-102 | 719.90 | | | 3117 | 25R-3, 52-54 | 830.78 | | | 4081 |
| 72R-2, 53-55 | 736.89 | | | 3412 | 25R-5, 51-53 | 833.61 | | | 4335 |
| 73R-1, 22-24 | 735.52 | | | 3169 | | | | | |

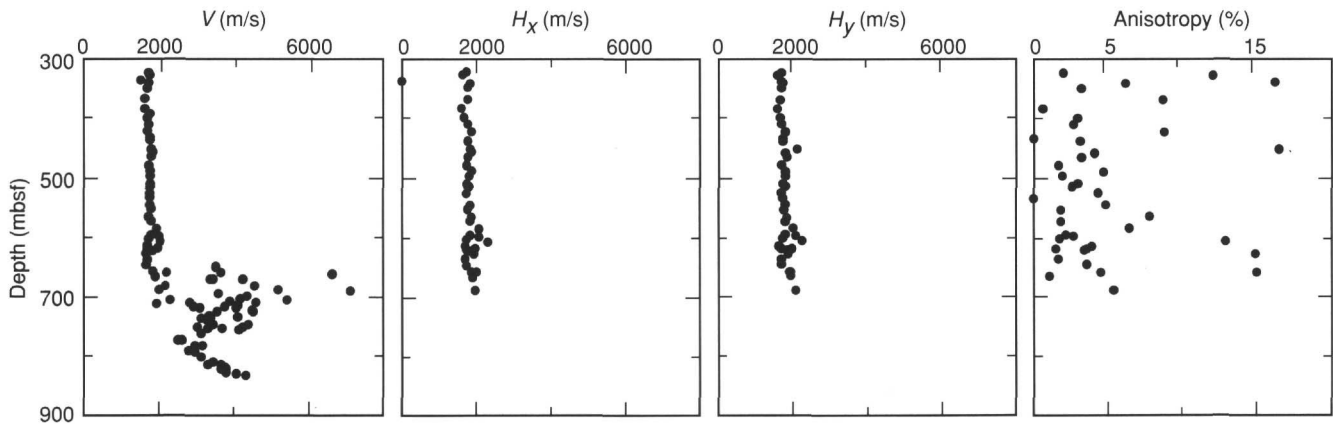


Figure 62. Hamilton Frame Velocimeter measurements and computed anisotropy for Holes 897C and 897D. The vertical velocity (V) was measured along the axis of the core. Horizontal velocities were measured perpendicular to the core axis and parallel to the core face (H_x) and normal to the core face (H_y).

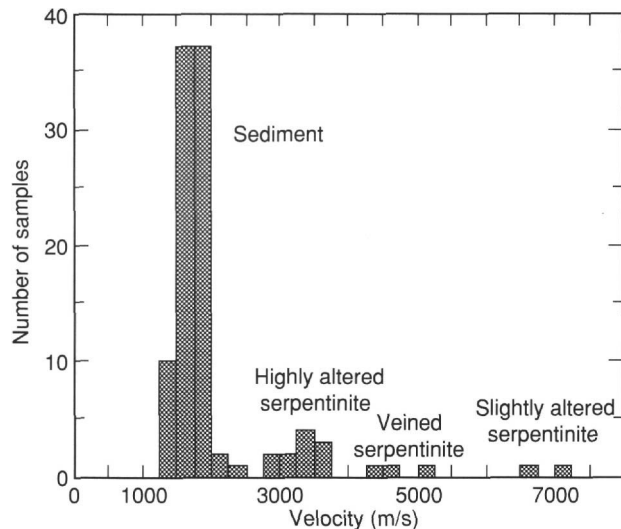


Figure 63. Histogram of velocities measured on cores from Hole 897C.

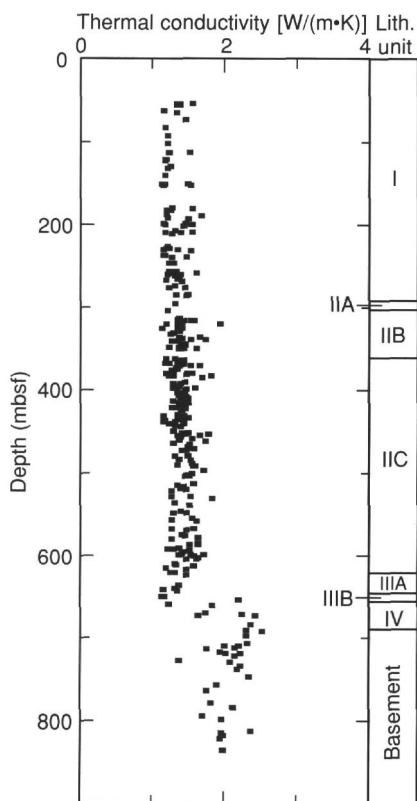


Figure 64. Thermal conductivity measurements for Holes 897C and 897D.

lated using 3168 s as the insertion time and modeling the data over the interval from 3233 to 4102 s. The shape of the temperature curve suggests that the tool was inserted only once and that the tool was stationary during the measurement, which suggests that this measurement is more reliable than the one at 55.2 mbsf.

The slope of a linear least-squares fit of the temperature to depth (Table 19) yields an estimate of 43 ± 10 mK/m (95% confidence level) for the temperature gradient in the upper 215 mbsf at Site 897. The slope of a linear least-squares fit of the temperature to vertically integrated thermal resistivity (Table 19) yields an estimate of $54 \pm$

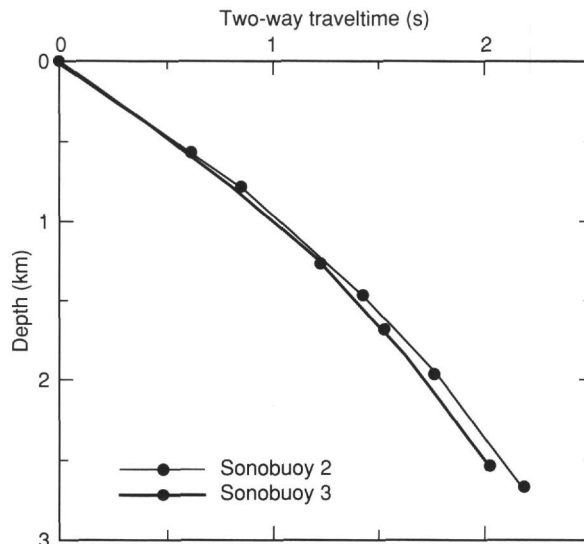


Figure 65. Graph relating two-way traveltime to depth in the Iberia Abyssal Plain. Curves are based on two sonobuoy lines shot at 40°22'N, 11°52'W (sonobuoy SB2) and 40°37'N, 12°52'W (sonobuoy SB3; Whitmarsh et al., 1990).

13 mW/m² (95% confidence level) for the heat flow (see "Explanatory Notes" chapter, this volume).

SUMMARY AND CONCLUSIONS

Site 897 is situated in the Iberia Abyssal Plain over a north-south basement ridge (Fig. 2), within the presumed ocean/continent transition (OCT) zone off western Iberia (see "Introduction" chapter, this volume). The site is one of a transect of drill sites across the OCT designed to study the petrological changes in the basement rocks within the OCT as a means of identifying the processes that accompanied continental break-up and the onset of steady-state seafloor spreading. Geophysical modeling had predicted that the ridge lay at, or close to, the ocean/continent boundary (Whitmarsh et al., 1990; Whitmarsh et al., 1993) and, by analogy with samples obtained from a 100-km-long ridge within the ocean/continent transition west of Galicia Bank (Boillot, Winterer, Meyer, et al., 1987; Boillot, Comas, et al., 1988), might consist of serpentinitized peridotite (Beslier et al., 1993). Four holes were drilled at 40°50.3'N, 12°28.4'W to test this hypothesis, with the primary scientific objective of penetrating basement to a depth sufficient to firmly establish its character. Up to 694 m of Pleistocene to Early Cretaceous age sediments were cored in Holes 897A, 897C, and 897D. Up to 143 m of basement were cored in Holes 897C and 897D.

The evolution of this site revealed in our cores began with exposure on the sea bed of a serpentinitized peridotite. About 90% of the peridotite sampled is undifferentiated harzburgite or lherzolite, whose mean original composition was 70%-80% olivine, 15%-20% pyroxene, and 1%-2% spinel. These rocks are heterogeneous and range from pyroxene-rich peridotite to dunite. The coexistence of plagioclase and spinel in the rocks suggests that they last equilibrated at low pressure (900-1000 MPa or about 30 km depth). The wide range of peridotite compositions and the locally high proportion of plagioclase (up to 40%) suggest that the peridotite may have experienced some melting and even mobility of magma. About 10% of the peridotite was brecciated during and after serpentinitization. The brecciation ranges from pervasive fracturing with serpentine and calcite veining to gravel-sized serpentinitized peridotite clasts embedded in a calcite and/or serpentine matrix. In a process yet to be determined, but that probably involved the (hydrothermally driven) circulation of large quantities of seawater,

Table 18. Depths of reflectors in Hole 897C.

| Reflector | Time (s TWT) | Computed depth (mbsf) | Estimated depth (mbsf) | Origin of reflector |
|-----------|--------------|-----------------------|------------------------|---------------------------------------------------------------------|
| R1 | | 0-300 | | Impedance contrasts at bases of turbidites |
| R2 | 0.37 | 340 | 325 | mid-Miocene hiatus/unconformity; acoustic formation 1A/1B boundary |
| R3 | 0.45 | 420 | ≥ 440 | Appearance of denser clays below 440 mbsf |
| R4 | 0.63 | 590 | ? | Appearance of claystone and chalk; acoustic formation 1B/2 boundary |
| Basement | 0.70 | 670 | 678 | Top of peridotite basement |

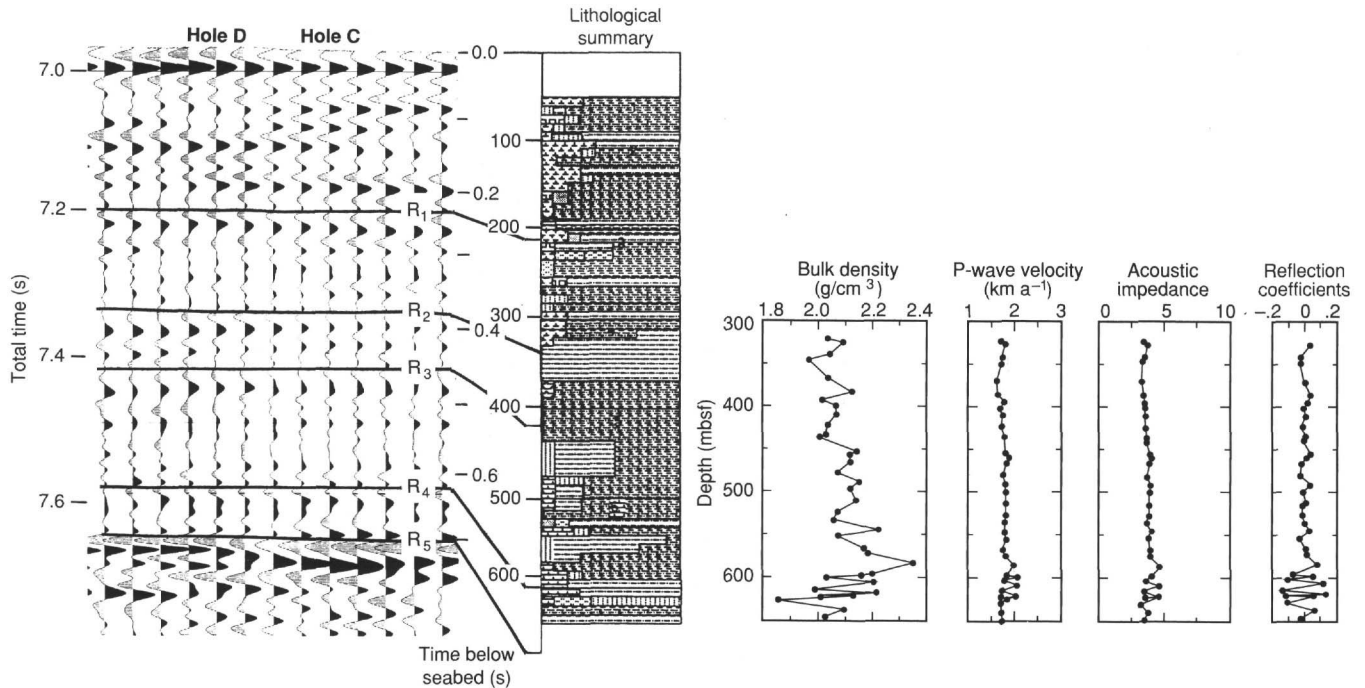


Figure 66. Expanded migrated seismic reflection profile section from Sonne Line 75-16 showing the principal reflectors R₁, R₂, etc., which are referred to in the text, and a summary lithology (see "Explanatory Notes" chapter, this volume, for an explanation of the symbols) and bulk density, velocity, impedance, and reflection coefficients computed from laboratory physical properties measurements.

Table 19. WSTP temperature measurements and vertically integrated thermal resistivity.

| Depth (mbsf) | Temperature (°C) | Vertically integrated thermal resistivity (m ² K/W) |
|--------------|------------------|----------------------------------------------------------------|
| 0 | 3.6 ± 0.1 | 0 |
| 55.2 | 7.3 ± 0.8 | 42.1 |
| 214.4 | 13.1 ± 0.1 | 169 |

western Galicia Bank margin. The extensive serpentinization is the result of the peridotite having reacted with seawater. The altered rocks have a range of physical properties that depends on their alteration state. Densities and velocities lie in the range of 2.3 to 2.5 g/cm³ and 2.8 to 7.1 km/s, respectively. Alteration also was accompanied by a reduction in magnetic susceptibility.

The oldest sediment recovered at this site is a mass flow deposit, found immediately above the basement, that contains peridotite blocks and a variety of sediments of late Hauterivian(?), early Barremian to late Aptian age that young upward. This age range includes the estimated Barremian (130 Ma) time of first seafloor spreading at this latitude (Whitmarsh et al., 1990). As the sequence young upward systematically, rather than showing a disordered age pattern, it is probable that several debris flows were emplaced during the Early Cretaceous, not in post-late Aptian time, and so are related to the last

stages of rifting and the earliest seafloor spreading. The provenance of the sediments in the flows is uncertain. The weak disruption, poor sorting, and absence of graded deposits suggest a relatively short transport path; yet, the deposit contains clasts of continental basement material that must have come from a continental margin or from submarine continental fault blocks. The peridotite must have been exposed at the seafloor during the late Hauterivian(?), early Barremian to late Aptian time, perhaps along a fault scarp, to have contributed clasts to the flows. An east-west seismic reflection profile shows that the crest of the ridge, 1.0 km east of the site, is capped by middle Eocene sediments. Thus, the problem is how to explain a gravity-driven deposit, which is much older than early Eocene, when seismic reflectors, inferred to be roughly contemporary with its age of emplacement, now appear to be several hundred meters deeper than the ridge crest in the basins that flank the ridge. If the ridge was at its present elevation with respect to the adjacent basins when the mass flows were deposited (and assuming that the mass flow could travel only 100 to 200 m uphill), then either all the material is of local origin (i.e., from the same ridge) or, more speculatively, the nonperidotite material was transported from the continental crust to the north, along the axis of the rift itself. Had the peridotite not yet been fully uplifted to form the present-day ridge when the mass flows occurred, then the nonperidotite material might have arrived from almost any direction. However, the implied upbending of reflectors toward the ridge, which

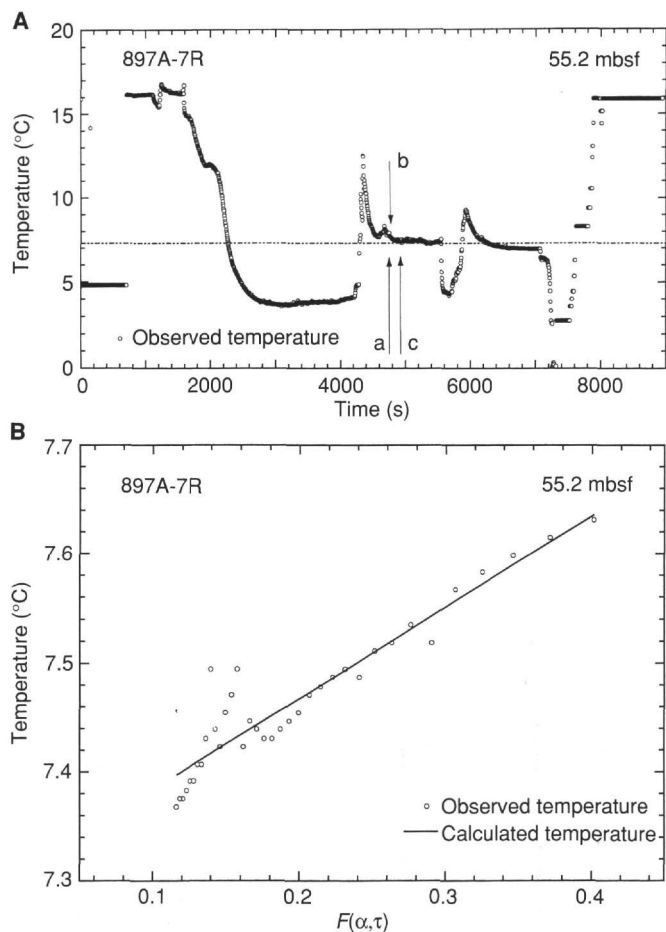


Figure 67. Deployment of the WSTP at 55.2 mbsf in Hole 897A. **A.** Observed temperature as a function of time. The temperature at the seafloor has been interpreted as 3.6 ± 0.1 °C, and the in-situ temperature was interpreted as 7.3 ± 0.8 °C. The curve does not show a normal decay after initial insertion at about 4400 s. The probe was pulled partially or completely out and then reinserted at about 5900 s. The insertion time used for curve fitting is indicated by arrow a. The portion of the temperature data used in the extrapolation is between arrows b and c. **B.** Observed temperature plotted vs. Bullard's "F" function (Bullard, 1954). The quality of the temperature extrapolation is reflected in the linearity of the plotted points.

should have accompanied any such uplift, is not seen. Either hypothesis implies that the peridotite ridge was exposed at the sea bed for several tens of millions of years.

Serpentinized peridotite breccias have been found frequently both at other DSDP/ODP sites where serpentinite was drilled (see Juteau et al., 1990, for a review) and elsewhere in ophiolites. During Leg 125, clasts of serpentinized tectonized peridotite and metabasalt were found at the base of Sites 778, 779, and 783, drilled on the flanks of seamounts behind the Izu-Bonin and Mariana arcs (Fryer, Pearce, Stokking, et al., 1990). Serpentinite breccias also were recovered from young Atlantic oceanic crust drilled during Leg 82 (Bougault, Cande, et al., 1985) and from the backarc Tyrrhenian Sea drilled during Leg 107 (Kastens, Mascle, et al., 1987). Surprisingly, no breccia was found at Site 637, which was drilled on the flank of a peridotite ridge off Galicia Bank (Boillot, Winterer, Meyer, et al., 1987). In the western Alps, a widespread opihcalcite sediment breccia exists around the Queyras Ophiolite, a relict of the Ligurian Tethys continental margin (Tricart and Lemoine, 1991); similar deposits also are known in the northern Apennines. Thus, serpentinite breccias are known from many different marine geological environments and

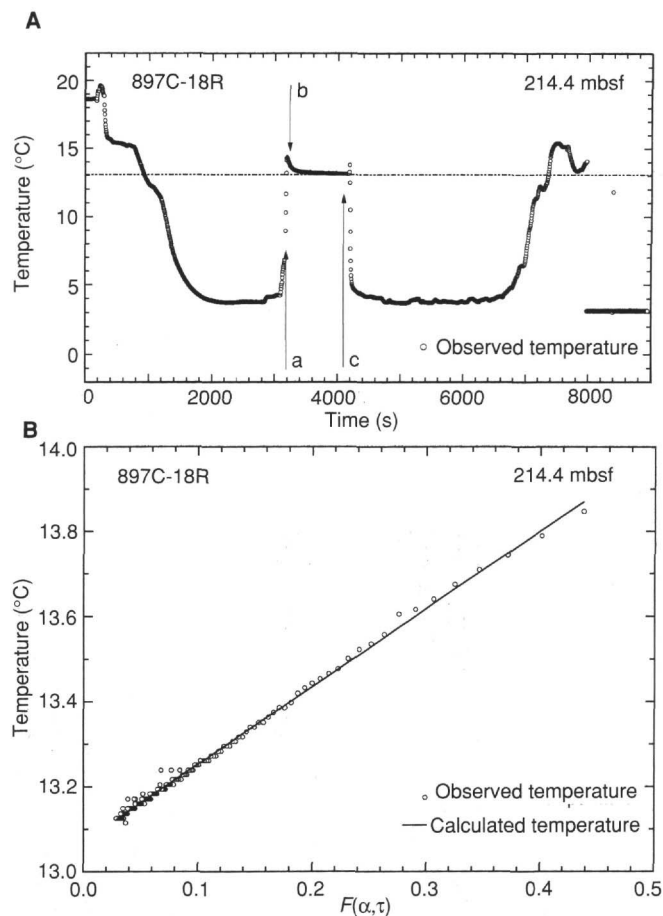


Figure 68. Deployment of WSTP at 214.4 mbsf in Hole 897C. **A.** Observed temperature as a function of time. The temperature at the seafloor has been interpreted as 3.6 ± 0.1 °C, and the in-situ temperature was interpreted as 13.1 ± 0.1 °C. The insertion time used for fitting the curve is indicated by arrow a. The portion of the temperature data used in the extrapolation is between arrows b and c. **B.** Observed temperature plotted vs. Bullard's "F" function (Bullard, 1954). The quality of the temperature extrapolation is reflected in the linearity of the plotted points.

attest to the ease with which serpentinized peridotite can become disaggregated when exposed on the seafloor. This may be because such outcrops are subject to extensive brittle deformation during their emplacement. The unusual, but not unique, aspect of the Site 897 mass flow deposit is the variety of sediments of different ages entrained with the serpentinite clasts.

Following the deposition of the mass flow deposit, a sequence of 29 m of unfossiliferous coarse-grained clastic rocks and claystones was deposited. Deposition below the CCD and the constraints posed by the age of immediately overlying beds suggest it was deposited during Eocene-late Paleocene time, when the regional CCD was relatively shallow (Tucholke and Vogt, 1979). Some of the sediment was deposited as debris flows or turbidites. Clasts suggest the existence of contemporary basaltic volcanism and the reworking of continental basement material.

The claystones pass abruptly upward into a 260-m-thick sequence of calcareous graded beds and carbonate-poor pelagic/hemipelagic sediments deposited below the CCD during middle Eocene to middle Miocene time. These sediments were deposited by turbidity currents and have been reworked by contour currents. Evidence of contour currents is sparse in cores of early Miocene age, but the calcareous turbidites persist. A 10.5-Ma hiatus in deposition began in the middle

Miocene and continued until the late Miocene. This hiatus correlates with the angular unconformity between the regional acoustic formations 1A and 1B, defined by Groupe Galice (1979), which is visible in multichannel seismic reflection profiles across the site. The unconformity represents the onlapping of horizontally bedded turbidites on to reflectors that were folded and uplifted by northwest-southeast compression on the western Iberia margin during the Betic compressional phase in southern Spain. This sediment deformation appears to be closely correlated with a monoclinical fold frequently found over the peridotite basement ridge within the Iberia Abyssal Plain (Masson et al., in press).

The lithology remained unchanged after the hiatus until the earliest Pliocene, when about 290 m of Pliocene to Pleistocene, fine-grained terrigenous turbidites, having thin intervening layers of nanofossil clay, began to accumulate at close to 60 m/m.y. The site appears to have been above the CCD. The reason for this sudden increase in sedimentation is not clear, but is possibly related to climatic changes.

The principal results from this site can be summarized as follows:

1. The basement is composed of serpentinitized, relatively undepleted peridotite that originated in the upper mantle and last equilibrated at a pressure of 9 to 10 kbars (about 30 km depth). The peridotite underwent extensive serpentinitization and calcitization in the upper part of the basement. The peridotite was exposed at the seafloor during, and for several tens of millions of years after, the time of continental break-up.

2. A mass flow unit containing late Hauterivian(?), early Barremian to late Aptian sediments immediately overlies basement and contains fragments of peridotite and continental basement rocks. The unit was likely deposited in multiple events at any time from the late Hauterivian(?), early Barremian to the late Aptian. The sediments suggest that continental basement rocks were located upslope, or only tens of meters downslope, of the site.

3. A significant break in the sedimentary record, starting in the middle Miocene, can be correlated with horizontally bedded turbidites that onlap onto a monoclinical fold of pre-late Miocene sediments. The hiatus can be correlated with a regional angular unconformity (seen in seismic reflection profiles) that may be related to northwest-southeast compression on this margin during a compressional phase in the Betic Mountains in southern Spain.

REFERENCES*

- Agrinier, P., Mével, C., and Girardeau, J., 1988. Hydrothermal alteration of the peridotites cored at the ocean/continent boundary of the Iberian Margin: petrologic and stable isotope evidence. *In* Boillot, G., Winterer, E.L., et al., *Proc. ODP, Sci. Results*, 103: College Station, TX (Ocean Drilling Program), 225-234.
- Beslier, M.-O., Ask, M., and Boillot, G., 1993. Ocean-continent boundary in the Iberia Abyssal Plain from multichannel seismic data. *Tectonophysics*, 218:383-393.
- Beslier, M.-O., Girardeau, J., and Boillot, G., 1990. Kinematics of peridotite emplacement during North Atlantic continental rifting, Galicia, NW Spain. *Tectonophysics*, 184:321-343.
- Boillot, G., Beslier, M.O., and Comas, M., 1992. Seismic image of undercrusted serpentinite beneath a rifted margin. *Terra Nova*, 4:25-33.
- Boillot, G., Comas, M.C., Girardeau, J., Kornprobst, J., Loreau, J.-P., Malod, J., Mougénot, D., and Moullade, M., 1988. Preliminary results of the Galinaute cruise: dives of the submersible *Nautille* on the Western Galicia Margin, Spain. *In* Boillot, G., Winterer, E.L., et al., *Proc. ODP, Sci. Results*, 103: College Station, TX (Ocean Drilling Program), 37-51.
- Boillot, G., Féraud, G., Recq, M., and Girardeau, J., 1989. "Undercrusting" by serpentinite beneath rifted margins: the example of the west Galicia margin (Spain). *Nature*, 341:523-525.
- Boillot, G., Girardeau, J., and Kornprobst, J., 1988. Rifting of the Galicia Margin: crustal thinning and emplacement of mantle rocks on the seafloor. *In* Boillot, G., Winterer, E.L., et al., *Proc. ODP, Sci. Results*, 103: College Station, TX (Ocean Drilling Program), 741-756.
- Boillot, G., Grimaud, S., Mauffret, A., Mougénot, D., Kornprobst, J., Mergoïl-Daniel, J., and Torrent, G., 1980. Ocean-continent boundary off the Iberian margin: serpentinite diapir west of the Galicia Bank. *Earth Planet. Sci. Lett.*, 48:23-34.
- Boillot, G., Winterer, E.L., et al., 1988. *Proc. ODP, Sci. Results*, 103: College Station, TX (Ocean Drilling Program).
- Boillot, G., Winterer, E.L., Meyer, A.W., et al., 1987. *Proc. ODP, Init. Repts.*, 103: College Station, TX (Ocean Drilling Program).
- Bougault, H., Cande, S.C., et al., 1985. *Init. Repts. DSDP*, 82: Washington (U.S. Govt. Printing Office).
- Bouma, A.H., 1962. *Sedimentology of Some Flysch Deposits: A Graphic Approach to Facies Interpretation*: Amsterdam (Elsevier).
- Boyce, R.E., 1973. Physical properties—methods. *In* Edgar, N.T., Saunders, J.B., et al., *Init. Repts. DSDP*, 15: Washington (U.S. Govt. Printing Office), 1115-1128.
- , 1976. Definitions and laboratory techniques of compressional sound velocity parameters and wet-water content, wet-bulk density, and porosity parameters by gravimetric and gamma ray attenuation techniques. *In* Schlanger, S.O., Jackson, E.D., et al., *Init. Repts. DSDP*, 33: Washington (U.S. Govt. Printing Office), 931-958.
- , 1980. Determination of the relationships of electrical resistivity, sound velocity, and density/porosity of sediment and rock by laboratory techniques and well logs from Deep Sea Drilling Project Sites 415 and 416 off the coast of Morocco. *In* Lancelot, Y., Winterer, E.L., et al., *Init. Repts. DSDP*, 50: Washington (U.S. Govt. Printing Office), 305-318.
- Bullard, E.C., 1954. The flow of heat through the floor of the Atlantic Ocean. *Proc. R. Soc. London A*, 222:408-429.
- Claypool, G.E., and Kvenvolden, K.A., 1983. Methane and other hydrocarbon gases in marine sediment. *Annu. Rev. Earth Planet. Sci.*, 11:299-327.
- Comas, M.C., and Maldonado, A., 1988. Late Cenozoic sedimentary facies and processes in the Iberian Abyssal Plain, Site 637, ODP Leg 103. *In* Boillot, G., Winterer, E.L., et al., *Proc. ODP, Sci. Results*, 103: College Station, TX (Ocean Drilling Program), 635-655.
- Deer, W.A., Howie, R.A., and Zussman, J., 1966. *An Introduction to the Rock-Forming Minerals*: London (Longman Group).
- Dick, H.J.B., 1989. Abyssal peridotites, very slow spreading ridges and ocean ridge magmatism. *In* Saunders, A.D., and Norry, M.J. (Eds.), *Magmatism in the Ocean Basins*. Geol. Soc. Spec. Publ. London, 42:71-105.
- Emerson, S., and Hedges, J.I., 1988. Processes controlling the organic carbon content of open ocean sediments. *Paleoceanography*, 3:621-634.
- Emery, K.O., and Uchupi, E., 1984. *The Geology of the Atlantic Ocean*: New York (Springer-Verlag).
- Evans, C.A., and Girardeau, J., 1988. Galicia Margin peridotites: undepleted abyssal peridotites from the North Atlantic. *In* Boillot, G., Winterer, E.L., et al., *Proc. ODP, Sci. Results*, 103: College Station, TX (Ocean Drilling Program), 195-207.
- Evans, H.B., and Cotterell, C.H., 1970. Gamma-ray attenuation density scanner. *In* Peterson, M.N.A., Edgar, N.T., et al., *Init. Repts. DSDP*, 2: Washington (U.S. Govt. Printing Office), 460-472.
- Féraud, G., Girardeau, J., Beslier, M.O., and Boillot, G., 1988. Dation $^{39}\text{Ar}/^{40}\text{Ar}$ de la mise en place des péridotites bordant la marge de la Galice (Espagne). *C. R. Acad. Sci. Ser. 2*, 307:49-55.
- Folk, R.L., 1980. *Petrology of Sedimentary Rocks*: Austin (Hemphill Publ.).
- Fryer, P., Pearce, J.A., Stokking, L.B., et al., 1990. *Proc. ODP, Init. Repts.*, 125: College Station, TX (Ocean Drilling Program).
- Gard, G., and Backman, J., 1990. Synthesis of Arctic and Subarctic coccolith biochronology and history of North Atlantic drift water influx during the last 500,000 years. *In* Bleil, U., et al. (Eds.), *Geologic History of the Polar Oceans: Arctic versus Antarctic*. NATO ASI Ser, Ser. C, 417-436.
- Gealy, E.L., 1971. Saturated bulk density, grain density, and porosity of sediment cores from the western Equatorial Pacific: Leg 7, *Glomar Challenger*. *In* Winterer, E.L., Riedel, W.R., et al., *Init. Repts. DSDP*, 7 (Pt. 2): Washington (U.S. Govt. Printing Office), 1081-1104.
- Gieskes, J.M., 1974. Interstitial water studies, Leg 25. *In* Simpson, E.S.W., Schlich, R., et al., *Init. Repts. DSDP*, 25: Washington (U.S. Govt. Printing Office), 361-394.
- , 1983. The chemistry of interstitial waters of deep-sea sediments: interpretation of deep-sea drilling data. *In* Riley, J.P., and Chester, R. (Eds.), *Chemical Oceanography* (Vol. 8): London (Academic Press), 222-269.

* Abbreviations for names of organizations and publication titles in ODP reference lists follow the style given in *Chemical Abstracts Service Source Index* (published by American Chemical Society).

- Girardeau, J., Evans, C.A., and Beslier, M.-O., 1988. Structural analysis of plagioclase-bearing peridotites emplaced at the end of continental rifting: Hole 637A, ODP Leg 103 on the Galicia Margin. *In* Boillot, G., Winterer, E.L., et al, *Proc. ODP, Sci. Results*, 103: College Station, TX (Ocean Drilling Program), 209-223.
- Groupe Galice, 1979. The continental margin off Galicia and Portugal: acoustical stratigraphy, dredge stratigraphy, and structural evolution. *In* Sibuet, J.-C., Ryan, W.B.F., et al., *Init. Repts. DSDP*, 47 (Pt. 2): Washington (U.S. Govt. Printing Office), 633-662.
- Juteau, T., Cannat, M., and Lagabrielle, Y., 1990. Serpentinized peridotites in the upper oceanic crust away from transform zones: a comparison of the results of previous DSDP and ODP Legs. *In* Detrick, R., Honnorez, J., Bryan, W.B., Juteau, T., et al. *Proc. ODP, Sci. Results*, 106/109: College Station, TX (Ocean Drilling Program), 303-308.
- Kastens, K.A., Mascle, J., Auroux, C, et al., 1987. *Proc. ODP, Init. Repts.*, 107: College Station, TX (Ocean Drilling Program).
- Laughton, A.S., Berggren, W.A., et al., 1972. *Init. Repts. DSDP*, 12: Washington (U.S. Govt. Printing Office).
- Lundberg, N., and Moore, J.C., 1986. Macroscopic structural features in Deep Sea Drilling Project cores from forearc regions. *In* Moore, J.C. (Ed.), *Structural Fabrics Preserved in Deep Sea Drilling Project Cores From Forearcs*. Mem.—Geol. Soc. Am., 166:13-44.
- Maldonado, A., 1976. Upper Cretaceous and Cenozoic depositional processes and facies in the distal North Atlantic continental margin off Portugal, DSDP Site 398. *In* Sibuet, J.-C., Ryan, W.B.F., et al., *Init. Repts. DSDP*, 47 (Pt. 2): Washington (U.S. Govt. Printing Office), 373-402.
- Martini, E., 1971. Standard Tertiary and Quaternary calcareous nannoplankton zonation. *In* Farinacci, A. (Ed.), *Proc. 2nd Int. Conf. Planktonic Microfossils Roma*: Rome (Ed. Tecnosci.), 2:739-785.
- Masson, D.G., Cattungh, J.A., Pinheiro, L.M., Whitmarsh, R.B., Beslieu, M.-O., Roeso, H., in press. Compressional deformation at the ocean-continent transition in the NE Atlantic. *J. Geol. Soc. London*.
- Mauffret, A., and Montadert, L., 1988. Seismic stratigraphy off Galicia. *In* Boillot, G., Winterer, E.L., et al., *Proc. ODP, Sci. Results*, 103: College Station, TX (Ocean Drilling Program), 13-30.
- Melver, R., 1975. Hydrocarbon occurrence from Joides Deep Sea Drilling Project. *Proc. Ninth Petrol. Congr.*, 269-280.
- Meyers, P.A., in press. Preservation of source identification of sedimentary organic matter during and after deposition. *Chem. Geol.*
- Meyers, P.A., and Brassell, S.C., 1985. Biogenic gases in sediments deposited since Miocene times on the Walvis Ridge, South Atlantic Ocean. *In* Caldwell, D.E., Brierly, J.A., and Caldwell, C.L. (Eds.), *Planetary Ecology*: New York (Wiley), 69-80.
- Müller, P.J., 1977. C/N ratios in Pacific deep sea sediments: effect of inorganic ammonium and organic nitrogen compounds sorbed by clays. *Geochim. Cosmochim. Acta*, 41:765-776.
- Peterson, M.N.A., Edgar, N.T., et al., 1970. Shipboard scientific procedures. *In* Peterson, M.N.A., Edgar, N.T., et al., *Init. Repts. DSDP*, 2: Washington (U.S. Govt. Printing Office), 451-490.
- Pickering, K.T., Stow, D.A.V., Watson, M.A., and Hiscott, R., 1986. Deep-water facies, processes and models: a review and classification for modern and ancient sediments. *Earth Sci. Rev.*, 223:75-174.
- Piper, D.J.W., 1978. Turbidite muds and silts on deep sea fans and abyssal plains. *In* Stanley, D.J., and Kelling, G. (Eds.), *Sedimentation in Submarine Canyons, Fans, and Trenches*: Stroudsburg, PA (Dowden, Hutchinson and Ross), 163-176.
- Ringwood, A.E., 1975. *Composition and Petrology of the Earth's Mantle*: New York (McGraw-Hill).
- Sibuet J.-C., Ryan, W.B.F., et al., 1979. *Init. Repts. DSDP*, 47 (Pt. 2): Washington (U.S. Govt. Printing Office).
- Sissingh, W., 1977. Biostratigraphy of Cretaceous nannoplankton. *Geol. Mijnbouw*, 56:37-50.
- Snowdon, L.R., and Meyers, P.A., 1992. Source and maturity of organic matter in sediments and rocks from Sites 759,760,761, and 764 (Wombat Plateau) and Sites 762 and 763 (Exmouth Plateau). *In* von Rad, U., Haq, B.U., et al., *Proc. ODP, Sci. Results*, 122: College Station, TX (Ocean Drilling Program), 309-315.
- Suess, E., 1980. Particulate organic carbon flux in the oceans—surface productivity and oxygen utilization. *Nature*, 288:260-263.
- Toumarkine, M., and Luterbacher, H., 1985. Paleocene and Eocene planktic foraminifera. *In* Bolli, H.M., Saunders, J.B., and Perch-Nielsen, K. (Eds.), *Plankton Stratigraphy*: Cambridge (Cambridge Univ. Press), 87-154.
- Tricart, P., and Lemoine, M., 1991. The Queyras Ophiolite west of Monte Viso (Western Alps): indicator of a peculiar ocean floor in the Mesozoic Tethys. *J. Geodyn.*, 13:163-181.
- Tucholke, B.E., and Vogt, P.R., 1979. Western North Atlantic: sedimentary evolution and aspects of tectonic history. *In* Tucholke, B.E., Vogt, P.R., et al., *Init. Repts. DSDP*, 43: Washington (U.S. Govt. Printing Office), 791-825.
- Van den Driessche, J., and Brun, J.P., 1987. Rolling structures at large shear strain. *J. Struct. Geol.*, 9:691-704.
- Waterman, L.S., 1973. Interstitial water studies on small core samples, Leg 20. *In* Heezen, B.C., MacGregor, I.D., et al., *Init. Repts. DSDP*, 20: Washington (U.S. Govt. Printing Office), 423-425.
- Whitmarsh, R.B., Miles, P.R., and Mauffret, A., 1990. The ocean-continent boundary off the western continental margin of Iberia, I. Crustal structure at 40°30'N. *Geophys. J. Int.*, 103:509-531.
- Whitmarsh, R.B., Pinheiro, L.M., Miles, P.R., Recq, M., and Sibuet, J.C., 1993. Thin crust at the western Iberia ocean-continent transition and ophiolites. *Tectonics*, 12:1230-1239.

Ms 149IR-104

NOTE: For all sites drilled, core-description forms ("barrel sheets") and core photographs have been reproduced on coated paper and can be found in Section 3, beginning on page 271. Forms containing smear-slide data can be found in Section 4, beginning on page 657. Thin-section data are given in Section 5, beginning on page 679. GRAPE, Index Property and MAGSUS data are presented on CD-ROM (back pocket).